Topology and Thermophoresis Characterization of Complex Polymers by Thermal Field-Flow Fractionation

D I S S E R T A T I O N

zur Erlangung des akademischen Grades
Doctor rerum naturalium
(Dr. rer. nat.)

vorgelegt

dem Bereich Mathematik und Naturwissenschaften
der Technischen Universität Dresden

von

M. Sc. Martin Geisler
geboren am 23.02.1988 in Lutherstadt Wittenberg

Eingereicht am 10.11.2020

Die Dissertation wurde in der Zeit von Januar 2017 bis Oktober 2020
am Leibniz-Institut für Polymerforschung Dresden e. V. angefertigt.

This dissertation was accomplished under the scientific supervision of:

Prof. Dr. Brigitte Voit and Prof. Dr. Albena Lederer.

First reviewer: Prof. Dr. Brigitte Voit
Second reviewer: Prof. Dr. Harald Pasch

Submitted: 10.11.2020
Defended: 09.02.2021

Abstract

Field-flow fractionation (FFF) is a versatile separation technique with high potential for in-depth characterization of complex macromolecular systems with multiple distributions. FFF has been proven to successfully tackle challenges in chromatography since it does not rely on a stationary phase with a high surface or interaction area and hence, provide information on a broader size range than column-based separation. To date, this potential is not fully exploited for the application of FFF as a routine method for the measurement of physicochemical properties due to lack of theoretical background or applicable calculation approaches. Among all FFF techniques, thermal FFF (ThFFF) still represents the so far least understood method from theoretical point of view. ThFFF has a great but still not fully explored potential in advanced polymer separation and characterization. Additionally, to separation prior to multidetection-based analysis, ThFFF has the capability to be used for analysis of the thermophoretic properties of polymers or particles. Unlike all other FFF subtypes, evaluations of ThFFF separations require a correction of effects induced due to temperature differences in the carrier liquid. One of the main goals in this dissertation is dedicated to extension and revision of the broad spectrum of solvents and experimental conditions used for ThFFF calculations. Optimizations of ThFFF separations required so far empirical attempts by trial-and-error approaches. Thus, the second goal of this work was to shorten this process and to allow precise predictions of the influence of the polymer solubility on the ThFFF separation efficiency.

The investigation of the potential of ThFFF for the multidetection-based analysis of polymers with complex topology was the third goal of this work. Initially, thermal diffusion was assumed to be independent on the molar mass and on the polymer topology. However, recent advances indicate a certain dependency of thermophoretic behavior on branching or microstructure. To shed light on this topic, ThFFF is theoretically assessed and designed to prove its capability to resolve polymer branching characteristics from the measured thermophoretic properties. Therefore, two different libraries of branched polymer model systems based on aliphatic-aromatic polyesters and on a new type of short chain branched polyethylene are investigated. Furthermore, the potential of the optimized ThFFF theory was assessed in the context of crosslinked polymer architectures. These investigations shine light onto the so far controversially debated topic of electron beam irradiation effects on thermoplastic polyurethane. This topic is addressed by a combination of multidetector ThFFF and supporting associated characterization methods showing the potential of ThFFF to evaluate crosslinked and ultra-high molecular weight macromolecular structures.

Zusammenfassung

Bislang ist die Feldflussfraktionierung (FFF) als Routinemethode zur Messung physikalisch-chemischer Stoffeigenschaften auf der Basis von Retentionsdaten mangels theoretischen Hintergrunds oder anwendbarer Berechnungsansätze noch nicht voll anwendbar. Gleichwohl hat sich FFF als erfolgreich erwiesen Herausforderungen in der Chromatographie zu kompensieren, da FFF keinerlei stationäre Phase benötigt und daher Informationen über einen breiteren Trennungsbereich im Vergleich zu säulenbasierter Separation liefert.

Von allen FFF-Techniken ist die thermische FFF (ThFFF) die bis dato theoretisch am wenigsten verstandene FFF-Methode. ThFFF hat ein großes, aber zugleich noch nicht vollständig ausgeschöpftes Potenzial im Bereich der modernen Polymercharakterisierung. Im Gegensatz zu allen anderen FFF-Subtypen erfordern Auswertungen von ThFFF-Trennungen allerdings eine Korrektur von Effekten aufgrund temperaturbedingter Unterschiede in den Eigenschaften des Eluenten. Eines der Hauptziele dieser Dissertation ist die Erweiterung und Überarbeitung des Spektrums an Lösungsmitteln und experimentellen Bedingungen, die bei Berechnungen von ThFFF-Analysenergebnissen (u. a. thermophoretischer Eigenschaften von Polymeren) angewandt werden können. Zudem erforderten Optimierungen von ThFFF-Trennungen bisher empirische Versuchsreihen. Das zweite Ziel dieser Arbeit war es daher, diesen Prozess zu verkürzen und genauere Vorhersagen über den Einfluss der Polymerlöslichkeit auf die ThFFF-Trennleistung zu ermöglichen.

Die Untersuchung des Potenzials von ThFFF für die multidetektionsbasierte Analyse von Polymeren mit komplexen Topologien war das dritte Ziel dieser Arbeit. Bisher wurde die thermische Diffusion als unabhängig von Molmasse oder Polymertopologie angenommen. Jüngste Erkenntnisse weisen jedoch auf eine gewisse Abhängigkeit des thermophoretischen Verhaltens von Verzweigung oder Mikrostruktur hin. Um diesen Aspekt näher zu beleuchten, wurde das ThFFF Retentionsverhalten und die thermische Diffusion selbst hinsichtlich der Verzweigungseigenschaften von Polymeren anhand zwei verschiedener Polymermodellsysteme mit je einer Bandbreite verschiedener Topologien untersucht. Im Zuge dieser Untersuchungen wurde auch durch eine Kombination von Multidetektor-ThFFF und unterstützenden zugehörigen Charakterisierungsmethoden ein substantieller Beitrag zur Aufklärung des bisher kontrovers diskutierten Themas der Elektronenbestrahlungseffekte auf thermoplastisches Polyurethan geleistet und so das Potenzial von ThFFF zur Analyse vernetzter Strukturen mit ultrahoher Molmasse genutzt.

Acknowledgements / Danksagung

First of all, I would like to express my gratitude to Prof. Dr. Brigitte Voit for giving me the opportunity to carry out my dissertation in the Institute of Macromolecular Chemistry at the Leibniz-Institut für Polymerforschung Dresden e. V. under her supervision, with her support and valuable scientific guidance. Furthermore, I would like to heartedly thank PD Dr. Albena Lederer for the co-supervision and all knowledge, experience and skills she shared with me or taught me as well as for her outstanding support and encouragement during my entire journey in science so far. The Graduate Academy of the TU Dresden is greatly acknowledged for their support by providing me a bridging grant during my time as PhD student. My sincere thanks go to our partners from the Colorado School of Mines Prof. Dr. Kim Williams and Dr. William C. Smith for sharing their expertise and experience and profound introduction in the field of FFF as well as for the great time we spend during exchange visits and conferences. Prof. Dr. Jan Merna and Dr. Robert Mundil from the University of Chemistry and Technology Prague as well as Dr. Anna Sharmak (formerly named Khalyavina) are greatly acknowledged for synthesizing and providing the polymer samples used in the investigations in this dissertation. A further thank is addressed to the former head of the Analytics Department Dr. Klaus-Jochen Eichhorn for the support during my work in the department. Sincere thanks go to my current and former colleagues form the Polymer separation group Dr. Susanne Boye, Christina Harnisch, Petra Treppe, Dr. Laura Plüschke, Dr. Raffaele Andrea Abbate, Shamila Firdaus, Mahmoud Alkhalaf, Johanna Engelke and Carolin Bunk for all the help, contributions and inspiring vibes throughout my time as PhD student. Great thanks go to all members of the Analytics Department for their contributions and support. In particular I would like to thank Franziska, Elisavet, Mikhail and Eileen for sharing spare time during lunch or coffee breaks, which refreshed my daily and sometimes lengthy working routine as well as for particular scientific discussions. Thanks to Dr. Kay Lederer for grilling the best Thuringian fried sausages I have savored so far.

Ein ganz besonders großer Dank geht an meine lieben Eltern für all die Unterstützung und die Möglichkeiten die sie mir geboten haben um meinen Weg gehen zu können und die in guten wie in schwierigen Zeiten stets an mich geglaubt haben. Auch meiner Freundin Asha, meiner Schwester Julia, meinen Großeltern, sowie der gesamten weiteren Familie sei gedankt für ihre bisherige und zukünftige Unterstützung in allen Lebenslagen.

TABLE OF CONTENT

Abstract V
Zusammenfassung (German Summary) VI
Acknowledgements / Danksagung VII
List of Figures and Tables 3
Symbols 6
List of Publications and Contributions 7
1. Introduction 9
1.1. Analytical Methods and Challenges in Polymer Characterization 12
1.1.1. Single-Detection Size-Exclusion Chromatography (SEC) 12
1.1.2. SEC coupled to Viscometry Detection 13
1.1.3. Light Scattering 14
1.1.3.1. Multi-Angle Static Light Scattering 14
1.1.3.2. Dynamic Light Scattering 16
1.1.4. Multidetector Liquid Chromatography 17
1.1.5. Alternative Flow-Based Separation 18
1.2. Objectives and Scope of the Thesis 19
2. Scientific Background 23
2.1. Tailoring of Polymer Properties 23
2.2. Quantification of Branching in Polymers 26
2.3. Field-Flow Fractionation 28
2.3.1 Derivation of the Basic FFF Separation Description 29
2.3.1.1 Concentration Distribution 29
2.3.1.2 Velocity Distribution 30
2.3.1.3 Normal Mode Retention in FFF 31
2.3.2. Physicochemical Parameters guiding Retention in FFF 32
2.3.3. Thermal Field-Flow Fractionation (ThFFF) 33
2.4. Approaches to Basic Theory and Prediction of Thermal Diffusion 36
2.5. Solubility Theories 38
3. State-of-the-Art 42
3.1. Polyesters with Tailored Degree of Branching 42

3.2. Characterization of Irradiated Thermoplastic Polyurethanes 43
3.3. Comprehensive Analysis of Polyolefins by Multidetector HT-SEC 45
3.4. Analysis of Branched Polymers by ThFFF 48
4. Experimental Part 51
4.1. Details to Polymer Model Systems 51
4.2. Electron Beam Irradiation 52
4.3. ThFFF Analysis 52
4.4. HT-SEC-d4 Analysis 53
4.5. Temperature-Dependent Dynamic Light Scattering 54
4.6. SEC-MALS-dRI at Room Temperature 54
4.7. Spectroscopic Methods 54
4.8. Thermal Analysis 55
5. Results and Discussion 56
5.1. Improvements in the Mathematical Description of ThFFF Retention 56
5.2. Tuning of ThFFF Separation and Analysis by Solubility and D_T Prediction 58
5.3. Branching Characterization of Polymer Model Systems by ThFFF 61
5.3.1. Architecture Characterization of Branched Aromatic-Aliphatic Polyesters 61
5.3.2. Topology Analysis of Chain Walk Polyethylene by ThFFF 64
5.4. ThFFF applied for Orthogonal Polymer Analysis of Electron Beam Irradiated Thermoplastic Polyurethane 70
6. Conclusions and Future Prospects 77
7. Bibliography 80
8. Publications 92
8.1. Non-Parabolicity correction for fifty-nine solvents and a retention study for strongly distorted flow-profiles in thermal field-flow fractionation 92
8.2. The Role of Solubility in Thermal Field Flow Fractionation – A Revisited Theoretical Approach for Tuning the Separation of Chain-Walking Polymerized Polyethylene 99
8.3. Thermal Field-Flow Fractionation for Characterization of Architecture in Hyperbranched Aromatic-Aliphatic Polyesters with Controlled Branching 116
8.4. Topology Analysis of Chain Walking Polymerized Polyethylene: An Alternative Approach for the Branching Characterization by Thermal FFF 135
8.5. Impact of Electron Beam Irradiation on Thermoplastic Polyurethanes Unraveled by Thermal Field-Flow Fractionation 159

LIST OF FIGURES AND TABLES

FIGURE 1.1 DIMENSIONS OF A LINEAR RANDOM POLYMER COIL. 11

FIGURE 1.2 DETECTOR DESIGN OF MALS 14

FIGURE 1.3 DETERMINATION OF THE WEIGHT AVERAGE MOLAR MASS MW AND Z-AVERAGE OF R_G FROM BATCH LIGHT SCATTERING DATA USING THE ZIMM FIT METHOD, EXEMPLARILY SHOWN FOR A THREE-ARM STAR POLYSTYRENE IN TETRAHYDROFURAN 15

FIGURE 1.4 INTENSITY FLUCTUATIONS OF SCATTERED LIGHT MEASURED IN DLS IN **A** AS RECORDED SIGNAL AND IN **B** AFTER AUTOCORRELATION OF THE DATA AND FITTED 16

FIGURE 1.5 GRAPHICAL ABSTRACT OF THE OBJECTIVES ACCOMPLISHED IN THIS DISSERTATION DEALING WITH THE OVERALL TOPIC OF THFFF AS SEPARATION AND CHARACTERIZATION METHOD 22

FIGURE 2.1 OVERVIEW OF POLYMER HETEROGENEITY IN CHEMICAL COMPOSITION, MOLECULAR TOPOLOGY AND THE CROSSOVER BETWEEN BOTH REPRESENTED BY GRAFTED BOTTLE-BRUSH COPOLYMERS 23

FIGURE 2.2 THE REPRESENTATIVE MORPHOLOGY OF SEGMENTED COPOLYMERS WITH CRYSTALIZING (HARD) SEGMENTS AND AMORPHOUS (SOFT) SEGMENTS, E.G. TYPICAL FOR THERMOPLASTIC POLYURETHANE 24

FIGURE 2.3 GENERALIZED STRUCTURE OF A HYPERBRANCHED POLYMER IN COMPARISON TO A DENDRIMER 27

FIGURE 2.4 GENERALIZED SEPARATION PRINCIPLE OF FFF: A) AFTER INJECTION, B) DURING FOCUS OR STOP FLOW AND C) ELUTION AND SUBSEQUENT SEPARATION. 28

FIGURE 2.5 TECHNICAL REALIZATION OF DIFFERENT SEPARATION FORCE FIELDS IN THE MOST COMMONLY USED FFF SUBTYPES: SDFFF, THFFF AND AF4 29

FIGURE 2.6 DIMENSIONLESS VELOCITY FLOW-PROFILES FOR A RECTANGULAR CHANNEL OF LOW AND HIGH ASPECT RATIO 31

FIGURE 2.7 PRINCIPLE OF THFFF DURING ELUTION WITH THE DISTORTED FLOW-PROFILE IN COMPARISON TO THE ISOVISCOUS PARABOLIC FLOW 35

FIGURE 2.8 HANSEN SOLUBILITY SPHERE CALCULATED FOR POLY(METHYL METHACRYLATE) WITH HSP AND THE SPHERE RADIUS REPORTED IN THE LITERATURE 39

FIGURE 3.1 SUMMARY OF THE SYNTHETIC STRATEGY TO TAILOR ARCHITECTURES OF DESIRED TOPOLOGY IN BETWEEN A DEGREE OF BRANCHING OF $0 - 50$ % 42

FIGURE 3.2 STRUCTURE OF A TPU WITH ALIPHATIC AND AROMATIC DIISOCYANATE, 1,4-BUTANE DIOL AS CHAIN EXTENDER AND A POLY(N-BUTYL ADIPATE) SOFT SEGMENT 44

FIGURE 3.3 PRINCIPLE OF ELECTRON BEAM PROCESSING IN A PROCESS LINE USING A HIGH VOLTAGE E-BEAM ACCELERATOR 44

FIGURE 3.4 COMPREHENSIVE CHARACTERIZATION BY HT-SEC-D4, SETUP SKETCHED IN (**A**) WITH SIMULTANEOUS RECORD OF FOUR INDEPENDENT DETECTIONS (**B**). DIFFERENT TYPES OF REGULAR PE OF LINEAR (LINPE, NIST) TO SHORT (LLDPE) AND LONG-CHAIN-BRANCHED STRUCTURE (BPE, HBPE, LDPE) WERE INVESTIGATED WITH REGARD TO THEIR TOPOLOGY BY CONFORMATION (**C, D**) CONTRACTION (**E, F**) ANALYSIS AND DENSITY-RELATED MEASURES (**G**) 46

FIGURE 3.5 A) EVOLUTION OF TOPOLOGY IN CWPE INDICATING THE GENERAL TREND TO DISORDERED DENDRITIC LIKE BOTTLE BRUSH POLYMERS WITH GROWING POLYMER CHAIN; TOPOLOGY IN COMPARISON BETWEEN EXPERIMENTAL FINDING BY AFM (HEIGHT MODE) AND STRUCTURES SIMULATED WITH REALISTIC CHAIN WALKING RATES OF AROUND 7 (**C**) AND 5 (**D**). 48

FIGURE 3.6 A) EXPERIMENTAL VERSUS PREDICTED MEAN SORET COEFFICIENTS FOR DIFFERENTLY STAR-SHAPED PS SAMPLES, AND **B)** SORET CONTRACTION FACTORS VS. THE NUMBER OF CHAIN ENDS FOR NON-LINEAR PS AND PMMA-STARS 49

TABLE 4.1 SYNTHESIS CONDITIONS, EXPECTED TOPOLOGY AND THE CHARACTERIZATION AVERAGE RESULTS OF THE CWPE MODEL LIBRARY USED IN THFFF STUDIES, FOUND BY HT-SEC-D4. 51

TABLE 4.2 LIST OF CARRIER LIQUIDS AND ADDITIVE CHEMICALS USED IN THFFF SEPARATIONS 53

FIGURE 5.1 D_T PREDICTED IN THIS STUDY IN COMPARISON TO THE PREDICTED D_T REPORTED PREVIOUSLY. BOTH PREDICTIONS ARE PLOTTED AGAINST EXPERIMENTAL D_T REPORTED FOR A BROAD CHOICE OF SOLVENTS 59

FIGURE 5.2 THFFF FRACTOGRAMS OF SEVEN CWPEWITH VARYING TOPOLOGY FROM HIGHLY BRANCHED (HB) TO LINEAR (LIN), SEPARATED IN THF (**A**), CHLOROFORM (**B**) AND CYCLOHEXANE (**C**). **D** ILLUSTRATES THE CALCULATED HANSEN SOLUBILITY SPHERE FOR PE TO APPROXIMATE THE SOLVENT QUALITY IN RELATION TO THEIR DISTANCE FROM THE SPHERE CENTER 60

FIGURE 5.3 CHEMICAL AND TOPOLOGY REPRESENTATION OF THE POLYMER MODEL LIBRARY COMPRISED OF SILYLATED ALIPHATIC-AROMATIC POLYESTERS CONTAINING ALL AN EQUAL FOCAL UNIT AS WELL AS LINEAR, DENDRITIC AND TERMINAL UNITS 61

FIGURE 5.4 A THFFF FRACTOGRAMS OF AN EXEMPLARY CHOICE OF SILYLATED POLYESTERS WITH DIFFERENT DB MEASURED IN CYCLOHEXANE WITH A CONSTANT ΔT. **B** DEPENDENCE OF D_T AND g'' ON DB IN CYCLOHEXANE AND THF. **C** DISTRIBUTION OF g'' CALCULATED FROM QUASI ONLINE DATA 63

FIGURE 5.5 SIMULATED APPEARANCE OF CWPE OF THE POLYMER MODEL LIBRARY INVESTIGATED IN THIS STUDY RANGING FROM **A)** HYPERBRANCHED (HB) TO **B)** LINEAR (LIN) TOPOLOGY, COMPRISED OF SHORT CHAIN BRANCHES, LONG CHAIN BRANCHES AS WELL AS BRANCH-ON-BRANCHES. 64

FIGURE 5.6 A CORRELATION OF D_T (THFFF) TO THE POLYMER TOPOLOGY EXPRESSED BY B AND M_{SEG}. **B** COMPARISON OF NORMALIZED D_T FROM TDFRS STUDIES OF N-ALKANES AND VALUES FROM THIS STUDY 65

FIGURE 5.7 A NORMALIZED DIFFERENTIAL WEIGHT DISTRIBUTION OF QUASI ONLINE g'' FOR SEVEN DIFFERENTLY BRANCHED CWPE. NORMALIZED LCB DISTRIBUTIONS CALCULATED ON THE BASIS OF THFFF RETENTION DATA BY AN OPTIMIZED FITTING PROCESS ARE DISPLAYED IN **B** IN COMPARISON TO LCB DISTRIBUTIONS FROM HT-SEC-D4 AND VALIDATED IN **C** 67

FIGURE 5.8 A CALCULATED BLOB DIAMETERS FROM EXPERIMENTAL D_T BY REVERSE APPLICATION OF THE MES D_T MODEL IN COMBINATION WITH THE HANSEN SOLUBILITY THEORY. **B** PERSISTENCE LENGTH OF REGULAR PE FROM SANS VERSUS THE NUMBER OF SHORT-CHAIN BRANCHES. 69

FIGURE 5.9 POSSIBLE REACTIONS IN MDI OR H_{12}MDI-BASED THERMOPLASTIC POLYURETHANES DISCUSSED IN THE LITERATURE 70

FIGURE 5.10 A) ATR-FTIR STUDY OF THE ALIPHATIC TPU IN A SERIES OF INCREASING IRRADIATION DOSE APPLIED ONTO THE MATERIAL. **B)** GLASS TRANSITION TEMPERATURES (T_g) OF THE ALIPHATIC TPU. **C)** INDICATES THE CORRESPONDING STEP HEIGHTS (HEAT CAPACITY DROPS) 71

FIGURE 5.11 A OPTIMIZED SEPARATION METHOD USED FOR THFFF SEPARATIONS OF ALL TPU IRRADIATION SERIES IN PUBLICATION 8.5 WITH TWO ASSIGNED REGIONS OF INTEREST FOR LOW AND HIGH MOLECULAR WEIGHT FRACTIONS BEING SEPARATED AND RECORDED IN THFFF FRACTOGRAMS SHOWN IN **B** FOR THE ALIPHATIC TPU. 72

FIGURE 5.12 NORMALIZED MOLAR MASS DIFFERENTIAL DISTRIBUTIONS OF THE ALIPHATIC TPU DETERMINED WITH THE DIFFERENT ANALYSIS APPROACHES SEC CALIBRATED WITH NARROW PS STANDARDS, SEC-MALS-DRI AND THFFF-MALS-DRI 73

FIGURE 5.13 DIFFERENTIAL S_T WEIGHT DISTRIBUTIONS CALCULATED FROM THE FULL THFFF FRACTOGRAMS OF THE ALIPHATIC TPU SERIES ILLUSTRATED IN FIG. 5.11 B 74

FIGURE 5.14 SUMMARY OF THE APPROXIMATE SECONDARY RELAXATION CORRECTION DEVELOPED IN THIS STUDY BASED ON S_T – MOLAR MASS CALIBRATION OF BROAD PS AND PMMA REFERENCE SAMPLES (**A**), WHICH IS USED TO EVALUATE THE SECONDARY RELAXATION INFLUENCE BY RETRACING THE EFFECTIVE ΔT FROM THE MEASURED MOLAR MASS RETENTION (**B**) 76

Abbreviations

SEC	Size exclusion chromatography
LC	Liquid chromatography (non-specified)
LAC	Liquid adsorption chromatography
LCCC	Liquid chromatography under critical conditions
KMHS	Kuhn-Mark-Houwink-Sakurada (plot or analysis)
MALS	Multi-angle (laser) light scattering detection
SANS	Small-angle neutron scattering
dRI	differential refractometric detection
DLS	Dynamic light scattering
TDFRS	Thermal diffusion forced Rayleigh scattering
FFF	Field-flow fractionation
HT-…	High temperature …
HT-SEC-d4	High temperature SEC with quadruple detection
FℓFFF	(Cross) flow-FFF
AF4	Asymmetric flow-FFF
SdFFF	Sedimentation FFF
ThFFF	Thermal FFF
EℓFFF	Electrical FFF
TPU	Thermoplastic polyurethane
PS	Polystyrene
PMA	Poly(methyl acrylate)
PBA	Poly(n-butyl acrylate)
PMMA	Poly(methyl mehacrylate)
PI	Polyisoprene
PP	Polypropylene
PE	Polyethylene
LLDPE	Linear low-density polyethylene
LDPE	Low-density polyethylene
HDPE	High-density polyethylene
cwPE	chain walking polymerized polyethylene
HST	Hansen solubility theory
HSP	Hansen solubility parameter
MEK	Methyl ethyl ketone (2-butanone)
THF	Tetrahydrofuran
ATR-FT-IR	Attenuated total reflection Fourier transform infrared spectroscopy
NMR	Nuclear magnetic resonance spectroscopy
DSC	Differential scanning calorimetry
UHMW	Ultra-high molecular weight
a. u.	Arbitrary units
hb.	Highly branched or hyperbranched
Eq(s).	Equation(s)
Fig.	Figure

SYMBOLS

M	Molar mass
index n	Number average moment
index w	Weight average moment
index z	Centrifugal average moment
index eq	Standard-equivalent
index Seg	Molar mass of a linear segment
$Đ$	Molar mass dispersity
η_0, η_S	Solvent viscosity
$dn\ dc^{-1}$	Refractive index increment
λ_L	Laser wavelength
θ	Scattering angle
n_0	Solvent refractive index
ϕ	Volume fraction
[η]	Intrinsic viscosity
R_G	Gyration radius
R_h	Hydrodynamic radius
τ_D	Decay time
$R_{[\eta]}$	Viscosity radius
α_{KMHS}, ν_R	Scaling exponents
K_{RMS}, K_{KMHS}	Scaling constants
K	(optical) constant
DB	Degree of branching
LCB	Long chain branches per 1000 monomers
SCB	Short chain branches per 1000 monomers
B	Number of branching points per molecule
g	Radius contraction factor
g'	Viscosity contraction factor
g''	Soret contraction factor
index bra.	branched analyte
index lin.	linear reference analyte
ε	Drainage parameter
S_T	Soret coefficient
t_0	Void time
t_R	Retention time
R	Retention ratio
u	Flow velocity
$\bar{u}$	Mean flow velocity
index p	parabolic
index 3rd	cubic
u_F	Analyte migration velocity
x/w	Relative height or thickness
w	(FFF-)Channel height
ℓ	Analyte cloud thickness
λ	Dimensionless FFF parameter (relative mean layer thickness)
D	Translational diffusion coefficient
D_T	Thermal diffusion coefficient
ν	Non-parabolicity parameter (Flow-profile asymmetry)
N_A	Avogadro constant
k_B	Boltzmann constant
T_h	Hot wall temperature [°C]
T_c	Cold wall temperature [°C]
T	Absolute temperature [K]
ΔT	Temperature gradient [K]
τ	Stop flow time (relaxation)
κ	Thermal conductivity
index c	… at the cold wall temperature
α_V, γ	Volumetric thermal expansion coefficient
δ *or* $\delta_{D,P,H}$	Hildebrandt or (partial) Hansen Solubility parameter(s) [$MPa^{0.5}$]
T_g	Glass transition temperature
c	Analyte mass concentration
J	Net flux
a_x	Polynomial coefficients
θ_b	Bond angle
l_b	Bond length
l_K	Kuhn length
χ	Flory-Huggins interact. parameter
index H	Enthalpic …
index S	Entropic …
C_∞	Characteristic ratio

List of Publications and Contributions

First Author Publications

1. **Non-Parabolicity correction for fifty-nine solvents and a retention study for strongly distorted flow-profiles in thermal field-flow fractionation**
   M. Geisler, A. Lederer, *Journal of Chromatography A*, **2020**, 1621 ,461082.
   doi: 10.1016/j.chroma.2020.461082 (referred as publication 8.1).

2. **The Role of Solubility in Thermal Field Flow Fractionation – A Revisited Theoretical Approach for Tuning the Separation of Chain-Walking Polymerized Polyethylene**
   M. Geisler, L. Plüschke, J. Merna, A. Lederer, *Analytical chemistry* **2020**, 92, 21, 14822-14829. doi: 10.1021/acs.analchem.0c03686 (referred as publication 8.2).

3. **Topology Analysis of Chain Walking Polymerized Polyethylene: An Alternative Approach for the Branching Characterization by Thermal FFF**
   M. Geisler, W. C. Smith, L. Plüschke, R. Mundil, J. Merna, S. K. R. Williams, A. Lederer, *Macromolecules* **2019**, 52, 22, 8662-8671. doi: 10.1021/acs.macromol.9b01410
   (referred as publication 8.4).

4. **Impact of Electron Beam Irradiation on Thermoplastic Polyurethanes Unraveled by Thermal Field-Flow Fractionation**
   M. Geisler, T. Subhra Pal, K. Arnhold, M. Malanin, M. T. Müller, B. Voit, J. Pionteck, A. Lederer, *Polymer Degradation and Stability* **2021**, 183, 109423.
   doi: 10.1016/j.polymdegradstab.2020.109423 (referred as publication 8.5).

Co-Author Publications

1. **Thermal field-flow fractionation for characterization of architecture in hyper-branched aromatic-aliphatic polyesters with controlled branching**
   W. C. Smith, M. Geisler, A. Lederer, S. K. R. Williams, *Analytical chemistry* **2019**, 91, 19, 12344-12351. doi: 10.1021/acs.analchem.9b02664. (referred as publication 8.3)
   The co-author performed and evaluated major parts of the experiments and edited the manuscript.

2. **Polyolefins Formed by Chain Walking Catalysis—A Matter of Branching Density Only?**
   R. Dockhorn, L. Plüschke, M. Geisler, J. Zessin, P. Lindner, R. Mundil, J. Merna, J.-U. Sommer, A. Lederer, *Journal of the American Chemical Society* **2019**, 141, 39, 15586−15596. doi: 10.1021/jacs.9b06785.
   The co-author contributed in performing and evaluation a part of the SEC experiments.

Conference proceedings

1. **Branching Characterization of Polymers by ThFFF in Various Solvents**
   M. Geisler, L. Plüschke, J. Merna, A. Lederer, FFF2020, Vienna, Austria, 23 – 27 February 2020, *Oral presentation.*

2. **Non-parabolicity correction for moderately and strongly distorted flow-profiles in Thermal FFF**
   M Geisler, A Lederer, FFF2020, Vienna (Austria), *Poster presentation.*

3. **Topology Analysis of Chain Walking Polymerized Polyethylene by Thermal Field-flow fractionation**
   M. Geisler, W. C. Smith, L. Plüschke, R. Mundil, J. Merna, S K. R. Williams, A. Lederer, FFF2020, Vienna, Austria, 23 – 27 February 2020, *Poster presentation.*

4. **Topology Analysis of Novel Short Chain Branched Polyethylene - A New Approach for the Branching Characterization by Thermal FFF**
   M. Geisler, W. C. Smith, L. Plüschke, R. Mundil, J. Merna, S K. R. Williams, A. Lederer, SCM-9, Amsterdam (The Netherlands), 30 January – 1 February 2019, *Poster presentation.*

5. **Short chain branched polyethylene with various topologies - evaluation of separation and detection approaches for conformational analysis**
   M. Geisler, W. C. Smith, L. Plüschke, R. Mundil, J. Merna, S K. R. Williams, A. Lederer, FFF2018, Columbia, SC (USA), 14 – 17 May 2018, *Oral presentation.*

6. **Thermal field-flow fractionation for characterization of architecture in dendritic aromatic-aliphatic polyesters with controlled branching**
   W. C. Smith, M. Geisler, A. Lederer, S. K. R. Williams, FFF2018, Columbia, SC (USA), 14 – 17 May 2018, *Oral presentation.*

1. Introduction

Within the family of macromolecules, polymers are a highly abundant class of material of either natural or synthetic basis.[1] Polymers are used by humans since about a thousand years[2] despite the fact that the exploration of their nature was initiated in comparably recent history. The term polymer originates from the Greek words “polys” (many) and “meros” (part) and describes a molecule consisting of repeating smaller building blocks called monomers. It was coined by Berzelius 1833, but its modern meaning was established far later in the 1920s, when Hermann Staudinger revised the definition of a macromolecule and set the base of polymer science as a new research area.[3] Many discoveries have been made since then in polymer science covering synthesis, properties, and structural understanding. Today synthetic polymers are the most abundant material for industry and consumer products such as packaging material,[4] adhesives,[5] optics,[6,7] coatings,[8] therapeutic drugs and -delivery,[9,10] and textiles[11] with an ever-growing variety and production scale representing in total a multibillion-dollar business.[12] Since the application possibilities of polymers are virtually endless, its market sector remains steadily expanding[13] with the trend from mass product to specific high-tech applications.[14]

Several strategies were discovered to adjust polymer material properties, such as blending of different polymers,[15] formulation of polymer composites with fillers[16] or fibers,[17] changing of the polymer architecture on the molecular level in terms of branching,[18] and crosslinking,[19,20] or copolymerization of different building blocks.[14,21] Continuously, polymer’s property enhancement establishes new fields of research in material and polymer science. Polymers are complex materials having more or less broad distributions in molar mass (chain length), chemical composition, microstructure (e.g. tacticity) as well as molecular architecture or topology.[22,23] For a homopolymer consisting only of one monomer type next to the molar mass already the dispersity may have major influence on bulk material properties such as crystallinity or toughness. For instance, very broad dispersity can lead to deviating crystallization behavior or phase separations in polymers of the same chemical identity, if the processing conditions are not suitable. This can be seen for instance in mixtures of n-alkanes with highly varying chain length.[24,25] Changing polymer architecture from linear to gradually or hyperbranched topology, further properties such as glass transition temperature (T_g), viscosity, solubility as well as mechanical and viscoelastic properties are altered. Tailoring of polymer properties on the basis of molecular topology is discussed comprehensively in section 2.1. With regard to multicomponent polymers like copolymers material property changes

are possible by varying sequence of different monomers. Copolymers can be in principle composed in random, alternating or block-wise order of their co-monomers. Depending on this order, properties of copolymers with the same overall composition can be tremendously different. A well-established example for a copolymer material family are polyurethanes and will be discussed in detail in section 5.4. Furthermore, the combination of architectural and chemical heterogeneity makes polymers today the most versatile type of material.

With the apparently endless variety of macromolecular structures and their heterogeneities, the ability to characterize these materials becomes necessary and hence, the demand of sophisticated analysis methods arises. Common batch techniques are applied targeting the chemical identity (NMR, IR, atomic spectroscopy) or molar mass and size (mass spectroscopy, solution viscometry, light scattering).[26] However, all these methods yield only average characteristics and are incapable of quantifying less abundant subpopulations when it comes to macromolecules with broader dispersity. Therefore, a separation and subsequent analysis distribution of subpopulations is essential for drawing a comprehensive conclusion on the polymer's intrinsic or bulk properties as well as performance.[27] A number of important methods based on different mechanisms were developed to separate polymers in solution. Well-established separation approaches are interaction based methods like size exclusion chromatography (SEC), liquid adsorption chromatography (LAC)[23,28] and liquid chromatography at critical conditions (LCCC)[28,29] or flow-based methods like hydrodynamic chromatography (HDC)[30] and the diverse family of field-flow fractionation (FFF).[31]

In this portfolio, SEC has become the most established and hence, the workhorse separation method in polymer analysis.[28,32] All column-based liquid chromatography (LC) types are carried out in columns packed with porous beads as stationary phase through which a liquid flow as mobile phase is forced carrying the polymer analyte to be separated.[33] In contrast to LAC, where the separation is based only on enthalpic interactions between solute and stationary phase, in SEC those are intentionally avoided or suppressed[34] and the separation is solely based on entropic interactions. Analytes are separated according to their hydrodynamic volume by their ability to diffuse into differently large pores of the packing material. The dimensions of a polymer coil in solution are sketched in Fig. 1.1 When the separation modes of SEC and LAC are precisely balanced, the separation happens in LCCC mode. LCCC is typically used for separation according to end-groups or functionalities of the polymer independent on molar mass.[28]

Upon calibration with polymer standards of comparable solution properties to those of the analyte, SEC represents a facile determination method for molar masses and distributions.

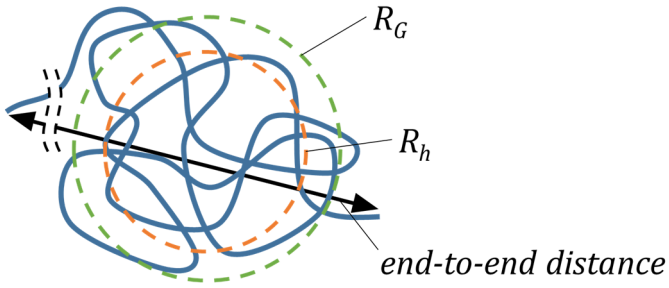

Figure 1.1 Dimensions of a linear random polymer coil with the hydrodynamic radius R_h, the gyration radius R_G and the statistical end-to-end-distance (typically much larger than R_G and R_h).

The characteristic molar mass moments are the number (M_n), weight (M_w) and centrifugal average (M_z), as defined in Eqs. (1.1) to (1.3) in dependence to the measured concentration c_i. The molar mass dispersity $Đ$ is given in Eq. (1.4).

$$M_n = \frac{\sum c_i}{\sum {c_i}/{M_i}} \tag{1.1}$$

$$M_w = \frac{\sum c_i M_i}{\sum c_i} \tag{1.2}$$

$$M_z = \frac{\sum c_i {M_i}^2}{\sum c_i M_i} \tag{1.3}$$

$$Đ = M_w {M_n}^{-1} \tag{1.4}$$

However, for complex macromolecular architectures or chemically heterogeneous polymers comparable polymer standards are not available. Consequently, not the same correlation between elution volume and molar mass exists and on the basis of calibration with established polymer standards the determination of molar masses becomes considerably erroneous.[28,32] The challenges arising in separation and characterization of complex polymer systems by classical methods is discussed in detail in section 1.1.

An alternative is provided by the family of FFF techniques that has attracted significant attention for the fractionation and characterization of complex macromolecules, colloids, aggregates or associates and particles.[35] Here, the limitations of column-based separations are avoided by the absence of a column packing material and – depending on the method – a choice of different separation-controlling parameters.[31] The key benefits of FFF are explained in section 1.1 and the fundamentals of FFF are discussed in section 2.3. FFF methods are nor-

mally named after the separation providing the driving separation force field applied externally perpendicular to the flow direction. One member of the FFF family is thermal field flow fractionation (ThFFF) where the separation force is provided by a temperature drop.[31,36] Improving the understanding of the separation mechanism, tuning the retention and interpreting the ThFFF retention behavior of polymers to understand polymer structure is the main focus of this thesis.

1.1. Analytical Methods and Challenges in Polymer Characterization

1.1.1. Single-Detection Size-Exclusion Chromatography

Undoubtedly, SEC has reached a quasi-monopole in macromolecular analysis[37] and its remarkable value will continue for this class of materials,[38] because it does not require extensive sample preparation or complicated data evaluation. However, for calibration-based molar mass determination accurate molar masses are only found, if standard procedures are employable and both the repeat unit chemistry and the architecture of the calibration standards are similar and in the same size range.[39] Molar masses from SEC calibration have to be considered only as standard equivalent molar masses M_{eq} and are only comparable within the frame of reference. However, often this is overlooked and M_{eq} are reported as true molar masses.[40] Relating those molar mass to sizes obtained through e.g. dynamic light scattering or microscopy can lead to significant bias or even complete misinterpretation up to physically unrealistic results, if the polymer standards do not resemble the retention behavior of the analyte.[39] This and further issues become problematic in particular for the analysis of copolymers by SEC due to an additional distribution in chemical composition besides the molar mass distribution. Already in correct separation mode SEC tends to an overestimation of molar mass dispersities caused by inner column band broadening.[33] Different chemical composition affects on one hand the hydrodynamic volume of the polymer in solution and on the other hand the optical contrast in respect to the solvent (refractive index increment) or the absorbance of ultraviolet or visible light (UV-VIS), which are measured by concentration-sensitive differential refractive index (dRI) or UV-VIS detectors, respectively. Hence, a correct analysis of absolute molar masses for complex polymers or copolymers by SEC with concentration detection is nearly impossible.[28]

1.1.2. SEC coupled to Viscometry Detection

To tackle issues in SEC regarding chemical differences SEC hyphenated to further detectors is used. The first step towards absolute molar mass and size characterization is the combination of online viscometry with concentration detection, which enables a quasi-absolute molar mass determination on the basis of a universal calibration. For a universal calibration the product of the intrinsic viscosity (the specific viscosity of a polymer solution extrapolated to infinite dilution) and the molar mass is fitted versus the retention volume. For a broad range of polymer architectures and chemical compositions an accurate measurement of molar masses and sizes was empirically confirmed.[41] However, for very compact particles, such as hyperbranched polymers a universal calibration is not valid anymore and may lead to erroneous results.[42] The universal law relies on Einstein's viscosity relation, discovered in the beginning of the 20th century (Eq. (1.5))[43]

$$\eta = \eta_0 \, (1 + 2.5 \, \phi) \tag{1.5}$$

with the volume fraction of the suspended analyte, and the Kuhn-Mark-Houwink-Sakurada (KMHS) equation (Eq. (1.6))

$$[\eta] = K_\alpha \, M^\alpha \tag{1.6}$$

where K_α and α are empirical parameters. The exponent α can be determined by fitting the intrinsic viscosity versus the molar mass in a double logarithmic plot and provides information about the shape or conformation of the polymer in solution and can range from 0 for ultra-compact objects over 0.5 for collapsed polymer coils and 0.7 for random coils in a thermodynamically good solvent up to 2 indicating a rigid rod-like shape.[44]

From the molar mass and the intrinsic viscosity, a hydrodynamic size is accessible. This relation is also based on Einstein's viscosity relation (Eq. (1.5)) and displays a size or volume of a sphere, which would have the same intrinsic viscosity. This hydrodynamic radius can be expressed as so-called viscosity radius, as defined in Eq. (1.7) with the Avogadro constant N_A.

$$R_{[\eta]} = \left(\frac{3 \, [\eta] \, M}{10 \, \pi \, N_A} \right)^{1/3} \tag{1.7}$$

1.1.3. Light Scattering

1.1.3.1. Multi-Angle Static Light Scattering

Another approach allowing a true, absolute molar mass measurement is the combination of multi angle light scattering (MALS) with concentration detection (typically dRI). The light scattering of polymers is mainly used in the Rayleigh regime of light scattering and is applicable for object sizes between ≈ 1 nm to 2 µm diameter.[45,46] The dependency of the scattered light on molar mass and radius is described by the reduced Rayleigh ratio (scattered light intensity of the polymer solution over the intensity of the solvent in the same detector environment) as defined for dilute solutions in Eq. (1.8)

$$R_\theta = M_w\, c\, (1 + cos^2\theta)\, \frac{2\pi\, {n_0}^2}{{\lambda_L}^4\, N_A} \left(\frac{dn}{dc}\right)^2 \tag{1.8}$$

with the analyte concentration c, the scattering angle θ, the solvent refractive index n_0, the laser wavelength λ_L and the refractive index increment $dn\, dc^{-1}$.[47] The principle of MALS is illustrated in Fig. 1.2.

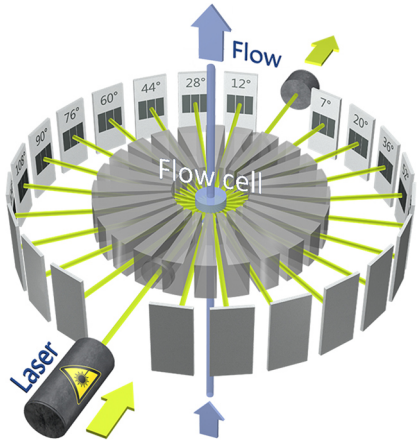

Figure 1.2 Detector design of MALS.[48] Courtesy © Postnova Analytics GmbH

In MALS detection the intensity of scattered (laser) light of the polymer solution in a quartz flow-cell is measured simultaneously for up to 21 angles. The intensity of scattered light is proportional to the concentration and the molar mass. Furthermore, a scattering anisotropy, for instance in scattering intensity dependence on the scattering angle is seen once the polymer is larger than 1/20 of the wavelength of the laser, i.e. R_G > 12 nm for 600 nm-laser.

As stated in Eq. (1.6), a molar mass determination by MALS always required a concentration information, either set by defined concentration in a series of differently diluted solutions in batch experiments or by combination of MALS with a concentration detector in online

mode, coupled to a separation method. The data evaluation of scattered light intensity in dependence on angle and concentration is typically done by a Zimm plot (batch measurements, multi-angle and multiple concentrations) or a Debye plot (online measurements, multiple angles only, for dilute solutions of one concentration)[49] in various formalisms such as Debye,[50] Zimm[47] and Berry.[51] Other plot and fit formalisms such as the Guinier plot or the shape-biased fits for sphere, random coil or rod-like objects are to be named for the sake of completeness. A typical evaluation of static light scattering data by Zimm plot and Zimm formalism is shown in Fig. 1.3. In this data evaluation method, the light scattering data are transformed and plotted in such a way, that the data can be fitted linearly according to equal concentration and equal scattering angle. The concentration and angle dependent fits are extrapolated to data points, where c $\rightarrow$ 0 and $\theta \rightarrow$ 0, respectively.

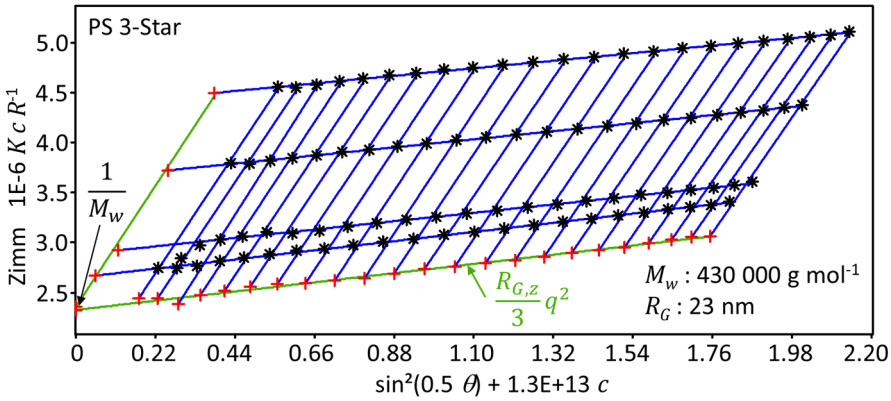

Figure 1.3 Determination of the weight average molar mass Mw and z-average of R_G from batch light scattering data by Zimm formalism using the Zimm fit method, exemplarily shown for a three-arm star polystyrene in tetrahydrofuran in four concentrations (own experiment, measured with a Fica 50 light scattering device, modernized by SLS-Systemtechnik, G. Baur, Germany).

These data points are fitted in the same way than the measured data point and the ordinate intercept of both fits become the reciprocal of the weight average molar mass. Furthermore, for analytes upon a minimum size the slope of the fit yielding the angle series at zero concentration contains the information about the z-average of the gyration radius $R_{G,z}$.

Molar mass and radii data from online MALS detection after separation can be used in the same way as stated for the KMHS analysis (Eq. (1.6) by double logarithmic plot and analogue fitting to obtain information about conformation or shape of polymers, respectively. The relation of M to R_G is defined as follows in Eq. (1.9)

$$R_G = K_{RMS}\, M^{\nu_R} \tag{1.9}$$

where K_R is again an empirical constant and ν_R is the scaling exponent. Typical values for ν_R range from 0.33 for dense (non-draining) spheres over 0.5 for collapsed random coil conformations and 0.58 for a random coil in a thermodynamically good solvent up to 1 for rigid-rod-like shapes.[52]

1.1.3.2. Dynamic Light Scattering

MALS is also used in combination with dynamic light scattering (DLS). Whereas in MALS the intensity of (monochromatic) scattered light is averaged over a certain time constant, in DLS instead the fluctuations of the scattered light are analyzed in a high time resolution.[53] These fluctuations are caused by interference effects of scattered light due to Brownian motion of the analyte's internal scattering centers. The fluctuating scattered light is detected and processed by a hardware autocorrelator according to intensity per increasing time intervals $I(t)$. In online detections after separation DLS is often applied only at one specific angle. For the data evaluation the autocorrelated data are fitted by different models which link the decay and trend of the data to the translational diffusion coefficient. Commonly used models are the cumulant fit (average D for the analyte)[54,55] and the regularization fit (various subpopulations resolvable).[56] The simplest case in DLS are monodisperse analytes, where the intensity g_T autocorrelated in dependence to the decay time τ_D is fitted by Eq. (1.10)[54]

$$g_T(\tau) = 1 + \beta \exp\left[-2\,D\,\frac{4\pi n_0}{\lambda}\,sin\left(\frac{\theta}{2}\right)\tau_D\right] \tag{1.10}$$

with β as a coherence factor. The data treatment in DLS is illustrated in Fig. 1.4.

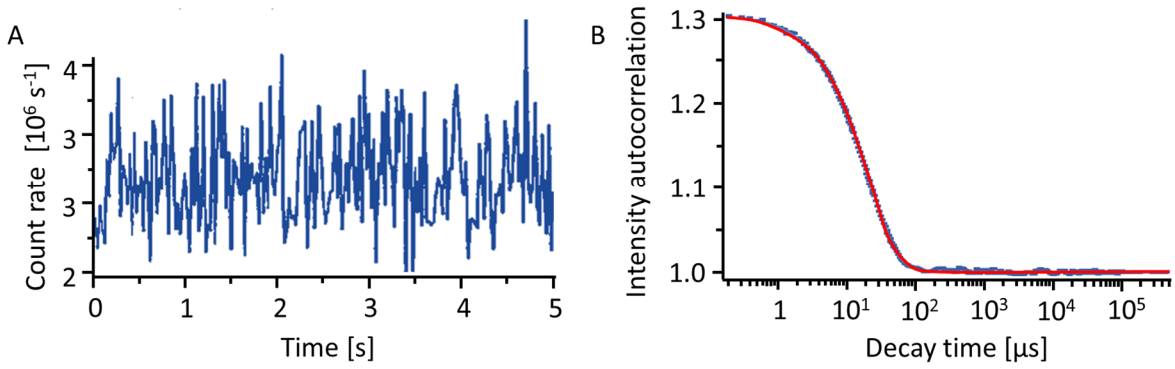

Figure 1.4 Intensity fluctuations of scattered light measured in DLS in **A** as recorded signal and in **B** after autocorrelation of the data (blue) and fitted (red). Plot in A adapted and reprinted with permission from Ref. [57] Copyright © 2016 Elsevier B.V., Plot in B adapted under Creative Commons Attribution License CC BY 4.0 from Ref. [58].

The translational diffusion coefficient D can then be translated into a size information such as the hydrodynamic radius R_h via the well-known Stokes-Einstein Equation (Eq. (1.11))[59]

$$D = \frac{k_B\, T}{6\pi\, \eta_0\, R_h} \tag{1.11}$$

where k_B denotes the Boltzmann constant, T is the absolute temperature in K and η_0 is the dynamic viscosity of the solvent.

1.1.4. Multidetector Liquid Chromatography

Multidetector approaches with up to 5 detection systems combining MALS, DLS, viscometry, UV-VIS and/or dRI have now become state-of–the-art for comprehensive polymer characterization at ambient temperature[28,60] as well as at elevated temperature (e.g. necessary for polyolefin analysis).[61] Other detection methods also used in hyphenation with SEC are offline-FTIR,[62,63] online-NMR[64–66] and mass spectrometry to elucidate compositional differences.[67–69] Yet, in terms of molar mass and size in some cases MALS is not applicable due to a too low optical contrast[70,71] or fluorescence.[72,73] In those cases, calibration-based SEC or a coupling to mass spectrometry remain better options. Multidetector approaches in liquid chromatography provide a plethora of information and can overcome the drawbacks for instance from calibrated SEC, because it is not directly dependent on the retention behavior. However, if the separation is strongly affected also multidetector approaches fail in yielding conclusive information due to co-elution of different subpopulations. Co-elution can occur on one hand by anchoring effects of side branches in branched or hyperbranched polymer structures in the pores of the stationary phase of SEC.[74] On the other hand, adsorption effects of side- or end groups in a fraction can lead to co-elution, too. This is a main challenge in the analysis of structurally complex homo- and copolymers[75] and biomacromolecules.[76] Problems of co-elution have to be therefore addressed by multidimensional chromatography such as coupling of SEC with LAC or LCCC with multidetector approaches[23,28] to unravel structural and compositional complexity.[77]

However, despite the fact that LC corresponding detection becomes costly with increasing dimensionality, the separation range is limited to a maximum molar mass and size due to upper and lower size exclusion limits of SEC and limits in reversible ad- and desorption in LAC, respectively. On one hand, upon a certain size or molar mass (beyond 10^7 g mol^{-1}) exceeding significantly the separation range of SEC[78] an inversion and hence, co-elution with

smaller fractions of different topology may occur due to an inversion of the separation mechanism from size exclusion to hydrodynamic chromatography mode.[30,79] On the other hand, fractions in the ultra-high molar mass (UHMW) region tend to degrade in SEC separations due to high flow induced shear forces.[80] Shear degradation becomes an increasing challenge in high-efficiency systems[38] exceeding 800 bar system pressure in order to maintain high flow rates for fast analysis.[81] Therefore, for separations of UHMW polymers or particles alternative separation methods are required.

1.1.5. Alternative Flow-Based Separation

An alternative separation method prior to any detection is given by FFF.[82] The basic concept of FFF was invented by J. C. Giddings in the mid-1960s,[83] who also developed the majority of the nowadays established FFF sub techniques. FFF can overcome some of the mentioned limitations of column-based LC. The principle of FFF is explained in detail in section 2.3. First of all, due to the absence of a column packing material adsorption to the stationary phase and shear degradation is tremendously reduced.[31,84] Analytes over a wide size range from 1 nm to several µm (normal retention mode) can be separated with a high overall resolution.[85] The mild flow conditions allow the analysis of fragile analytes such as colloidal-sized dendronized glycopolymers,[86] liposomes[87,88], polymersomes,[89,90] protein assemblies,[91,92] supramolecular assemblies[93] like biohybrid structures[94,95] or whole cells.[96–98] However, within the separation range, LC-based separations maintain a higher peak resolution. A superior advantage of FFF over LC are programmable separations, which enable 3-5 times higher peak capacity than in SEC and analysis time, which can be kept in reasonable limits.[38] Depending on the FFF subtype, polymers can be fractionated simultaneously according to physicochemical properties like size, composition, effective mass, electrostatic or magnetic response.[31,99]

However, a disadvantage of FFF is peak broadening under constant separation conditions, which needs to be addressed by optimization with tuned separation conditions. Another remaining challenge in macromolecular characterization can be found in the versatility of FFF, which increases the opportunities and thus, the effort for optimization. This fact hinders the exploitation of FFF's for an easy routine analysis.[31,100,101] Meanwhile, for specific applications FFF has made a great step towards routine analytics, like for quality control of pigment nanoparticles[102], nanomedicines[103] or adhesive dispersions.[104] So far, only ThFFF has already become a full established routine characterization method for styrene-butadiene copolymer blends[105–107] and polyisoprene rubber[108] for industrial products. Though, high performance

polymers like polyolefins will remain challenging regardless of the separation method because all flow-related parts must be kept at high temperature to avoid precipitation and clogging of capillaries. Nevertheless, contributions to method optimizations as necessary for FFF can be done by investigation of polymer model systems of the same chemistry and in dependence to molecular topology, but readily soluble at ambient temperature. This is substantial part of this thesis and section 5.3.2 is mainly devoted to the application of ThFFF for polyolefin characterization.

1.2. Objectives and Scope of the Thesis

Early ThFFF retention studies by Giddings and Schimpf with polystyrene (PS) of linear and star-architecture showed a certain dependency of the retention according to architecture, but related it to the temperature dependence of the translational diffusion only. They concluded that for the specific polymer solvent combination the thermal diffusion as underlying driving force for the retention is neither dependent on molar mass nor on branching.[109] However, the generality of these findings remained unclear. Thermal diffusion or thermophoresis is a phenomenon of concentration imbalance in a solution being under influence of a temperature difference and is explained in detail in section 2.4. This concentration imbalance is always partially counterbalanced by translational diffusion. The ratio between thermal diffusion coefficient D_T and translational diffusion coefficient D is called Soret coefficient S_T (Eq. (1.12)).

$$S_T = \frac{D_T}{D} \tag{1.12}$$

In extension to Giddings, Runyon found in later studies also a correlation to the number of chain ends in regular star-shaped non-aromatic homo- and copolymers.[110] In that context, copolymers of methyl and butyl acrylate may be also considered as crossover of copolymer and variation of side chains[110] and is in agreement with earlier studies where ThFFF was confirmed to provide a separation towards copolymer composition.[35,111,112]

The independence of D_T to polymer architecture was accounted to be generic in the previously mentioned first studies without specific investigation. However, for a potential use of the Soret coefficient as parameter to describe or provide information about branching, it is necessary to elucidate the influence of polymer branching on thermal diffusion. Greyling and coworkers found a certain dependence of D_T to the polymer architecture for PS and indicated

furthermore that solvent selectivity plays a significant role.[113] Although the reported D_T values were calculated without corrections for nonuniformities of the flow, they confirm qualitatively the observed trend.

Objective 1

In fact, the lack of sufficiently precise flow and temperature nonuniformity corrections made accurate D_T calculations elaborate and challenging. Therefore, Belgaied and coworkers developed in the mid-1990s a polynomial approach to provide an applicable correction, based on coefficients reported for the most common solvents used in ThFFF at that time.[114] Hence, the **first objective in this thesis is to improve and extend applicable solutions as a basis for accurate calculation of D_T from measured ThFFF retention data**. This matter is discussed in detail in section 5.1.

Objective 2

The influence of branching on thermophoretic behavior was the basis for investigation of the solvent selectivity and the influence of the thermodynamic quality of the solvent on thermophoresis. Generally, to find a suitable solvent for ThFFF separations where the thermal diffusion is sufficiently high to provide a good retention and separation has so far remained an elaborate trial and error process. Although thermophoresis is practically used for separation or accumulation applications (e.g thermophoretic trapping),[115,116] the phenomenon itself is not fully understood and hence, a complete fundamental theory does not exist yet. Numerous approximate approaches were developed to predict thermal diffusion based on physicochemical parameters such as thermal conductivity, activation energy of the viscous flow or the Hamaker constant.[117] The latest D_T prediction model was proposed by Mes, Kok and Tjissen[118] (heinafter named Mes D_T model) is confirmed to provide better predictions than compared to theories reported earlier. However, the accuracy of predictions by the Mes D_T model strongly relies on the approximated segment size information from the polymer and to some extend on the solubility model. D_T predictions reported so far used either monomer sizes extrapolated from polymer dimensions [119] or approximated this information by the bulk density and molar mass of the monomer and are in consequence still of lower accuracy. Therefore, the **second objective in this thesis was to improve the prediction capability of the Mes D_T model** with input data on a more comprehensive basis for the segment size information and by using a three-dimensional solubility model (Hansen solubility).[120,121] The improved prediction power of the Mes D_T model as basis then allows to **probe segment size information from experimentally measured D_T based on the improved model.** Segment

size in polymer chains indicates the local stiffness (persistence) within polymer structures in dependence to branching and solvent interaction. The prediction power improvement of the Mes D_T model and its reverse application to retrace polymer stiffness in solution is discussed in section 5.2.

Objective 3

With the improved calculation methods to derive accurate thermophoretic data from ThFFF experiments as a basis (discussed in objective 1), the **third objective of this thesis was to thoroughly investigate the correlation between the molecular topology and thermal diffusion** without influences of chemical composition. Therefore, a library of silylated polyesters with tailored degree of branching was investigated in solvents with varied selectivity. This study is discussed in section 5.3.1. Confirmation of the relation between polymer topology and thermal diffusion was aimed based on another polymer model system having the lowest possible intrinsic chemical heterogeneity. For this study (section 5.3.2) a library of polyethylene (PE) samples with varying polymer topology was studied. The type of PE used here was synthesized by late-transition metal chain walking catalysis. The general structure of this PE is characterized equally high short chain branching but varying long chain branching (*LCB*). The definition of *LCB* is described in section 2.2. Due to its unique structure this chain walking PE (cwPE) is entirely amorphous and readily soluble at room temperature in a broad variety of solvents untypical for regular PE. Therefore, it represents a suitable model system to be studied without the challenges of high temperature characterization. Based on the fin-dings in this study, **a branching characterization method for polyethylene is developed on the basis of Soret coefficients measured by ThFFF.** Thus, the concept of the Soret contraction, proposed by Runyon a decade ago, has to be validated.[122] The results of this investigation are discussed in section 5.2.

Objective 4

Another unresolved problem is the accurate treatment of thermophoretic data from ThFFF experiments in programmed field conditions. From sedimentation FFF[123,124] and flow-FFF[125,126] effects of delays in retention induced by fast-changing field force due to the so called secondary relaxation phenomena[127] are known. However, for ThFFF the increment changes in field strength were accounted to be relatively slow and delays in retention, thus, to be negligible without experimental validation.[128] Therefore, the **fourth objective in this thesis is to investigate and implement a secondary relaxation correction in ThFFF data treatment of field-programmed experiments** and to apply it in thermophoretic anal-

ysis as a novel, complementary investigation of electron-beam irradiated thermoplastic polyurethane (TPU) material. In this investigation multidetector ThFFF is applied to separate degraded, branched and crosslinked fractions and to enable a characterization of molar masses and distributions not sufficiently understood by SEC. Since about 40 years, the irradiation influence on polyurethane materials is an intensively investigated and still ongoing research interest in that comprehensive absolute molar mass characterization has not been part, yet. Hence, findings and proposed mechanisms of irradiation impact on TPU remained partially inconclusive. Details on this study are given in section 5.4. A graphical summary of all objectives outlined above and their contribution to the outcome of this thesis is given in Fig. 1.5.

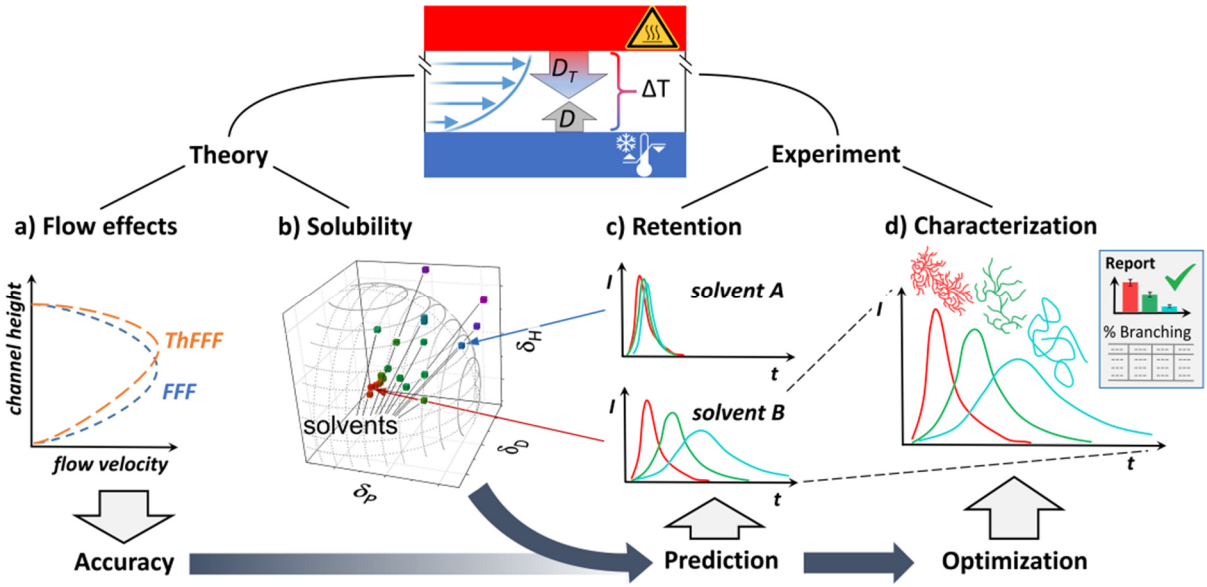

Figure 1.5 Graphical abstract of the objectives accomplished in this dissertation dealing with the overall topic of ThFFF as separation and characterization method, which comprise advances from the theory improving the accuracy of ThFFF derived physicochemical parameters in objective 1 (**a**), the predictability of themophoretical and ThFFF retention behavior in objective 2 (**b**) and the application of optimized ThFFF as comprehensive characterization method complementary to established techniques in objectives 3 and 4. Sketches in b and c reprinted under Creative Commons Attribution License CC BY-NC-ND 4.0 from publication 8.2; ThFFF scheme and sketch in d reprinted with permission from publication 8.4. Copyright © 2019 American Chemical Society.

2. Scientific Background

2.1. Tailoring of Polymer Properties

Physical properties of polymer material such as mechanical strength, viscoelasticity, melting point or melt viscosity are in first instance defined by the morphology, which is a result of interaction between the molecules.[129] For industrial applications mechanically tough polymers are established since almost a century, which originates in high crystallinity as found for regular linear homopolymers without bulky pendant groups like high density polyethylene (HDPE). However, a demand to specifically adapt polymer properties arises either the processing conditions need to be optimized or the application profile in the final product is not sufficiently matched. A purely physical property adaptation is achieved by blending of different polymers, which could lead to possess undesired phase separations. Adaptations from the chemical point of view are achieved by changing the monomer composition or the polymer topology, as well as by combination of both options as shown in Fig. 2.1, A and B.

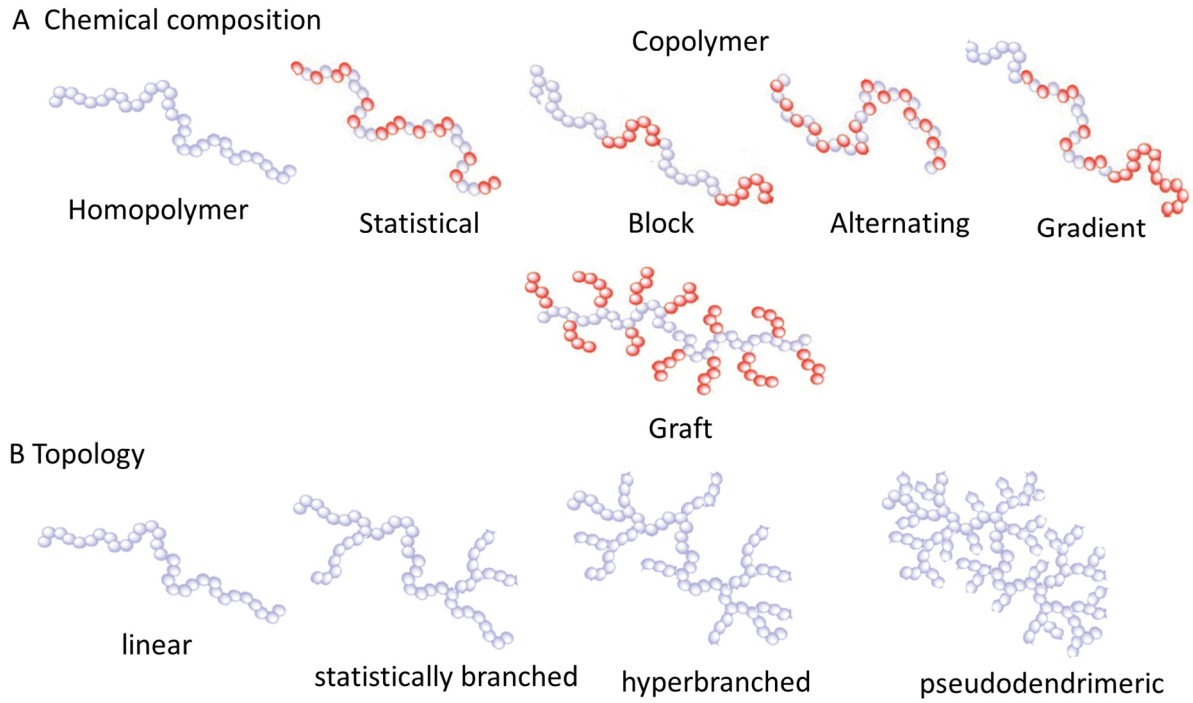

Figure 2.1 Overview of polymer heterogeneity in chemical composition (A), molecular topology (B) and the crossover between both represented by grafted bottle-brush copolymers. Adapted with permission from Ref. [130] Copyright © 2009, Springer Nature.

By using copolymerization to induce property changes, the tendency for crystallization is intrinsically reduced, since they contain more than one repeating unit in the chain. In random

or statistical arrangements of repeating units the resulting copolymer becomes entirely amorphous.[131] A subsequent change to more ordered structures leads on one hand to gradient copolymers, which enables to combine the properties of two or more materials in a continuous manner without uncontrolled phase separation.[132] In addition, there are also perfectly alternating copolymers providing desired properties like for microporous materials as used in gas permeation membranes[133] or as backbone for hierarchically composed multifunctional polymers in for instance supramolecular or colloids-based applications.[86,134,135]

A widely applied copolymer type are block or segmented copolymers, which possess sequences of repeating units, or domains with different length defining their properties. Often block copolymers are composed of one crystallizing block in which the degree of crystallinity is related to the size of the crystallizable domain. A typical example for such material are thermoplastic polyurethanes (TPU). As illustrated in Fig. 2.2, depending on the composition of the crystallizing hard segments and the amorphous remaining soft segments TPU materials can be tailored from brittle, highly crystalline to soft, flexible, thoroughly amorphous morphology in that a particular property can be "build in" without significant reduction of other targeted properties.[136]

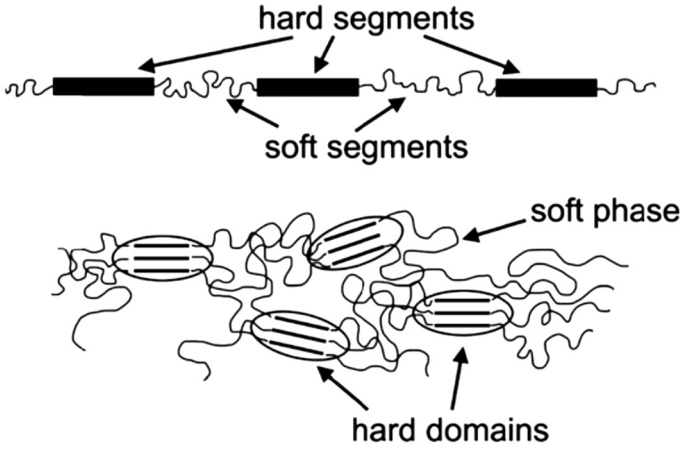

Figure 2.2 The representative morphology of segmented copolymers with crystalizing (hard) segments and amorphous (soft) segments, e.g. typical for thermoplastic polyurethane. Reprinted with permission from Ref. [137] Copyright © 2015 Society of Chemical Industry.

Meanwhile, changing the topology or in relation to that, the microstructure without significant change in chemical composition is a complementary way to adjust desired polymer properties. Brittle, highly crystalline materials composed of linear homopolymer can be plasticized without the need of low molecular and possibly hazard plasticizers. An introduction of side branches onto the main chain, by postmodification (synthesis or irradiation) or by synthesis of initially branched polymers imped crystallization of the polymer. A further increase of branching leads to a lower T_g, lower melting point, lower melt viscosity, higher ductility, but

also non-preferentially to a lower stability of the bulk material. Prominent examples showing the versatility in tailoring polymer properties by topology design with varying branch length and keeping about the same chemical identity are polyethylene (PE) and polypropylene (PP). Innovations in catalysis and/or with combination of different α-olefin co-monomers a broad portfolio of properties can be realized ranging from liquid, waxy to solid tough material of varying ductility even at high molar mass, which promoted PE and PP to materials with the largest polymer market sector in the world.[138]

The third dimension in tailoring polymer properties next to chemical composition and topology is dispersity regarding all polymer characteristics discussed above such as dispersity in molar mass, branching (lengths, branch or graft density) or copolymer composition (blockiness, block length). Broad molar mass dispersity may enhance processability of polymers by improving the rheology in molten state at high shear rate. In contrast, a narrow molar mass dispersity improve materials stability, impact resistance, toughness at low temperatures, and higher resistance to environmental stress cracking but processing of these materials at high molar masses would be more challenging.[139,140] Thus, dispersity in composition can be used to adjust phase segregation, crystallinity and in consequence also the melting behavior of copolymer materials.[139] Overall, superimposed to the effects of composition, topology and molar mass, a variation in dispersity enlarges the tailoring possibilities of polymer properties. However, it also increases tremendously the complexity of the system making an understanding of the structure-property relation challenging. Therefore, comprehensive characterization with suitable separation and detection methods is required to retrace effects of changed synthesis and processing parameters in material development.

2.2. Quantification of Branching in Polymers

In order to quantify branching in polymers in a comparable manner several generic definitions have been introduced. The oldest concept to express branching was introduced by Zimm[141] 1949, who defined a radius contraction factor g (Eq. (2.1))

$$g = \left(\frac{{R_{g,bra}}^2}{{R_{g,lin}}^2} \right)_M \tag{2.1}$$

with R_g of the branched polymer and R_g, of a linear analogue with equal molar mass.

Following the same principle, Zimm and Kilb introduced later a related quantity named viscosity contraction factor g' (Eq. (2.2))[142]

$$g' = g^{\varepsilon} = \left(\frac{[\eta]_{bra}}{[\eta]_{lin}} \right)_M \tag{2.2}$$

which is defined by the corresponding intrinsic viscosities of the branched and the linear polymer, respectively. g' and g are directly convertible to each other with the help of a drainage parameter ε, which ranges from 0.5 to 1.5.

Based on the contraction concept, several further application-based measures were defined for comparison of branching. For a monodisperse polymer (also valid for online data from separation- and multidetector- based characterization) having trifunctional type of branching the contraction model was defined by Zimm as given in Eq. (2.3) using the quantity of the number of branching points per molecule B.

$$g_3 = \left[\left(1 + \frac{B}{7} \right)^{0.5} + \frac{4B}{9\pi} \right]^{-0.5} \tag{2.3}$$

Other contraction models like for tetrafunctional and comb-like structures as well as for polymers of broader dispersity are reported in the literature. A well-established parameter in polyolefin characterization is the number of long chain branches LCB as defined in Eq. (2.4)

$$LCB = 1000 \cdot B \cdot \frac{M_{RU}}{M} \tag{2.4}$$

where M is the polymer molar mass and M_{RU} is the molar mass of the repeat unit. As alternative quantity for branching in a macromolecule, the theoretical molar mass of a long chain branch segment M_{Seg} has been defined (Eq. (2.5)).

$$M_{Seg} = \frac{M}{(B+2)+(B-1)} = \frac{M}{2B+1} \tag{2.5}$$

Here, the term (B − 1) refers to a linear segment in between two branching points, whereas the term (B + 2) represents the segments attached to the same branching point on both sites.

To practically calculate values for *LCB* or M_{Seg} from experimental data, *B* needs to be extracted from *g*. For a trifunctional monodisperse polymer this quantity is directly accessible by solving Eq. (2.4) to *B*, as illustrated in Eq. (2.6)

$$B = \frac{504\,\pi + 81\,\pi^2\,g^2 - 567\,\pi\,g\,\sqrt{\frac{16\,\pi}{63} + \frac{\pi^2\,g^2}{49} + \frac{64\,g^2}{81}}}{224\,g^2} \tag{2.6}$$

A simple expression of the degree of branching (DB) particularly for polycondensation AB_2-polymers not related to measured size information was defined by Frechét[143] and Kim[144] (independently), stated in Eq. (2.7)

$$DB_{Frechét} = \frac{T + D}{T + L + D} \tag{2.7}$$

where *D*, *T* and *L* are the molar quantities of dendritic, terminal or linear incorporated units in the hyperbranched polymer, e. g. measured by NMR upon signal integration. The definition of the different units in an AB_2-polymer as well as the difference between a hyperbranched polymer and a dendrimer is explained in Fig. 2.3.

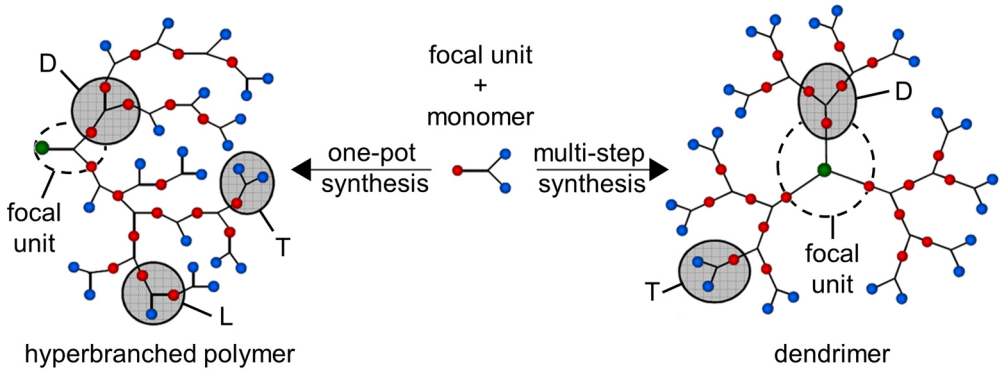

Figure 2.3 Generalized structure of a hyperbranched polymer in comparison to a dendrimer. Adapted and reprinted from Ref. [145].

This definition for DB was later refined by Frey and coworkers (Eq. (2.8)), because they recognized that Frechét's definition is only suitable for polymers of high molar mass and overestimates the DB in the molar mass range typically yielded in polyester synthesis.

$$DB_{Frey} = \frac{2\,D}{2\,D + L} \tag{2.8}$$

Frey's refined definition of DB allows the comparison of polymers to a great extend regardless of the molar mass.

2.3. Field-Flow Fractionation

Field-flow fractionation (FFF) is a generic concept of a flow-based separation technique exhibiting a distinct advantage in separating macromolecules and colloids by its essential one-phase nature.[83] It was conceived in the mid-1960s by J. C. Giddings in order to overcome challenges in column based chromatographic separations due to slow equilibration, precarious distribution between two phases or high shear forces, particularly in SEC.[83,146] The basic principle of FFF relies on the combination of a non-uniform axial flow and different transverse concentration profiles induced by an applied separation force field. A general description of the separation is illustrated in Fig. 2.4.

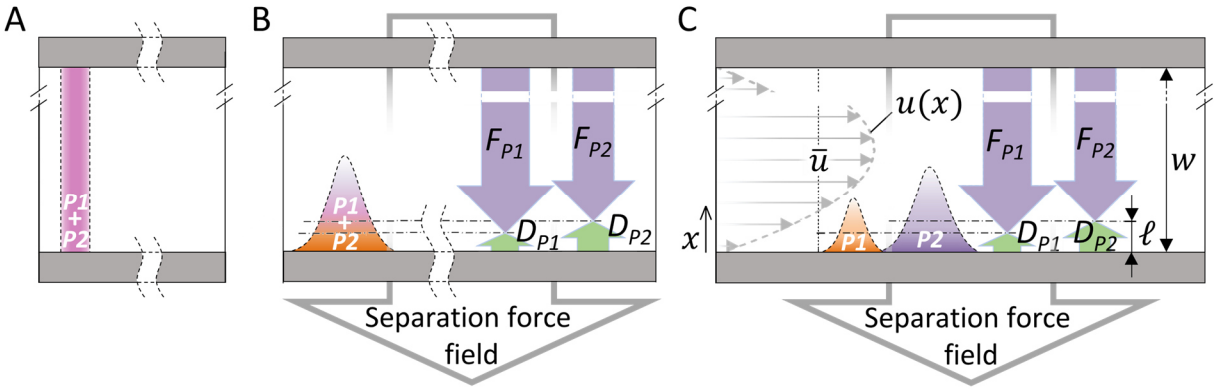

Figure 2.4 Generalized separation principle of FFF: A) after injection, B) during focus or stop flow (relaxation) and C) elution and subsequent separation.

A hypothetical mixture of analytes with different sizes P1 and P2 is injected at the beginning of the separation channel of the height w. Under influence of an externally applied separation force field perpendicular to the channel orientation a field-driven mass transport (F_{P1}, F_{P2}) is induced, which is counteracted by a diffusion-driven mass transport (D_{P1}, D_{P2}) leading to a relaxation of the analytes to different mean layer thicknesses ℓ from the accumulation wall during focus or stop flow, respectively. Once carrier fluid is pumped through the channel during elution, the analytes are subsequently separated by migration through the channel in different flow velocities $u(x)$ of the laminar parabolic flow having the mean flow velocity $\bar{u}$.

The criteria to achieve a relevant separation are sufficient strength and selectivity of an effective field and its feasibility in technical realization. Each type of field induces a different response of analytes to be separated based on a specific physicochemical property. Up to now a vast number of different fields have been successfully verified to enable separation. Hence, FFF has become a relatively large family of separation methods. Typical fields include centrifugal force, gravitational force, temperature gradient, a cross-flow stream, electrical potential,

standing acoustic wave or magnetic fields. The resulting FFF subtypes are in general named after the applied field. Examples are symmetric (generally FℓFFF) or asymmetric cross-flow (AF4), thermal (ThFFF), electrical (EℓFFF), sedimentation (SdFFF), gravitational (GrFFF), dielectrophoretic (DEP-FFF), acoustic (AcFFF) and magnetic (MgFFF) field-flow fractionation.[99] FFF can be in principle set up in any flow or field geometry. Most commonly a thin ribbon-like parallel plate configuration with typical dimensions of 20 - 80 cm in length, 1 - 2 cm in breadth and 70 - 500 µm in thickness is used. From all invented FFF subtypes so far, AF4, ThFFF, and SdFFF were commercialized and established as separation and analysis methods. An example for an established FFF subtype with a different geometry is hollow fiber flow FFF (HF5), which is a derivation of AF4. The technical realization of established FFF techniques is illustrated in Fig. 2.5.

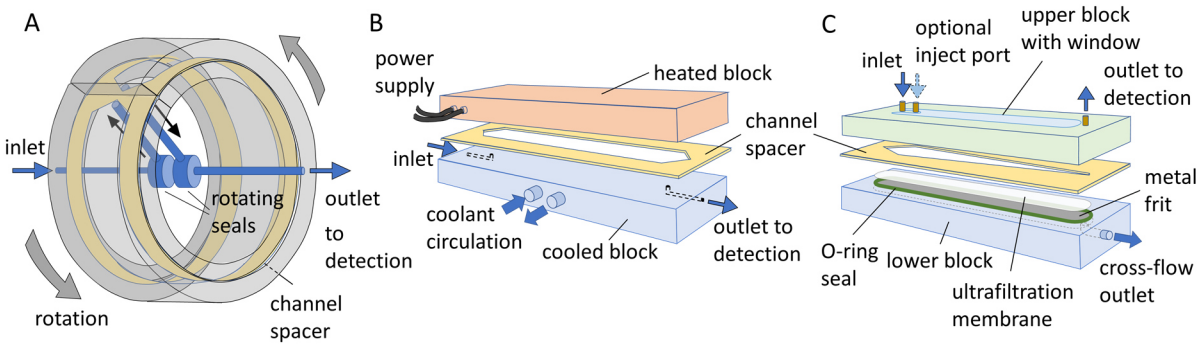

Figure 2.5 Technical realization of different separation force fields in the most commonly used FFF subtypes: SdFFF with a centrifugal force field (A), ThFFF with a thermal field by temperature drop (B) and AF4 with a hydrodynamic field realized with a cross-flow superimposed to the channel flow (C).

Often pressurized channels up to 20 atm are used to enable a good flow control in FℓFFF or to extend the application to prevent boiling of the carrier liquid in case the heated block in ThFFF reaches a higher temperature than the boiling point of the carrier liquid. Channels with high pressure stability furthermore allow separations with supercritical carrier fluids.[147]

2.3.1 Derivation of the Basic FFF Separation Description

2.3.1.1 Concentration Distribution

Under influence of a force field, analytes are forced to migrate towards one channel wall. Their accumulation is counteracted by the normal diffusion process due to concentration imbalance and Brownian motion. The resulting analyte flux as expressed Eq. (2.9) is defined as sum of a convective and a diffusive term.

$$J_x = u_F\, c(x) - D\frac{\partial c}{\partial x} \tag{2.9}$$

The convective term is described by the analyte's migration velocity u_F towards the accumulation wall forced by the field and the local analyte concentration $c(x)$ at distance x from the accumulation wall, whereas the diffusive part is represented by the first Fick law including D. At steady state (fully established relaxation) an equilibration between field-induced convective flux and the diffusive flux is reached and overall flux becomes 0 for all x. The local concentration is then described by an exponentially decaying profile as given in Eq. (2.10)

$$c(x) = c_0\, e^{-\frac{x\, u_F}{D}} = c_0\, e^{-\frac{x}{\ell}} \tag{2.10}$$

Thus, the local concentration depends on the mean layer thickness ℓ, which represents the height of the analyte cloud's center of gravity with one half of the analyte's total mass above and the other half below ℓ. In dimensionless form, the mean layer thickness is expressed by the FFF parameter λ as the ratio of ℓ to the channel height w.[146]

$$\lambda = \ell\, w^{-1} \tag{2.11}$$

λ, depends on the underlying physicochemical property causing a reaction to the field and controlling retention in FFF.[148] Properties defining λ are discussed in section 2.3.2.

2.3.1.2 Velocity Distribution

FFF relies on a laminar carrier flow perpendicular to the force field orientation. The laminar flow of an isothermal, incompressible fluid between two stationary infinite parallel plates is expressed by the reduced form of the Navier–Stokes equation (Eq. (2.12))[149]

$$\eta \frac{d^2}{dx^2} = \frac{dp}{dz} \tag{2.12}$$

with the viscosity η, and the system pressure p. Double integration of Eq. (2.12) by neglecting side wall friction yields the formula of the classical Poiseuille flow[150] describing the laminar parabolic flow-profile with constant η (Eq. (2.13)) and a pressure drop Δp due to friction.

$$u(^x/_w) = \frac{w^2 \Delta p}{2\, \eta\, L} \left[\left(\frac{x}{w}\right) - \left(\frac{x}{w}\right)^2\right] \tag{2.13}$$

The first fraction term in Eq. (2.13) mean flow velocity $\bar{u}$ is and the local deviation forming the flow velocity profile is represented by the parabolic term in brackets.

The dimensionless form of the flow-profile is given in Eq. (2.14).

$$\frac{u}{\bar{u}_p} = 6\left[\left(\frac{x}{w}\right) - \left(\frac{x}{w}\right)^2\right] \tag{2.14}$$

Typical FFF channels are designed in flat ribbon-like appearance with rectangular cross section of large aspect ratio, which allows neglecting side wall effects. However, for other geometries friction at the side walls are to be respected by implementation of a correction term.[151,152] The velocity profile then becomes

$$\frac{u_x}{\bar{u}}\left(\frac{x}{w};\frac{y}{b}\right) = 6\left[\left(\frac{x}{w}\right) - \left(\frac{x}{w}\right)^2\right] \cdot \left[1 - \frac{cosh\left(\sqrt{3}b\right) - 1}{cosh\left(\sqrt{3}y\right) - 1}\right] \tag{2.15}$$

where $u_x/\bar{u}$ also dependent on the breath b of the channel. The influence of side wall effects on flow velocity profiles is illustrated in Fig. 2.6 for small and large aspect ratios.

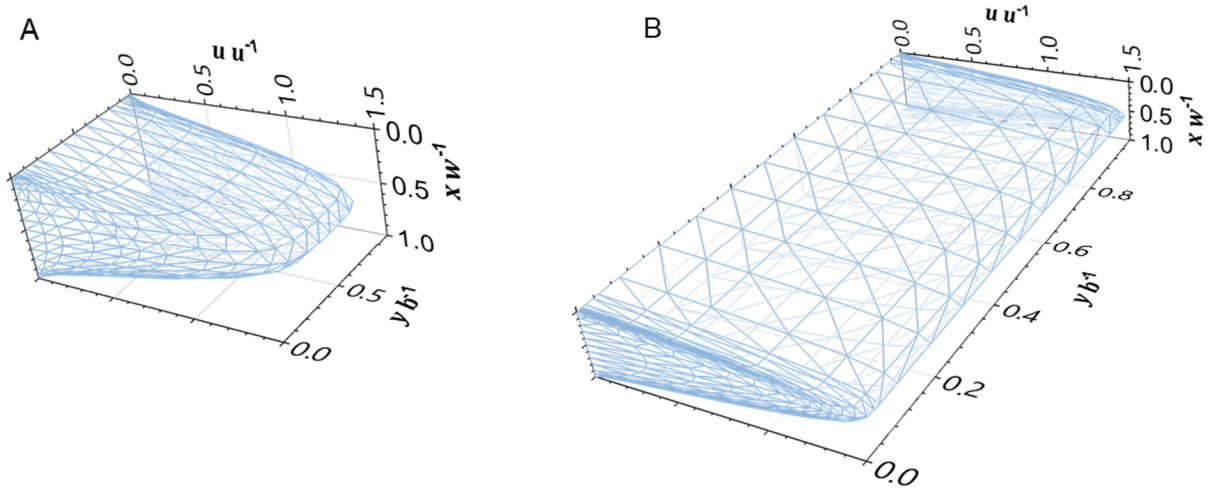

Figure 2.6 Dimensionless velocity flow-profiles calculated by Eq. (2.15) for a rectangular channel of low aspect ratio $w\,b^{-1}$ = 5 (A) and high aspect ratio $w\,b^{-1}$ = 80 (B) as normally used in flat channel-based FFF. The scale in $y\,b^{-1}$ and $x\,w^{-1}$ was adapted for better view.

2.3.1.3 Normal Mode Retention in FFF

To describe retention of analytes in chromatography the retention ratio has been defined as the ratio of the zone migration velocity of an unretained solute (equal to $\bar{u}$) to the zone migration of a retained analyte u_{zone}, which is equal to the ratio of the void time t_0 to the retention time t_R. The zone migration can be described by combination of the concentration and flow velocity distribution. The retention ratio can be then expressed as given in Eq. (2.16)

$$R = \frac{u_{zone}}{\bar{u}} = \frac{t_0}{t_R} = \frac{\int_0^w [c(x)\,u(x)]dx}{\int_0^w c(x)dx \int_0^w u(x)dx} \tag{2.16}$$

Subsequent partial integration, substitution and rearrangement yields the analytic solution for the well-known FFF retention equation,[153,154] given in Eq. (2.17) for analytes retained in an isoviscous laminar parabolic flow.

$$R_p = 6\,\lambda\left[\frac{(1-2\lambda)exp(\lambda^{-1})+1+2\lambda}{exp(\lambda^{-1})-1}\right] = 6\,\lambda\left(coth\left(\frac{1}{2\,\lambda}\right)-2\,\lambda\right) \tag{2.17}$$

For well retained analytes having values of λ lower than 0.06 (equal to R ≤ 0.4) the retention ratio can be approximated within a deviation of 5 % by the asymptotic form in Eq. (2.18)

$$R_\infty = 6\,\lambda \tag{2.18}$$

Next to the normal mode retention describable by Eqs. (2.16) and (2.17), other retention modes occur once analytes (typically nano- and microparticles) have a hydrodynamic size where the analytes center of gravity does not reach the vicinity of the accumulation wall anymore. Particles of a significantly large size are oriented in zones of higher flow velocity than smaller analytes. Furthermore, they have an increasing flow resistance and are accelerated by the flow. Both effects lead to a so-called steric inversion of the retention order, which is used for particles separated in steric-FFF mode e.g. by SdFFF. Additionally, large objects occupying zones of differing flow velocities experience lift forces induced by the carrier flow. In gravitational FFF this effect is purposefully used to realize separations in the so called hyperlayer-FFF mode.[155] Both retention modes typically occur far beyond the size range of polymers in solution and are therefore not further discussed here.

2.3.2. Physicochemical Parameters guiding Retention in FFF

The retention of analytes in FFF is directly related to their characteristics defining the response to the separation force field, which are comprised in the dimensionless FFF parameter λ. This parameter can be therefore generally defined as a ratio of the diffusion driven mass transport to the field-induced mass transport as described in Eq. (2.19)

$$\lambda = \frac{\ell}{w} = \frac{k_B\,T}{F\,w} = \frac{D}{u_F\,w} \tag{2.19}$$

in that F stands for a local field induced force on the analyte. In this context the parameter λ gets a true physical meaning. The theoretical tractability of FFF furthermore allow the measurement of physicochemical parameters directly related to experimentally measured retention data, which are either intrinsic physicochemical properties or associated to the interaction of the analyte with the carrier liquid.[148]

For AF4 λ is defined by the hydrodynamic size like the radius, as shown in Eq. (2.20)

$$\lambda = \frac{k\,T\,V_0}{6\,\pi\,V_{CF} r_H} \tag{2.20}$$

where the field is described by the ratio of the channel flow rate V_0 to the flow rate of the cross-flow V_{CF}. Meanwhile in SdFFF, analytes are separated according to their effective mass m_{eff} where the field is provided by the centrifugal acceleration G.

$$\lambda = \frac{k\,T\,V_0}{m_{eff}\,G\,w} \tag{2.21}$$

Instead, separations by EℓFFF are associated with the analyte's environment, which is described by the electrophoretic mobility μ in an applied electric field E.

$$\lambda = \frac{D}{\mu\,E\,w} \tag{2.22}$$

In this thesis the potential of ThFFF to achieve the objectives if this work was investigated. Therefore, ThFFF and the underlying phenomenon behind that are described more in depth in the following sections.

To obtain physicochemical parameters from FFF retention experiments below the high retention limit t Eq. (2.18) is to be applied, Eq. (2.17) can only be solved numerically by root-finding algorithms since an analytical solution is mathematically impossible. Additionally, for fairly accurate calculations of λ from given R the simple approximation given in Eq. (2.23) has been suggested by Schimpf, Schure and Schettler.[156]

$$\lambda \approx \frac{R}{6\,(1-R)^{1/3}} \tag{2.23}$$

2.3.3. Thermal Field-Flow fractionation (ThFFF)

In ThFFF retention is caused by thermophoresis. This phenomenon was discovered by Ludwig[157] and further understood by Soret[158] in the mid-1800's, who observed a concentration difference in solutions induced by a temperature gradient ΔT being the difference between the hot wall temperature T_h and the cold wall temperature T_c. This concentration shift is a result of a thermophoretic mass transport described by the thermal diffusion coefficient D_T, which is counteracted by the normal diffusion. The ratio of both is defined as the Soret coefficient S_T (see Eq. (1.12)). Hence, for ThFFF λ is related to S_T and the field force ΔT (Eq. (2.24))

$$\lambda = \frac{1}{(S_T + \gamma)\Delta T} \cong \frac{D}{D_T\,\Delta T} \tag{2.24}$$

The thermal expansion coefficient γ of the carrier liquid is for the vast majority of solvents of a small quantity (< 10^{-3} K^{-1}) and is therefore often neglected.[159]

However, the measurement of S_T from ThFFF retention data is a more complex matter, because unlike for all other FFF subtypes, the viscosity of the carrier fluid is not constant over the channel height. This needs to be respected in the derivation of the flow velocity profile. In this case the Navier-Stokes equation for an incompressible fluid with non-constant viscosity is defined as given in Eq. (2.25)

$$\frac{d}{dx}\left(\eta(T)\frac{du}{dx}\right) = \eta(T)\frac{d^2u}{dx^2} + \frac{d\eta(T)}{dx}\cdot\frac{du}{dx} \tag{2.25}$$

The integrated form of the dimensionless flow-profile then becomes as shown in Eq. (2.26),

$$\frac{u}{\bar{u}_{exact}} = \frac{\int_0^{x/w}\frac{x/w}{\eta(T)}d(x/w) - \frac{\int_0^1\frac{x/w}{\eta(T)}d(x/w)}{\int_0^1\frac{d(x/w)}{\eta(T)}}\int_0^{x/w}\frac{d(x/w)}{\eta(T)}}{\int_0^1\left(\int_0^{x/w}\frac{x/w}{\eta(T)}d(x/w) - \frac{\int_0^1\frac{x/w}{\eta(T)}d(x/w)}{\int_0^1\frac{d(x/w)}{\eta(T)}}\int_0^{x/w}\frac{d(x/w)}{\eta(T)}\right)d(x/w)} \tag{2.26}$$

The calculation of $\eta(T)$ in this expression requires the knowledge of the exact temperature profile $T(x\,w^{-1})$ across the channel. This has also to a minor extend a non-linearity between T_h and T_c due to a slight temperature dependency of the thermal conductivity κ of the carrier fluid. The exact formulation of $T(x\,w^{-1})$ is described in Eq. (2.27)

$$T(x/w) = T_c + \frac{\kappa_c}{d\kappa/dT}\cdot\left(\sqrt{1 + \frac{\kappa_c}{2\ d\kappa/dT}\Delta T\left(1 + \frac{d\kappa}{dT}\cdot\frac{\Delta T}{2\ \kappa_c}\right)x/w} - 1\right) \tag{2.27}$$

The cumbersome expression of the exact flow-profile in Eq. (2.26) solved with $T(x/w)$ in Eq. (2.26) requires elaborate numerical calculations and does not allow for an analytical solution for the retention equation after Eq. (2.13) as derived for an isoviscous flow in Eq. (2.17). Therefore, a simplified approximation was derived by extension of Eq. (2.14) to a cubic formula and the introduction of a parameter ν describing the distortion of the flow-profile, as given in Eq. (2.28).

$$\frac{u}{\bar{u}_{3rd}} \cong 6\left[(1+\nu)\left(\frac{x}{w}\right) - (1+3\,\nu)\left(\frac{x}{w}\right)^2 + 2\,\nu\left(\frac{x}{w}\right)^3\right] \tag{2.28}$$

The influence of the flow-profile distortion in the frame of basic separation in ThFFF is illustrated in Fig. 2.7 with its exact and approximate solution as well as comparison to an

isoviscous flow. The combination of Eqs. (2.10) and (2.28) yields the established analytical solution of the ThFFF retention equation (2.29) for a cubic velocity flow-profile.

$$R_{3rd} = 6\,\lambda\,\nu\left(1 - R_p\right) + R_p = 6\,\lambda\left[\nu + (1 - 6\,\lambda\,\nu)\left(coth\left(\frac{1}{2\,\lambda}\right) - 2\,\lambda\right)\right] \tag{2.29}$$

The parameter ν (hereinafter coined non-parabolicity parameter) can be derived by the initial slope ε of the exact flow-profile in the limit of $x\,w^{-1} \longrightarrow 0$, as shown in Eq. (2.30).[114]

$$\varepsilon(^{x}/_{w} \to 0) \triangleq \frac{1}{6}\left(\frac{d\left(\frac{u}{\bar{u}}(^{x}/_{w})\right)}{d(^{x}/_{w})}\right) - 1 = \nu \tag{2.30}$$

Other possibilities to approximate ν are described within section 5.1 of this thesis.

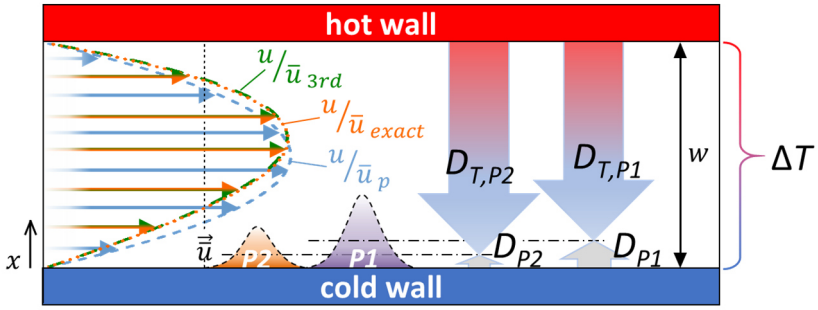

Figure 2.7 Principle of ThFFF during elution. The exact solution of the distorted flow-profile (orange) and for the corresponding cubic approximation (green) with ν = −0.3 (e.g. cyclohexane at ΔT = 75 K, T_c = 25 °C, pressurized) is illustrated in comparison to the isoviscous parabolic flow (blue). Adapted with permission from Ref. [160]. Copyright © 2019 American Chemical Society.

For very well retained samples the distortion of the flow-profile becomes of lower significance influence for the retention. In this case, Eq. (2.18) can be modified by the term of λ for ThFFF to fairly approximate thermophoretic properties based on ThFFF retention data.[36]

$$R_\infty = \frac{6\,D}{D_T\,\Delta T} = \frac{6}{S_T\,\Delta T} \tag{2.31}$$

Unlike for Eq. (2.18), approximations by Eq. (2.31) are only fairly reliable and recommended for lower ΔT and/or solvents exhibiting rather low flow-profile distortions, because the impact of ν in Eq. (2.28) remains of higher quantity than the approximation error in λ.

2.4. Approaches to Basic Theory and Prediction of Thermal Diffusion

Thermal diffusion or also coined as thermophoresis or Ludwig-Soret-effect describes the phenomenon of a directional movement of molecularly dissolved molecules as well as solid dispersed particles which are driven by a temperature gradient. Thermal diffusion is generally about two orders of magnitude lower than translational diffusion by Brownian motion and has been observed in gases,[161] liquids,[162] supercritical fluids[147,163] and even in solids.[164] Although it is often overlooked due to its small quantity, the understanding of this phenomenon is of essential importance. It was reported to have significant contribution in the polymerization of ribonucleic acids to ribosomes during the chemical evolution of life on earth, reinforced by a temperature gradient from submarine volcanic activity.[165]

In principle thermophoresis can be described with the irreversible thermodynamic theory by Onsager.[166] However, this theory provides only a formal framework for non-equilibrium phenomena, but it does not allow the calculations of distinct values D_T or S_T.[167] For gases the effect is quite well understood and can be sufficiently described with a kinetic theory by Chapman: in a temperature gradient gas molecules in the environment of a different molecule or particle, which continuously collide with it have a slightly higher kinetic energy on the hotter side than on the colder side. Consequently, the object experiences statistically a net momentum and moves towards the colder site.[168] The object then shows a so-called thermophobic behavior. Since a fundamental theory has not been found yet, thermal diffusion is described with the help of phenomenological and to some extend experimentally verified laws. A general description of the net flux under a temperature gradient $J_{T,x}$ can be defined in relation to Eq. (2.9) by introduction of a convective term (dependent on the temperature gradient) to Fick's diffusion law (Eq. (2.32))

$$J_{T,x} = D_T \frac{\partial T}{\partial x} - D \frac{\partial c}{\partial x} \tag{2.32}$$

However, this theory fails to thermophoresis in liquids and solids where for low molecular substances as well as for polymeric species up to a certain limit also movements towards the hotter side, i.e. thermophilic behavior have been observed.[169–172] Previous studies indicated, that in liquid systems thermophoresis is the resulting effect of multiple and potentially superimposed contributions such as electrostatic charge, interfacial effects and molecular interactions.[162] In that, the dependency of the molecular weight on D_T has been found to play a significant role only for low molar mass systems, which were found to be both either thermophilic or thermophobic.[173–175] Instead, non-charged macromolecules of molar mass far

bigger than the molar mass of the solvent molecules were found to be generally thermophobic with a constant D_T independent on the molar mass.[109,174] Hence, many theory approaches have been developed to describe the complex nature of thermophoresis in liquids, which are for instance linked to a difference in the heat of transport,[176,177] related to molar enthalpies[178,179] or use the activation energy of viscous flow.[180,181] With these theories notable correlations between predictions and experiment, measured by batch techniques such as thermogravitational column[161,182] or thermal diffusion forced Rayleigh scattering (TDFRS),[183] were found within their limited frame of reference. However, still in 2020 thermal diffusion discovered over 150 years ago is still full of surprises even in the limited frame of dilute macromolecular solutions and appears almost random in both magnitude and direction.[184]

Meanwhile several theories with focus on polymer thermal diffusion have been derived with contributions and assessments by Khazanovich,[185] Bender,[186] Schimpf and Giddings,[117] or Schimpf and Semenov[187,188] with varying success in D_T predictions. The latest D_T prediction model with so far the highest prediction power is the Mes D_T model, which was reported 2003 by Mes, Kok and Tjissen[118]. Their model describes D_T in dependence on the polymer-solvent interaction using the relationship presented in Eq. (2.33)

$$D_T = {\phi^2}_S \left(\frac{k_b T}{6\pi\, \eta_S(T)\, r_m}\right)\left(2\frac{\partial \chi}{\partial T} + T\frac{\partial^2 \chi}{\partial T^2}\right) \tag{2.33}$$

with the Boltzmann constant k_B, the solvent's dynamic viscosity $\eta_S(T)$, the volume fraction ϕ_S and the first and second partial derivative of the polymer solvent interaction parameter χ from the Flory–Huggins solution theory,[189,190] differentiated to T. Insights on χ (also coined as Floy-Huggins parameter) and its calculation e.g. with the help of solubility theories is explained in the following section. For dilute polymer solutions ϕ_S is normally set to a value of 1. r_m represents a radius of a local segment of the polymer chain in the size region of a monomer, which has been approximated so far by extrapolation of polymer scaling data down to monomer molar mass[118,186] or calculated from state equations for crystal of spheres.[188,191] This is in fact a weakness of the Mes D_T model, because the quantity of r_m has a large effect on the prediction result. However, since thermophoresis is practically used for ThFFF separations the interest and relevance in the accurate prediction of D_T has increased, which could avoid in future elaborate trial-and-error process to find conditions for high and selective retention in ThFFF. Furthermore, an improved D_T prediction model may allow a better understanding of possible trends in D_T linked to polymer properties, which is essential for a possible application of ThFFF as polymer characterization method.

2.5. Solubility Theories

The term "solution" generally describes a dynamic equilibrium state where the interaction between solvent molecules and solute becomes greater than the interactions between the material's molecules itself. In this case (spontaneous dissolution), the change in Gibbs free energy ΔG_{mix} as the difference of the enthalpy of mixing ΔH_{mix} and the corresponding entropy ΔS_{mix} times the temperature becomes negative, which is additionally dependent on the relative molar amounts of the components (molar ratio, x_i).

$$\Delta G_{mix} = \Delta H_{mix} - T\,\Delta S_{mix} = n\,R\,T\,(x_1 \ln x_1 + x_2 \ln x_2) \tag{2.34}$$

Solutions appear in all (classical) states of matter from mixing of gases to metal alloys. In this context, the term "solubility" describes quantitatively to which extend a solute interacts thermodynamically with a solvent. Understanding solubility or the influence of a solvent environment is of great importance e. g. for optimization of chemical syntheses,[192] industrial processes such as extractions[193] or crystallizations,[194] pharmaceutical aspects[195] or – within the scope of this thesis – for improvements in physicochemical analyses.

Similar to the demand of prediction methods for D_T stated in the previous section, since the early times of chemical industry there is a great interest to find possible solvents or better solvents, respectively, to avoid elaborate solvent testing, costly time and resource-consuming trial and error processes. A rather simple theory was introduced already in 1936 by Hildebrand, who defined a single solubility parameter δ on the basis of cohesive energy density, as shown in Eq. (2.35).[196]

$$\delta^2 = \frac{\Delta H_v - RT}{V_m} \tag{2.35}$$

with the heat of vaporization ΔH_v and the molar volume V_m. Values of δ are given in SI conform units of $MPa^{0.5}$. Values in older references given in $(cal\ cm^3)^{0.5}$ may be converted by multiplication with a factor of factor of 2.0455. Substances with similar solubility parameters are more alike to interact with each other resulting in solvation. Instead, solvents differing by more than about 2 $MPa^{0.5}$ (empirically found) are considered as nonsolvents.

However, Hildebrandt's single parameter approach has significantly limited prediction power and it clearly cannot capture the full complexity of real solubility including all possible solute–solvent interactions. Therefore, Charles Hansen refined Hildebrandt's theory to a three-dimensional model, where δ is a sum of three partial contributions as given in Eq. (2.36)

$$\delta^2 = {\delta_D}^2 + {\delta_P}^2 + {\delta_H}^2 \tag{2.36}$$

with dispersive interactions (δ_D) including London-dispersion and van-der-Waals forces, polar contributions (δ_P) from dipole-dipole or electrostatic interactions as well as π-π interactions in or by aromatic systems, and hydrogen-bonding contributions (δ_P) significant for polar-protic compounds.[120] δ_D, δ_P, δ_P are also coined as Hansen's solubility parameters (HSP). Furthermore, Hansen extended the meaning of the difference of δ between compounds from Hildebrand's theory in the sense of a sphere radius *Ra* (Eq. (2.37))

$$Ra^2 = (\Delta\delta_D)^2 + {}^1/_4\,(\Delta\delta_P(T))^2 + {}^1/_4\,(\Delta\delta_H(T))^2 \tag{2.37}$$

where the regarded compound marks the center of a sphere in a three-dimensional Cartesian coordinate system with its partial solubility parameters as $\delta_D \triangleq x$, $\delta_P \triangleq y$, $\delta_H \triangleq z$ coordinates and is probed to a compound to be dissolved in or mixed with. The fraction ${}^1/_4$ in Eq. (2.37) reflects the different impact quantity of the partial contributions on the HSP distance. At a certain maximum distance from the sphere center *Ro* the interactions of solute or solvent molecules become equal to the solute-solvent interactions. This distance marks the radius of the Hansen solubility sphere for the regarded compound and indicates the border between soluble (inside) and insoluble (outside).[121] An example for a modelled solubility survey with the Hansen's theory is illustrated in Fig. 2.8. The ratio $Ra\ Ro^{-1}$ is defined as the relative energy difference *RED* and may be used to express solvent quality on a scale even without the need of 3D modelling. HSP are nowadays widely available in the literature or for not reported substances accessible e.g., by calculations using group contribution models.[197,198]

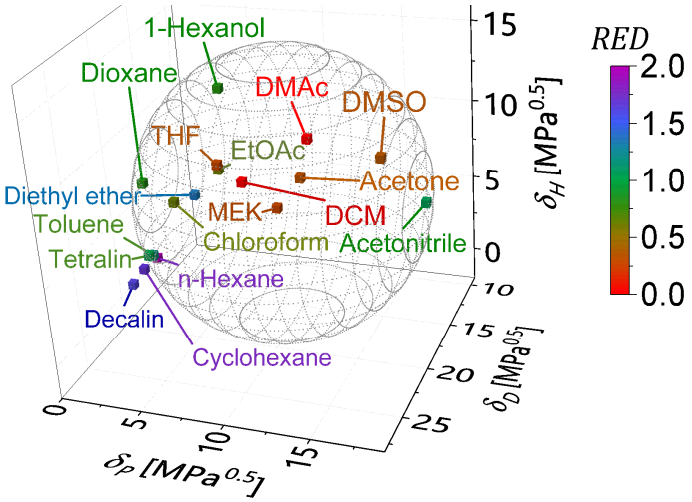

Figure 2.8 Hansen solubility sphere calculated for poly(methyl methacrylate) with HSP and the sphere radius reported in the literature.[121] The color scale indicates the relative energy distance (*RED*) of the solvent to the sphere center.

However, despite its multidimensional concept, the Hansen solubility theory (HST) exhibits limits in prediction power. One drawback is the determination of *Ro* (*RED* = 1), which needs to be approximated empirically by testing of poor and "border" solvents. Furthermore, it can only predict positive deviations from Raoult's law (linear approximation of the vapor pressure in binary mixtures). In fact, HST may accurately predict cosolvency effects where a substance becomes soluble in a mixture of two nonsolvents, but it fails in the description of the opposite effect when a substance becomes insoluble in a mixture of two solvents with competing interactions, named co-nonsolvency. Meanwhile, improved, but more complex solubility models have been reported more recently, like the MOSCED[199] model or regression-based models (QSAR, QSPR).[200,201] Other limitations have been addressed later by Hansen and coworkers and extend the validity range of the model.[121] They introduced a relation to yield HSP in dependency to pressure or temperature (Eqs. (2.38) to (2.40))

$$\frac{\delta_{D,ref.}}{\delta_D(T)} = \left(\frac{V_{ref.}}{V(T)}\right)^{-1.25} \tag{2.38}$$

$$\frac{\delta_{P,ref.}}{\delta_P(T)} = \left(\frac{V_{ref.}}{V(T)}\right)^{-0.5} \tag{2.39}$$

$$\frac{\delta_{H,ref.}}{\delta_H(T)} = exp\left[-0.00122\left(T_{ref.} - T\right) - ln\left(\frac{V_{ref.}}{V(T)}\right)^{0.5}\right] \tag{2.40}$$

with the ratio of the reference volume $V_{ref.}$, typically at the reference temperature $T_{ref.}$ to the volume at the regarded temperature $V(T)$. The ratio $V_{ref.}\ V(T)^{-1}$ can be either calculated temperature-dependent by volumetric thermal expansion coefficients or pressure-dependent by compressibility coefficients. With that, calculations including supercritical fluids have become possible.[202]

Close after Hildebrandt and around 25 years earlier than Hansen, Flory and Huggins developed independently a rather simple lattice model to describe the solubility of particular polymers on the basis of enthalpic and entropic contributions. They derived a relation on the basis of the Gibbs free energy (Eq. (2.34)), linked the solubility of a polymer to its volume fraction ϕ and introduced a polymer-solvent interaction parameter χ,[189,190] known as the Flory-Huggins parameter (Eq. (2.41).

$$\Delta G_{mix} = R\ T\ (n_1 \ln \phi_1 + n_2 \ln \phi_2 + n_1 \ln \phi_2\ \chi) \tag{2.41}$$

The parameter χ describes the sum of all solute-solvent interactions and is in the simple model defined as sum of an enthalpic part χ_H and an entropic contribution χ_S. χ_H can be approximated on the basis of the molar volume using the squared solubility distance either from Hildebrandt's theory or from HST (Eq. (2.42)).

$$\chi_H = \frac{V_m\,(Ra)^2}{RT} \tag{2.42}$$

Despite assumptions and certain oversimplifications, the Flory–Huggins solution theory and the parameter χ are still widely used for predictions and interpretations related to polymers.

3. State-of-the-Art

3.1. Polyesters with Tailored Degree of Branching

Among branched polymers hyperbranched polyesters represent a prominent progress in industrial polymer chemistry due to their industrially attractive properties like low solution or melt viscosity and a high number of terminal groups, which can be modified with functionalities for targeted applications. For this reason, they are well-established in commercial products like coatings, resins or in blends for polyurethane foams.[203] Initial key benefit of these polymers is the relatively facile production by "one pot" synthesis procedure leading in the first instance to statistically branched polyesters when unmodified AB_2-monomers are polymerized.[204,205] Further synthesis approaches allow to tune the properties of the originally statistically branched materials either by modification of the monomer's end groups with protective groups or my postmodification of the polyester's functional groups with additional monomers. A scheme of this synthetic tailoring approach using differently modified AB_2-monomers is outlined for silylated aromatic-aliphatic polyesters in Fig. 3.1.[206]

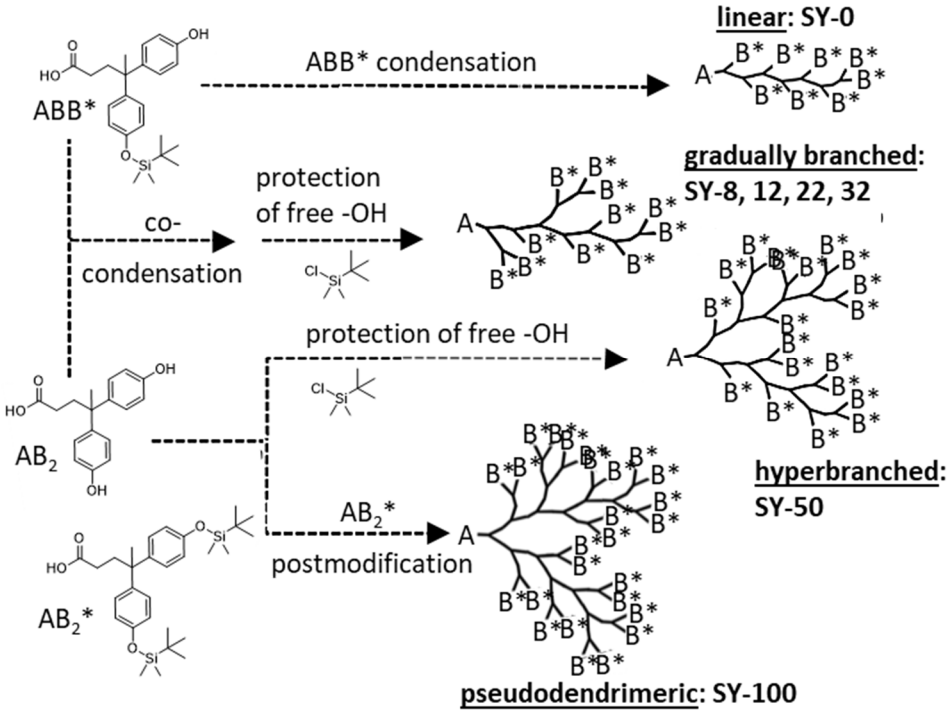

Figure 3.1 Summary of the synthetic strategy to tailor architectures of desired topology in between a degree of branching 0 – 50 %. The pseudodendrimer with DB = 100% is yield by postmodification of linear units in the hyperbranched polyester with DB = 50 % with double protected monomers. Adapted with permission from Ref. [206] Copyright © 2010 American Chemical Society.

This system has been used as a library of model polymers in the research conducted in this thesis by means of ThFFF (outlined in section 5.3.1). Therein, the pre- and postmodification allow for variation of the properties by extending the range of realizable topologies from linear polymers up to pseudodendrimeric structures. Pseudodendrimers have irregular structure, but similar branching density as regularly branched dendrimers without the need of elaborate and costly multi-step synthesis.[18,207] Depending on the generation the irregular structure of the so-called pseudodendrimers may lead potentially to an even higher local density of terminal units than in dendrimers.[208,209] Therefore and due to their facile synthesis stated above, they are also of great research interest for potential pharmaceutical applications such as drug-delivery[210] or for treatment of neurodegenerative diseases.[211–213]

Unlike the relatively facile synthesis of the polyesters introduced above, the characterization of hyperbranched polymers or pseudodendrimers, which often have additional functionalities on their terminal units, is more challenging and requires sophisticated separation and analysis approaches.[214] The polymer system given in Fig. 3.1 has been thoroughly investigated in the last decade by means of multidetector SEC,[206] interaction-LC,[215] 2D-LC,[216] small-angle neutron scattering[42,217] and thermal analysis.[218] With these investigations it could be also elucidated, that the universal law of the Flory-Fox-equation applied in SEC with universal calibration is not valid anymore for hyperbranched structures.[42] Thus, comprehensive characterization results are reported, which allow to use these polyesters as initial model system to develop new characterization methods, e.g., by means of ThFFF.

3.2. Characterization of Irradiated Thermoplastic Polyurethanes

Since their invention in the late 1930's,[219] thermoplastic polyurethanes (TPU) have become an established, versatile class of material with widely used properties, including modulable flexibility, mechanical strength, elasticity, good abrasion resistance, and transparency[220,221] and a broad application range from elastic foams over textile fibers, innovative rubber material[222] up to 3D additive manufacturing[223,224] or shape-memory materials.[225] TPU are segmented block copolymers (see section 2.1) consisting of a polydiisocyanate hard segment, often extended with a low molecular weight chain extender, and longer aliphatic soft segments. The typical structures of TPU (and of the materials used in this thesis) is illustrated in Fig. 3.2. Hard segments can possess aliphatic as well as of aromatic nature. Aromatic TPU may vary in their bulk properties from low to high crystallinity,[226] whereas aliphatic TPU is more likely an amorphous material.[227]

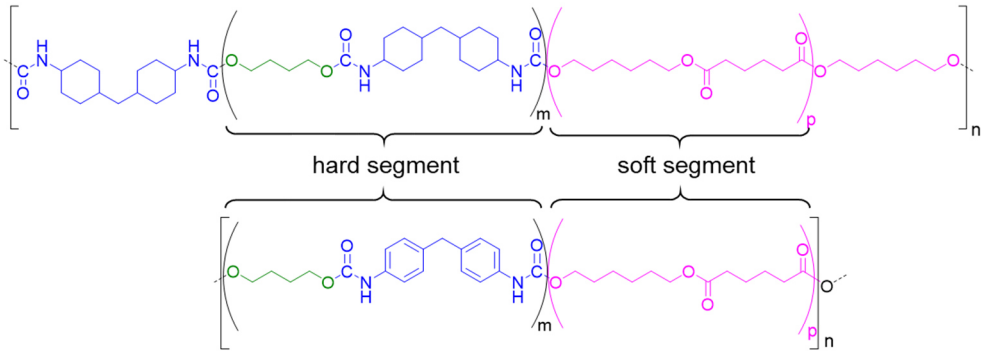

Figure 3.2 Structure of a TPU with aliphatic and aromatic diisocyanate (blue), 1,4-butane diol as chain extender (green) and a poly(n-butyl adipate) soft segment (magenta), precopolymerized with a short aliphatic diol.

To improve material properties by post synthetic modification to the final product, polymers can be reactivated by the formation of radicals induced using high energy gamma or electron beam irradiation. An example of electron beam irradiation in a production process is sketched in Fig. 3.3. High energy irradiation is established in industrial polymer processes like the fabrication of heat-resistant cable insulations[228] or high performance tires,[229] as well as in lower dose for sterilization of medical products.[230,231] The higher the energies involved in the interaction of polymer material with high-energy irradiation the greater the electron binding energy to an atomic nucleus.[232] Hence, irradiation results in complex and random superimposed processes in the material where reactivity of formed radicals combined with other bulk properties such as crystallinity leads to isomerization (branching), crosslinking or degradation by chain scission. Polymers are classified in generic types which are like polyethylene or polyacrylates prone to crosslinking or to polyisobutylene or polytetrafluoroethylene, which mainly undergo chain scission.[232]

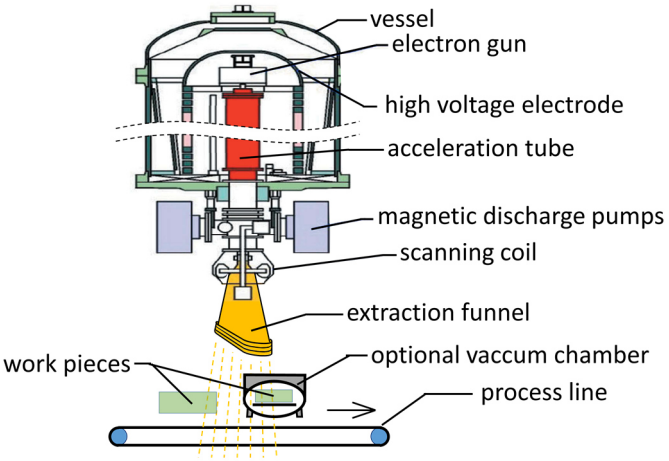

Figure 3.3 Principle of electron beam processing in a process line using a high voltage e-beam accelerator. Reprinted under Creative Commons Attribution License CC BY 4.0 from Ref. [233].

The classification of PS and polypropylene varies in the literature.[232,234] Also for TPU the classification has remained unclear since about 40 years of research and seems to depend on chemical composition, crystallinity and process conditions. For both, aliphatic and aromatic TPU either crosslinking[235,236] or degradation[237,238] was reported in the literature so far. Most of the studies dealing with irradiated TPU mainly focused on characterization techniques in bulk such as x-ray diffraction with differential scanning calorimetry,[239–241] gel-content studies or infrared and Raman spectroscopy.[240,242,243] Fewer studies included molar mass characterization mainly monitored by single-detector SEC with standard calibration[244–247] and rarely by absolute molar mass determination with SEC-MALS.[248] Despite the known facts of potential topological changes or increased amount of functional groups by cleavage of ester or urethane groups leading both to affected elution behavior in SEC as explained in section 1.1, recent studies on beam irradiated TPU still are done with standard calibration SEC only. It needs to be emphasized, that (highly) branched species of larger molar masses or with higher amount of functional groups could elute later than less branched fractions of lower molar mass. Therefore, the comparison of standard-equivalent molar masses by calibrated SEC is not appropriate and may lead to erroneous results and wrong conclusions. To shed light on this topic and to elucidate the predominant mechanisms in electron beam irradiation of TPU material, studies by channel-based fractionation have been carried out within the frame of this thesis.

3.3. Comprehensive Analysis of Polyolefins by Multidetector HT-SEC

Since polyolefins like PE and PP are only soluble above their melting temperature, separation-based characterizations have to be carried out at elevated temperatures in organic solvents of high boiling point with sufficient thermal stability and low polarity, such as 1,2,4-trichlorobenzene or 1-chloronaphthalene. Therefore, high-temperature (HT) chromatography such as HT-SEC coupled to MALS and dRI has been established to characterize polyolefins of varying molecular architecture.[249] Thereby HT-SEC provides a faster analysis than other fractionation techniques used in polyolefin analysis such as temperature rising elution fractionation or crystallization analysis fractionation, which clearly also provide valuable information about composition and crystallinity, but are highly time-consuming with analysis times up to 20 h.[62,250,251] It is well known, that linear PE (HDPE) has an open structure forming random coils in dilute solution. Instead, branched types of PE such as LDPE or LLDPE exhibit rather compact conformation as a result of their branching density.

However, polymers of similar chain arrangement but with significantly differing topology cannot be clearly identified by means of power law relations using data from the established HT-SEC approach with triple detection using MALS, dRI and viscometry. For this reason, Plüschke and coworkers extended triple detection HT-SEC by additional online DLS detection introducing quadruple detection HT-SEC (HT-SEC-d4).[61] This extended analysis approach allows to simultaneously determine molecular conformation, topology properties and the calculation of the structure parameters based on hydrodynamic and viscosity radii in terms of the ratios $\rho = R_G R_h^{-1}$ and $\kappa = R_{[\eta]} R_G^{-1}$ or the apparent density. With this set of information topological variations in polyolefins can be better resolved. An illustration of the method's capability is displayed in Fig. 3.4.

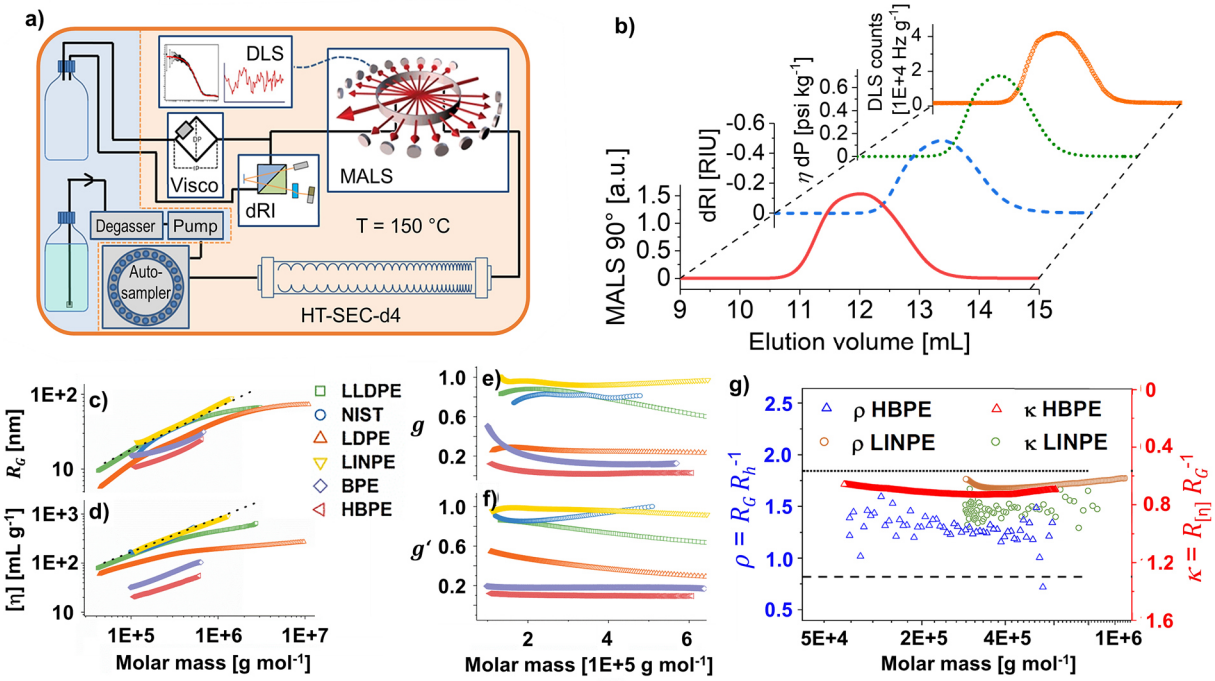

Figure 3.4 Comprehensive characterization by HT-SEC-d4, setup sketched in (**a**) with simultaneous record of four independent detections (**b**). Different types of regular PE of linear (LINPE, NIST) to short (LLDPE) and long-chain-branched structure (BPE, HBPE, LDPE) were investigated with regard to their topology by conformation (**c, d**) contraction (**e, f**) analysis and density-related measures (**g**). MALS image in (a) Courtesy © Wyatt Technology Corp., images **a** to **e**) reprinted with permission from Ref. [61] Copyright © 2018 American Chemical Society.

Next to the comprehensive characterization and elucidation of regular established types of polyethylene, HT-SEC-d4 furthermore has opened the opportunity to unravel structure property-relations of a new type of highly short-chain-branched polyethylene synthesized by the so-called chain walk catalysis (cwPE) after a concept introduced by Brookhart and Guan about two decades ago.[252] In contrast to regular-type PE synthesized by Ziegler-Natta

catalysis (Lewis-acid metal-complexes e.g. titanium, zirconium chlorides with aluminum alkyls)[253,254] or Kaminsky-type metallocene catalysis (aromatic sandwich complexes with titanium or zirconium),[255] this type of PE is synthesized with a late transition metal α-diimine catalyst of the type developed by Brookhart and coworkers.[256,257] This type of catalyst with a palladium(II) catalytic center yields PE with properties differing tremendously from regular PE such as an entirely amorphous structure and a solubility at room temperature even in normally pretty untypical solvents for PE due to a high number of short chain branches (verified by NMR).[258] By adjusting the synthesis conditions like ethylene pressure, reaction temperature, synthesis time and catalyst concentration, different topologies can be realized. Thereby, cwPE from different synthesis parameters exhibit analytical measures variations in long chain branching ranging from highly branched to almost linear, whereas the number of short-chain branches remains constant. Low synthesis pressure leads to predominantly hyperbranched structures, whereas high pressure generates polymers of linear topology. The synthesis temperature affects the topology to a minor extend and influences mainly the molar mass of the polymers.

HT-SEC-d4 furthermore allowed in a combined approach with other characterization techniques such as small-angle neutron scattering, atomic force microcopy and the comparison to simulations with varying chain walking probabilities, to unravel the structure formation during synthesis of this PE type.[259] Previous studies reported for cwPE spherical nanoobjects observed by AFM lead in combination with theory to the conclusion, that cwPE may cover a broad range of structures from compact globular up to coil-like linear topology. However, the recent study by Dockhorn, Plüschke and coworkers revealed, that the walking-to-insertion ratio of the catalyst remains constant over the polymerization time. This consequently limits the walking distance of the catalyst to a certain segmental range. Above a certain polymer size, monomers cannot be homogeneously implemented anymore along the entire molecule and are instead added or inserted in a distinct region of the growing molecule. Hence, during chain growth the polymer undergoes a transition from dendritic towards linear topology, which leads for all synthesis parameters more or less to disordered dendritic bottlebrush polymers. An overview about the outcome of this comprehensive study is summarized in Fig. 3.5.

The unique properties and the topological variety of the cwPE used in the study stated above represents a perfect polymer system, which allows to develop complementary branching characterization approaches as aimed in this thesis by ThFFF for polyethylene in general without the need of elevated temperatures and in an extended choice of solvents.

Studies of regular-type PE by ThFFF in high temperature mode have been in fact already reported, but they required high technical effort (immanent in high temperature techniques regardless of the separation technique) and were in first instance a proof of principle.[260–262] However, cwPE may allow for optimizations of ThFFF separations under easier experimental conditions and cost-effective, readily available equipment.

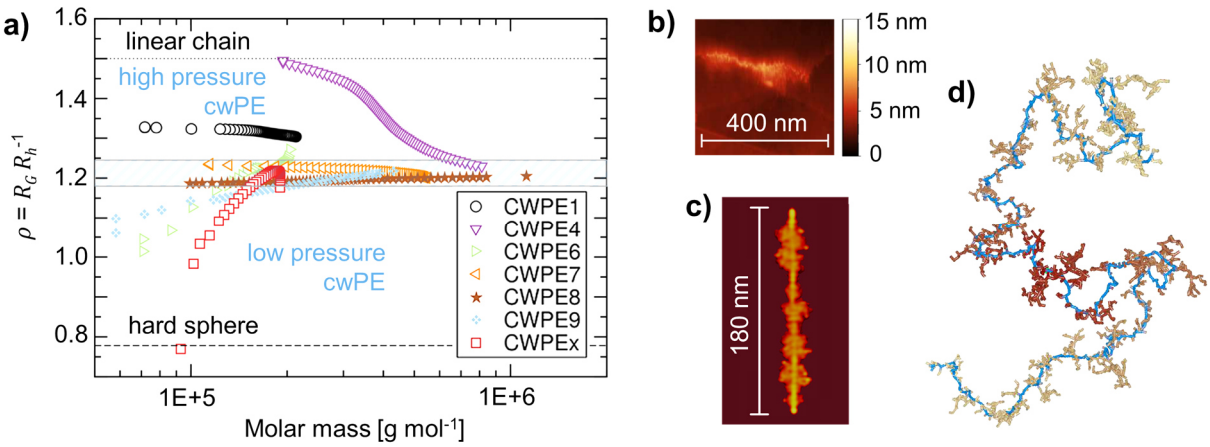

Figure 3.5 a) Evolution of topology in cwPE indicating the general trend to disordered dendritic like bottle brush polymers with growing polymer chain; topology in comparison between experimental finding by AFM (height mode) and structures simulated with realistic chain walking rates of around 7 (**c**) and 5 **(d**). Theoretical chain walking rates range from 1 for a linear chain to 100 for a dendrimer. Reprinted in part with permission from Ref. [259] Copyright © 2019 American Chemical Society.

3.4. Analysis of Branched Polymers by ThFFF

Branching was accounted for long time to have no effect on polymer thermal diffusion. This assumption was based on results by Schimpf and Giddings, who found that for star-shaped PS of different number of arms and combs of different length the FFF parameter λ falls in line with the translational diffusion coefficient. They concluded that D_T is independent on branching and molar mass for the system PS in ethylbenzene[109] and implied this independency to be generic referencing theoretical considerations by Brochard and de Gennes.[263] While the independency on molar mass has been widely verified by different experimental techniques (see section 2.4), the branching dependency remained experimentally unclarified up to recent investigations (explained below) and is therefore addressed in detail in objective 3 and 4 of this thesis.

Branching analysis is in principle possible assuming D_T to be constant, since the resulting S_T still scales with the changing translational diffusion coefficient D by a difference in hydrodynamic size for molecules of the same molar mass and different branching. This assumption was also used by Runyon as a basis in his work, in which he found that macromolecules with

a higher number of side chains have in the ThFFF channel shorter retention times, which represents a connection of S_T to differences in architecture. In his work this was expressed by the number of chain ends. Based on that, he introduced the concept of the Soret contraction factor g'' in analogy to the viscosity contraction factor g' and the radius contraction factor g (see section 2.2) being a ratio of the branched structure's S_T and of the linear analogue with the same molar mass (Eq. (3.1)).[122]

$$g'' = \left(\frac{S_{T,bra}}{S_{T,lin}}\right)_M = \left(\frac{D_{T,bra}\, D_{lin}}{D_{T,lin}\, D_{bra}}\right)_M \tag{3.1}$$

g'' was in fact found to be linearly related to the number of chain ends in the macromolecule, which confirms its ability to express an information about branching as a third independent parameter next to g, and g'. Assuming D_T being unaffected by branching ($D_{T,bra} = D_{T,lin}$) would lead to a shortened form of g'' being the ratio of the translational diffusion coefficients only. For the system PS in 2-butanone (MEK) in fact an agreement to the initial findings of Schimpf and Giddings was found. However, for poly(methyl methacrylate) (PMMA) in MEK significant differences from this trend were observed, which remained unclear so far. The correlation of S_T to the number of chain ends was investigated for homo- as well as for copolymer star molecules and furthermore, correlations between experimentally found S_T and values predicted by the Mes D_T model were investigated (see Fig. 3.6).[122] Both matters, the information incorporated in the Soret contraction and the predictability of D_T by model are regarded in objective 3 in this thesis and are reported in publication 8.3 to 8.5, respectively.

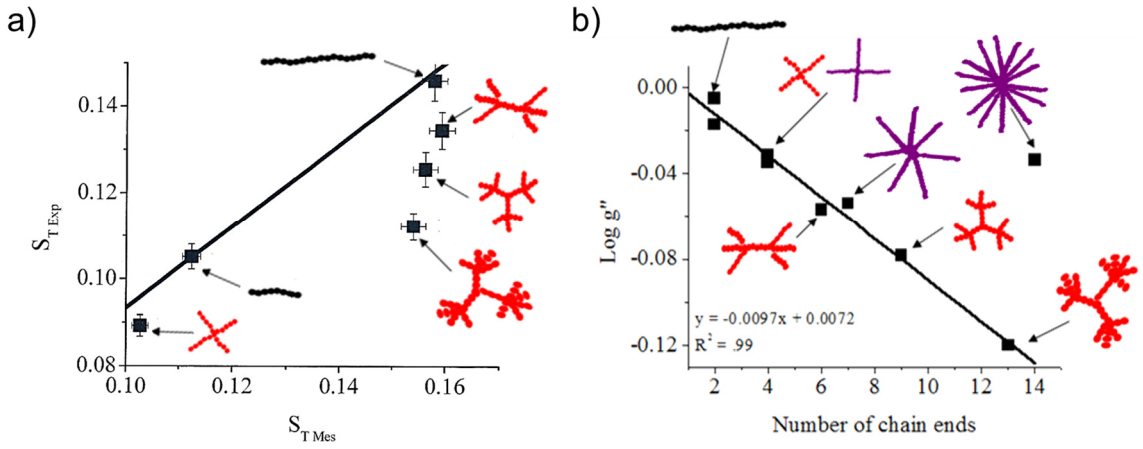

Figure 3.6 a) Experimental versus predicted mean Soret coefficients for differently star-shaped PS samples, and **b)** Soret contraction factors log(g'') vs. the number of chain ends for non-linear PS (red) and PMMA-stars (purple). Adapted from Ref. [122], Illustration concept by J. R. Runyon.

Another approach to a potential branching-selective separation by ThFFF was chosen by Greyling 2018, who reassessed to some extend the work by Schimpf and Giddings stated above for PS stars and linear samples and found an influence of the solvent on the selectivity in separation of branched and linear structures. Furthermore, he found indications for a branching dependency of D_T.[113] However, despite the stated trend of D_T to the number of arms holds true qualitatively, the reported D_T have to be seen critically, because they were calculated with the simplified high retention approximation (Eq. (2.30)) even though the actual measured retention apparently did not fulfill the requirements of high retention. Additional errors are expected by the disregard of the flow-profile distortion in the calculation, although the necessity of its correction has been known for more than 30 years[114,264,265] and is confirmed by numerous comparisons of experimental D_T from ThFFF and other measurement methods.[118,191]

Next to topological differences, other influencing parameters have to be considered when ThFFF is used as branching analysis method. The dependency of S_T and D_T may be superimposed by other differences in polymer microstructure and copolymer composition. Investigations by Greyling[266] and Muza[267] indicated exemplary for PMMA a dependency of the thermophoretic behavior on the stereoregularity (tacticity) of polymers. This is in agreement to findings by Köhler and coworkers, who concluded upon thermophoretic studies by TDFRS that the polymer chain stiffness may have an influence on thermal diffusion.[174]

4. Experimental Part

4.1. Details to Polymer Model Systems

Silylated aromatic-aliphatic polyesters of designed *DB* from 0 to 50 % were synthesized by polycondensation of 4,4-bis(4- hydroxyphenyl) valeric acid (AB2) with a tert-butyldimethyl-silyl protected version of the monomer (ABB*) as reported previously.[268] The preset ABB*/AB2 ratio yields a tailored degree of branching of the resultant polymer. These samples are after their targeted *DB* as follows: SY-0, -8, -12, -22, -32, and -50. SY denotes the presence of a silyl group. The SY-100 sample was produced following a postmodification process where the statistically branched OH-50 (analogue to SY-50 but with OH end groups for further modification) was reacted with additional AB*2 monomer having two silyl groups.[208] This replaced any remaining linear regions formerly present in the hyperbranched sample with an AB*2 terminal chain yielding a pseudodendrimer of a nominal *DB* = 100 %. Molar masses and dispersities measured by SEC-MALS analysis are summarized in publication 8.3.

The model library of cwPE used in this work were synthesized with α-diimine palladium catalyst ([(N, N'-bis(2,6-diisopropylphenyl)-2,3-dimethyl-1,4-diazabutane)Pd$(CH_2)_3COOCH_3$]$^+$ [BAr^F_4]$^-$ (Ar^F=3,5-bis-(trifluoro-methyl)phenyl)) as described elsewhere[61,259,269] based on the synthesis approach of Brookhart *et al.*[256] with the conditions shown in Table 4.1. All samples contain ~ 100 branches per 1000 total carbon atoms according to ^{1}H NMR analysis but differ in topology mainly influenced by ethene pressure[252].

Both polymer model systems used in objective 3 were derived from previous works. Their synthesis was not part of this dissertation.

Table 4.1 Synthesis conditions, expected topology and the characterization average results of the cwPE model library used in ThFFF studies, found by HT-SEC-d4.

Synthesis conditions					Average results found by HT-SEC-D4		
Sample	p [bar][a]	T [°C]	Reaction time [h]	Expected topology	M_w [kg mol^{-1}]	$R_{G,z}$ [nm]	ν_R
hb1	0.14	35	24	highly branched, medium M_w	230 ± 6	15.8 ± 0.3	0.56 ± 0.3
hb2	0.09	0	24	highly branched, lower M_w	161.3 ± 2.2	12.9 ± 0.2	0.45 to 1.15*
b1	4	0	20	linear, lower M_w	140 ± 3	16.6 ± 0.4	0.60 ± 0.09
b2	2	0	20	branched, lower M_w	136 ± 2	16.3 ± 0.2	0.65 ± 0.08
sb	2	10	20	slightly branched, higher M_w	313 ± 8	25.4 ± 0.5	0.47 to 0.73*
lin1	8	0	20	linear, lower M_w	175.4 ± 0.5	18.5 ± 0.2	0.53 ± 0.02
lin2	8	10	20	linear, higher M_w	384 ± 7	30.4 ± 0.3	0.35 to 0.74*

Pd catalyst 10 µmol, chlorobenzene 30 mL, [a] absolute ethene pressure

*) dependent on the molar mass

The thermoplastic polyurethane materials L780D10 (aliphatic polyester-TPU) of the composition 4,4′-dicyclohexylmethane diisocyanate (H_{12}MDI) copolymerized with 1,4-butane diol (BD) and a segment of poly(1,6-hexylene adipate), and C74D50 (aromatic polyester-TPU) composed of diphenylmethane diisocyanate (MDI), BD and poly(1,4-butylene adipate) used in the electron beam irradiation study reported in publication 8.5 were produced and provided by BASF Polyurethanes GmbH. The structures and further experimental details are given in the Supporting information of publication 8.5.

4.2. Electron Beam Irradiation

Rectangular samples of dimension approximately 40 mm x 10 mm were cut from a bulk polyurethane sheet and were irradiated in a special irradiation chamber[270] using an electron accelerator ELV-2 (manufactured by Budker Institute of Nuclear Physics, Novosibirsk, Russia).[271] Prior to irradiation the samples were dried at 40 °C for 4 h under vacuum in the vacuum oven. After the drying process the polyurethane sheet were place into the irradiation chamber. Before irradiation, the temperature was firstly heated up to 80 °C and kept for 5 minutes under vacuum in order to remove moisture and oxygen. Subsequently, the temperature was cooled down to the target irradiation temperatures in the nitrogen atmosphere. The irradiation was carried out with constant electron energy (1.5 MeV) and electron current (4 mA), the dose was applied by several steps of 25 kGy until the target dose had been reached.

4.3. ThFFF Analysis

ThFFF experiments were carried out with a TF2000 set up, consisting of an isocratic pump, degasser, auto-sampler, actively heated and cooled ThFFF channel, PN3621 21-angle light scattering (MALS) detector with a laser of the wavelength 532 nm and PN3150 differential refractive index (dRI) detector (all by Postnova Analytics GmbH, Germany). The cold wall block was cooled by a liquid cooling circuit with a refrigeration unit Unichiller® 025-MPC (2.5 kW) by Peter Huber Kältemaschinenbau GmbH (now AG), Germany. The channel dimensions were 45.6 cm tip-to-tip length, width 2 cm and a thickness of 250 µm, realized by spacers made of Mylar A® and Teonex® by DuPont Teijin Films Ltd. A constant flow rate of 0.2 or 0.3 mL min^{-1} was applied for all separations. This is specified further in the supporting information of the publications 8.2 to 8.5. A channel pressure of about 0.6 to 1 MPa was adjusted

for the used flow rate by a back-pressure tubing (inner diameter 0.001“) between the ThFFF channel and the MALS detector in order to maintain the stability of the dRI baseline and to avoid possible accumulation of gas bubbles due to residual dissolved gas in the carrier fluid or boiling of the solvent. The samples were injected in a concentration of 4 to 5 mg mL^{-1}. The injection volume for all TPU separations was 102.5 µL. Separations of cwPE and the silylated polyesters were done with 102.5 µL or 49 µL. The data recording and analysis was carried out with the TF2000 version of the NovaFFF software. A list of carrier liquids used in ThFFF separations comprised in this dissertation is given in Table 4.2. ThFFF Measurements of TPU material, dissolved in *N,N*-dimethylacetamide with di-n-butyl amine were carried out without LiCl to avoid corrosion damage in the separation channel.

Table 4.2 List of carrier liquids and additive chemicals used in ThFFF separations

Carrier liquid	Purity	Supplier, Remarks
Tetrahydrofuran	ReagentPlus®, ≥ 99 %	Sigma-Aldrich Chemie, GmbH, Germany
Cyclohexane	EMSURE®, ≥99.5 %	Merck KGaA, Germany
Mesitylene	99%, Acros Organics™	Fisher Scientific GmbH, Germany
Chloroform	Chromasolv™ 99%	Honeywell Int. Inc. USA
N,N-dimethylacetamide	ReagentPlus®, ≥ 99 %	Sigma-Aldrich Chemie, GmbH, Germany
Paraffin oil (C9-C13 alkanes)	favorit® Lampenöl klar < 0.2 mol-% residual aromatic compounds (Py-GC/MS, ^{1}H-NMR)	Alschu-Chemie GmbH, Germany, fractionated by vacuum distillation over Vigreux fractional column, Purification and analysis, see SI of publication 8.5
Additive chemicals	**Purity**	**Supplier, Remarks**
Lithium chloride	EMSURE®, ≥99 %	Merck KGaA, Germany
Di-n-butyl amine	99%, Acros Organics™	Fisher Scientific GmbH, Germany

4.4. HT-SEC-d4 Analysis

High temperature quadruple-detector size exclusion chromatography (HT-SEC-d4) experiments were done with a PL-GPC220 (Polymer Laboratories Ltd., U. K.) setup, connected to a MALS detector (Wyatt Technology Corporation, USA), a dRI detector and an online viscometer (both Agilent Technologies, Inc., USA) as described in our previous report.[61] The carrier fluid 1,2,4-trichlorobenzene was purchased from Sigma Aldrich with a purity of ≥ 99 % and stabilized with 1 g L^{-1} 2,6-di-tert-butyl-4-methylphenol (Carl Roth, Germany, purity ≥ 98 %) to prevent thermo-oxidative decomposition. Data recording and analysis was done with the Astra® software, version 6.1.2.84 (Wyatt Technology Corporation, USA).

4.5. Temperature-Dependent Dynamic Light Scattering

Temperature dependent dynamic light scattering (DLS) experiments were performed with a DynaPro® NanoStar® instrument (Laser λ = 658 nm) by Wyatt Technology Corporation, USA using a 1.25 µl quartz cuvette (total volume approximately 1 mL). In all experiments, the cuvette was completely filled with ca. 0.8 mL sample solution to avoid cavities, containing 1 mg mL^{-1} of polymer solution, which was filtered through a 0.45 µm PTFE syringe filter (Carl Roth, Germany). The cuvette was closed with an affiliated PTFE lid and sealed with Parafilm® wax foil to prevent evaporation of solvent. The data recording and analysis was done with the software Dynamics® by Wyatt Technology Corporation, USA, versions 7.6.0.48 and 7.8.0.26 using the cumulant fit method.[272] During the run of all experiments (T = 20 to 60 °C in stages of 5 K, total time ca. 6 h) no solvent lost due to evaporation of volatile solvents or leakage of the sealing was observed.

4.6. SEC-MALS-dRI at Room Temperature

SEC-MALS-DRI analysis was performed at room temperature with a set up composed of an HPLC-Pump 1200, a Polar Gel-M separation column (300 x 7.5 mm; 8 µm) (both by Agilent Technologies, Inc.) coupled to a TREOS II 3-angle light scattering detector by Wyatt Technology, Corp. and a K-2301 dRI detector (generic) by KNAUER Wissenschaftliche Geräte GmbH, Germany (with *N,N*-dimethyl-acetamide) or a viscosity/differential refractive index (dRI) dual detector ETA-2020 by WGE Dr. Bures, Germany (THF). The samples were dissolved in 500 µl of solvent. TPU was dissolved in *N,N*-dimethylacetamide with 0,5% di-n-butyl amine and filled up to 1 mL with *N,N*-dimethylacetamide (+ 3 g L^{-1} LiCl). cwPE and silylated aromatic-aliphatic polyesters were measured in THF (stabilized with 0.025% butylated hydroxytoluene). For each run, a sample volume of 20 µL was injected and separated with a flowrate of 1.0 mL min^{-1}. Data recording and evaluation was done with the Astra® Software by Wyatt Technology Corporation, USA, version 6.1.2 and 7.3.1.9.

4.7. Spectroscopic Methods

Attenuated total internal reflection-Fourier transform infrared analysis (ATR-FTIR) was carried out at room temperature using a TENSOR 27 infrared spectrometer (Bruker Optik GmbH, Germany) equipped with a MIRacle^{TM} diamond crystal ATR accessory (PIKE Technologies, Inc., USA). 32 scans were taken and averaged per spectrum in the spectral region 4000 to

400 cm^{-1} at a resolution of 4 cm^{-1}. Data evaluation, including baseline correction and vector normalization[273,274] for valid comparison, was done with the spectroscopic software OPUS, version 7.5 (Bruker Optik GmbH).

^{1}H-NMR spectra were recorded with a Bruker Avance III spectrometer operating at 500.13 MHz. DMSO-d6 was used as solvent, lock, and internal standard [δ(^{1}H) 2.50 ppm]. The spectra were recorded using the standard pulse programs included in the Bruker Topspin software package, version 3.2.

4.8. Thermal Analysis

Thermogravimetric Analysis was performed using a TA Instruments TGA Q 500 (V20.13 Build 39) in the range between 35 and 600 °C. The experiments were performed under constant nitrogen purge of 25 ml min^{-1} and a nominal heating ramp of 10 °C min^{-1}.

DSC analysis was performed with a DSC 2500 differential scanning calorimeter by TA Instruments, Inc., USA, equipped with a liquid nitrogen accessory. For all analyses, a sample weight of approximately 10 mg per measurement was analyzed under a constant nitrogen purge in Tzero-Al hermetic with perforated lid. The aliphatic TPU L780D10 was analyzed by the following method: Isothermal equilibration at −90 °C for 5 min, followed by a preheating run to 80 °C. After a 30 s isothermal hold, the sample was cooled down again to −90 °C with another 5 min isothermal equilibration. Then the first heating scan was performed to 250 °C. After a 30 s isothermal hold the cooling scan was performed to −90 °C with an isothermal equilibration step for 5 min, before the second heating run up to 280 °C was done. All heating and cooling scans/runs in this method were carried out with a ramp of +/−10 °C min^{-1}.
The aromatic TPU C74D50 was analyzed instead by the following method: Isothermal equilibration at −90 °C for 5 min, followed by the first heating scan to 250 °C. After a 30 s isothermal hold the cooling scan was performed down to −90 °C with an isothermal equilibration step for 5 min, before the second heating run up to 280 °C was done. The heating scans were performed with a ramp of +40 °C min^{-1} and the cooling scans a ramp of −10 °C min^{-1}. Melting (T_m) and crystallization temperatures ($T_{c,m}$) were taken as the maximum of the endothermic transition, whereas glass transition temperatures (T_g) were taken as onset and as midpoint at half of the step height in heat capacity Δc_p. Data recording and analysis of both, TGA and DSC analyses was done with the Software Universal V4.5A by TA Instruments, Inc., USA.

5. Results and Discussion

5.1. Improvements in the Mathematical Description of ThFFF Retention

In order to simplify calculations for accurate ThFFF investigations as outlined in section 2.3.3, Belgaied, Hoyos and Martin[114] developed a polynomial based approach for an easy determination of the non-parabolicity parameter ν in dependency to the cold wall temperature T_c and ΔT, as shown in Eq. (5.1) with solvent specific polynomial coefficients.

$$\nu = (a_1 T_c + a_2)\,\Delta T + (a_3 T_c + a_4)\,\Delta T^2 + (a_5 T_c + a_6)\,\Delta T^3 \tag{5.1}$$

For the commonly used in ThFFF 12 organic solvents in total (until 1994), they computed the solvent specific coefficients a_1 to a_6, numerically by a linear fitting process (involving Eqs. (2.26) to (2.30)) in the range of moderate cold wall temperatures T_c. In the meantime research continued and ThFFF investigations were performed in many other solvents[113,117,191,275–280] and even at elevated T_c as high temperature ThFFF,[260,261] which are not covered in their report. For these studies values for ν had to be computed by elaborate calculations for specific experimental conditions or the distortion of the flow-profile was completely ignored, which led to imprecise thermophoretical data[113,281,282] mainly affecting results for polymers with typically poorer ThFFF retention than observed for larger objects like latex particles,[283–285] micelles or other vesicle-like objects.[286–288] To yield accurate thermophoretical data from ThFFF experiments comparable to data from other methods such as TDFRS an applicable way for the non-parabolicity correction in the processing of ThFFF data is definitely needed. This issue has been tackled in the first objective of this thesis and is outlined in **publication 8.1**.

The first goal in this study was to extend and revise the reported list of solvents and the corresponding coefficients a_1 to a_6 needed for calculations of ν (Eq. (5.1)). The coefficients of in total fifty-nine solvents were computed with 210 calculation sets per solvent on the basis of sophisticated experimental literature (dynamic viscosity and thermal conductivity) and their temperature dependency in ranges of T_c = −10 °C to 120 °C and ΔT up to 120 K involving application ranges of normal and high temperature ThFFF. The full list is reported in publication 8.1. In this survey, coefficients of solvents like n- and cycloalkanes were summarized in fits for the homologue series in dependency to the number of carbon atoms in the alkane chain or ring.

The second goal of this study evolved during the computation of the velocity flow-profiles in the first goal. In principle all nonpolar and aprotic-polar solvents were accurately

resembled by the cubic flow-profile approximation (see Eq. (2.28)). Even for high field conditions (ΔT = 100 K) only a moderate distortion of the flow-profile of $\nu < -0.4$ was found. However, polar-protic solvents such as alcohols and water exhibited severe flow-profile distortions reaching non-parabolicity parameters up to $\nu \approx -0.6$. For such tremendous distortions, an increasing inability of the cubic flow-profile approximation to match the exact flow-profile (computed with Eqs. (2.26), (2.27)), roughly correlating with the solvents' polarity, was found. In consequence, also the retention description (Eq. (2.29)) becomes increasingly inaccurate. Hence, the coefficients reported for such solvents have a quite limited validity range. In order to maintain the key benefit of having only one adjustable parameter in the non-parabolicity correction for accurate ThFFF calculations, an empirically found modification of the original ThFFF retention, given in the following Eq. (5.2) is proposed in this study.

$$R = R_p + 6\,\lambda\left(\nu + 0.5\,R_p\,\nu^{3}\right)\left(1 - R_p\right) \tag{5.2}$$

This relation incorporates a higher influence of ν on R for severe flow-profile distortions and improves in general the accuracy of the retention description compared to descriptions of R on the basis of higher polynomial flow-profile approximations reported in the literature,[159,289–291] which are not equally universal and always require specific physicochemical solvent data in their application. The flow-profile distortion and a comparison of the retention descriptions given above is illustrated in Figs. 1 and 2 of publication 8.1.

The third goal in this study was to provide a simple tool to approximate λ from measured retention ratios without numerical solution. For ThFFF calculations such a relation, which incorporates the flow distortions as the main issue affecting the accuracy of the calculation, was not available yet. Therefore, the approximation equation proposed by Schimpf and coworkers (Eq. (2.23)) was refined empirically and adapted by introduction of polynomial terms with ν, which yielded the following equation (5.3):

$$\lambda \cong \frac{\left({}^{5}/_{4}\,\nu^{2} - {}^{5}/_{4}\,\nu + {}^{101}/_{100}\right)R}{6\left[1 - R^{\left({}^{20}/_{6}\,\nu^{2} - {}^{12}/_{5}\nu + {}^{4}/_{3}\right)}\right]^{\left({}^{10}/_{9}\nu^{2} - {}^{1}/_{4}\,\nu + {}^{68}/_{155}\right)}} \tag{5.3}$$

The accuracy of this approximation is verified in Fig. 3 of publication 8.1.

It is believed, that this study will contribute to greatly improve the applicability of ThFFF as characterization method for thermophoretic studies. The coefficients being yielded in this study set furthermore the basis for significantly simplified calculations of S_T or D_T from measured ThFFF retention times and are used in the objectives 3 and 4 of this thesis.

5.2. Tuning of ThFFF Separation and Analysis by Solubility and D_T Prediction

Finding a polymer solvent combination that yields sufficiently high D_T for a good retention in ThFFF analysis as presented in the studies from objective 3 (publication 8.3 and 8.4) had to be performed still to a greater extend in a trial-and-error process. The latest D_T prediction model by Mes, Kok and Tijssen helps to shorten this process already tremendously and provide an orientation, but up to this study they have not reached a prediction level yet accurately matching experimentally found D_T.[118,191] Reassessments of available D_T prediction theories by Runyon indicated, that their predictive power depends to a great extent on the quantity of the segmental size information r_m and to a minor extend on the temperature dependency of the Hildebrandt solubility parameter used in the prediction.[191] D_T values were so far predicted with theoretically approximated r_m of 0.201 nm[118,186] or 0.29 nm[191] for PS and 0.153 nm[186] or 0.27 nm[191] for PMMA, respectively, derived either by extrapolation of the scaling laws of these polymers down to monomer molar mass or via sphere-equivalent closest packing models.[188,191] It is questionable, whether such small length scales stated above are still meaningful in thermodynamic sense. Furthermore, the temperature dependency of the Hildebrandt solubility parameter $\delta(T)$ was calculated by the liquid thermal expansion of the regarded polymers in melt (taken from the literature). Both, r_m and $\delta(T)$ provide room for optimizations in prediction accuracy. Therefore, in the **second objective** in this thesis reported **in publication 8.2** the prediction capability of the Mes D_T model (defined in Eq. (2.33)) was targeted to be improved with data input on a more comprehensive and thermo-dynamically reasonable basis. This concerns segment size information and more comprehensive Hansen solubility theory[120,121] to model $\delta(T)$ and hence, the partial derivatives $^{\partial\chi}/_{\partial T}$, $^{\partial^2\chi}/_{\partial T^2}$. This combination has not been attempted before. In this approach, r_m was approximated as given in Eq. (5.4) in relation to the Kuhn length l_K

$$l_K = l_b\, C_\infty \cos\left(^{\theta_b}/_2\right) \approx 2\, r_m \tag{5.4}$$

which can be approximated with the bond length l_b, the bond angle θ_b and the characteristic ratio C_∞. l_K represents in principle the average length of a segment in the theoretical description of a (long) polymer chain by the freely-jointed-chain-model and is for worm-like polymer chains about twice the persistence length and hence, a measure of the chain stiffness. C_∞ is defined in this model as a correction factor for the deviation of the polymer's behavior as a real chain from the freely-jointed-chain-model and represents also a dimensionless measure

of the chain flexibility.[292] The parameters l_b , C_∞ and θ are tabulated in comprehensive reference literature[293], for instance from experimental work or rotational isomeric state modelling.[294] Indications that D_T dependents potentially on l_K or a related segment length, was already described previously.[174,184] Eventually, this sets a direct physiochemical or thermodynamic basis for the Mes D_T model. The temperature derivatives of χ_H in this study were modelled with temperature-dependent HSP according to Eqs. (2.38) to (2.40). For that, also the volumetric thermal expansion coefficient α_V valid for the regarded temperature range was used to consider phase transitions of amorphous polymers in solubility parameter calculations. The necessity for this was already reported previously.[295] This was accounted to be more realistic, since α_V is also a result of the cohesive energy density at given temperature.

The prediction results of the Mes D_T model with newly assessed input revealed a superior prediction power to resemble experimentally found D_T as shown in Fig. 5.1 than compared to the previous study by Runyon and Williams.[191] This confirms at least for unipolar and as well for aprotic polar systems a general validity and accuracy of the Mes D_T model and has a fundamental character despite that the complete fundamental D_T theory has still not been developed yet. The Mes D_T model can in principle also display negative D_T in case of thermophilic behavior. However, further work is needed for the validation of this matter as well as for protic-polar systems, *i.a.* to elucidate the contribution of electrostatic interactions.

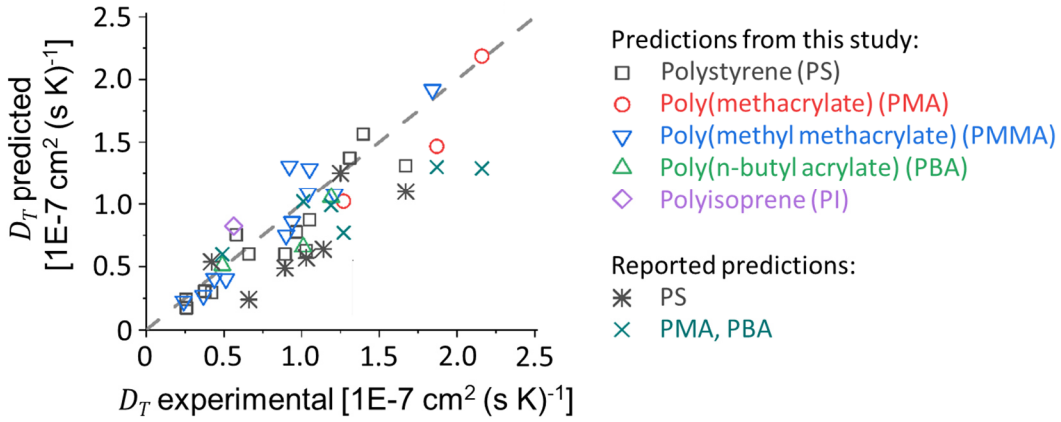

Figure 5.1 D_T predicted with Eqs. (2.33),(2.38)-(2.40) and (5.7) in comparison to the predicted D_T reported previously.[118,191] Both predictions are plotted against experimental D_T reported for the presented polymers in a broad choice of solvents. The full overview of predictions and list of references is reported in publication 8.2. The dashed line is guide for the eye at $D_{T,\,exp.} = D_{T,\,predict.}$. Adapted with permission from publication 8.2. Copyright © 2020 American Chemical Society.

The D_T predictions assessed in this study indicated to some extent also a correlation of the thermal diffusion and consequently the retention in ThFFF to the thermodynamic quality of the solvent for the regarded polymer. With the improved input, the Mes D_T model may provide a great help to find an optimal solvent for ThFFF separation, however, trends to the solvent quality may not directly be derivable and require certain effort of calculations and experiments to yield D and D_T. To shorten the optimization process, the ThFFF retention and selectivity was probed for the cwPE system (investigated also in objective 3) for several solvents and correlated to the solvent quality modeled by HST. In fact, a direct correlation of the experimentally measured ThFFF retention was found in dependency to the relative energy distance, i.a. to the distance of the solvent's HSP from the sphere center of the polymer. This correlation is indicated in Fig. 5.2 for 3 out of in total 5 investigated solvents. According to the observed trend, a solvent yielding an optimal retention and selectivity will be located closest to the sphere center. In fact, the highest retention in this study was found for cwPE in n-decane which's HSP are located in the vicinity of the sphere center. Separations in n-decane were found to require even less than one third of the field strength to yield an equal retention than compared to the separation in cyclohexane (comparison shown in publication 8.2). A slightly lower retention, but in the same order of magnitude was found for an aliphatic hydrocarbon mixture (paraffin oil). This outcome in fact allows to find a preferential solvent for ThFFF separations without comprehensive calculations.

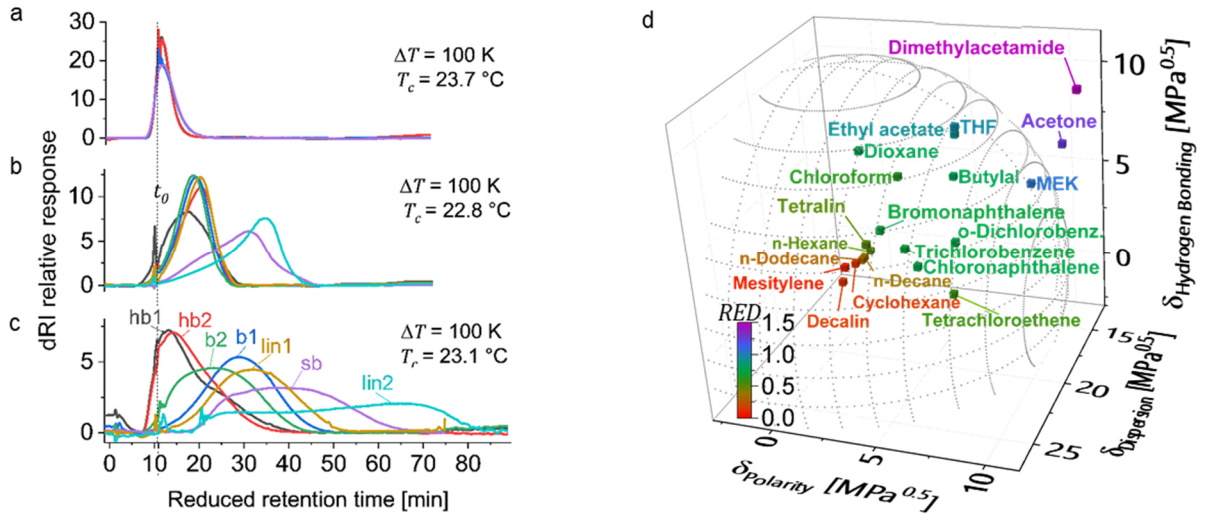

Figure 5.2 ThFFF fractograms of seven cwPE (investigated also in objective 3) with varying topology from highly branched (hb) to linear (lin), separated in THF (**a**), chloroform (**b**) and cyclohexane (**c**). **d** illustrates the calculated Hansen solubility sphere for PE to approximate the quality of the probed solvents in relation to their distance from the sphere center (*RED*). Adapted with permission from publication 8.2. Copyright © 2020 American Chemical Society.

5.3. Branching Characterization of Polymer Model Systems by ThFFF

5.3.1. Architecture Characterization of Branched Aromatic-Aliphatic Polyesters

In the study reported **in publication 8.3** ThFFF was applied to characterize the architecture of aromatic–aliphatic polyesters with varying tailored degree of branching. This study addresses objective 3 and is intended to elucidate the correlation between the molecular topology and thermal diffusion. This polymer system investigated here was derived from the synthesis development study by Khalyavina and coworkers[206] as summarized in section 3.1 and represents in contrast to star-shaped polymers investigated previously by ThFFF (see section 3.4) a polymer system with irregular random type of branching. The model library illustrated in Fig. 5.3 containing polymers with degree of branching 0, 8, 12, 22, 32, 50 and 100 % was investigated by ThFFF for two aprotic solvents of different polarity (THF and cyclohexane), supported by offline temperature dependent DLS.

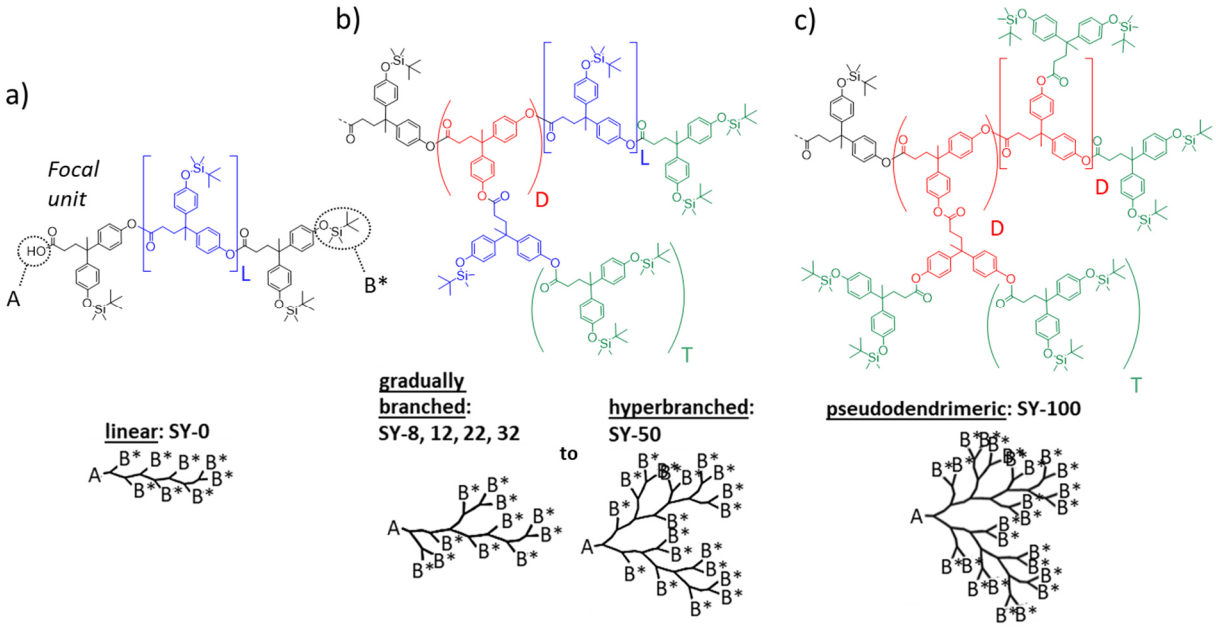

Figure 5.3 Chemical and topology representation of the polymer model library comprised of silylated aliphatic-aromatic polyesters containing all an equal focal unit as well as linear (index L, blue), dendritic (index D, red) and terminal (index T, green) units. DB ranges from a) 0 % (linear) over b) 8 to 32 % (gradually branched) and 50 % (hyperbranched) up to c) ≈ 100 % (pseudodendrimeric).

Thereby, a generally higher retention was observed in THF, which is in first instance attributed to the overall larger hydrodynamic size of all model samples observed by DLS. However, in a second instance additionally clear dependencies of D_T to the solvent and to the degree of branching are found, as indicated in Fig. 5.4 b. This confirms previous findings by Greyling,[113] and proves that there are branching-selective and nonselective solvents for

separations by in ThFFF. This may be an explanation for the findings by Runyon for dendritic PMMA in MEK, which remained unexplained at that time (see section 3.4).[122] D_T values were extracted from the measured ThFFF retention times from the MALS peak maximum (exemplarily shown in Fig. 5.3 a) by computational root-finding solution of Eq. (2.29) with non-parabolicity correction by coefficients reported by Belgaied et al. [114] combined with diffusion coefficients measured by offline DLS. Therefore, D_T values reported in this work are accounted to be accurate and well-comparable to values potentially measured by optical batch techniques despite the polymers have a broader $Đ$ from 1.8 to 2.5. For cwPE representing homopolymers of a lower chemical heterogeneity also retention behavior in more and less selective manner depending on the solvent was observed. This was investigated in detail in the second goal of this objective (publication 8.4) and is summarized in section 5.3.2.

Next to D_T dependency also the ability of the Soret contraction concept was probed in this study. For both solvents a direct correlation of g'' to the degree of branching (DB) was found (see Fig. 5.4 b). Surprisingly, the dependency of g'' to DB becomes lower for a D_T-non-selective solvent. This behavior could be explained with a copolymer-like thermal diffusion behavior due to the chemical heterogeneity of the monomers having aromatic components and ester groups in the center and terminal silyl groups. According to the Mes D_T model and studies by Köhler et al. regarding the influence of coil draining on polymer thermal diffusion,[296] the thermophoretic behavior of copolymers is to a great extend described dependent on polymer–solvent interactions at the interface and also a combination of contributions from in this case both intramonomer “blocks” with two distinct chemistries. It appears, that the silyl groups on the global polymer solvent interface are better solvated in THF guiding D_T and causing a dependency of D_T to branching, whereas the aromatic rings more in the center of the molecule are better solvated in cyclohexane but cannot significantly contribute to the resulting D_T of the polymer.

The molar mass trace of the linear reference polyester was found to cover the molar mass range of the main fraction of all investigated polyesters (Fig. 5.4 a). This allowed to generate quasi online data of g'', calculated per discrete retention time slice. Unlike the mean values of g'' (from peak apex retention data) stated above, here the broad molar mass dispersity is an advantage for the analysis. The differential weight distribution of g'' shown in Fig. 5.4 c confirmed the results and trend of the g'' mean values in good agreement. However, the outcome in Fig. 5.4 c additionally reveals the existence of small subpopulations with positive $\log(g'')$ or g'' above 1 in the samples of lower DB and predominantly in the linear reference, respectively.

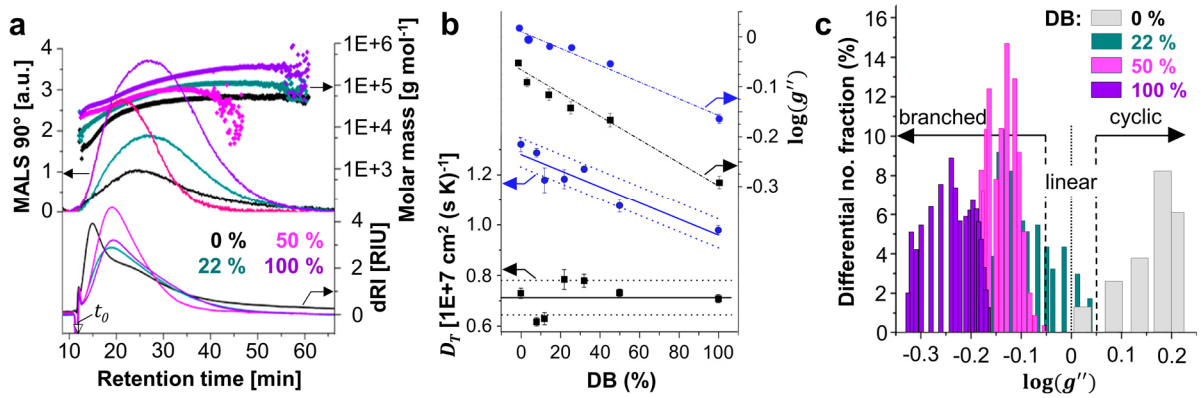

Figure 5.4 a ThFFF fractograms of an exemplary choice of silylated polyesters with different DB measured in cyclohexane with a constant ΔT = 100 K (T_c = 23 °C). **b** Dependence of D_T and g'' (both from MALS peak apex) on DB in cyclohexane (black) and THF (blue). **c** Distribution of g'' calculated from quasi online data from slices of the fractogram data displayed in a. The solid line represents the fit for trend in THF and mean value in CH. Dotted lines represents one standard deviation. Adapted with permission from publication 8.3. Copyright © 2019 American Chemical Society.

Fraction collection and subsequent analysis by matrix assisted laser desorption ionization with time-of-flight mass spectroscopy (MALDI-TOF) confirmed these fractions as cyclic subpopulations of lower molar mass. These small molar mass fractions were also observed in complementary analysis of the polyesters by SEC-MALS-dRI. This first report of the thermal diffusion behavior of cyclic polymers is a promising development. The Soret contraction analysis has been confirmed to display accurately the architecture of polymers and could additionally lead to advances in the analysis of cyclic polymers, particularly in mixtures. Unlike the other contraction factors g and g', which indicate also for cyclic structures contracted conformations (g ≈ 0.5), g'' allows to distinguish between branched or cyclic structures. The formation of cyclic structures is a general phenomenon in polycondensation reactions, which occurs mainly due to so-called back-biting and end-to-end condensation at higher monomer conversion degree.[297,298] For the polyester system used in this study etherification as side reaction during polycondensations can be also discussed as origin for cycles.[299]

5.3.2. Topology Analysis of Chain Walk Polyethylene by ThFFF

Parallel to the ThFFF branching analysis study outlined above, the second aim in the study of objective 3 was the investigation of a polymer model system with broad range of topological differences, but also with the lowest possible chemical heterogeneity. This study is reported **in publication 8.4.** cwPE represents a perfect polymer model system due to the importance of polyethylene in research and industry on one hand and the unique properties of palladium catalyzed cwPE on the other hand being readily soluble at room temperature in an extended portfolio of solvents. For this reason, the retention behavior of a library of seven model polymers with variations in their global topology was investigated with ThFFF hyphenated to absolute molar mass and size detection. The generalized topological features and the local chemical structure of the cwPE samples is illustrated in Fig. 5.5.

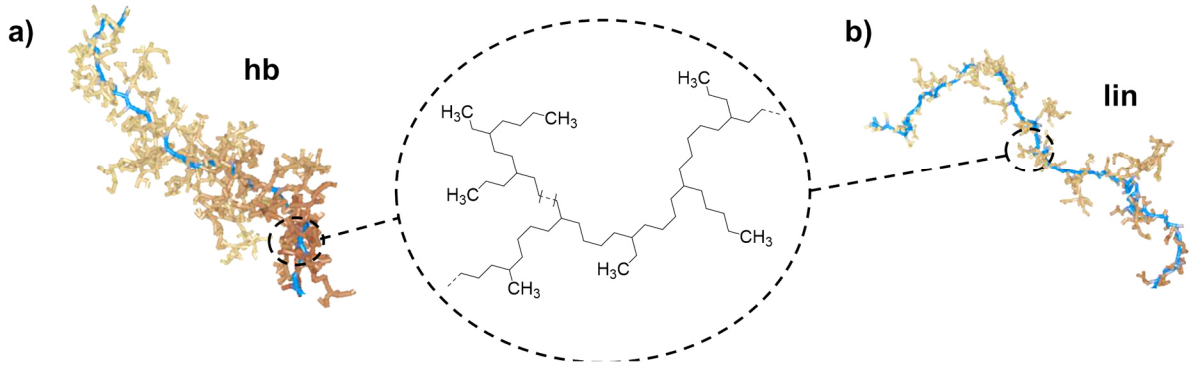

Figure 5.5 Simulated appearance of cwPE of the polymer model library investigated in this study ranging from **a)** hyperbranched (hb) to **b)** linear (lin) topology, comprised of short chain branches, long chain branches as well as branch-on-branches. Adapted with permission from Ref. [259] Copyright © 2019 American Chemical Society.

Prior to the ThFFF study, the polymers were comprehensively characterized by the state-of-the-art approach HT-SEC-d4 (see section 3.3) in order to set a validated basis for the development of a potential branching analysis approach based on ThFFF retention. Thereby, branching characteristics were expressed by the radius contraction factor g, B, LCB and M_{Seg}. Unlike the polyester system, for polyethylene in general no real linear reference material is available for the calculation of the contraction factors, which would additionally be soluble under the same experimental conditions. Instead, theoretical extrapolation-derived scaling models can be applied for the calculation of $R_{G,lin} = 0.023\ M^{0.58}$ and $[\eta]_{lin} = 0.053\ M^{0.70}$, respectively. The validity of these models was confirmed by Plüschke and coworkers for regular types of PE[61] as well as for cwPE.[259]

Like in the ThFFF study of the silylated polyesters, also in this study the ThFFF results were combined with offline temperature dependent DLS measurements to allow an accurate calculation of thermal diffusion coefficients with DLS-determined values of D and accurately calculated Soret coefficients. In contrast to the polyester samples, the cwPE samples have very narrow molar mass dispersity, which allowed a well reliable calculation of average D_T from dRI peak apex retention times and offline-measured D. The required S_T were calculated again with non-parabolicity correction and numerically solved ThFFF retention parameter from measured retention times. The evaluation of the recorded data from ThFFF-MALS-dRI analysis were found to be in good agreement with the results obtained by HT-SEC-d4. A comparative summary of the polymer properties is reported in Table 1 of publication 8.4.

As a first outcome of this work, for the first time, a clear **dependency of D_T on the polymer topology** could be **undoubtedly confirmed**. As illustrated in Fig. 5.6 a, D_T shows an exponentially decreasing trend with shortening linear segments in the polymer structure or with a growing number of branches per molecule, respectively. A trend to even negative D_T can be approximated, which would describe a thermophilic behavior for oligomeric segments. On the other hand, it indicates the trend that D_T apparently becomes independent on the molar mass for large linear segments e.g. represented by entirely linear polymers. Both findings are in agreement with results from Stadelmaier and Köhler, who found a thermophilic behavior for n-alkanes and other mono-/oligomers in various solvents and contrarily a thermophobic behavior of their polymeric analogues upon M_w of 10 000 g mol^{-1}.[174]

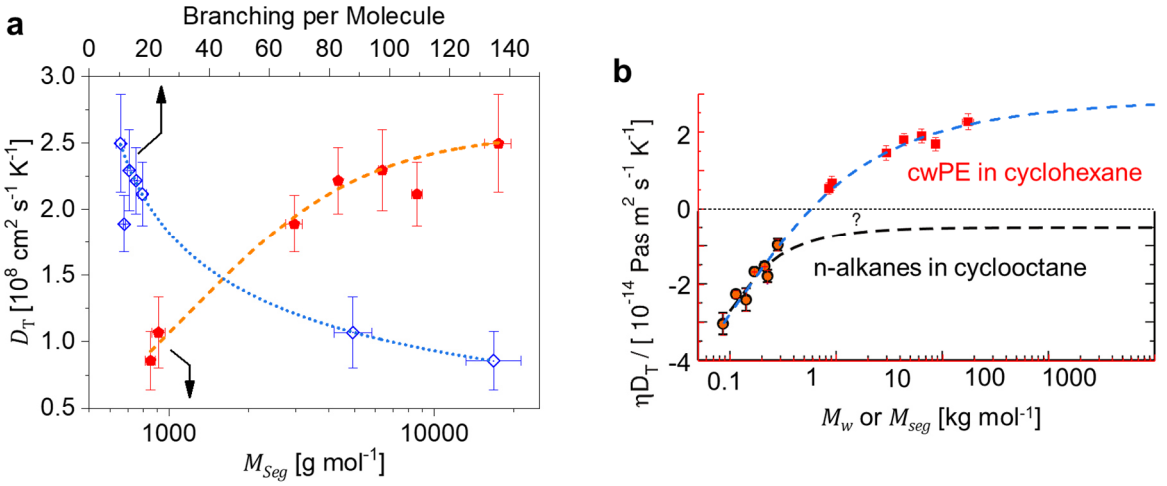

Figure 5.6 a Correlation of D_T (ThFFF, constant ΔT = 101 K, T_c = 23 °C) to the polymer topology expressed by B and M_{Seg}. The dotted and dashed lines are for guiding the eye. **b** Comparison of normalized D_T from TDFRS studies with n-alkanes and values from this study. Orange circles indicate replotted data for n-alkanes in cyclooctane from the original report (for exact alignment).[174] Plot in a reprinted with permission from publication 8.4, plot in b adapted with permission from Ref. [174]. Copyright © 2019 (a), © 2009 (b) American Chemical Society.

This system furthermore allows in sufficient comparability to elucidate the by Köhler assumed trend of n-alkane's thermal diffusion scaling with the chain length (shown in Fig. 5.6 b with superimposed normalized D_T from this study). It was not possible to directly investigate this trend due to the insolubility of long n-paraffins at ambient temperatures. The physicochemical properties of cyclohexane are, except of the dynamic viscosity, closely similar to cyclooctane as used in the work by Stadelmaier and Köhler. The comparison indicated in Fig. 5.6 b confirms, that polymers above a certain molecular size generally become thermophobic. This trend is also reported for PS,[173,175] polydimethylsiloxane or poly(alkyl acrylates) in various solvents.[175]

In contrast to the polyester system investigated in the study above, the calculation of Soret contraction factors was more challenging. Unlike for g and g' from the HT-SEC-d4 analysis, here no theoretical reference model available or alternatively, D_T for a linear polyethylene are not yet reported. To enable a calculation of Soret contraction factors despite this lack of information, a model to predict S_T for linear analogues of the same M_w has been developed by extrapolation of S_T versus M_{Seg} to an assumed linear segment equal to the molar mass of the entire polymer (Eq. (5.5)).

$$S_{T,lin} = \frac{(a_1 \cdot \Delta T + a_2) \cdot lnM_w - (a_3 \cdot \Delta T + a_4)}{\Delta T} \tag{5.5}$$

The polynomial coefficients for several experimental conditions (T_c, stop flow) are reported in publication 8.4. The model was in fact found to be consistent and so derived g'' were found in very close agreement to the mean radius contraction factors g from HT-SEC, which indicates next to the Soret contraction study reported above and in publication 8.3 also in this study its profound capability to provide information about polymer topology.

However, to provide a resolved information per sample from the fractograms in terms of quasi-online data, another subsequent fitting approach had to be developed. The very narrow dispersity of the samples being useful for accurate average data obstructs the generation of online data in this study. The approach to calculate $S_{T,lin}$ from a calibration of the molar mass versus retention time of an almost linear sample was also not applicable, due to the very narrow dispersity of the cwPE samples, which is impaired in the calculations by the broad retention range in ThFFF fractograms due to a highly selective separation and a certain portion of non-equilibrium band broadening (a general effect in FFF separations). Therefore, a recursive fitting approach was developed using *LCB* data from HT-SEC-d4 analysis and peak apex data from ThFFF separation as a supporting basis. In that, *LCB* data from HT-SEC-d4 were fitted against the molar mass and rematched to the molar mass trace from the ThFFF

analysis. This approach (fully outlined in publication 8.4) allowed to calculate *LCB* on the basis of ThFFF retention data. *LCB* are originally defined on the basis of the radius contraction factor only. Therefore, it is required to transform *g''* and vice versa for *LCB* calculations, which can be done using a similar exponential relation like between *g* and *g'* (Eq. (2.1)). As indicated in Fig. 5.5 b and c, the developed recursive fitting approach provides on one hand reliable *LCB* distributions, validated for the model library of cwPE samples as well as for unknown samples which were not part of the fitting process. On the other hand, it enables the generation of quasi online data for the Soret contraction analysis of very narrowly dispersed polyethylene samples with equal ThFFF retention characteristics (Fig. 5.7 a). This can be assessed as a limitation of this approach. For broadly distributed systems (regarding M_w and branching) only an online determination by a separate detection may generate reliable data for an accurate online branching analysis on the basis of ThFFF separation and the Soret contraction concept. Another challenge in current ThFFF analyses is the relatively low analyte concentration per slice, which makes a reliable measurement of *D* by online-DLS challenging. In that case *D* could be alternatively accessed indirectly via $R_{[\eta]}$ from online viscometric detection, although a certain systematic error needs to be taken into account, because R_h and $R_{[\eta]}$ potentially differ for various polymers and topologies despite both are sphere-equivalent radii.[61,300] Advances in technical development e.g. flow cell design of online MALS[301] and potentially DLS could also enable more sensitive detection in future.

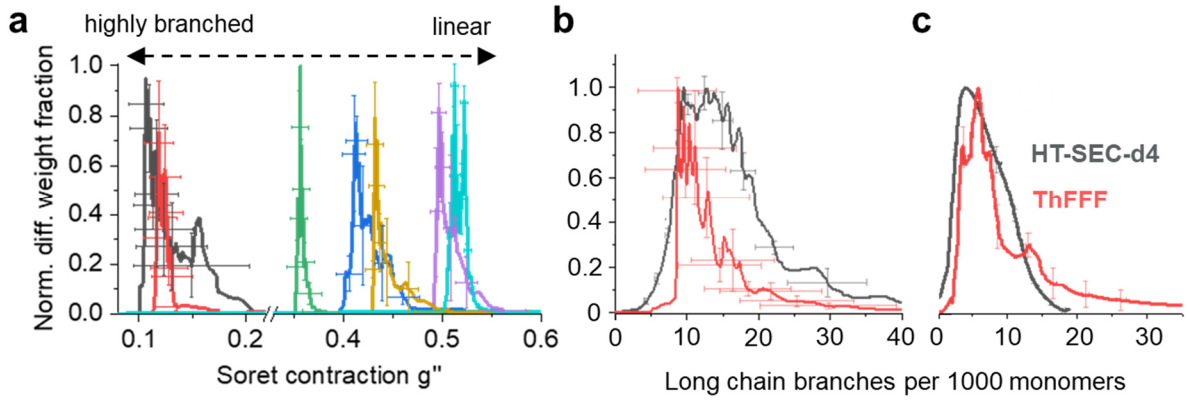

Figure 5.7 a Normalized differential weight distribution of generated quasi online data of *g''* for seven differently branched cwPE. Normalized *LCB* distributions calculated on the basis of ThFFF retention data by an optimized fitting process are displayed in **b** in comparison to *LCB* distributions from HT-SEC-d4 state-of-the-art analysis for the most branched sample shown in a and in **c** validated with a sample, which was not part of the fitting process. Reprinted with permission from publication 8.4. Copyright © 2019 American Chemical Society.

In publication 8.2 in this thesis, the Mes D_T model was proven to predict D_T in high and improved accuracy with the help of HSP and segmental sizes for a particular polymer. By taking this as a basis, **an additional outcome** was derived by applying the Mes D_T model in reverse mode to obtain information about molecular chain stiffness or branching density directly from thermophoretic data by calculation of r_m from experimentally measured D_T. Depending on the underlying polymer model, r_m or the corresponding diameter can be somewhat interpreted as the Kuhn length, persistence length or a related segment length such as the size of a thermal blob as defined by de Gennes[302] with the Flory theory.[292] A thermal blob in a polymer chain may actually become theoretically equal to the Kuhn segment length for a polymer depending on the solvent conditions. To avoid misinterpretation, with r_m we referred in this study to a thermophoretically effective blob size. The elucidation of relations to blob sizes of other polymer models was not part of this study and is delegated to future work.

The calculation of blob diameters from experimental D_T measured for the cwPE model library from publication 8.4 by ThFFF combined with offline DLS (shown in Fig. 5.6 exemplarily in cyclohexane) yielded in fact an increasing trend in correlation to increasing branching degree (expressed here by *LCB*) for data measured in good solvents such as cyclohexane and paraffin oil as indicated in Fig. 5.8 a. Instead, blob diameters probed in chloroform are found to remain about constant regardless of branching with general slightly larger sizes, indicating somewhat an increased chain stiffness. A similar or even slightly reverse trend is assumed for THF. However, the found blob diameter for THF can only be seen as lower limit of its actual size, because D_T data from ThFFF are not fully resolved due to the very low retention (see Fig. 5.2 a). The trend seen in good solvents is in agreement with the theory, because with higher branching the stiffness of the polymer should increase accordingly due to increasing steric hindrance by a higher density of branches along the main backbone chain.[259] In a thermodynamically good solvent, the solvent can freely drain through the (brush-like) polymer coil. In a poor solvent instead, the polymer coil is rather collapsed with reduced interaction to the solvent, which leads to a generally larger blob diameter without significant dependency on *LCB*.[302]

The blob diameter of cwPE in collapsed state as well as in high branching limit is consistent to the blob size of cwPE (about 8 to 10 nm) found by atomic force microscopy (AFM) and SANS reported in previous studies (see Fig. 3.5 b).[259] The trend of increasing segment lengths with increasing number of branching is also reported for short chain branched (*SCB*), regular type PE as indicated in Fig. 5.8 b.[303] Although this system is not directly comparable to cwPE in terms of *LCB*, it can be discussed to indicate the same trend.

Combining the results from publication 8.2 and 8.4 in fact confirm, that the local stiffness of a polymer can be validated by thermal diffusion measurements. Among other methods to determine D_T, this can be accurately done by ThFFF analysis. This allows a new, alternative access to local chain conformation, microstructure or fractals, respectively, normally measured by scattering methods such as small-angle neutron or x-ray scattering.[303,304]

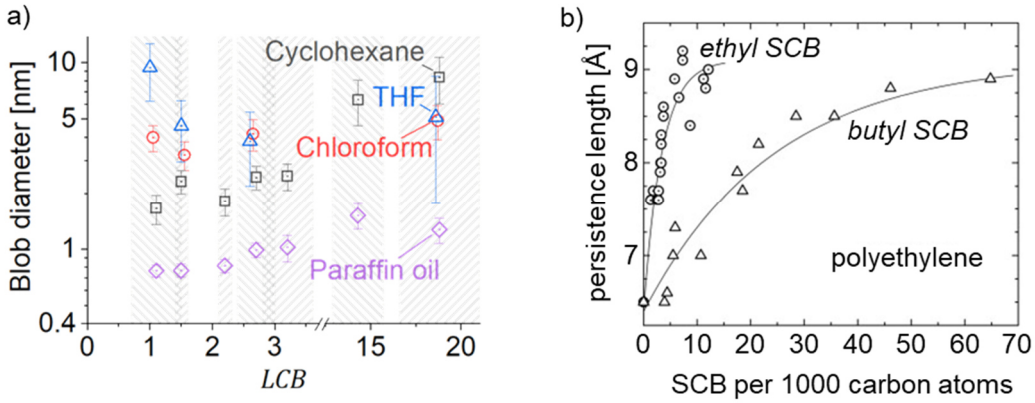

Figure 5.8 a Calculated blob diameters from experimental D_T by reverse application of the Mes D_T model in combination with the Hansen Solubility theory. The hashed regions indicate the error bars of the *LCB* values (from HT-SEC-d4, publication 8.4). Reprinted with permission from publication 8.2. Copyright © 2020 American Chemical Society. **b** Persistence length of regular PE from SANS versus the number of ethyl (circles)[305] or butyl (triangles)[303] short-chain branches per 1000 carbon atoms. Reprinted with permission from Ref. [306] Copyright © 2013 Elsevier Inc.

Furthermore, next to the ThFFF study of the silylated polyesters in publication 8.3 the existence of highly selective and rater non-selective solvents (e.g. chloroform) in terms of thermal diffusion is proven. The correlation of thermal diffusion to the thermodynamic solvent quality is also in certain aspects in agreement to Köhler et al., who concluded, that mainly the (Kuhn) segments from the thin drained outer layer of the polymer coil take part in the thermophoretic motion.[296] However, regarding the variety of blob sizes depending on polymer architecture and solvent quality found in this study (Fig. 5.8 a), their conclusion needs to be reevaluated concerning the question to which depth towards the center of the polymer coil segments contribute to the overall thermal diffusion.

5.4. ThFFF applied for Orthogonal Polymer Analysis of Electron Beam Irradiated Thermoplastic Polyurethane

In the study reported **in publication 8.5** ThFFF was used as a complementary method to clarify open questions about the structure of thermoplastic polyurethane material upon irradiation and whether crosslinking or chain scission occurs predominantly, which cannot be fully understood by data from classical polymer analysis only, like from DSC, FTIR and SEC. Therefore, the impact of electron beam irradiation on TPU in doses up to 300 kGy applied under inert atmosphere at room temperature and at 100 °C was investigated for an aliphatic and an aromatic commercially available thermoplastic polyurethane material with an equal quantitative composition of hard and soft segments. Possible radiation-induced reactions and mechanisms in TPU discussed in the literature are summarized and illustrated in Fig. 5.9. Irradiation-caused changes in chemical structure, molar mass and size were characterized by means of infrared spectroscopy (ATR-FTIR), differential scanning calorimetry (DSC), SEC and, complementary to that, by ThFFF. Both separation techniques were coupled to MALS and dRI detection. SEC with molar mass calibration was used additionally for comparison.

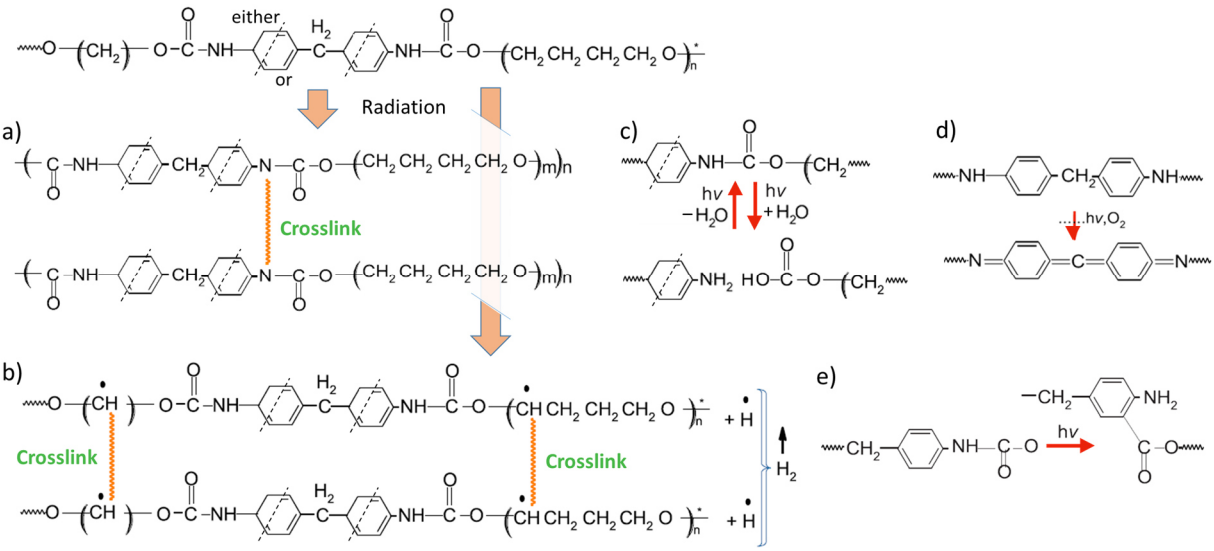

Figure 5.9 Possible reactions in MDI or H_{12}MDI-based thermoplastic polyurethanes discussed in the literature: Crosslinking in **a)** between hard segments or in **b)** between hard segments,[235] **c)** cleavage and recombination of urethane bonds,[307] **d)** oxidization of the central methylene group (only in aromatic TPU)[235] or **e)** formation of primary amines e.g. by Photo-Fries rearrangement.[308] Adapted with permission from Ref. [235] (a to d) and Ref. [308]. Copyright © 2013 (a to d) and © 2009 (e) Elsevier B.V.

Initial investigations by ATR-FT-IR indicated for both materials, that electron beam irradiation initiates a cascade of parallel chemical reactions by formed radicals including chain scission and chain recombination leading to an increase of branching (seen by changes in

bands of methylene stretching vibrations), crosslinking and the emerge of new functional groups and linkages such as amines, amides or carboxylic acids, which are not apparent initially. Notable changes in the material were recognized already upon low irradiation doses.

Parallel studies by DSC yielded in agreement with the findings from the ATR-FTIR study in both materials signs for isomerization or branching, indicated by a slight decrease in their glass transition temperatures. The most prominent changes observed in ATR-FTIR and DSC are shown in Fig. 5.10 for the aliphatic material. Radiation related differences between the materials were mainly attributed to their different morphology. The aliphatic TPU appeared as thoroughly amorphous material with a distinct glass transition, whereas the aromatic TPU showed a highly crystalline character with a complex phase transition behavior seen in multiple melting and crystallization peaks. Instead, the aromatic TPU indicated only a barely recognizable glass transition related to its soft segments. Meanwhile the impact of irradiation affected tremendously the morphology of the aromatic material. A transformation of the hard domains from well-ordered to increasingly disordered crystallites were found.

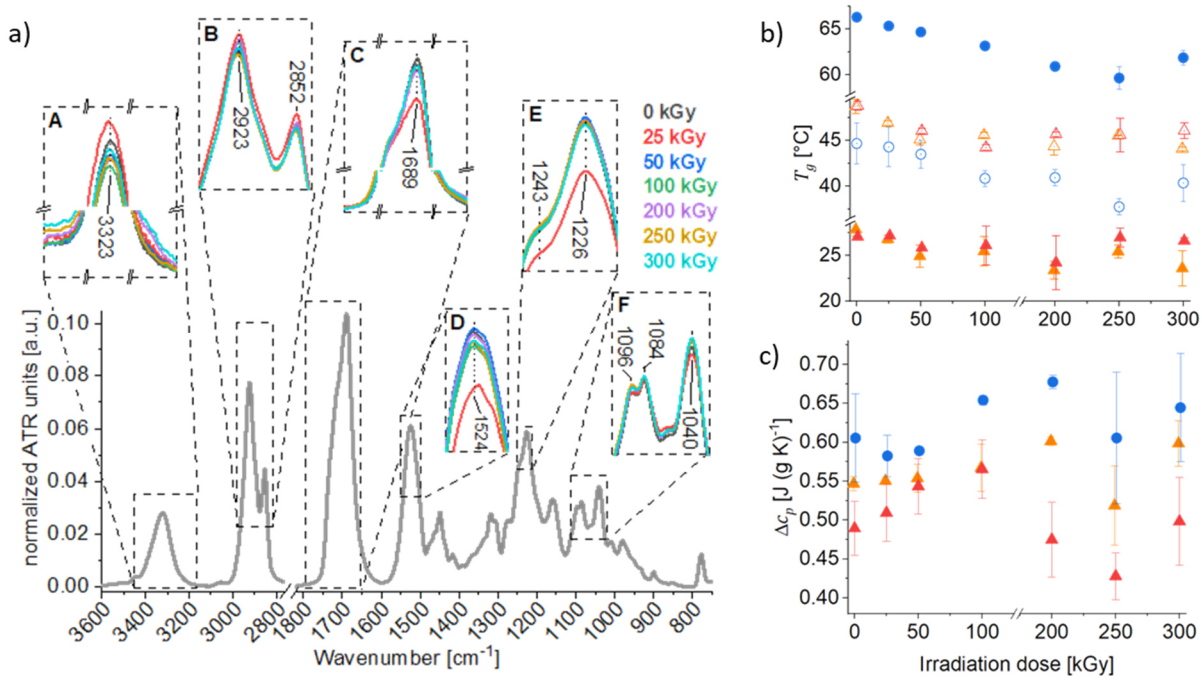

Figure 5.10 a) ATR-FTIR study of the aliphatic TPU in a series of increasing irradiation dose applied onto the material with changes observed in bands of amide A (A), methylene stretching vibrations (B), amide I, II and III (C, D and E) and the region of C–O–C stretching vibrations from both, urethane and (soft segment) ester groups (F). **b)** Glass transition temperatures (T_g) of the aliphatic TPU from the first DSC heating scan (orange), from the cooling scan (blue) and the second heating scan (red). Filled symbols indicate onset T_g and open symbols show mid-point T_g at half step height. **c)** indicates the corresponding step heights (Heat capacity drops). Adapted with permission from publication 8.5.

However, the characterization of radiation induced changes was partially obstructed by superimposed reorganization effects being typical for TPU with high hard segment content,[309,310] which did not allow the elucidation whether different crystallite polymorphs in the material are formed or the observed multiple melting behavior is rather related to micro-phase mixing assumingly on the outer part of the increasingly disordered crystallites. Overall, the combination of the findings from both ATR-FT-IR and DSC allowed the conclusion that in the aliphatic TPU both hard and soft segments are equally affected upon irradiation, whereas in the aromatic TPU predominantly the soft segments degrade earlier, indicated by signs of isomerization in the polyol segments.

Despite the fact that ATR-FT-IR and DSC indicated mainly signs of degradation, previous studies also reported crosslinking as a dominant mechanism[235,236]. However, the conclusions in the literature were contradictory. Therefore, molar mass and size characterizations were carried out to address this question. Thereby, initial analysis by SEC-MALS-dRI revealed for both materials on one hand the formation of a highly crosslinked fraction with ultra-high molar masses far beyond the separation range resolvable by SEC, but on the other hand also an increasing fraction of lower molar masses representing degradation products and a partial co-elution of several fractions due to apparently differing topology. These interferences may have significant influence on the comparability of the molar masses and sizes. However, in recently reported studies this issue had been overlooked or ignored so far[237,246,311,312] even though abnormal elution behavior of TPU material is already known for longer time.[313]

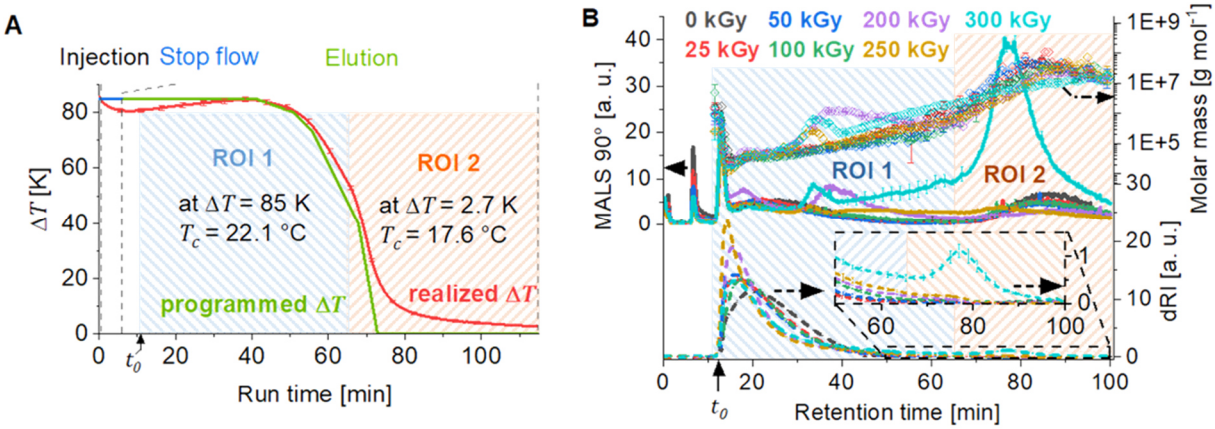

Figure 5.11 A Optimized separation method used for ThFFF separations of all TPU irradiation series in publication 8.5 with two assigned regions of interest ROI 1 ad ROI 2 for low and high molecular weight fractions being separated and recorded in ThFFF fractograms shown in **B** for the aliphatic TPU. The realized field strength shown in A is a result of the control in autosampled measurements. Changes in ΔT also affect T_c due to a non-programmable cooling, which had to be respected in ThFFF calculations of this study. Image in B reprinted with permission from publication 8.5. Copyright © 2021 Elsevier B.V.

For this reason, ThFFF separation coupled to absolute molar mass determination has been applied in this study to resolve molar mass, size, and scaling with focus on the ultra-high molecular weight fraction. The ThFFF separation was carried out in programmed field conditions to maintain on one hand a separation of the lower molecular weight fraction and to keep the analysis time in a reasonable time limit on the other hand. The optimized field-programmed method applied in all separations in this study and exemplary the fractograms of the aliphatic TPU investigated as irradiation series is shown in Fig. 5.11. The fractograms given in Fig. 5.11 B clearly indicate the need of another separation method next to SEC. A detailed quantification per region of interest is shown in Fig. 5 reported in publication 8.5. With the help of ThFFF it was possible to resolve in particular the region of the high molar mass fraction. However, ThFFF was not intended to substitute SEC in this study, because it is unable to sufficiently resolve the low molar mass range of the apparently degraded material. A comparison of the differential molar mass distribution as illustrated in Fig. 5.12 between the different methods indicate their optimal separation range. For comparison it is indicated, that SEC with relative molar mass calibration (often done on the basis of narrow PS standards) overestimate both, average molar mass moments as well as the molar mass dispersity and is hence not recommended for investigations of irradiated polymer materials. It is to be noted, that molar mass characterization with MALS may not resemble in general low molar masses in the range of oligomers due to their very low scattering intensity. However, in the current case it is questionable if significant amount of such low molar masses found by standard-calibrated SEC are truly apparent in the material or rather an artefact of delayed elution.

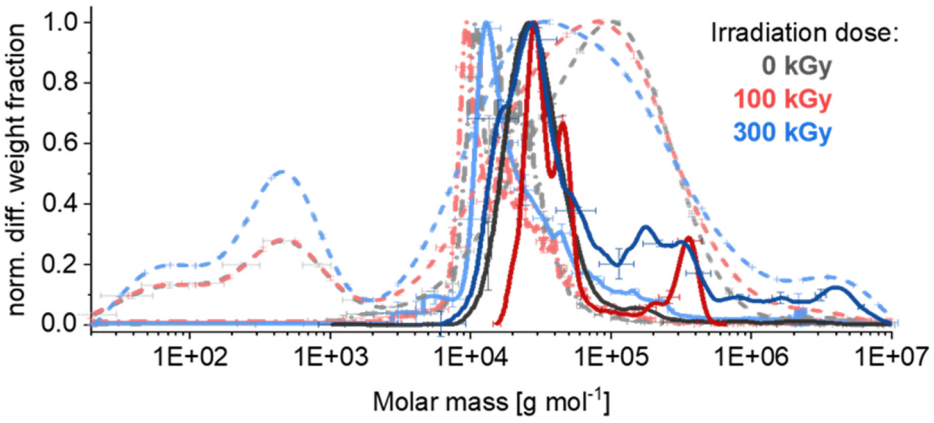

Figure 5.12 Normalized molar mass differential distributions of the aliphatic TPU determined with the different analysis approaches SEC calibrated with narrow PS standards (dashed), SEC-MALS-dRI (dashed-dotted) and ThFFF-MALS-dRI. Reprinted with permission from publication 8.5. Copyright © 2021 Elsevier B.V.

Meanwhile due to the much greater separation range and the absence of any potentially interfering stationary phase ThFFF is found superior in resolving particularly the high molar mass region showing fractions, which cannot be seen by SEC.

Additionally, MALS-dRI detection allowed for an evaluation of the molecular shape of the fractions above the required minimum size (see section 1.1.3.1) with the help of the scaling exponent ν_R yielded by conformation analysis. In both, SEC and ThFFF ν_R showed a general trend to lower values approaching the theoretical limit for a dense sphere with increasing irradiation dose, which confirms the findings by ATR-FTIR and DSC of irradiation-induced isomerization, branching or crosslinking as causes for the observed compaction.

However, the conformation analysis allowed the quantification of only a small population in the materials since the majority of the material has molecular sizes below the limit for measuring gyration radii (< 12 nm). To gain a better overview over an extended fraction of the material, changes in topology were addressed by a thermophoretic analysis as a second independent investigation based on the ThFFF calculation procedures outlined in the sections above, since the Soret coefficients were confirmed in previous investigations to display changes in topology or branching (see section 3.4). Alterations in chemical composition found by ATR-FTIR are accounted to have a negligible effect on S_T of the irradiated TPU materials, because its influence on S_T was reported to be of lower quantity than the influence of changing polymer architecture in terms of branching[112,113,282] or tacticity.[266,267] The differential distributions of S_T as exemplarily shown in Fig. 5.13 for the aliphatic TPU material show a trend towards lower S_T roughly correlating with the irradiation dose applied in other material, which indicates a shortening of linear segments in the polymer chains. This agrees with the findings reported in publication 8.3 and 8.4 of this thesis. The influence of branching on S_T was investigated in objective 3 and 4 as summarized in the following sections.

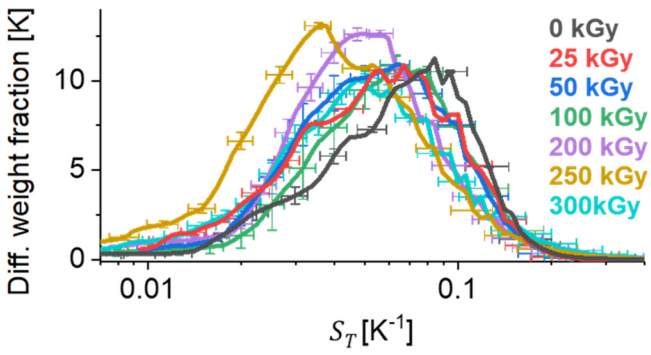

Figure 5.13 Differential S_T weight distributions calculated from the full ThFFF fractograms of the aliphatic TPU series illustrated in Fig. 5.11 B. Reprinted with permission from publication 8.5. Copyright © 2021 Elsevier B.V.

The aromatic TPU material did not show significant trends in its S_T distribution on the first view regardless if the irradiation temperature. However, small differences regarding irradiation dose and temperature were found by further analysis of the cumulative S_T distribution using alternative measures. This matter is further explained in publication 8.5.

For calculation of S_T values used in the weight distributions the influence of secondary relaxation had to be respected. Secondary relaxation in FFF separations is an effect of delayed elution in non-constant field conditions with large increments. Under conditions of fast decreasing field force the dynamic relaxation equilibrium lags increasingly behind the change rate of the field force resulting in later retention times than expected for an instantaneous reaction of the analytes on the field strength. This can be generally described for the retention ratio R by introduction of a departure term Δ as stated in Eq. (5.6)

$$R = R_{instant} \cdot (1 + \Delta) \tag{5.6}$$

In SdFFF, where separations e.g. of particles are carried out to a great extend in field programming conditions, an approximation for Δ based on the particle diffusion coefficient and the field increment has been developed.[124] However, for solvated polymers separated by ThFFF no investigation of this phenomenon has been carried out yet. So far, polymers were assumed to adapt instantaneously to a non-constant field force.

In order to approximate the influence of secondary relaxation in the programmed method used in this study on one hand, but also to skip experiments exceeding the scope of this study, an approach based on reference experiments with known polymer standards has been chosen. For that, broad reference samples of PS and PMMA covering a wide retention range were first analyzed by ThFFF under constant field conditions. Based on these retention data, Soret coefficients were calculated by Eq. (5.3) incorporating the non-parabolicity of the flow-profile with the help of the newly tabulated polynomial coefficients reported in publication 8.1. The so calculated S_T were fitted against the molar mass in a double logarithmic plot as S_T calibration defined by the molar mass. The validity of this calibration approach and the direct proportionality of S_T to M_w for linear polymers had been confirmed in previous studies.[262,314,315] The S_T - M_w calibration allowed in the following to retrace the effective ΔT from the molar mass trace recorded in field programmed separations) of the same reference samples with the help of Eqs. (2.24) and (5.3). Next to the original ΔT method shown in Fig. 5.11 also a shortened version was tested without the constant part in the beginning in order to acquire a sufficiently resolved molar mass trace for the calculation and to probe the robustness of this approach. Thereby S_T was assumed to remain constant independently on the cold wall temperature.

This simplification holds true for a change of not more than 5 K as reported previously in universal calibrations tested for ThFFF.[316] The retraced effective ΔT showed in fact a significant departure from the actual recorded field strength for fast decreasing ΔT, which confirms that this effect cannot be ignored in accurate calculations. With the help of this reference experiment an approximation of departure term Δ given in Eq. (5.7) was empirically found by matching the retraced effective ΔT.

$$\Delta = \frac{-0.005}{R_{init.}} \cdot ln\left(\left|\frac{d\Delta T}{dR}\right|\right) \tag{5.7}$$

This Δ-approximation for ThFFF is inspired by the approximation reported for SdFFF, which also relies on the field decay (expressed here as $^{d\Delta T}/_{dR}$) and the retention ratio R_{init} at the initial time of the field decay.[124] As confirmed in Fig. 5.14, the calculated retention time with correction of the secondary relaxation delay (plotted with the actual recorded ΔT) are found to be in good agreement to the retraced effective ΔT with nominal retention time.

Overall, this study unraveled, that crosslinking is the dominating effect under irradiation influence prevailing chain scission and degradation, which is in agreement to the literature for aliphatic[236] and aromatic TPU.[235] Thereby, the aliphatic TPU indicated a stronger tendency to crosslinking than the aromatic material, which instead showed a higher resistance to irradiation.

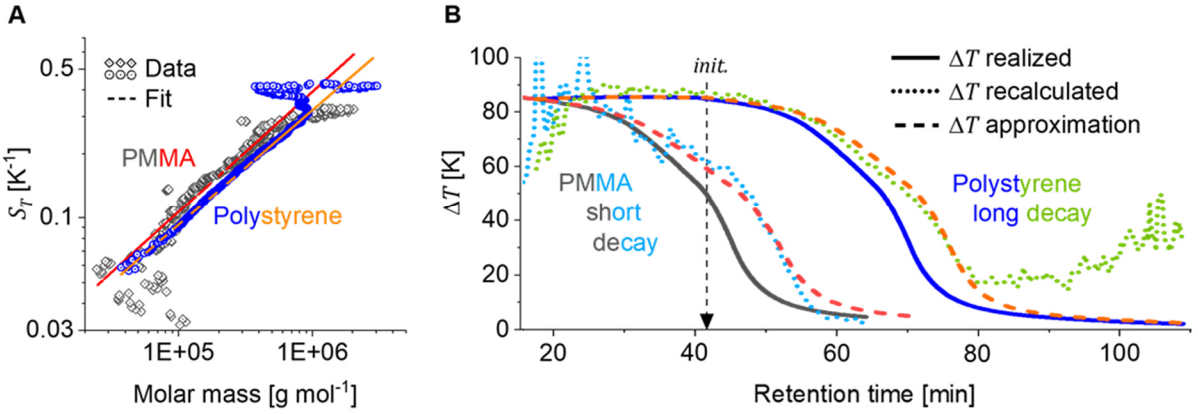

Figure 5.14 Summary of the approximate secondary relaxation correction developed in this study based on S_T – molar mass calibration of broad PS and PMMA reference samples (**A**), which is used to evaluate the secondary relaxation influence by retracing the effective ΔT from the measured molar mass retention (**B**). The moment indicated with init. refers to the initial time of the field decay. Reprinted with permission from publication 8.5. Copyright © 2021 Elsevier B.V.

6. Conclusions and Future Prospects

Field flow fractionation (FFF) in its specific subtypes is established to successfully address and overcome challenges of column-based separations, because it does not rely on a stationary phase and provides a far broader separation range with higher selectivity compared to column-based separation methods such as size exclusion chromatography (SEC). However, the potential of FFF for application as alternative or complementary separation technique is not fully understood due to the lack of profound theoretical background and optimization in the interpretation of results. In particular, in Thermal FFF (ThFFF) the underlying separation mechanism is not yet fully understood. Furthermore, calculations for generation and interpretation of results were so far elaborate due to lack of applicable mathematical solutions. Main scope of this dissertation was therefore to generate advances in the theoretical understanding of ThFFF and validation by experiment.

In order to obtain accurate thermophoretic data from ThFFF experiments a correction of the distortion in the laminar velocity flow-profile occurring in ThFFF is inevitable. Therefore, the first outcome of this thesis is the provision of solvent specific coefficients, numerically calculated for in total 59 solvents, allowing an easy applicable and accurate non-parabolicity correction of the laminar flow-profiles This work represents an extension and revision of the previous theoretical considerations including the field of normal and high temperature ThFFF. Additionally, a modified solution of the ThFFF retention equation is proposed to match severely distorted flow-profiles, maintaining an easy and user-friendly non-parabolicity correction with only one adjustable parameter. Furthermore, a fast and still accurate approximation was empirically developed, which avoids numerical, iterative computation for the calculation of physicochemical properties from ThFFF retention data.

The second outcome of this dissertation is the advance in the understanding of polymer thermal diffusion phenomena and to use this knowledge to establish ThFFF as a convenient characterization method. Due to a lack of a fundamental theory to model thermophoresis in particular for liquids, finding solvents that yield sufficiently high retention in ThFFF remained so far an elaborate trial-and-error process. The latest thermal diffusion prediction theories proved to shorten this process tremendously, but up to this study they have not reached a prediction level yet which accurately matches experimentally found data. Therefore, advances in polymer thermal diffusion have been made using a revisited approach of the latest thermal diffusion prediction model combined with the Hansen solubility theory. Suggestions for a highly selective solvents were derived for a potential ThFFF investigation of regular

polyolefins in a high temperature approach without the requirement of costly and difficult technical effort. The improved prediction power allowed to validate local segmental sizes as measures of the stiffness or microstructure in polymer chains of varying topology using the revisited thermal diffusion prediction approach in inverse mode with experimental thermal diffusion data.

In the third research outcome, ThFFF has been proven to be used as branching characterization method of two different polymer model systems, silylated aromatic-aliphatic polyesters and disordered bottlebrush-like polyethylene, by resolving their topology characteristics based on their ThFFF retention behavior. This study clearly indicates, that thermophoretic properties measured by ThFFF provide a new complementary route to polymer architecture analysis. Based on differences in the thermal diffusion behavior, a new model has been developed for the application of ThFFF as an alternative to the established branching calculation approaches relying on light scattering or online viscometric detection. These results demonstrate for the first time the usefulness of the Soret contraction concept to characterize (highly)-branched polymer systems on the basis of thermophoresis and its additional sensitivity to cyclic polymers is underlined.

Next to the application of ThFFF as branching analysis method, ThFFF was applied to amend limited characterization capabilities by size exclusion chromatography to elucidate native properties and induced alterations in complex polymer systems. The impact of electron beam irradiation on thermoplastic polyurethane (TPU) is such a controversially discussed topic in polymer research. In this work, the impact of electron beam irradiation on TPU was studied using infrared spectroscopy, differential scanning calorimetry, SEC and complementarily ThFFF. Material alterations were correlated with trends regarding degradation, crosslinking or branching. Thereby, as fourth research outcome the high potential of ThFFF coupled to light scattering detections is shown for thermophoretic analysis and to elucidate molar mass and conformation distributions of highly crosslinked and ultra-high-molecular polymer systems. This study has unraveled, that crosslinking is the dominating effect in TPU under irradiation prevailing chain scission and degradation, which is also indicated in previously reported studies, but were not clearly proven in terms of molar mass and related measures. Additionally, an empirically derived approach in respect to secondary relaxation phenomena occurring in non-constant separation conditions is proposed. This phenomenon is known and considered in analysis by sedimentation and crossflow-based FFF, but had been so far ignored in ThFFF.

The overall outcome of this thesis opens new avenues for correct interpretation of the physicochemical properties of macromolecules like topology and conformation, showing that ThFFF is highly suitable as thermophoretic and potentially as complementary branching characterization method of complex macromolecular architectures. Yet, there is still need for fundamental understanding of thermophoresis and accurate modelling of ThFFF retention for embedding ThFFF in the portfolio of combined polymer characterization techniques. To enhance the selectivity in ThFFF separations also binary solvent mixtures were successfully tested previously.[317,318] However, the non-parabolicity correction for solvent mixtures reaches only a limited accuracy with the polynomial approach developed in the thesis. Hence, future works is needed to encounter mixing phenomena seen in the vast majority of non-ideal solvent mixtures, which show regularly nonlinear and occasionally complex dependencies of dynamic viscosity and thermal conductivity to the molar mixing ratio. Solutions such as empirical interaction parameters[319,320] or approaches based on the free energy of activation[321] are proposed to be implemented in the flow-profile correction of ThFFF calculations.

Furthermore, despite great advances in the predictability of thermal diffusion being achieved with this work, further effects need to be assessed and implemented in future prediction models. Such effects are electrostatic contributions or hydrogen bonding. Additionally, the prediction models need to be enhanced regarding the transition from dissolved polymers to dispersed nano- or microparticles. For well predictable systems instead, thermal diffusion models may be tested in the future with regard to the nature and comparability of a local size measure indicating the stiffness or microstructure in a dissolved polymer, which can be probed by experimentally measured thermal diffusion.

Regarding the investigation of chemically and topologically complex polymer systems by ThFFF hyphenated to absolute molar mass and size detection, further improvements are accounted by implementation of a direct measurement of diffusion coefficients by online dynamic light scattering or in case of very low concentrations indirectly by online viscometry. This will allow a comprehensive branching characterization by multidetection ThFFF encountering dispersities in molar mass, chemical composition and topology.

7. BIBLIOGRAPHY

[1] Jenkins, A. D.; Stepto, R. F. T.; Kratochvíl, P.; Suter, U. W. *Pure Appl. Chem.* **1996**, *68* (12), 2287–2311. doi: 10.1351/pac199668122287.

[2] Hurley, P. E. *J. Macromol. Sci. Part A - Chem.* **1981**, *15* (7), 1279–1287. doi: 10.1080/00222338108056785.

[3] Nicholson, J. W. In *The Chemistry of Polymers*; The Royal Society of Chemistry: London, 2017; Vol. 1, pp 2–5. doi: 10.1039/c000660m.

[4] Piringer, O. G.; Baner, A. L. *Plastic Packaging: Interactions with Food and Pharmaceuticals*; WILEY-VCH Verlag GmbH & Co. KGaA, 2008, pp. 32–59. doi: 10.1002/9783527621422.

[5] Awaja, F.; Gilbert, M.; Kelly, G.; Fox, B.; Pigram, P. J. *Prog. Polym. Sci.* **2009**, *34* (9), 948–968. doi: 10.1016/j.progpolymsci.2009.04.007.

[6] Beecroft, L. L.; Ober, C. K. *J. Macromol. Sci. Part A* **1997**, *34* (4), 573–586. doi: 10.1080/10601329708014985.

[7] Wei, Q.; Pötzsch, R.; Liu, X.; Komber, H.; Kiriy, A.; Voit, B.; Will, P. A.; Lenk, S.; Reineke, S. *Adv. Funct. Mater.* **2016**, *26* (15), 2545–2553. doi:10.1002/adfm.201504914.

[8] Liang, S.; Neisius, N. M.; Gaan, S. *Prog. Org. Coatings* **2013**, *76* (11), 1642–1665. doi: 10.1016/j.porgcoat.2013.07.014.

[9] Voit, B.; Haag, R.; Appelhans, D.; Welzel, P. B. *Bio-and Multifunctional Polymer Architectures*; John Wiley & Sons, Inc.: Hoboken, New Jersey, 2016. doi: 10.1002%2F9781119188896.

[10] Rehm, B. H. A.; Moradali, M. F. *Advances in Biopolymers for Biomedical and Biotechnological Applications*; Advanced Biotechnology; Wiley-VCH: Weinheim, 2020.

[11] Hu, J.; Chen, S. *J. Mater. Chem.* **2010**, *20* (17), 3346–3355. doi: 10.1039/B922872A.

[12] Eling, B.; Tomović, Ž.; Schädler, V. *Macromol. Chem. Phys.* **2020**, *221* (14), 2000114. doi: 10.1002/macp.202000114.

[13] Krause, M. Glauner, P., Plugmann, P., Eds.; Springer International Publishing: Cham, 2020; pp 233–243. doi: 10.1007/978-3-030-41309-5_15.

[14] Matyjaszewski, K.; Gnanou, Y.; Leibler, L. *Macromolecular Engineering: Precise Synthesis, Materials Properties, Applications*. September 23, 2011, pp 1–6. doi: 10.1002/9783527631421.ch1.

[15] Higgins, J. S.; Tambasco, M.; Lipson, J. E. G. *Prog. Polym. Sci.* **2005**, *30* (8–9), 832–843. doi: 10.1016/j.progpolymsci.2005.06.001.

[16] Rothon, R. *Fillers for Polymer Applications*; Springer, 2017. doi: 10.1007/978-3-319-28117-9.

[17] Tong, L.; Mouritz, A. P.; Bannister, M. K. *3D Fibre Reinforced Polymer Composites*; Elsevier Science, 2002.

[18] Voit, B. I.; Lederer, A. *Chem. Rev.* **2009**, *109* (11), 5924–5973. doi: 10.1021/cr900068q.

[19] Améduri, B.; Boutevin, B.; Czub, P.; Penczek, P.; Pielichowski, J.; Rodríguez-Pérez, M. A.; Taguet, A. *Crosslinking in Materials Science*; Abe, A., Dušek, K., Kobayashi, S., Eds.; Advances in Polymer Science; Springer Berlin Heidelberg, 2005; Vol. 184. doi: 10.1007/b136215.

[20] Pötzsch, R.; Voit, B. *Macromol. Rapid Commun.* **2012**, *33* (8), 635–639. doi: 10.1002/marc.201100795.

[21] Spontak, R. J.; Patel, N. P. *Curr. Opin. Colloid Interface Sci.* **2000**, *5* (5–6), 333–340. doi: 10.1016/s1359-0294(00)00070-4.

[22] Pasch, H. In *Polymer Science: A Comprehensive Reference, 10 Volume Set*; Matyjaszewski, K., Möller, M. B. T.-P. S. A. C. R., Eds.; Elsevier: Amsterdam, 2012; Vol. 2, pp 33–64. doi: 10.1016/B978-0-444-53349-4.00021-2.

[23] Pasch, H. *Polym. Chem.* **2013**, *4* (9), 2628–2650. doi: 10.1039/c3py21095b.

[24] Senra, M.; Panacharoensawad, E.; Kraiwattanawong, K.; Singh, P.; Fogler, H. S. *Energy and Fuels* **2008**, *22* (1), 545–555. doi: 10.1021/ef700490k.

[25] Srivastava, S. P.; Handoo, J.; Agrawal, K. M.; Joshi, G. C. *J. Phys. Chem. Solids* **1993**, *54* (6), 639–670. doi: 10.1016/0022-3697(93)90126-C.

[26] *Modern Methods of Polymer Characterization*; Barth, H. G., Mays, J. W., Eds.; John Wiley & Sons, 1991; Vol. 115.

[27] Smith, W. C. Doctoral disseration, Colorado School of Mines, Golden, CO, USA, 2019. available online: https://hdl.handle.net/11124/173266.

[28] Pasch, H.; Trathnigg, B. *Multidimensional HPLC of Polymers*; Springer, 2013. doi: 10.1007/978-3-642-36080-0.

[29] Belenky, B. G.; Gankina, E. S.; Tennikov, M. B.; Vilenchik, L. Z. *J. Chromatogr. A* **1978**, *147* (C), 99–110. doi: 10.1016/S0021-9673(00)85121-3.

[30] Striegel, A. M.; Brewer, A. K. *Annu. Rev. Anal. Chem.* **2012**, *5* (1), 15–34. doi: 10.1146/annurev-anchem-062011-143107.

[31] Schimpf, M. E.; Caldwell, K.; Giddings, J. C. *Field-Flow Fractionation Handbook*; John Wiley & Sons, Inc.: New York, USA, 2000.

[32] Striegel, A. M. *Anal. Bioanal. Chem.* **2008**, *390* (1), 303–305. doi: 10.1007/s00216-007-1417-6.

[33] Striegel, A. M.; Yau, W. W.; Kirkland, J. J.; Bly, D. D. In *Modern Size-Exclusion Liquid Chromatography*; Wiley Online Books; John Wiley & Sons, Inc., 2009; p 496. doi: 10.1002/9780470442876.ch2.

[34] Estrin, Y. I.; Perepelitsina, E. O.; Grishchuk, A. A. *Russ. J. Phys. Chem. A* **2016**, *90* (7), 1474–1478. doi: 10.1134/S0036024416070086.

[35] Greyling, G. H. Doctoral disseration, Stellenbosch University, South Africa, 2016. available online: http://hdl.handle.net/10019.1/98503.

[36] Greyling, G.; Pasch, H. Greyling, G., Pasch, H., Eds.; Springer International Publishing: Cham, 2019; pp 13–29. doi: 10.1007/978-3-030-10650-8_2.

[37] Gaborieau, M.; Castignolles, P. *Anal. Bioanal. Chem.* **2011**, *399* (4), 1413–1423. doi: 10.1007/s00216-010-4221-7.

[38] Giddings, J. C. *J. Chromatogr. A* **1976**, *125* (1), 3–16. doi: 10.1016/S0021-9673(00)93808-1.

[39] Engelke, J.; Brandt, J.; Barner-Kowollik, C.; Lederer, A. *Polym. Chem.* **2019**, *10* (25), 3410–3425. doi: 10.1039/c9py00336c.

[40] *Handbook Of Size Exclusion Chromatography And Related Techniques*, 2nd ed.; Wu, C. S., Ed.; Chromatographic science; CRC Press: Boca Raton, 2003. doi: 10.1201/9780203913321.

[41] Grubisic, Z.; Rempp, P.; Benoit, H. *J. Polym. Sci. Part B Polym. Lett.* **1967**, *5* (9), 753–759. doi: 10.1002/pol.1967.110050903.

[42] Lederer, A.; Burchard, W.; Khalyavina, A.; Lindner, P.; Schweins, R. *Angew. Chemie Int. Ed.* **2013**, *52* (17), 4659–4663. doi: 10.1002/anie.201209228.

[43] Einstein, A. *Ann. Phys.* **1911**, *339* (3), 591–592. doi: 10.1002/andp.19113390313.

[44] Lederer, A.; Burchard, W. In *Hyperbranched Polymers: Macromolecules in between Deterministic Linear Chains and Dendrimer Structures*; The Royal Society of Chemistry: Cambridge, Great Britain, 2015; pp 88–135. doi: 10.1039/9781782622468-00088.

[45] Wyatt, P. J. *J. Nanoparticle Res.* **2018**, *20* (12), 322. doi: 10.1007/s11051-018-4397-x.

[46] Wyatt, P. J. *J. Nanoparticle Res.* **2019**, *21* (2), 30. doi: 10.1007/s11051-019-4469-6.

[47] Zimm, B. H. *J. Chem. Phys.* **1948**, *16* (12), 1093–1099. doi: 10.1063/1.1746738.

[48] Meier, F.; Heinzmann, G. *www.chemie.de* **2017**, No. September.

[49] Podzimek, S. In *Light Scattering, Size Exclusion Chromatography and Asymmetric Flow Field Flow Fractionation*; John Wiley & Sons, Inc.: Hoboken, New Jersey, 2011; pp 37–98. doi: 10.1002/9780470877975.ch2.

[50] Debye, P. *J. Phys. Colloid Chem.* **1947**, *51* (1), 18–32. doi: 10.1021/j150451a002.

[51] Berry, G. C. *J. Chem. Phys.* **1966**, *44* (12), 4550–4564. doi: 10.1063/1.1726673.

[52] Lederer, A.; Burchard, W. In *Hyperbranched Polymers: Macromolecules in between Deterministic Linear Chains and Dendrimer Structures*; The Royal Society of Chemistry: Cambridge, Great Britain, 2015; pp 136–192. doi: 10.1039/9781782622468-00136.

[53] Bloomfield, V. A.; Lim, T. K. In *Methods in Enzymology*; Academic Press, 1978; Vol. 48, pp 415–494. doi: 10.1016/S0076-6879(78)48021-8.

[54] Burchard, W. In *Light Scattering from Polymers*; Springer Berlin Heidelberg: Berlin, Heidelberg, 1983; pp 1–124. doi: 10.1007/3-540-12030-0_1.

[55] Frisken, B. J. *Appl. Opt.* **2001**, *40* (24), 4087. doi: 10.1364/ao.40.004087.

[56] Provencher, S. *Die Makromol. Chemie* **1979**, *180* (1), 201–209. doi: 10.1002/macp.1979.021800119.

[57] Bhattacharjee, S. *J. Control. Release* **2016**, *235*, 337–351. doi: 10.1016/j.jconrel.2016.06.017.

[58] Hsieh, V. H.; Wyatt, P. J. *Sci. Rep.* **2017**, *7* (1), 10030. doi: 10.1038/s41598-017-09051-1.

[59] Einstein, A. *Ann. Phys.* **1906**, *324* (2), 289–306. doi: 10.1002/andp.19063240204.

[60] Rowland, S. M.; Striegel, A. M. *Anal. Chem.* **2012**, *84* (11), 4812–4820. doi: 10.1021/ac3003775.

[61] Plüschke, L.; Mundil, R.; Sokolohorskyj, A.; Merna, J.; Sommer, J.-U.; Lederer, A. *Anal. Chem.* **2018**, *90* (10), 6178–6186. doi: 10.1021/acs.analchem.8b00619.

[62] Macko, T.; Schulze, U.; Brüll, R.; Albrecht, A.; Pasch, H.; Fónagy, T.; Häussler, L.; Iván, B. *Macromol. Chem. Phys.* **2008**, *209* (4), 404–409. doi: 10.1002/macp.200700398.

[63] Beskers, T. F.; Hofe, T.; Wilhelm, M. *Polym. Chem.* **2015**, *6* (1), 128–142. doi: 10.1039/c4py01043d.

[64] Hiller, W.; Sinha, P.; Hehn, M.; Pasch, H.; Hofe, T. *Macromolecules* **2011**, *44* (6), 1311–1318. doi: 10.1021/ma102750s.

[65] Cudaj, M.; Guthausen, G.; Hofe, T.; Wilhelm, M. *Macromol. Rapid Commun.* **2011**, *32* (8), 665–670. doi: 10.1002/marc.201000760.

[66] Botha, C.; Höpfner, J.; Mayerhöfer, B.; Wilhelm, M. *Polym. Chem.* **2019**, *10* (18), 2230–2246. doi: 10.1039/c9py00140a.

[67] Veloso, A.; Leal, G. P.; Agirre, A.; Leiza, J. R. *Eur. Polym. J.* **2018**, *105*, 265–273. doi: 10.1016/j.eurpolymj.2018.06.003.

[68] Salhi, S.; Tessier, M.; Blais, J. C.; Gharbi, R. El; Fradet, A. *E-Polymers* **2005**, *5* (1), 42. doi: 10.1515/epoly.2005.5.1.446.

[69] Jayakannan, M.; Van Dongen, J. L. J.; Behera, G. C.; Ramakrishnan, S. *J. Polym. Sci. Part A Polym. Chem.* **2002**, *40* (24), 4463–4476. doi: 10.1002/pola.10527.

[70] Dong, S.; Striegel, A. M. *Chromatographia* **2013**, *76* (13–14), 725–733. doi: 10.1007/s10337-013-2472-0.

[71] Striegel, A. M. *Chromatographia* **2017**, *80* (6), 989–996. doi: 10.1007/s10337-017-3294-2.

[72] Zinovyev, G.; Sulaeva, I.; Podzimek, S.; Rössner, D.; Kilpeläinen, I.; Sumerskii, I.; Rosenau, T.; Potthast, A. *ChemSusChem* **2018**, *11* (18), 3259–3268. doi: 10.1002/cssc.201801177.

[73] Lange, H.; Rulli, F.; Crestini, C. *ACS Sustain. Chem. Eng.* **2016**, *4* (10), 5167–5180. doi: 10.1021/acssuschemeng.6b00929.

[74] Podzimek, S.; Vlcek, T.; Johann, C. *J. Appl. Polym. Sci.* **2001**, *81* (7), 1588–1594. doi: 10.1002/app.1589.

[75] Pasch, H.; Malik, M. I. Pasch, H., Malik, M. I., Eds.; Springer International Publishing: Cham, 2014; pp 75–145. doi: 10.1007/978-3-319-08632-3_3.

[76] Stoll, D. R.; Carr, P. W. *Anal. Chem.* **2017**, *89* (1), 519–531. doi: 10.1021/acs.analchem.6b03506.

[77] Plüschke, L.; Ndiripo, A.; Mundil, R.; Merna, J.; Pasch, H.; Lederer, A. *Macromolecules* **2020**, *53* (10), 3765–3777. doi: 10.1021/acs.macromol.0c00314.

[78] Striegel, A. M. *Anal. Bioanal. Chem.* **2013**, *405* (28), 8959–8967. doi: 10.1007/s00216-013-7198-1.

[79] Isenberg, S. L.; Brewer, A. K.; Côté, G. L.; Striegel, A. M. *Biomacromolecules* **2010**, *11* (9), 2505–2511. doi: 10.1021/bm100687b.

[80] Striegel, A. M. *J. Liq. Chromatogr. Relat. Technol.* **2008**, *31* (20), 3105–3114. doi: 10.1080/10826070802480024.

[81] Uliyanchenko, E. *Anal. Bioanal. Chem.* **2014**, *406* (25), 6087–6094. doi: 10.1007/s00216-014-8041-z.

[82] Giddings, J. C.; Yang, F. J. F.; Myers, M. N. *Science* **1976**, *193* (4259), 1244–1245. doi: 10.1126/science.959835.

[83] Giddings, J. C. *Sep. Sci.* **1966**, *1* (1), 123–125. doi: 10.1080/01496396608049439.

[84] Podzimek, S. In *Light Scattering, Size Exclusion Chromatography and Asymmetric Flow Field Flow Fractionation*; John Wiley & Sons, Inc.: Hoboken, New Jersey, 2011; pp 259–305. doi: 10.1002/9780470877975.ch5.

[85] Giddings, J. C. *Science* **1993**, *260* (5113), 1456–1465. doi: 10.1126/science.8502990.

[86] Boye, S.; Appelhans, D.; Boyko, V.; Zschoche, S.; Komber, H.; Friedel, P.; Formanek, P.; Janke, A.; Voit, B. I.; Lederer, A. *Biomacromolecules* **2012**, *13* (12), 4222–4235. doi: 10.1021/bm301489s.

[87] Iavicoli, P.; Urbán, P.; Bella, A.; Ryadnov, M. G.; Rossi, F.; Calzolai, L. *J. Chromatogr. A* **2015**, *1422*, 260–269. doi: 10.1016/j.chroma.2015.10.029.

[88] Kirkland, J. J.; Yau, W. W.; Szoka, F. C. *Science* **1982**, *215* (4530), 296–298. doi: 10.1126/science.7053578.

[89] Gumz, H.; Boye, S.; Iyisan, B.; Krönert, V.; Formanek, P.; Voit, B.; Lederer, A.; Appelhans, D. *Adv. Sci.* **2019**, *6* (7), 1801299. doi: 10.1002/advs.201801299.

[90] Yassin, M. A.; Appelhans, D.; Wiedemuth, R.; Formanek, P.; Boye, S.; Lederer, A.; Temme, A.; Voit, B. *Small* **2015**, *11* (13), 1580–1591. doi: 10.1002/smll.201402581.

[91] Abbate, R. A.; Raak, N.; Boye, S.; Janke, A.; Rohm, H.; Jaros, D.; Lederer, A. *Food Hydrocoll.* **2019**, *92*, 117–124. doi: 10.1016/j.foodhyd.2019.01.043.

[92] Raak, N.; Abbate, R.; Lederer, A.; Rohm, H.; Jaros, D. *Separations* **2018**, *5* (1), 14. doi: 10.3390/separations5010014.

[93] Haladjova, E.; Rangelov, S.; Geisler, M.; Boye, S.; Lederer, A.; Mountrichas, G.; Pispas, S. *Macromol. Chem. Phys.* **2015**, *216* (18), 1862–1867. doi: 10.1002/macp.201500177.

[94] Ennen, F.; Boye, S.; Lederer, A.; Cernescu, M.; Komber, H.; Brutschy, B.; Voit, B.; Appelhans, D. *Polym. Chem.* **2014**, *5* (4), 1323–1339. doi: 10.1039/c3py01152f.

[95] Boye, S.; Ennen, F.; Scharfenberg, L.; Appelhans, D.; Nilsson, L.; Lederer, A. *Macromolecules* **2015**, *48* (13), 4607–4619. doi: 10.1021/acs.macromol.5b00824.

[96] Janča, J. *Trends Anal. Chem.* **1983**, *2* (12), 278–281. doi: 10.1016/0165-9936(83)87054-X.

[97] Williams, S. K. R.; Caldwell, K. D. *Field-Flow Fractionation in Biopolymer Analysis*; Springer: Vienna, 2012. doi: 10.1007/978-3-7091-0154-4.

[98] Ratanathanawongs Williams, S. K.; Lee, D. *J. Sep. Sci.* **2006**, *29* (12), 1720–1732. doi: 10.1002/jssc.200600151.

[99] Messaud, F. A.; Sanderson, R. D.; Runyon, J. R.; Otte, T.; Pasch, H.; Williams, S. K. R. *Prog. Polym. Sci.* **2009**, *34* (4), 351–368. doi: 10.1016/j.progpolymsci.2008.11.001.

[100] Qureshi, R. N.; Kok, W. T. *LCGC Eur.* **2010**, *23* (1), 18–25.

[101] Schimpf, M. E. *J. Liq. Chromatogr. Relat. Technol.* **2002**, *25* (13–15), 2101–2134. doi: 10.1081/JLC-120013997.

[102] de la Calle, I.; Menta, M.; Klein, M.; Maxit, B.; Séby, F. *Spectrochim. Acta - Part B At. Spectrosc.* **2018**, *147*, 28–42. doi: 10.1016/j.sab.2018.05.012.

[103] Hu, Y.; Crist, R. M.; Clogston, J. D. *Anal. Bioanal. Chem.* **2020**, *412* (2), 425–438. doi: 10.1007/s00216-019-02252-9.

[104] Lohmann, C. A.; Haseltine, W. G.; Engle, J. R.; Williams, S. K. R. *Anal. Chim. Acta* **2009**, *654* (1), 92–96. doi: 10.1016/j.aca.2009.07.023.

[105] Lewandowski, L.; Sibbald, M. S.; Johnson, E.; Mallamaci, M. P. *Rubber Chem. Technol.* **2000**, *73* (4), 731–742. doi: 10.5254/1.3547617.

[106] Sibbald, M.; Lewandowski, L.; Mallamaci, M.; Johnson, E. *Macromol. Symp.* **2000**, *155* (1), 213–228. doi: 10.1002/1521-3900(200004)155:1<213::AID-MASY213>3.0.CO;2-I.

[107] Colvin, H. A.; Senyek Jr, M. L. U.S. patent, US6455655B1, September 24, 2002.

[108] Kerns, M.; Rachita, M. U.S. patent, US10626230B2, April 2015.

[109] Giddings, J. C.; Schimpf, M. E. *Macromolecules* **1987**, *20* (7), 1561–1563. doi: 10.1021/ma00173a022.

[110] Runyon, J. R.; Williams, S. K. R. *J. Chromatogr. A* **2011**, *1218* (38), 6774–6779. doi: 10.1016/j.chroma.2011.07.076.

[111] Schimpf, M. E.; Giddings, J. C. *J. Polym. Sci. Part B Polym. Phys.* **1990**, *28* (13), 2673–2680. doi: 10.1002/polb.1990.090281313.

[112] Schimpf, M. E.; Wheeler, L. M.; Romeo, P. F. In *Chromatography of Polymers*; ACS Symposium Series; American Chemical Society, 1993; Vol. 521, pp 63–76. doi: 10.1021/bk-1993-0521.ch005.

[113] Greyling, G.; Lederer, A.; Pasch, H. *Macromol. Chem. Phys.* **2018**, *219* (24), 1800417. doi: 10.1002/macp.201800417.

[114] Belgaied, J. E.; Hoyos, M.; Martin, M. *J. Chromatogr. A* **1994**, *678* (1), 85–96. doi: 10.1016/0021-9673(94)87077-2.

[115] Hill, E. H.; Li, J.; Lin, L.; Liu, Y.; Zheng, Y. *Langmuir* **2018**, *34* (44), 13252–13262. doi: 10.1021/acs.langmuir.8b01979.

[116] Fränzl, M.; Thalheim, T.; Adler, J.; Huster, D.; Posseckardt, J.; Mertig, M.; Cichos, F. *Nat. Methods* **2019**, *16* (7), 611–614. doi: 10.1038/s41592-019-0451-6.

[117] Schimpf, M. E.; Giddings, J. C. *J. Polym. Sci. Part B Polym. Phys.* **1989**, *27* (6), 1317–1332. doi: 10.1002/polb.1989.090270610.

[118] Mes, E. P. C.; Kok, W. T.; Tijssen, R. *Int. J. Polym. Anal. Charact.* **2003**, *8* (2), 133–153. doi: 10.1080/10236660304888.

[119] Striegel, A. M. *Chromatographia* **2016**, *79* (15–16), 945–960. doi: 10.1007/s10337-016-3078-0.

[120] Hansen, C. M.; Beerbower, A. In *Kirk-Othmer Encyclopedia of Chemical Technology*; Mark, H. F., McKetta, J. J., Othmer, D. F., Eds.; John Wiley & Sons: New York, 1971; Vol. 2, pp 889–910.

[121] Hansen, C. M.; Durkee, J.; Kontogeorgis, G.; Panayiotou, C.; Willliams, L. L.; Poulsen, T. S.; Priebe, H.; Redelius, P. *Hansen Solubility Parameters: A User's Handbook, Second Edition*, 2nd ed.; CRC Press, 2007. doi: 10.1201/9781420006834.

[122] Runyon, J. R. Doctoral dissertation, Colorado School of Mines, Golden, CO, USA, 2009. available online: https://hdl.handle.net/11124/174030

[123] Beckett, R.; Nicholson, G.; Hart, B. T.; Hansen, M.; Giddings, J. C. *Water Res.* **1988**, *22* (12), 1535–1545. doi: 10.1016/0043-1354(88)90166-2.

[124] Hansen, M. E.; Giddings, J. C.; Schure, M. R.; Beckett, R. *Anal. Chem.* **1988**, *60* (14), 1434–1442. doi: 10.1021/ac00165a018.

[125] Magnusson, E.; Håkansson, A.; Janiak, J.; Bergenståhl, B.; Nilsson, L. *J. Chromatogr. A* **2012**, *1253*, 127–133. doi: 10.1016/j.chroma.2012.07.005.

[126] Håkansson, A.; Magnusson, E.; Bergenståhl, B.; Nilsson, L. *J. Chromatogr. A* **2012**, *1253*, 120–126. doi: 10.1016/j.chroma.2012.07.029.

[127] Giddings, J. C. *Anal. Chem.* **1986**, *58* (4), 735–740. doi: 10.1021/ac00295a018.

[128] Pasti, L.; Bedani, F.; Contado, C.; Mingozzi, I.; Dondi, F. *Anal. Chem.* **2004**, *76* (22), 6665–6680. doi: 10.1021/ac049399q.

[129] Andrews, E. H. *Int. J. Polym. Mater. Polym. Biomater.* **1973**, *2* (4), 337–359. doi: 10.1080/00914037308072367.

[130] Matyjaszewski, K.; Tsarevsky, N. V. *Nat. Chem.* **2009**, *1* (4), 276–288. doi: 10.1038/nchem.257.

[131] Seymour, R. B.; Carraher, C. E.; Seymour, R. B.; Carraher, C. E. In *Structure—Property Relationships in Polymers*; Seymour, R. B., Carraher, C. E., Eds.; Springer US: Boston, MA, 1984; pp 1–17. doi: 10.1007/978-1-4684-4748-4_1.

[132] Matyjaszewski, K.; Ziegler, M. J.; Arehart, S. V.; Greszta, D.; Pakula, T. *J. Phys. Org. Chem.* **2000**, *13* (12), 775–786. doi: 10.1002/1099-1395(200012)13:12<775::AID-POC314>3.0.CO;2-D.

[133] Zhang, J.; Jin, J.; Cooney, R.; Fu, Q.; Qiao, G. G.; Thomas, S.; Merkel, T. C. *Polym. Chem.* **2015**, *6* (28), 5003–5008. doi: 10.1039/c5py00570a.

[134] Geisler, M. Master thesis, Hochschule für Technik und Wirtschaft Dresden, Germany, 2016.

[135] Majoinen, J.; Haataja, J. S.; Appelhans, D.; Lederer, A.; Olszewska, A.; Seitsonen, J.; Aseyev, V.; Kontturi, E.; Rosilo, H.; Österberg, M.; Houbenov, N.; Ikkala, O. *J. Am. Chem. Soc.* **2014**, *136* (3), 866–869. doi: 10.1021/ja411401r.

[136] Kenney, J. F. *Polym. Eng. Sci.* **1968**, *8* (3), 216–226. doi: 10.1002/pen.760080307.

[137] Javni, I.; Bilić, O.; Bilić, N.; Petrović, Z. S.; Eastwood, E. A.; Zhang, F.; Ilavský, J. *Polym. Int.* **2015**, *64* (11), 1607–1616. doi: 10.1002/pi.4960.

[138] Geyer, R.; Jambeck, J. R.; Law, K. L. *Sci. Adv.* **2017**, *3* (7), e1700782. doi: 10.1126/sciadv.1700782.

[139] Kim, J. D.; Soares, J. B. P.; Rempel, G. L. *J. Polym. Sci. Part A Polym. Chem.* **1999**, *37* (3), 331–339. doi: 10.1002/(SICI)1099-0518(19990201)37:3<331::AID-POLA10>3.0.CO;2-V.

[140] Gentekos, D. T.; Sifri, R. J.; Fors, B. P. *Nat. Rev. Mater.* **2019**, *4* (12), 761–774. doi: 10.1038/s41578-019-0138-8.

[141] Zimm, B. H.; Stockmayer, W. H. *J. Chem. Phys.* **1949**, *17* (12), 1301–1314. doi: 10.1063/1.1747157.

[142] Zimm, B. H.; Kilb, R. W. *J. Polym. Sci.* **1959**, *37* (131), 19–42. doi: 10.1002/pol.1959.1203713102.

[143] Hawker, C. J.; Lee, R.; Frécnet, J. M. J. *J. Am. Chem. Soc.* **1991**, *113* (12), 4583–4588. doi: 10.1021/ja00012a030.

[144] Kim, Y. H.; Webster, O. W. *Macromolecules* **1992**, *25* (21), 5561–5572. doi: 10.1021/ma00047a001.

[145] Boye, S. Doctoral dissertation, Technische Universität Dresden, Germany, 2013. available online: https://nbn-resolving.org/urn:nbn:de:bsz:14-qucosa-107514

[146] Martin, M.; Williams, P. S. In *Theoretical Advancement in Chromatography and Related Separation Techniques*; Dondi, F., Guiochon, G., Eds.; Springer Netherlands: Dordrecht, 1992; pp 513–580. doi: 10.1007/978-94-011-2686-1_18.

[147] Gunderson, J. J.; Myers, M. N.; Giddings, J. C. *Anal. Chem.* **1987**, *59* (1), 23–28. doi: 10.1021/ac00128a006.

[148] Dondi, F.; Martin, M. In *Field Flow Fractionation Handbook*; Schimpf, M., Caldwell, K., Giddings, J., Ed.; John Wiley & Sons: New York, USA, USA, 2000; pp 103–132.

[149] Happel, J.; Brenner, H. Happel, J., Brenner, H., Eds.; Springer Netherlands: Dordrecht, 1983; pp 23–57. doi: 10.1007/978-94-009-8352-6_2.

[150] Cornish, R. J.; Milne, E. A. *Proc. R. Soc. London. Ser. A, Contain. Pap. a Math. Phys. Character* **1928**, *120* (786), 691–700. doi: 10.1098/rspa.1928.0175.

[151] Takahashi, T.; Gill, W. N. *Chem. Eng. Commun.* **1980**, *5* (5–6), 367–385. doi: 10.1080/00986448008935976.

[152] Janča, J. *Int. J. Polym. Anal. Charact.* **2017**, *22* (1), 62–71. doi: 10.1080/1023666X.2016.1232558.

[153] Giddings, J. C.; Yoon, Y. H.; Caldwell, K. D.; Myers, M. N.; Hovingh, M. E. *Sep. Sci.* **1975**, *10* (4), 447–460. doi: 10.1080/00372367508058032.

[154] Hovingh, M. E.; Thompson, G. H.; Giddings, J. C. *Anal. Chem.* **1970**, *42* (2), 195–203. doi: 10.1021/ac60284a003.

[155] Caldwell, K. In *Field Flow Fractionation Handbook*; Schimpf, M. E., Caldwell, K. D., Giddings, J. C., Eds.; John Wiley & Sons: New York, USA, 2000; pp 79–93.

[156] Schure, M. R.; Schimpf, M. E.; Schettler, P. D. In *Field-Flow Fractionation Handbook*; Schimpf, M. E., Caldwell, K. D., Giddings, J. C., Eds.; Wiley-Interscience Inc.: New York, USA, 2000; pp 31–48.

[157] Ludwig, C. *Sitzungber. Bayer. Akad. Wiss. Wien Math.-Naturwiss. Kl.* **1856**, *20*, 539.

[158] Soret, C. *J. Phys. Theor. Appl.* **1880**, *9* (1), 331–332.

[159] Martin, M.; Van Batten, C.; Hoyos, M. Köhler, W., Wiegand, S., Eds.; Springer Berlin Heidelberg: Berlin, Heidelberg, 2002; pp 250–284. doi: 10.1007/3-540-45791-7_13.

[160] Geisler, M.; Smith, W. C.; Plüschke, L.; Mundil, R.; Merna, J.; Williams, S. K. R.; Lederer, A. *Macromolecules* **2019**, *52* (22), 8662–8671. doi: 10.1021/acs.macromol.9b01410.

[161] Clusius, K.; Dickel, G. *Naturwissenschaften* **1938**, *26* (33), 546. doi: 10.1007/BF01675498.

[162] Köhler, W.; Morozov, K. I. *J. Non-Equilibrium Thermodyn.* **2016**, *41* (3), 151–197. doi: 10.1515/jnet-2016-0024.

[163] Mishakov, G. V.; Popov, V. K.; Bagratashvili, V. N. *Russ. J. Phys. Chem. B* **2015**, *9* (8), 1143–1147. doi: 10.1134/S1990793115080072.

[164] Barreiro, A.; Rurali, R.; Hernández, E. R.; Moser, J.; Pichler, T.; Forró, L.; Bachtold, A. *Science* **2008**, *320* (5877), 775–778. doi: 10.1126/science.1155559.

[165] Koonin, E. V. *Proc. Natl. Acad. Sci. U. S. A.* **2007**, *104* (22), 9105–9106. doi: 10.1073/pnas.0702699104.

[166] De Groot, S. R.; Mazur, P. *Non-Equilibrium Thermodynamics*; Dover Books on Physics; Dover Publications: New York, USA, 1984.

[167] Würger, A. *Eur. Phys. J. E* **2014**, *37* (10), 1–11. doi: 10.1140/epje/i2014-14096-y.

[168] Chapman, S.; Cowling, T. G. *The Mathematical Theory of Non-Uniform Gases: An Account of the Kinetic Theory of Viscosity, Thermal Conduction and Diffusion in Gases*; Cambridge University Press: Cambrige, New York, Melbourne, 1939.

[169] Wang, J.; Li, Z. *Phys. Rev. E - Stat. Nonlinear, Soft Matter Phys.* **2012**, *86* (1), 11201. doi: 10.1103/PhysRevE.86.011201.

[170] Leng, J.; Guo, Z.; Zhang, H.; Chang, T.; Guo, X.; Gao, H. *Nano Lett.* **2016**, *16* (10), 6396–6402. doi: 10.1021/acs.nanolett.6b02815.

[171] Kita, R.; Wiegand, S.; Luettmer-Strathmann, J. *J. Chem. Phys.* **2004**, *121* (8), 3874–3885. doi: 10.1063/1.1771631.

[172] Kita, R.; Polyakov, P.; Wiegand, S. *Macromolecules* **2007**, *40* (5), 1638–1642. doi: 10.1021/ma0621831.

[173] Rauch, J.; Köhler, W. *Macromolecules* **2005**, *38* (9), 3571–3573. doi: 10.1021/ma050231w.

[174] Stadelmaier, D.; Köhler, W. *Macromolecules* **2009**, *42* (22), 9147–9152. doi: 10.1021/ma901794k.

[175] Stadelmaier, D.; Köhler, W. *Macromolecules* **2008**, *41* (16), 6205–6209. doi: 10.1021/ma800891p.

[176] Dougherty, E. L.; Drickamer, H. G. *J. Chem. Phys.* **1955**, *23* (2), 295–309. doi: 10.1063/1.1741957.

[177] Denbigh, K. G. *Transactions of the Faraday Society*. 1952, pp 1–8. doi: 10.1039/tf9524800001.

[178] Haase, R. *Zeitschrift für Phys.* **1950**, *127* (1–2), 1–10. doi: 10.1007/BF01338979.

[179] Würger, A. *J. Phys. Condens. Matter* **2014**, *26* (3), 35105. doi: 10.1088/0953-8984/26/3/035105.

[180] Eslamian, M.; Ziad, S. M. *Journal of Non-Equilibrium Thermodynamics*. 2009, p 97. doi: 10.1515/JNETDY.2009.007.

[181] Tichacek, L. J.; Kmak, W. S.; Drickamer, H. G. *J. Phys. Chem.* **1956**, *60* (5), 660–665. doi: 10.1021/j150539a038.

[182] Washall, T. A.; Melpolder, F. W. *Ind. Eng. Chem. Process Des. Dev.* **1962**, *1* (1), 26–28. doi: 10.1021/i260001a004.

[183] Köhler, W. *J. Chem. Phys.* **1993**, *98* (1), 660–668. doi: 10.1063/1.464610.

[184] Pur, B.; Schock, F.; Köhler, W.; Morozov, K. I. *J. Phys. Chem. Lett.* **2020**, *11* (11), 4498–4502. doi: 10.1021/acs.jpclett.0c01303.

[185] Khazanovich, T. N. *J. Polym. Sci. Part C Polym. Symp.* **1967**, *16* (4), 2463–2468. doi: 10.1002/polc.5070160457.

[186] Bender, M. *Macromolecules* **1995**, *28* (4), 1309–1311. doi: 10.1021/ma00108a071.

[187] Schimpf, M. E.; Semenov, S. N. *J. Phys. Chem. B* **2000**, *104* (42), 9935–9942. doi: 10.1021/jp994334q.

[188] Semenov, S.; Schimpf, M. *Phys. Rev. E - Stat. Physics, Plasmas, Fluids, Relat. Interdiscip. Top.* **2004**, *69* (1), 8. doi: 10.1103/PhysRevE.69.011201.

[189] Flory, P. J. *J. Chem. Phys.* **1942**, *10* (1), 51–61. doi: 10.1063/1.1723621.

[190] Huggins, M. L. *J. Chem. Phys.* **1941**, *9* (5), 440. doi: 10.1063/1.1750930.

[191] Runyon, J. R.; Williams, S. K. R. *J. Chromatogr. A* **2011**, *1218* (39), 7016–7022. doi: 10.1016/J.CHROMA.2011.08.007.

[192] Reichardt, C.; Welton, T. *Solvents and Solvent Effects in Organic Chemistry*, 4th ed.; Wiley-VCH Verlag GmbH & Co. KGaA: Weinheim, Germany, 2011. doi: 10.1002/9783527632220.

[193] Gani, R.; Brignole, E. A. *Fluid Phase Equilib.* **1983**, *13* (C), 331–340. doi: 10.1016/0378-3812(83)80104-6.

[194] Adjiman, C. S. In *Encyclopedia of Optimization*; Floudas, C. A., Pardalos, P. M., Eds.; Springer US: Boston, USA, 2008; pp 2750–2757. doi: 10.1007/978-0-387-74759-0_474.

[195] Abramov, Y. A.; Sun, G.; Zeng, Q.; Zeng, Q.; Yang, M. *Mol. Pharm.* **2020**, *17* (2), 666–673. doi: 10.1021/acs.molpharmaceut.9b01138.

[196] Hildebrand, J. H.; Prausnitz, J. M.; Scott, R. L. *Regular and Related Solutions: The Solubility of Gases, Liquids, and Solids*; Van Nostrand Reinhold Company, 1970, p 190.

[197] Stefanis, E.; Panayiotou, C. *Int. J. Thermophys.* **2008**, *29* (2), 568–585. doi: 10.1007/s10765-008-0415-z.

[198] Mathieu, D. *ACS Omega* **2018**, *3* (12), 17049–17056. doi: 10.1021/acsomega.8b02601.

[199] Thomas, E. R.; Eckert, C. A. *Ind. Eng. Chem. Process Des. Dev.* **1984**, *23* (2), 194–209. doi: 10.1021/i200025a002.

[200] Gramatica, P. *QSAR Comb. Sci.* **2007**, *26* (5), 694–701. doi: 10.1002/qsar.200610151.

[201] Roy, K.; Kar, S.; Das, R. N. *A Primer on QSAR/QSPR Modeling: Fundamental Concepts*; SpringerBriefs in Molecular Science; Springer International Publishing: Cham, Heidelberg, Dordecht, London, New York, 2015.

[202] Williams, L. L.; Rubin, J. B.; Edwards, H. W. *Ind. Eng. Chem. Res.* **2004**, *43* (16), 4967–4972. doi: 10.1021/ie0497543.

[203] Ziemer, U. A. Doctoral dissertation. Technische Universität Dresden, Germany, Tenea Verlag Ltd., Dresden, 2003. available online: https://nbn-resolving.org/urn:nbn:de:swb:14-1055234737562-37907

[204] Flory, P. J. *J. Am. Chem. Soc.* **1952**, *74* (11), 2718–2723. doi: 10.1021/ja01131a008.

[205] Voit, B. *J. Polym. Sci. Part A Polym. Chem.* **2000**, *38* (14), 2505–2525. doi: 10.1002/1099-0518(20000715)38:14<2505::AID-POLA10>3.0.CO;2-8.

[206] Khalyavina, A.; Schallausky, F.; Komber, H.; Al Samman, M.; Radke, W.; Lederer, A. *Macromolecules* **2010**, *43* (7), 3268–3276. doi: 10.1021/ma100037n.

[207] Voit, B.; Komber, H.; Lederer, A. In *Materials Science and Technology*; Wiley-VCH Verlag GmbH & Co. KGaA: Weinheim, Germany, 2012; pp 701–740. doi: 10.1002/9783527603978.mst0434.

[208] Lederer, A.; Hartmann, T.; Komber, H. *Macromol. Rapid Commun.* **2012**, *33* (17), 1440–1444. doi: 10.1002/marc.201200223.

[209] Lederer, A.; Burchard, W.; Hartmann, T.; Haataja, J. S.; Houbenov, N.; Janke, A.; Friedel, P.; Schweins, R.; Lindner, P. *Angew. Chemie Int. Ed.* **2015**, *54* (43), 12578–12583. doi: 10.1002/anie.201504059.

[210] Cook, A. B.; Perrier, S. *Adv. Funct. Mater.* **2020**, *30* (2), 1901001. doi: 10.1002/adfm.201901001.

[211] Firdaus, S.; Geisler, M.; Friedel, P.; Banerjee, S.; Appelhans, D.; Voit, B.; Lederer, A. *Macromol. Rapid Commun.* **2018**, *39* (16), 1800364. doi: 10.1002/marc.201800364.

[212] Geisler, M. Bachelor thesis, Hochschule für Technik und Wirtschaft Dresden, Germany, 2015.

[213] Firdaus, S. Master thesis, Indian Institute of Technology Kharagpur, India, 2016.

[214] Voit, B. *J. Polym. Sci. Part A Polym. Chem.* **2005**, *43* (13), 2679–2699. doi: 10.1002/pola.20821.

[215] Al Samman, M.; Radke, W.; Khalyavina, A.; Lederer, A. *Macromolecules* **2010**, *43* (7), 3215–3220. doi: 10.1021/ma902537e.

[216] Al Samman, M.; Radke, W. *Polymer* **2016**, *99*, 734–740. doi: 10.1016/J.POLYMER.2016.07.077.

[217] Burchard, W.; Khalyavina, A.; Lindner, P.; Schweins, R.; Friedel, P.; Wiemann, M.; Lederer, A. *Macromolecules* **2012**, *45* (7), 3177–3187. doi: 10.1021/ma300031g.

[218] Khalyavina, A.; Häußler, L.; Lederer, A. *Polymer* **2012**, *53* (5), 1049–1053. doi: 10.1016/j.polymer.2012.01.020.

[219] Bayer, O.; Rinke, H.; Stiefken, W.; Orthner, L.; Schild, L. German patent, DE728981C, 1942.

[220] Engels, H. W.; Pirkl, H. G.; Albers, R.; Albach, R. W.; Krause, J.; Hoffmann, A.; Casselmann, H.; Dormish, J. *Angew. Chemie - Int. Ed.* **2013**, *52* (36), 9422–9441. doi: 10.1002/anie.201302766.

[221] Datta, J.; Kasprzyk, P. *Polym. Eng. Sci.* **2018**, *58* (S1), E14–E35. doi: 10.1002/pen.24633.

[222] Mattfeld, P. German patent, DE102017118314A1, 2017.

[223] Raasch, J.; Ivey, M.; Aldrich, D.; Nobes, D. S.; Ayranci, C. *Addit. Manuf.* **2015**, *8*, 132–141. doi: 10.1016/j.addma.2015.09.004.

[224] Bates, S. R. G.; Farrow, I. R.; Trask, R. S. *Mater. Des.* **2016**, *112*, 172–183. doi: 10.1016/j.matdes.2016.08.062.

[225] Fu, Y. Q.; Huang, W. M.; Luo, J. K.; Lu, H. In *Shape Memory Polymers for Biomedical Applications*; Yahia, L. B. T.-S. M. P. for B. A., Ed.; Woodhead Publishing, 2015; pp 167–195. doi: 10.1016/B978-0-85709-698-2.00009-X.

[226] Fridman, I. D.; Thomas, E. L. *Polymer* **1980**, *21* (4), 388–392. doi: 10.1016/0032-3861(80)90007-5.

[227] Mishra, A.; Maiti, P. *J. Appl. Polym. Sci.* **2011**, *120* (6), 3546–3555. doi: 10.1002/app.33525.

[228] Bly, J. H. *Radiat. Phys. Chem.* **1981**, *18* (5–6), 1331–1340. doi: 10.1016/0146-5724(81)90325-3.

[229] Sarma, K. S. S.; Rawat, K. P.; Benny, P. G.; Kader, S. A. *BARC News Lett. ISSN0976-2108* **2011**, No. 323, 38–41.

[230] Mrad, O.; Saunier, J.; Aymes Chodur, C.; Rosilio, V.; Agnely, F.; Aubert, P.; Vigneron, J.; Etcheberry, A.; Yagoubi, N. *Radiat. Phys. Chem.* **2010**, *79* (1), 93–103. doi: 10.1016/j.radphyschem.2009.08.038.

[231] Wakalopulos, G.; Urgiles, E. R. U.S. patent, US6140657A, October 31, 2000.

[232] Dawes, K.; Glover, L. C.; Vroom, D. A. In *Physical Properties of Polymers Handbook*; Mark, J. E., Ed.; Springer New York: New York, NY, 2007; pp 867–887. doi: 10.1007/978-0-387-69002-5_52.

[233] Abd-Elghany, A. A.; Diab, H. M.; Sulieman, A. *J. Radiat. Res. Appl. Sci.* **2020**, *13* (1), 246–251. doi: 10.1080/16878507.2020.1727676.

[234] Tamada, M. Kudo, H., Ed.; Springer Singapore: Singapore, 2018; pp 63–80. doi: 10.1007/978-981-10-7350-2_8.

[235] Murray, K. A.; Kennedy, J. E.; McEvoy, B.; Vrain, O.; Ryan, D.; Cowman, R.; Higginbotham, C. L. *Eur. Polym. J.* **2013**, *49* (7), 1782–1795. doi: 10.1016/j.eurpolymj.2013.03.034.

[236] Adem, E.; Angulo-Cervera, E.; González-Jiménez, A.; Valentín, J. L.; Marcos-Fernández, A. *Radiat. Phys. Chem.* **2015**, *112*, 61–70. doi: 10.1016/j.radphyschem.2015.03.017.

[237] Navarro, R.; Rubio Hernández-Sampelayo, A.; Adem, E.; Marcos-Fernández, A. *Radiat. Phys. Chem.* **2020**, *174*, 108905. doi: 10.1016/j.radphyschem.2020.108905.

[238] Guignot, C.; Betz, N.; Legendre, B.; Le Moel, A.; Yagoubi, N. *Nucl. Instruments Methods Phys. Res. Sect. B Beam Interact. with Mater. Atoms* **2001**, *185* (1–4), 100–107. doi: 10.1016/S0168-583X(01)00850-3.

[239] Sui, H. L.; Liu, X. Y.; Zhong, F. C.; Li, X. Y.; Ju, X. *Polym. Degrad. Stab.* **2013**, *98* (1), 255–260. doi: 10.1016/j.polymdegradstab.2012.10.003.

[240] Sui, H.; Ju, X.; Liu, X.; Cheng, K.; Luo, Y.; Zhong, F. *Polym. Degrad. Stab.* **2014**, *101* (1), 109–113. doi: 10.1016/j.polymdegradstab.2013.11.021.

[241] Ghobashy, M. M.; Abdeen, Z. I. *J. Polym.* **2016**, *2016*, 1–9. doi: 10.1155/2016/9802514.

[242] Wilhelm, C.; Rivaton, A.; Gardette, J. L. *Polymer* **1998**, *39* (5), 1223–1232. doi: 10.1016/S0032-3861(97)00353-4.

[243] Wilhelm, C.; Gardette, J. L. *Polymer* **1998**, *39* (24), 5973–5980. doi: 10.1016/S0032-3861(97)10065-9.

[244] Ravat, B.; Grivet, M.; Grohens, Y.; Chambaudet, A. *Radiat. Meas.* **2001**, *34* (1–6), 31–36. doi: 10.1016/S1350-4487(01)00116-0.

[245] Ravat, B.; Oudot, B.; Grivet, M.; Grohens, Y.; Chambaudet, A. *Radiat. Phys. Chem.* **2002**, *63* (1), 93–99. doi: 10.1016/S0969-806X(01)00488-1.

[246] Tian, Q.; Takács, E.; Krakovský, I.; Horváth, Z. E.; Rosta, L.; Almásy, L. *Polymers (Basel).* **2015**, *7* (9), 1755–1766. doi: 10.3390/polym7091481.

[247] Deng, Y. W.; Yu, T. L.; Ho, C. H. *Polym. J.* **1994**, *26* (12), 1368–1376. doi: 10.1295/polymj.26.1368.

[248] Cooke, S. L.; Whittington, A. R. *J. Chem.* **2018**, *2018*, 7312147. doi: 10.1155/2018/7312147.

[249] Grinshpun, V.; O'Driscoll, K. F.; Rudin, A. In *ACS Symposium Series*; ACS Symposium Series; American Chemical Society, 1984; Vol. 245, pp 273–280. doi: 10.1021/bk-1984-0245.ch018.

[250] Pasch, H. *Polym. Adv. Technol.* **2015**, *26* (7), 771–784. doi: 10.1002/pat.3479.

[251] Pasch, H.; Malik, M. I.; Macko, T. In *Advances in Polymer Science*; Abe, A., Kausch, H.-H., Möller, M., Pasch, H., Eds.; Springer Berlin Heidelberg: Berlin, Heidelberg, 2013; Vol. 251, pp 77–140. doi: 10.1007/12_2012_167.

[252] Guan, Z.; Cotts, P. M.; McCord, E. F.; McLain, S. J. *Science* **1999**, *283* (5410), 2059–2062. doi: 10.1126/science.283.5410.2059.

[253] Ziegler, K.; Holzkamp, E.; Breil, H.; Martin, H. *Angew. Chemie* **1955**, *67* (19-20), 541–547.

[254] Natta, G.; Danusso, F.; Vaccaroni, L. M.; Di Pietro, J. *Stereoregular Polymers and Stereospecific Polymerizations. Volume 2 : The Contributions of Giulio Natta and His School to Polymer Chemistry*; Natta, G., Dannusso, F., Eds.; Stereoregular Polymers and Stereospecific Polymerizations: The Contributions of Giulio Natta and His School to Polymer Chemistry; Symposium Publications Division, Pergamon Press: Michigan, USA, 1967. doi: 10.1016/C2013-0-07967-4.

[255] Kaminsky, W. *J. Chem. Soc. - Dalt. Trans.* **1998**, No. 9, 1413–1418. doi: 10.1039/a800056e.

[256] Johnson, L. K.; Killian, C. M.; Brookhart, M. *J. Am. Chem. Soc.* **1995**, *117* (23), 6414–6415. doi: 10.1021/ja00128a054.

[257] Ittel, S. D.; Johnson, L. K.; Brookhart, M. *Chem. Rev.* **2000**, *100* (4), 1169–1204. doi: 10.1021/cr9804644.

[258] Cotts, P. M.; Guan, Z.; McCord, E.; McLain, S. *Macromolecules* **2000**, *33* (19), 6945–6952. doi: 10.1021/ma000926r.

[259] Dockhorn, R.; Plüschke, L.; Geisler, M.; Zessin, J.; Lindner, P.; Mundil, R.; Merna, J.; Sommer, J.-U.; Lederer, A. *J. Am. Chem. Soc.* **2019**, *141* (39), 15586–15596. doi: 10.1021/jacs.9b06785.

[260] Brimhall, S. L.; Myers, M. N.; Caldwell, K. D.; Giddings, J. C. *Sep. Sci. Technol.* **1981**, *16* (6), 671–689. doi: 10.1080/01496398108058122.

[261] Pasti, L.; Roccasalvo, S.; Dondi, F.; Reschiglian, P. *J. Polym. Sci. Part B Polym. Phys.* **1995**, *33* (8), 1225–1234. doi: 10.1002/polb.1995.090330808.

[262] Pasti, L.; Melucci, D.; Contado, C.; Dondi, F.; Mingozzi, I. *J. Sep. Sci.* **2002**, *25* (10–11), 691–702. doi: 10.1002/1615-9314(20020701)25:10/11<691::AID-JSSC691>3.0.CO;2-L.

[263] Brochard, F.; Gennes, P.-G. de. *Comptes rendus l ' Académie des Sci. Paris II* **1981**, *293*, 1025–1027.

[264] Geisler, M.; Lederer, A. *J. Chromatogr. A* **2020**, *1621*, 461082. doi: 10.1016/j.chroma.2020.461082.

[265] Martin, M.; Reynaud, R. *Anal. Chem.* **1980**, *52* (14), 2293–2298. doi: 10.1021/ac50064a014.

[266] Greyling, G.; Pasch, H. *Anal. Chem.* **2015**, *87* (5), 3011–3018. doi: 10.1021/ac504651p.

[267] Muza, U. L.; Greyling, G.; Pasch, H. *Anal. Chem.* **2018**, *90* (23), 13987–13995. doi: 10.1021/acs.analchem.8b03590.

[268] Khalyavina, A.; Schallausky, F.; Komber, H.; Al Samman, M.; Radke, W.; Lederer, A. *Macromolecules* **2010**, *43* (7), 3268–3276. doi: 10.1021/ma100037n.

[269] Mundil, R.; Hermanová, S.; Peschel, M.; Lederer, A.; Merna, J. *Polym. Int.* **2018**, *67* (7), 946–956. doi: 10.1002/pi.5593.

[270] Korber, H.; Lappan, U.; Geißler, U.; Lunkwitz, K.; Hanke, R. German patent, DE19930742, 2001.

[271] Dorschner, H.; Jenschke, W.; Lunkwitz, K. *Nucl. Instruments Methods Phys. Res. Sect. B Beam Interact. with Mater. Atoms* **2000**, *161*, 1154–1158. doi: 10.1016/S0168-583X(99)00811-3.

[272] Koppel, D. E. *J. Chem. Phys.* **1972**, *57* (11), 4814–4820. doi: 10.1063/1.1678153.

[273] Gohs, U.; Böhm, R.; Brünig, H.; Fischer, D.; Häußler, L.; Kirsten, M.; Malanin, M.; Müller, M. T.; Cherif, C.; Wolz, D. S. J.; Jäger, H. *Radiat. Phys. Chem.* **2019**, *156*, 22–30. doi: 10.1016/j.radphyschem.2018.10.012.

[274] Lee, B. J.; Zhou, Y.; Lee, J. S.; Shin, B. K.; Seo, J. A.; Lee, D.; Kim, Y. S.; Choi, H. K. *PLoS One* **2018**, *13* (4), e0196315. doi: 10.1371/journal.pone.0196315.

[275] Giddings, J. C.; Caldwell, K. D.; Myers, M. N. *Macromolecules* **1976**, *9* (1), 106–112. doi: 10.1021/ma60049a021.

[276] Melucci, D.; Contado, C.; Mingozzi, I.; Reschiglian, P.; Dondi, F. *Chromatographia* **1999**, *49* (3–4), 131–136. doi: 10.1007/BF02575274.

[277] Lou, J.; Myers, M. N.; Giddings, J. C. *J. Liq. Chromatogr.* **1994**, *17* (14–15), 3239–3260. doi: 10.1080/10826079408013201.

[278] Kirkland, J. J.; Boone, L. S.; Yau, W. W. *J. Chromatogr. A* **1990**, *517* (C), 377–393. doi: 10.1016/S0021-9673(01)95735-8.

[279] Ponyik, C. A.; Wu, D. T.; Williams, S. K. R. *Anal. Bioanal. Chem.* **2013**, *405* (28), 9033–9040. doi: 10.1007/s00216-013-7282-6.

[280] Kassalainen, G. E.; Williams, S. K. R. *Anal. Chem.* **2003**, *75* (8), 1887–1894. doi: 10.1021/ac020594j.

[281] Greyling, G.; Pasch, H. Greyling, G., Pasch, H., Eds.; Springer International Publishing: Cham, 2019; pp 31–99. doi: 10.1007/978-3-030-10650-8_3.

[282] Radebe, N. W.; Beskers, T.; Greyling, G.; Pasch, H. *J. Chromatogr. A* **2019**, *1587*, 180–188. doi: 10.1016/J.CHROMA.2018.12.012.

[283] Mes, E. P. C.; Tijssen, R.; Kok, W. T. *J. Chromatogr. A* **2001**, *907* (1–2), 201–209. doi: 10.1016/S0021-9673(00)01010-4.

[284] Shiundu, P. M.; Williams, S. K. R. In *Particle Sizing and Characterization*; ACS Symposium Series; American Chemical Society, 2004; Vol. 881, pp 185–198. doi: 10.1021/bk-2004-0881.ch012.

[285] Schimpf, M. E.; Semenov, S. N. *J. Phys. Chem. B* **2001**, *105* (12), 2285–2290. doi: 10.1021/jp0005221.

[286] Muza, U. L.; Greyling, G.; Pasch, H. *J. Chromatogr. A* **2018**, *1562*, 87–95. doi: 10.1016/J.CHROMA.2018.05.065.

[287] Muza, U. L.; Greyling, G.; Pasch, H. *Anal. Chem.* **2017**, *89* (13), 7216–7224. doi: 10.1021/acs.analchem.7b01445.

[288] Greyling, G.; Pasch, H. *Polym. Int.* **2017**, *66* (6), 745–751. doi: 10.1002/pi.5350.

[289] Gunderson, J. J.; Caldwell, K. D.; Giddings, J. C. *Sep. Sci. Technol.* **1984**, *19* (10), 667–683. doi: 10.1080/01496398408060668.

[290] Asten, A. C. Van; Boelens, H. F. M.; Kok, W. T.; Poppe, H.; Williams, P. S.; Giddings, J. C. *Sep. Sci. Technol.* **1994**, *29* (4), 513–533. doi: 10.1080/01496399408002159.

[291] Schimpf, M. E.; Williams, P. S.; Giddings, J. C. *J. Appl. Polym. Sci.* **1989**, *37* (7), 2059–2076. doi: 10.1002/app.1989.070370725.

[292] Rubinstein, M.; Colby, R. H. In *Polymer Physics*; Oxford university press: New-York, 2003; Vol. 100, pp 97–133.

[293] Fetters, L. J.; Lohse, D. J.; Colby, R. H. In *Physical Properties of Polymers Handbook*; Mark, J. E., Ed.; Springer: New York, USA, 2007; pp 447–454. doi: 10.1007/978-0-387-69002-5_25.

[294] Rehahn, M.; Mattice, W. L.; Suter, U. W. In *Rotational Isomeric State Models in Macromolecular Systems*:; Springer: Berlin, Heidelberg, 1997; pp 19–476. doi: 10.1007/bfb0050961.

[295] Chen, X.; Yuan, C.; Wong, C. K. Y.; Zhang, G. *J. Mol. Model.* **2012**, *18* (6), 2333–2341. doi: 10.1007/s00894-011-1249-3.

[296] Morozov, K. I.; Köhler, W. *Langmuir* **2014**, *30* (22), 6571–6576. doi: 10.1021/la501695n.

[297] Duda, A.; Penczek, S. *Biopolymers Online*. January 15, 2002, pp 382 - 383. doi: 10.1002/3527600035.bpol3b12.

[298] Chen, G. -f; Jones, F. N. *J. Appl. Polym. Sci.* **1990**, *41* (9–10), 2517–2520. doi: 10.1002/app.1990.070410951.

[299] Komber, H.; Ziemer, A.; Voit, B. *Macromolecules* **2002**, *35* (9), 3514–3519. doi: 10.1021/ma011747s.

[300] Brewer, A. K.; Striegel, A. M. *Anal. Bioanal. Chem.* **2008**, *393* (1), 295. doi: 10.1007/s00216-008-2319-y.

[301] Tosoh Bioscience LLC. *White Paper*. 2019. url: www.tosohbioscience.com. available on request.

[302] de Gennes, P. G. *Scaling Concepts in Polymer Physics*; Cornell University Press, 1979; Vol. 33. doi: 10.1063/1.2914118.

[303] Ramachandran, R.; Beaucage, G.; Kulkarni, A. S.; McFaddin, D.; Merrick-Mack, J.; Galiatsatos, V. *Macromolecules* **2008**, *41* (24), 9802–9806. doi: 10.1021/ma801775n.

[304] Fetters, L. J.; Graessley, W. W.; Krishnamoorti, R.; Lohse, D. J. *Macromolecules* **1997**, *30* (17), 4973–4977. doi: 10.1021/ma961408c.

[305] Ramachandran, R.; Beaucage, G.; McFaddin, D.; Merrick-Mack, J.; Galiatsatos, V.; Mirabella, F. *Polymer* **2011**, *52* (12), 2661–2666. doi: 10.1016/j.polymer.2011.04.005.

[306] Roland, C. M. In *The Science and Technology of Rubber*; Mark, J. E., Erman, B., Roland, C. M. B. T.-T. S. and T. of R. (4th E., Eds.; Academic Press: Boston, USA, 2013; pp 115–166. doi: 10.1016/B978-0-12-394584-6.00003-0.

[307] Dannoux, A.; Esnouf, S.; Amekraz, B.; Dauvois, V.; Moulin, C. *J. Polym. Sci. Part B Polym. Phys.* **2008**, *46* (9), 861–878. doi: 10.1002/polb.21419.

[308] Rosu, D.; Rosu, L.; Cascaval, C. N. *Polym. Degrad. Stab.* **2009**, *94* (4), 591–596. doi: 10.1016/j.polymdegradstab.2009.01.013.

[309] Balko, J.; Fernández-D'Arlas, B.; Pöselt, E.; Dabbous, R.; Müller, A. J.; Thurn-Albrecht, T. *Macromolecules* **2017**, *50* (19), 7672–7680. doi: 10.1021/acs.macromol.7b00871.

[310] Saiani, A.; Daunch, W. A.; Verbeke, H.; Leenslag, J. W.; Higgins, J. S. *Macromolecules* **2001**, *34* (26), 9059–9068. doi: 10.1021/ma0105993.

[311] Scholz, P.; Wachtendorf, V.; Panne, U.; Weidner, S. M. *Polym. Test.* **2019**, *77*, 105881. doi: 10.1016/j.polymertesting.2019.04.028.

[312] Scholz, P.; Wachtendorf, V.; Elert, A. M.; Falkenhagen, J.; Becker, R.; Hoffmann, K.; Resch-Genger, U.; Tschiche, H.; Reinsch, S.; Weidner, S. *Polym. Test.* **2019**, *78*, 105996. doi: 10.1016/j.polymertesting.2019.105996.

[313] Lederer, A.; Elrehim, M. A.; Schallausky, F.; Voigt, D.; Voit, B. *E-Polymers* **2006**, *6* (1), 1–14. doi: 10.1515/epoly.2006.6.1.510.

[314] Nguyen, M. T.; Beckett, R. *Polym. Int.* **1993**, *30* (3), 337–343. doi: 10.1002/pi.4990300310.

[315] Nguyen, M.; Beckett, R. *Sep. Sci. Technol.* **1996**, *31* (3), 291–317. doi: 10.1080/01496399608000697.

[316] Cao, W.; Williams, P. S.; Myers, M. N.; Giddings, J. C. *Anal. Chem.* **1999**, *71* (8), 1597–1609. doi: 10.1021/ac981094m.

[317] Sisson, R. M.; Giddings, J. C. *Anal. Chem.* **1994**, *66* (22), 4043–4053. doi: 10.1021/ac00094a029.

[318] Rue, C. A.; Schimpf, M. E. *Anal. Chem.* **1994**, *66* (22), 4054–4062. doi: 10.1021/ac00094a030.

[319] Grunberg, L.; Nissan, A. H. *Nature* **1949**, *164* (4175), 799–800. doi: 10.1038/164799b0.

[320] Van Der Wyk, A. J. A. *Nature* **1936**, *138* (3498), 845–846. doi: 10.1038/138845b0.

[321] McAllister, R. A. *AIChE J.* **1960**, *6* (3), 427–431. doi: 10.1002/aic.690060316.

8. Publications

8.1. Non-Parabolicity correction for fifty-nine solvents and a retention study for strongly distorted flow-profiles in thermal field-flow fractionation

Journal of Chromatography A 1621 (2020) 461082

Contents lists available at ScienceDirect

Journal of Chromatography A

journal homepage: www.elsevier.com/locate/chroma

Non-Parabolicity correction for fifty-nine solvents and a retention study for strongly distorted flow-profiles in thermal field-flow fractionation

Martin Geisler[a,b], Albena Lederer[a,b,*]

[a] Polymer Separation Group, Department Analysis, Leibniz-Institut für Polymerforschung Dresden e. V., Hohe Straße 6, 01069 Dresden, Germany
[b] Faculty of Chemistry and Food Chemistry, Technische Universität Dresden, 01062 Dresden, Germany

ARTICLE INFO

Article history:
Received 8 February 2020
Revised 24 March 2020
Accepted 25 March 2020
Available online 15 April 2020

ABSTRACT

The non-parabolicity correction of the laminar flow profiles was numerically calculated for fifty-nine solvents. The exact flow profiles were simulated based on sophisticated experimental literature data of dynamic viscosity and thermal conductivity and their dependency on the temperature in between cold wall temperatures of −10 °C up to 120 °C and temperature gradients up to $\Delta T = 120$ K. Based on this computation the polynomial coefficients for the calculation of the non-parabolicity parameter ν is tabulated for each solvent. For this calculation a third-degree polynomial velocity profile was applied, which approximates in a good agreement the exact profile for moderately distorted flow profiles. Instead, for strongly distorted flow profiles a more exact solution with keeping ν as only adjustable parameter is proposed. Additionally, an empirically derived solution is presented to calculate the dimensionless retention parameter λ in fair accuracy directly from retention data.

1. Introduction

Since J. C. Giddings had developed the basic idea of Field flow fractionation (FFF) in 1965 [1], numerous further varieties of FFF techniques were invented with different underlying separation force fields. All they are based on the principle of a separation occurring in a thin ribbon-like channel with a laminar parabolic flow profile and an applied separation force field perpendicular to the flow direction. Once an analyte is introduced at the inlet of the channel via an injection step, the separation force induces an exponential concentration profile of the analyte with the highest concentration at the accumulation wall. Thus, by combination of the exponential concentration profile and the parabolic flow profile, the retention in FFF can be generally described by the well-known retention equation in its integrated form as given in Eq. (1) [2]:

$$R_p = \frac{t_0}{t_R} = 6\lambda\left(coth\left(\frac{1}{2\lambda}\right) - 2\lambda\right) \quad (1)$$

where the retention ratio for a parabolic flow profile R_p is the quotient of the void time t_0 and the retention time t_R measured at the outlet of the channel and is defined as a relationship to a dimensionless retention parameter λ. It describes the center of gravity's relative height of the analyte concentration distribution from the accumulation wall (mean layer thickness) under influence of the separation force field and is consequently defined by a relation to a physico-chemical parameter of the analyte.

For Thermal FFF (ThFFF) λ is defined as the ratio of the translational diffusion coefficient D caused by the Brownian motion and the thermal diffusion coefficient D_T induced by the separation force field, divided by the field strength ΔT. Here, the inverse ratio describes the so-called Soret coefficient $S_T = D_T\, D^{-1}$.

For most FFF techniques, Eq. (1) works sufficiently well and changes of the carrier liquid's viscosity are negligible. In contrast, in ThFFF the separation is performed in a pressurized channel (typically 10 bar) [3–5] to prevent boiling of the carrier liquid and the separation force field is realized by a temperature gradient between the upper (heated) wall and the actively cooled bottom wall. Consequently, the temperature gradient leads to a non-uniformity of the viscosity and to a falsified description of the retention by Eq. (1) with increasing field force due to a distortion of the flow profile. Therefore, Eq. (1) needs to be corrected by an introduction of a non-parabolicity factor ν [6,7] to calculate the retention ratio R, as stated in Eq. (2).

$$R = 6\lambda\left[\nu + (1 - 6\lambda\nu)\left(coth\left(\frac{1}{2\lambda}\right) - 2\lambda\right)\right] \quad (2)$$

* Corresponding author at: Faculty of Chemistry and Food Chemistry, Technische Universität Dresden, 01062 Dresden, Germany
E-mail address: lederer@ipfdd.de (A. Lederer).

https://doi.org/10.1016/j.chroma.2020.461082
0021-9673/

which was developed based on a third-degree polynomial approximation of the distortable flow profile, as given here in Eq. (3).

$$\frac{u(x)}{\overline{u}_{3rd}} \cong 6\left[(1+\nu)\left(\frac{x}{w}\right) - (1+3\nu)\left(\frac{x}{w}\right)^2 + 2\nu\left(\frac{x}{w}\right)^3\right] \tag{3}$$

For most solvents investigated in a previous work [8] as well as in this article, Eq. (3) provides a sufficiently accurate match of the exact flow profile. However, for strongly distorted flow profiles an increasing deviation to Eq. (3) is found. Thus, a more complex but more accurate relation for R on the basis of a fifth-degree polynomial approximation as shown by Eq. (4) is reported [9–12].

$$\frac{u(x)}{\overline{u}}_{5th} = d_1\left(\frac{x}{w}\right)^1 + \ldots + d_5\left(\frac{x}{w}\right)^5 \tag{4}$$

Here, ν can be still derived from the polynomial coefficient d_1, but a calculation of Eq. (4) or R, respectively, cannot be done on a basis of only one adjustable parameter such as ν.

Belgaied, Hoyos and Martin [8] developed a polynomial based approach for an easy determination of ν in dependency on the cold wall temperature T_c and ΔT, as shown in Eq. (5)

$$\nu = (a_1 T_c + a_2)\Delta T + (a_3 T_c + a_4)\Delta T^2 + (a_5 T_c + a_6)\Delta T^3 \tag{5}$$

The polynomial coefficients a_1 to a_6, computed numerically by a linear fitting process for ThFFF at moderate T_c, have been reported for 12 organic solvents. Yet, ThFFF investigations have been performed in many other solvents [13–21] and even at elevated T_c as high temperature ThFFF [22,23], which are not covered by the report of Belgaied et al. [8], where values for ν were computed by complex algorithms for specific experimental conditions or the distortion of the flow profile was completely ignored leading to rather incorrect thermophoretical data [4,16,24], particularly for polymers with typically poorer retention than observed for larger objects such as latex particles [25–27], micelles or other vesicle-like objects [28–30]. In order to determine thermophoretical data from ThFFF experiments in comparable accuracy to data from other methods such as thermal diffusion forced Rayleigh scattering (TDFRS) [31–33], thermogravitational methods [34,35] or optical beam deflection techniques [36,37], an applicable way for the non-parabolicity correction in the processing of ThFFF data is definitely needed. The requirement of this correction and its impact on the accuracy of thermophoretical data derived from ThFFF retention in comparison to batch methods as described above has been already reported [2] and confirmed [9,38,39] decades ago. The major aim of this study is to extend and revise the list of solvents and the applicable temperature range of the polynomial coefficients a_1 to a_6 used in Eq. (5) as an easy and user-friendly way to calculate ν.

The calculation of λ containing the physicochemical information of interest from a measured R needs to be typically done by numerical iterative methods such as root-finding algorithms since the analytical solution of Eq. (1) or Eq. (2) to λ does not exist. For a conditionally precise approximation of λ Schimpf, Schure and Schettler [40] proposed an empirical relation for retention in a parabolic flow as given in Eq. (6).

$$\lambda \cong \frac{R_p}{6(1-R_p)^{\frac{1}{3}}} \tag{6}$$

2. Theory

The parabolic profile of a laminar isoviscous flow between two infinite parallel plates with a distance w to each other is derived by integration and simplification of the one directional form of the Navier-Stokes-equation [41], given by Eq. (7)

$$\left(\frac{u}{\overline{u}}\right)_p = 6\left[(x/w) - (x/w)^2\right] \tag{7}$$

in which the ratio of the local flow velocity u and the mean flow velocity $\overline{u}$ depends only on the relative height x/w of the flow layer.

For a one-directional flow with non-constant viscosity the Navier stokes equation is defined as in Eq. (8)

$$\frac{d}{dx}\left(\eta(T)\frac{du}{dx}\right) = \eta(T)\frac{d^2u}{dx^2} + \frac{d\eta(T)}{dx}\cdot\frac{du}{dx} \tag{8}$$

with the temperature dependent dynamic viscosity $\eta(T)$,which after integration and transformation is used for definition of the flow profile [6,8,9,12] in Eq. (9). Effects like pressure drops, edge effects of the non-infinite channel and thermal expansion have been neglected due to their insignificant contributions at the used low flow velocity, large channel aspect ratio and thermal expansion coefficients of the carrier liquids being of the order of 10^{-3} K^{-1} [12,41,42]. To generate such a velocity flow profile in dependence of $\eta(T)$, the temperature profile across the channel thickness needs to be known and can be calculated as described earlier [6,8,9,12].

$$\frac{u}{\overline{u}} = \frac{\int_0^{x/w}\frac{x/w}{\eta(T)}d(x/w) - \frac{\int_0^1\frac{x/w}{\eta(T)}d(x/w)}{\int_0^1\frac{d(x/w)}{\eta(T)}}\int_0^{x/w}\frac{d(x/w)}{\eta(T)}}{\int_0^1\left(\int_0^{x/w}\frac{x/w}{\eta(T)}d(x/w) - \frac{\int_0^1\frac{x/w}{\eta(T)}d(x/w)}{\int_0^1\frac{d(x/w)}{\eta(T)}}\int_0^{x/w}\frac{d(x/w)}{\eta(T)}\right)d(x/w)} \tag{9}$$

The non-parabolicity parameter ν can be determined with the help of the relative deviation ε (Eq. (10) of the flow profile generated by Eq. (9) to the parabolic flow profile in Eq. (7) in dependency of x/w

$$\varepsilon(x/w) = \frac{\frac{u}{\overline{u}}(x/w) - \left(\frac{u}{\overline{u}}\right)_p(x/w)}{\left(\frac{u}{\overline{u}}\right)_p(x/w)} \tag{10}$$

ν can be then found either in the initial slope of $u/\overline{u}(x/w \to 0)$ at the cold wall or extrapolated as close approximation from ε in the vicinity of $x/w \cong 0$ (ε becomes undefined at exactly 0) [8], both described in Eq. (11).

$$\varepsilon(x/w \to 0) \hat{=} \frac{1}{6}\left(\frac{d\left(\frac{u}{\overline{u}}(x/w)\right)}{d(x/w)}\right)_{x/w\to 0} - 1 = \nu \tag{11}$$

3. Data processing

Eq. (9) and the integrations included were solved by numerical trapezoidal integration with a step width of $x/w = 8\cdot 10^{-3}$ and with an expression of $\eta(T)$. Therefore, the exact temperature profile along the channel thickness was calculated by an adapted version of the exact temperature profile (Eq. (12)) as described earlier [6,8,9,12] with the cold wall temperature T_c and $\kappa'(T)$ as the first derivative of $\kappa(T)$, in order to consider partial non-linearities of experimental thermal conductivity data $\kappa(T)$, in particular at elevated temperatures.

$$T_i(x_i/w) = T_c + \frac{\kappa_{i-1}}{\kappa'(T_{i-1})} \times\left(\sqrt{1 + \frac{\kappa'(T_{i-1})}{\kappa_{i-1}}\Delta T\left(1 + \frac{\kappa'(T_{i-1})}{\kappa_{i-1}}\frac{\Delta T}{2}\right)x_i/w} - 1\right) \tag{12}$$

The computation of Eq. (9) and Eq. (12) was done by fitting of sophisticated experimental literature data of η and κ (references see Table 1). For each solvent the exact velocity flow profile (Eq. (9)) was calculated in 210 sets with T_c = −10 to 120 °C and ΔT = −20 to 120 K (minus indicates inversion between hot and cold wall), both T_c and ΔT with a step width of 10 K. The resulting values of ν were then fitted by a third-degree polynome as a function of T_c and ΔT. Here, the polynomial coefficients a_1 to

Table 1
Coefficients a_i for the calculation of v in dependency of T_c [°C] and ΔT [K] with the polynome given in Eq. (5).

Solvent	CAS	$10^5\ a_1$	$10^3\ a_2$	$10^7\ a_3$	$10^5\ a_4$	$10^9\ a_5$	$10^7\ a_6$	T_c [°C] min	T_c [°C] max	ΔT_{max} [K]	Ref. for η, κ
Normal temperature ThFFF											
Acetonitrile	75–05–8	2.81123	−4.11188	−2.95309	2.02670	1.02557	−0.72112	−10	50	120	[44]
Diisopropyl ether	108–20–3	2.62068	−4.01912	−2.13706	1.68458	0.69925	−0.44164	−10	50	100	[47,48]
Methyl *tert*-butyl ether	1634–04–4	4.49603	−4.78493	−1.47717	2.60296	0.07636	−0.62683	−10	50	120	[44,49]
Dichloromethane	75–09–2	1.78974	−3.58977	−0.45358	1.28545	0.05291	−0.19628	−10	50	120	[44]
Acetone	67–64–1	2.32625	−3.99199	−1.57742	1.72781	0.64776	−0.41366	−10	50	120	[44,50]
Methanol	67–56–1	2.18760	−5.18911	−1.90968	2.17026	0.82145	−0.57395	−10	50	85	[44,47,51–54]
Ethanol	64–17–5	2.08800	−7.01762	−1.57244	2.99908	0.67626	−0.71352	−10	50	50	[44,52–56]
n-Propanol	71–23–8	5.53139	−9.56185	−5.05499	5.85375	1.80902	−1.76513	−10	50	50	[44,53,54,57–59]
n-Butanol	71–36–3	4.24315	−9.80667	−1.93859	5.05883	0.53406	−1.23832	−10	50	50	[44,54,57,60]
n-Pentanol	71–41–0	7.86996	−11.9714	−8.80312	8.96036	3.48033	−3.11385	−10	50	50	[57,61,62]
n-Hexanol	111–27–3	5.73534	−11.5606	−3.36441	6.84638	0.63774	−1.79163	−10	50	50	[44,57,62,63]
2-Propanol	67–63–0	9.37518	−11.9367	−4.15953	8.38247	0.43086	−2.39815	0	50	100	[44,45,64]
2-Butanol	78–92–2	12.1401	−15.6858	−8.65824	11.9579	1.97072	−3.64193	−10	50	50	[57,61]
Isobutanol	78–83–1	7.36831	−13.1154	−2.73631	7.78315	0.14484	−1.89911	−10	50	50	[57,61]
2,2,2-Trifluoroethanol	75–89–8	6.16181	−10.2666	−5.59704	6.92823	2.23231	−2.22817	$(0.8\Delta T - 25)$		100	[61,65]
Tetrahydrofuran	109–99–9	2.43693	−4.04762	−1.50392	1.69946	0.44876	−0.42922	0	50	120	[44,45]
Toluene	108–88–3	2.92379	−4.85476	−1.95288	2.19741	0.60389	−0.57440	0	50	120	[44,66,67]
Ethyl acetate	141–78–6	2.50711	−4.49963	−1.49405	2.02702	0.33271	−0.50931	0	50	120	[43–45]
N,N-Dimethylacetamide	127–19–5	3.01170	−5.21419	−1.95502	2.32825	0.67272	−0.58089	0	50	120	[61,62,68]
N,N-Dimethylformamide	68–12–2	2.84429	−4.84601	−1.77355	2.01790	0.53384	−0.47440	0	50	120	[61,62,68]
Chloroform	67–66–3	2.14342	−3.76849	−2.05018	1.45971	0.75091	−0.41200	0	50	120	[43,44,52]
2-Butanone (MEK)	78–93–3	2.53888	−4.13048	−0.56049	1.72162	−0.03280	−0.32350	0	50	120	[44,52,69]
1,2-Dichloroethane	107–06–2	2.91575	−5.03710	−0.61179	1.61337	−0.05934	0.11818	0	60	120	[43,44,52]
Dioxane	123–91–1	3.78397	−6.53012	−2.80239	3.34993	0.93981	−0.94134	0	60	120	[44,61,70]
n-Alkanes*	$a_1 = (4.1067 - 1.5732\ C + 0.2440\ C^2 - 7.7246\cdot10^{-3}\ C^3)\ 10^{-5}$ $a_2 = (-6.7739 + 1.5610\ C - 0.2182\ C^2 + 6.6972\cdot10^{-3}\ C^3)\ 10^{-3}$ $a_3 = (-6.8320 + 2.4600\ C - 0.3180\ C^2 + 9.3715\cdot10^{-3}\ C^3)\ 10^{-7}$ $a_4 = (4.2438 - 1.4362\ C + 0.1971\ C^2 - 5.8661\cdot10^{-3}\ C^3)\ 10^{-5}$ $a_5 = (4.4766 - 1.4596\ C + 0.1658\ C^2 - 4.7602\cdot10^{-3}\ C^3)\ 10^{-9}$ $a_6 = (-1.1696 + 0.4657\ C - 6.6192\cdot10^{-2}C^2 + 1.9433\cdot10^{-3}C^3)\ 10^{-7}$							0	60	120	[44,61,71–75]
Cycloalkanes#	$a_1 = (-90.063 + 46.481\ C - 7.481\ C^2 + 0.3966\ C^3)\ 10^{-5}$ $a_2 = (53.381 - 30.460\ C + 5.082\ C^2 - 0.2808\ C^3)\ 10^{-3}$ $a_3 = (110.433 - 55.891\ C + 8.913\ C^2 - 0.4662\ C^3)\ 10^{-7}$ $a_4 = (-69.303 + 36.397\ C - 5.947\ C^2 + 0.3204\ C^3)\ 10^{-5}$ $a_5 = (-37.396 + 19.283\ C - 3.0991\ C^2 + 0.1623\ C^3)\ 10^{-9}$ $a_6 = (29.800 - 15.192\ C + 2.4460\ C^2 - 0.1297\ C^3)\ 10^{-7}$							0	50	120	[44,61,76–80]
Methyl-Cyclohexane	108–87–2	2.95476	−5.18671	−2.44689	2.68028	0.88834	−0.79714	0	80	120	[44]
Chlorobenzene	108–90–7	2.79788	−4.65199	−1.82235	2.05211	0.55728	−0.52586	−10	60	120	[45,61,81,82]
o-Dichlorobenzene	95–50–1	11.5967	−8.48723	−14.7743	7.59760	6.59895	−3.06355	−10	60	120	[22,61,62,83]
Tetralin	119–64–2	3.30505	−7.21433	−0.83193	3.50186	−0.17205	−0.83744	30	60	120	[47,84–86]
Mesitylene	108–67–8	8.54042	−6.80595	−10.36893	5.29134	4.84328	−2.10632	10	45	120	[47,62,79,84,87–89]
Water	7732–18–5	7.12565	−9.39143	−3.73205	5.48428	0.88645	−1.46677	5	60	120	[44,46,62,90,91]
1,2-Dimethoxyethane	110–71–4	2.18188	−4.38560	−1.81788	2.00954	0.71375	−0.56094	−20	60	120	[61,92,93]
2-Butoxyethanol	111–76–2	10.7068	−11.8822	−8.82060	9.41055	2.92923	−3.17925	15	80	120	[61,94,95]
Normal and high temperature ThFFF											
Di-n-butyl ether	142–96–1	2.72237	−5.12796	−0.92398	2.15602	0.14004	−0.40833	−10	120	120	[44,48]
N-Methylformamide	123–39–7	2.45269	−6.00623	−0.82956	2.27296	0.11321	−0.43192	−25	120	100	[61,62,83]
Formamide	75–12–7	13.9786	−13.8246	−15.1285	13.5836	6.54463	−5.47944	−10	120	120	[61,83,96]
Dimethyl sulfoxide	67–68–5	3.38833	−7.15379	−2.05741	2.92986	0.53748	−0.67149	20	110	120	[44,90,97,98]
m-Cresol	108–39–4	8.14388	−14.7403	−8.84976	12.5907	3.54416	−4.70915	$(0.4\Delta T - 29)$		120	[82,83,99,100]
Cumene	98–82–8	2.71242	−5.17945	−1.08585	1.88081	0.29181	−0.40651	0	120	120	[47,79,101,102]
N-Methylpyrrolidone	872–50–4	3.80140	−6.20843	−1.61194	2.97338	0.33056	−0.69039	−10	120	120	[44,83]
High temperature ThFFF											
1,2,4-Trichlorobenzene	120–82–1	4.67106	−7.81572	−2.33886	4.30904	0.52980	−1.09473	60	120	120	[61,83,103,104]
Tetralin	119–64–2	2.67157	−6.33490	−2.46034	3.73248	0.54116	−1.02966	60	110	120	[61,84–86]
Mesitylene	108–67–8	2.56978	−4.43306	−0.85776	1.65643	0.12884	−0.30901	45	115	120	[47,62,79,84,87–89]
Sulfolane	126–33–0	5.12406	−9.84136	−4.05327	6.53778	1.14323	−1.94998	60	120	120	[44,83,105]
Chlorobenzene	108–90–7	1.54266	−4.06701	−0.78833	1.58054	0.21238	−0.37031	60	120	120	[45,61,81,82]
o-Dichlorobenzene	95–50–1	2.32822	−4.77209	−1.68232	2.56593	0.57274	−0.78800	60	120	120	[22,61,62,83]
Cyclooctane	292–64–8	2.70823	−6.96898	−1.91163	3.62100	0.61399	−1.02085	60	120	120	[44,61,79]
n-Alkanes**	$a_1 = (5.5813 - 1.535\ C + 0.1567\ C^2 - 4.5572\cdot10^{-3}C^3)\ 10^{-5}$ $a_2 = (-8.2538 + 1.6911\ C - 0.1830\ C^2 + 5.240\cdot10^{-3}C^3)\ 10^{-3}$ $a_3 = (-2.1672 + 0.6149\ C - 0.0641\ C^2 + 1.8942\cdot10^{-3}C^3)\ 10^{-7}$ $a_4 = (4.6778 - 1.217\ C + 0.12624\ C^2 - 3.64117\cdot10^{-3}C^3)\ 10^{-5}$ $a_5 = (0.4821 - 0.1103\ C + 0.0113\ C^2 - 3.3275\cdot10^{-3}C^3)\ 10^{-9}$ $a_6 = (-0.9922 + 0.2647\ C - 2.7973\cdot10^{-2}C^2 + 8.1827\cdot10^{-4}C^3)\ 10^{-7}$							60	120	120	[44,61,71–75]
Decalin	91–17–8	$a_1 = (3.6337 - 1.0655\ x + 0.25467\ x^2)\ 10^{-5}$						50	120	120	[44,106–111]
cis (1) + trans (2)§	iso. mix.	$a_2 = (-7.3400 + 1.4600\ x - 0.34546\ x^2)\ 10^{-3}$									
	493–01–6	$a_3 = (-1.4880 + 0.6786\ x - 0.19491\ x^2)\ 10^{-7}$									
	cis	$a_4 = (3.4066 - 1.1598\ x + 0.297854\ x^2)\ 10^{-5}$									
	493–02–7	$a_5 = (0.2622 - 0.1605\ x + 0.058696\ x^2)\ 10^{-9}$									
	trans	$a_6 = (-0.7206 + 0.3297\ x - 0.100542\ x^2)\ 10^{-7}$									

C: Number of carbon atoms per n- or cycloalkane molecule, valid for: * C5 to C16.
C5 to C8; ** C9 to C16.
§ *x: molar ratio, defined as* $x = x_1\ (x_1 + x_2)^{-1}$.

a_6 (Eq. (5)) were be determined by linear fits of the third-degree polynomial coefficients $B_X = a_{(i==x)}\ T_c + a_{(i==x+1)}$ for defined temperature ranges (given in Table 1).

4. Results and discussion

The fitting of the computed values of ν by a third-degree polynome revealed, that the polynomial coefficients B_X from Eq. (5) can be described by a linear relation to T_c only for limited ranges of computed T_c, reported earlier [8]. For the broad range of T_c used here, a polynomial fit would be necessary for an accurate fit. However, the coefficients a_i in Eq. (5) were found to also partly counterbalance their contribution to ν. Therefore, they compensate effects caused by deviations from the linear fit to T_c to rematch ν calculated by Eq. (5) compared to the computationally derived ν by Eq. (11). The ranges of T_c and ΔT in Eq. (5) can be calculated to accurately match the computed values, which depends on the properties and the limitations given by the melting and boiling points of the solvent (in the pressurized channel). Changes in the dynamic viscosity by slightly elevated pressure used in ThFFF have been found to be negligible (e. g. for Cyclohexane = 3% and for Ethyl acetate = 2% from 1 to 25 bar) [43–45]. The influence of the pressure on the thermal conductivity, which contributes in general only to a small extend to the computed flow profiles, have been also found to be negligible (e.g. for water < 0.1% at 100 °C between 2 and 20 bars) [46]. The observed compensational effect between the coefficients a_i enables the approach by Belgaied et al. [8] to cover reasonably large intervals of T_c and ΔT for all solvents regarded in this article for ThFFF with T_c around room temperature (normal temperature ThFFF) or elevated T_c (high temperature ThFFF). In some cases even the full range from normal to high temperature ThFFF can be described by the linearly fitted coefficients a_i in Eq. (5). A sophisticated summary of all computed coefficients is given in Table 1. The computed polynomial coefficients a_1 to a_6 (Table 1) allow to describe the velocity flow profile in its 3rd-degree approximation as well as the retention ratio (Eq. (2)) with a deviation of ±2% in the given limits of T_c and ΔT. Thereby, the values of ν calculated by the a_i coefficients of cyclohexane, ethyl acetate and tetrahydrofuran computed as reference and cross check are in good agreement to ν from a_i reported by Belgaied et al. [8]. Furthermore, the values of ν in the high temperature range reported for chlorobenzene by Pasti [22] are in good agreement with our results. This confirms the reliability of the a_i coefficients computed by Eq. (9) to (12) with sophisticated experimental data from the literature and verifies the validity of previously reported [8] a_i in their limits of T_c and ΔT.

For the vast majority of solvents, a moderate non-parabolicity is found with ν < –0.4 at high field conditions of ΔT = 100 K, which confirms very accurate match of the simplified flow profile (Eq. (3)) and the retention ratio (Eq. (2)) even at high force field conditions. However, polar and in particular protic solvents such as alcohols and water exhibit severe distortions at higher field conditions reaching ν = –0.6, which significantly deviates from the third-degree polynomial approximation. A precise description of those solvents requires the application of the fifth-degree approximation (Eq. (4)), where the approach of ν as a single adjustable parameter is incapable. An example of an extremely distorted flow profile is shown in Fig. 1. In contrast to the cyclo and n-alkanes, no accurate homologue series could be correlated for n- and isoalcohols to the number of carbons in the molecule. This can be discussed as hint of an increasing distorting influence by hydrogen bonds or polarity with decreasing chain length.

Consequently, the a_i given in Table 1 for alcohols are only sufficiently precise for lower ΔT (up to 50 K) when used with Eq. (2). In order to extend the applicable range of ΔT for the summarized a_i and improve the description of R for strongly distorted flow profiles a modified relation of R is proposed as presented in Eq. (13)

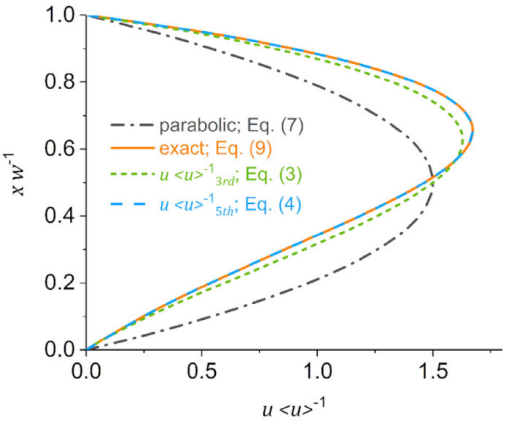

Fig. 1. The flow profile shown for 2-Butanol at ΔT = 100 K, T_c = 20 °C, representing an example of a strongly distorted flow profile. The third-degree polynomial expression (Eq. (3)) does not sufficiently match anymore at ν = –0.63 with T_c and ΔT as shown here, whereas a precise match is still given by the fifth-degree polynomial expression (Eq. (4)).

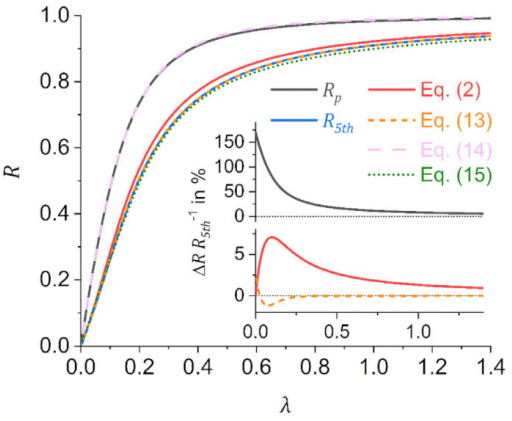

Fig. 2. The retention ratios calculated by differently precise definitions for 2-Butanol for ΔT = 100 K, T_c = 20 °C and their relative deviation to the most accurately accounted relation R_{5th} (Eq. (4)). The curve for Eq. (14) shows R recalculated from Eq. (1) with λ processed from given R, analoguely the curve for Eq. (14) shows R recalculated from Eq. (2).

$$R = R_p + 6\lambda\left(\nu + \frac{R_p}{2}\nu^3\right)(1 - R_p) \qquad (13)$$

With this solution the retention of all alcohols with their a_i given in Table 1 can be described in the full range of ΔT up to 120 K by keeping the simplicity of having only one adjustable parameter for the non-parabolicity correction. The accuracy of the different relations for R is shown in Fig. 2.

To avoid complex numerical iterative solution of R from λ Schimpf, Schure and Schettler [40] proposed an approximation to calculate λ directly from retention data (Eq. (6)) as an inversion of the general retention equation. For undistorted FFF, their solution provides a fairly accurate approximation of λ for $R \leq 0.6$. However, for ThFFF a revision of Eq. (6) is required to keep the deviations with increasing field strength in acceptable limits. Therefore,

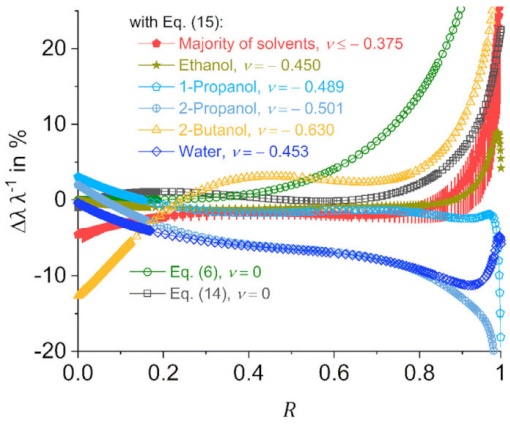

Fig. 3. The precision of calculated λ compared to given λ, both plotted in relation to *R*. All curves were processed for $\Delta T = 100$ K, $T_c = 20$ °C. The reference curves of Eq. (3) and (14) were processed for $T_c = 20$ °C without separation force field.

Eq. (14) can be proposed as a more accurate alternative of Eq. (6)

$$\lambda \cong \frac{\frac{101}{100}R}{6\left(1-R^{\frac{4}{3}}\right)^{\frac{68}{155}}} \tag{14}$$

Thus, an improved approximation of λ has been developed (Eq. (15)), where the non-parabolicity correction is implemented by a simple polynomial relation with the variable parameter ν.

$$\lambda \cong \frac{\left(\frac{5}{4}\nu^2 - \frac{5}{4}\nu + \frac{101}{100}\right)R}{6\left(1-R^{\left(\frac{20}{6}\nu^2 - \frac{12}{5}\nu + \frac{4}{3}\right)}\right)^{\left(\frac{10}{9}\nu^2 - \frac{1}{4}\nu + \frac{68}{155}\right)}} \tag{15}$$

A validity check of Eq. (14) and (15) is presented in Fig. 2, where λ is calculated from given *R* and is then applied in their corresponding inverse relation (Eq. (1) and (2)) to revalidate *R*. For the majority of solvents studied in this work, Eq. (15) is found to resemble λ with a precision of ±5% for $R \leq 0.94$. The precision of the λ prediction for the protic solvents, which tend to strong flow profile distortions, varies due to the solvent's nature from similar precise match of λ (compared to a given λ) to a discrepancy up to 13% in the range of *R* from ≈ 0 to 1. Furthermore, for FFF in general, Eq. (14) is found to allow more accurate calculation of λ than the approximation suggested previously in the literature [40]. A detailed precision evaluation of resembled λ by Eq. (15) is shown in Fig. 3.

5. Conclusions

For the purpose of thermophoretical studies using ThFFF a correction of the distortion in the laminar velocity flow profile caused by changes in the thermal conductivity and viscosity of the carrier liquid with the change of the temperature is inevitable. Therefore a modification of the basic retention equation for FFF has been developed based on a third-degree polynomial flow profile approximation by the introduction of a single adjustable non-parabolicity parameter ν. This non-parabolicity correction is the basis for an accurate derivation of physical thermophoretical data via the dimensionless FFF parameter λ from the retention measured in ThFFF experiments. Belgaied, Hoyos and Martin proposed earlier a numerical polynomial based approach for the coefficients for 12 solvents to allow for an easy calculation of ν [8]. As a revision and extension of this approach a non-parabolicity correction of fifty-nine solvents was computed and tabulated. Their derivation was obtained by processing of the exact flow profiles with the help of sophisticated experimental literature data of $\eta(T)$ and $\kappa(T)$. 210 sets of calculations were performed for each solvent at cold wall temperatures between −10 °C and 120 °C and temperature gradients up to 120 K in order to provide coefficients for an easy calculation of ν for normal and high temperature ThFFF applications. This sophisticated computation revealed, that the majority of solvents of unipolar and aprotic nature can be well described by the established retention equation for ThFFF and ν. Thereby, ν calculated with coefficients reported previously [8] within their reported range of validity and calculated with our apporach are in good agreement. Yet, for protic polar solvents deviations were found due to an increasing inability of the underlying third-degree polynomial flow profile to sufficiently match the more severe distorted flow profiles of these solvents. Thus, they require a more complex computation by a fifth-degree polynomial flow profile. In order to improve the accuracy of the retention description for strong flow profile distortions found for protic-polar solvents at $\Delta T > 50$ K a modified solution of the ThFFF retention equation is proposed, which keeps the non-parabolicity correction easy and user-friendly by including only one adjustable parameter ν.

To enhance the selectivity in ThFFF separations also binary solvent mixtures have been used [112,113]. However, for solvent mixtures, the polynomial approach for calculation of ν (Eq. (5)), using the coefficients given in Table 1 weighted by the molar ratio can be applied only in rare cases, when the miscibility of the solvents is close to thermodynamically ideal [114]. Future work needs to be done to cover all the diversity of solvent mixtures, which is a challenging task, taking into account the non-linear and sometimes complex dependency of $\eta(T)$ and $\kappa(T)$ on the molar mixing ratio due to non-ideal thermodynamic behavior of real liquid mixtures. To encounter these mixing phenomena, consideration of empirical interaction parameters [115,116] or the free energy of activation [117] will be of significant importance.

Since no analytical inversion of the FFF or ThFFF retention equations existsts, the calculation of thermophoretical data from measured retention requires numerical iterative solution, often carried out by more complex computation with root-finding algorithms. To avoid large calculation effort, Schimpf, Schure and Schettler [40] suggested an empirically found approximation for FFF assuming a parabolic flow. By adaption of their approach, an approximation for ThFFF is proposed in this article, in that the non-parabolicity correction with the adjustable parameter ν is implemented. The newly suggested approximation equation is found to generate data for λ in fairly good agreement for ThFFF, as well as in its reduced form for FFF in general.

Declaration of Competing Interests

The authors declare that they have no known competing financial interests or personal relationships that could have appeared to influence the work reported in this paper.

CRediT authorship contribution statement

Martin Geisler: Writing - original draft, Data curation, Conceptualization. **Albena Lederer:** Supervision, Writing - review & editing.

References

[1] J.C. Giddings, A new separation concept based on a coupling of concentration and flow nonuniformities, Sep. Sci. 1 (1966) 123–125, doi:10.1080/01496396608049439.

[2] M.E. Hovingh, G.H. Thompson, J.C. Giddings, Column parameters in thermal field-flow fractionation, Anal. Chem. 42 (1970) 195–203, doi:10.1021/ac60284a003.

[3] M. Geisler, W.C. Smith, L. Plüschke, R. Mundil, J. Merna, S.K.R. Williams, A. Lederer, Topology analysis of chain walking polymerized polyethylene: an alternative approach for the branching characterization by thermal FFF, Macromolecules 52 (2019) 8662–8671, doi:10.1021/acs.macromol.9b01410.

[4] G. Greyling, H. Pasch, Springer International Publishing, Cham, 2019, pp. 31–99, doi:10.1007/978-3-030-10650-8_3.

[5] J.C. Giddings, L.R.K. Smith, M.N. Myers, Thermal field-flow fractionation. extension to lower molecular weight separations by increasing the liquid temperature range using a pressurized system, Anal. Chem. 47 (1975) 2389–2394, doi:10.1021/ac60364a036.

[6] M. Martin, M.N. Myers, J.C. Giddings, Nonequilibrium and polydispersity peak broadening in thermal field-flow fractionation, J. Liq. Chromatogr. 2 (1979) 147–164, doi:10.1080/01483917908060055.

[7] M. Martin, J.C. Giddings, Retention and nonequilibrium peak broadening for a generalized flow profile in field-flow fractionation, J. Phys. Chem. 85 (1981) 727–733, doi:10.1021/j150606a025.

[8] J.E. Belgaied, M. Hoyos, M. Martin, Velocity profiles in thermal field-flow fractionation, J. Chromatogr. A 678 (1994) 85–96, doi:10.1016/0021-9673(94)87077-2.

[9] J.J. Gunderson, K.D. Caldwell, J.C. Giddings, Influence of temperature gradients on velocity profiles and separation parameters in thermal field-flow fractionation, Sep. Sci. Technol. 19 (1984) 667–683, doi:10.1080/01496398408060668.

[10] A.C. Van Asten, H.F.M. Boelens, W.T. Kok, H. Poppe, P.S. Williams, J.C. Giddings, Temperature dependence of solvent viscosity, solvent thermal conductivity, and soret coefficient in thermal field-flow fractionation, Sep. Sci. Technol. 29 (1994) 513–533, doi:10.1080/01496399408002159.

[11] M.E. Schimpf, P.S. Williams, J.C. Giddings, Accurate molecular weight distribution of polymers using thermal field-flow fractionation with deconvolution to remove system dispersion, J. Appl. Polym. Sci. 37 (1989) 2059–2076, doi:10.1002/app.1989.070370725.

[12] M. Martin, C. Van Batten, M. Hoyos, Determination of thermodiffusion parameters from thermal field-flow fractionation retention data, in: W. Köhler, S. Wiegand (Eds.), Springer Berlin Heidelberg, 2002: pp. 250–284. doi: 10.1007/3-540-45791-7_13.

[13] J.C. Giddings, K.D. Caldwell, M.N. Myers, Thermal diffusion of polystyrene in eight solvents by an improved thermal field-flow fractionation methodology, Macromolecules 9 (1976) 106–112, doi:10.1021/ma60049a021.

[14] D. Melucci, C. Contado, I. Mingozzi, P. Reschiglian, F. Dondi, Properties of decalin as a solvent in thermal field-flow fractionation, Chromatographia 49 (1999) 131–136, doi:10.1007/BF02575274.

[15] M.E. Schimpf, J.C. Giddings, Characterization of thermal diffusion in polymer solutions by thermal field-flow fractionation: dependence on polymer and solvent parameters, J. Polym. Sci. Part B Polym. Phys. 27 (1989) 1317–1332, doi:10.1002/polb.1989.090270610.

[16] G. Greyling, A. Lederer, H. Pasch, Thermal field-flow fractionation for the investigation of the thermoresponsive nature of star and linear polystyrene, Macromol. Chem. Phys. 219 (2018) 1800417, doi:10.1002/macp.201800417.

[17] J. Lou, M.N. Myers, J.C. Giddings, Separation of polysaccharides by thermal field-flow fractionation, J. Liq. Chromatogr. 17 (1994) 3239–3260, doi:10.1080/10826079408013201.

[18] J.J. Kirkland, L.S. Boone, W.W. Yau, Retention effects in thermal field-flow fractionation, J. Chromatogr. A. 517 (1990) 377–393, doi:10.1016/S0021-9673(01)95735-8.

[19] C.A. Ponyik, D.T. Wu, S.K.R. Williams, Separation and composition distribution determination of triblock copolymers by thermal field-flow fractionation, Anal. Bioanal. Chem. 405 (2013) 9033–9040, doi:10.1007/s00216-013-7282-6.

[20] G.E. Kassalainen, S.K.R. Williams, Coupling thermal field-flow fractionation with matrix-assisted laser desorption/ionization time-of-flight mass spectrometry for the analysis of synthetic polymers, Anal. Chem. 75 (2003) 1887–1894, doi:10.1021/ac020594j.

[21] J.R. Runyon, S.K.R. Williams, A theory-based approach to thermal field-flow fractionation of polyacrylates, J. Chromatogr. A 1218 (2011) 7016–7022, doi:10.1016/J.CHROMA.2011.08.007.

[22] L. Pasti, S. Roccasalvo, F. Dondi, P. Reschiglian, High temperature thermal field-flow fractionation of polyethylene and polystyrene, J. Polym. Sci. Part B Polym. Phys. 33 (1995) 1225–1234, doi:10.1002/polb.1995.090330808.

[23] S.L. Brimhall, M.N. Myers, K.D. Caldwell, J.C. Giddings, High temperature thermal field-flow fractionation for the characterization of polyethylene, Sep. Sci. Technol. 16 (1981) 671–689, doi:10.1080/01496398108058122.

[24] N.W. Radebe, T. Beskers, G. Greyling, H. Pasch, Online coupling of thermal field-flow fractionation and Fourier transform infrared spectroscopy as a powerful tool for polymer characterization, J. Chromatogr. A 1587 (2019) 180–188, doi:10.1016/J.CHROMA.2018.12.012.

[25] E.P.C. Mes, R. Tijssen, W.T. Kok, Influence of the carrier composition on thermal field-flow fractionation for the characterisation of sub-micron polystyrene latex particles, J. Chromatogr. A 907 (2001) 201–209, doi:10.1016/S0021-9673(00)01010-4.

[26] P.M. Shiundu, S.K.R. Williams, Thermal field-flow fractionation for particle analysis: opportunities and challenges, in: Part. Sizing Charact., American Chemical Society, 2004, pp. 185–198, doi:10.1021/bk-2004-0881.ch012.

[27] M.E. Schimpf, S.N. Semenov, Latex particle thermophoresis in polar solvents, J. Phys. Chem. B 105 (2001) 2285–2290, doi:10.1021/jp0005221.

[28] U.L. Muza, G. Greyling, H. Pasch, Core microstructure, morphology and chain arrangement of block copolymer self-assemblies as investigated by thermal field-flow fractionation, J. Chromatogr. A 1562 (2018) 87–95, doi:10.1016/J.CHROMA.2018.05.065.

[29] U.L. Muza, G. Greyling, H. Pasch, Characterization of complex polymer self-assemblies and large aggregates by multidetector thermal field-flow fractionation, Anal. Chem. 89 (2017) 7216–7224, doi:10.1021/acs.analchem.7b01445.

[30] G. Greyling, H. Pasch, Characterisation of block copolymer self-assemblies by thermal field-flow fractionation, Polym. Int. 66 (2017) 745–751, doi:10.1002/pi.5350.

[31] W. Köhler, Thermodiffusion in polymer solutions as observed by forced Rayleigh scattering, J. Chem. Phys. 98 (1993) 660–668, doi:10.1063/1.464610.

[32] W. Köhler, C. Rosenauer, P. Rossmanith, Holographic grating study of mass and thermal diffusion of polystyrene/toluene solutions, Int. J. Thermophys. 16 (1995) 11–21, doi:10.1007/BF01438953.

[33] D. Stadelmaier, W. Köhler, Thermal diffusion of dilute polymer solutions: the role of chain flexibility and the effective segment size, Macromolecules 42 (2009) 9147–9152, doi:10.1021/ma901794k.

[34] O. Ecenarro, J.A. Madariaga, J.L. Navarro, C.M. Santamaria, J.A. Carrión, J.M. Savirón, Thermogravitational thermal diffusion in liquid polymer solutions, Macromolecules 27 (1994) 4968–4971, doi:10.1021/ma00096a018.

[35] J.D. Hoffman, B.H. Zimm, Rate of thermal diffusion of polymer molecules in solution, J. Polym. Sci. 15 (1955) 405–411, doi:10.1002/pol.1955.120158008.

[36] V.G. Meyerhoff, H. Lütje, B. Rauch, Zur methodik thermischer diffusionsmessungen von makromolekülen in Lösung, Die Makromol. Chemie 44 (1961) 489–496, doi:10.1002/macp.1961.020440140.

[37] B. Rauch, G. Meyerhoff, Thermal diffusion of polystyrene in solution, J. Phys. Chem. 67 (1963) 946–947, doi:10.1021/j100798a521.

[38] J.C. Giddings, M.E. Hovingh, G.H. Thompson, Measurement of thermal diffusion factors by thermal field-flow fractionation, J. Phys. Chem. 74 (1970) 4291–4294, doi:10.1021/j100718a021.

[39] M.N. Myers, K.D. Caldwell, J. Calvin Giddings, A study of retention in thermal field-flow fractionation, Sep. Sci. 9 (1974) 47–70, doi:10.1080/01496397408080043.

[40] M.E. Schimpf, K. Caldwell, J.C. Giddings, Field-Flow Fractionation Handbook, John Wiley & Sons, Inc., New York, USA, 2000.

[41] M. Martin, P.S. Williams, Theoretical basis of field-flow fractionation,, in: F. Dondi, G. Guiochon (Eds.), Theor. Adv. Chromatogr. Relat. Sep. Tech., Springer, Netherlands, Dordrecht, 1992, pp. 513–580, doi:10.1007/978-94-011-2686-1_18.

[42] J.C. Giddings, M.R. Schure, Theoretical analysis of edge effects in field-flow fractionation, Chem. Eng. Sci. 42 (1987) 1471–1479, doi:10.1016/0009-2509(87)85019-4.

[43] L. Qun-Fang, L. Rui-Sen, N. Dan-Yan, H. Yu-Chun, Thermal conductivities of some organic solvents and their binary mixtures, J. Chem. Eng. Data 42 (1997) 971–974, doi:10.1021/je960351m.

[44] J. Gmehling, ed., Datasheet from "Dortmund Data Bank (DDB) – Thermophysical Properties Edition 2014" in SpringerMaterials, 2014.

[45] T.E. Daubert, R.P. Danner, Physical and Thermodynamic Properties of Pure chemicals: Data compilation, Taylor & Francis, New York, USA, 1998.

[46] B. Le Neindre, P. Bury, R. Tufeu, B. Vodar, Thermal conductivity coefficients of water and heavy water in the liquid state up to 370°C, J. Chem. Eng. Data 21 (1976) 265–274, doi:10.1021/je60070a018.

[47] C. Wohlfarth, Datasheet from landolt-börnstein - Group Iv physical chemistry volume 25: "Supplement to IV/18" in springermaterials, (2008). doi: 10.1007/978-3-540-75486-2_216.

[48] X. Li, J. Wu, Q. Dang, Thermal conductivity of liquid diethyl ether, diisopropyl ether, and di-n-butyl ether from (233 to 373) K at pressures up to 30MPa, J. Chem. Eng. Data 55 (2010) 1241–1246, doi:10.1021/je900615b.

[49] D. Li, X. Qin, W. Fang, M. Guo, H. Wang, Y. Feng, Densities, viscosities and refractive indices of binary liquid mixtures of methyl tert-butyl ether or ethyl tert-butyl ether with a hydrocarbon fuel, Exp. Therm. Fluid Sci. 48 (2013) 163–168, doi:10.1016/J.EXPTHERMFLUSCI.2013.02.019.

[50] Viscosity of acetone. https://wiki.anton-paar.com/de-de/aceton/ (accessed October 27, 2019).

[51] Viscosity of methanol. https://wiki.anton-paar.com/de-de/methanol/ (accessed October 27, 2019).

[52] D.J.G. Speight, Lange's Handbook of Chemistry, Seventeenth Edition, 17th editi, McGraw-Hill Education, New York, 2017.

[53] M.A. Motin, M.H. Kabir, M.E. Huque, Viscosities and excess viscosities of methanol, ethanol and n-propanol in pure water and in water+surf excel solutions at different temperatures, Phys. Chem. Liq. 43 (2005) 123–137, doi:10.1080/00319100420000303572.

[54] E.D. Dikio, S.M. Nelana, D.A. Isabirye, E.E. Ebenso, Density, dynamic viscosity and derived properties of binary mixtures of methanol, ethanol, n-propanol, and n-butanol with pyridine at T=(293.15, 303.15, 313.15 and 323.15) K, Int. J. Electrochem. Sci. 7 (2012) 11101–11122.

[55] J. Petravic, Thermal conductivity of ethanol, J. Chem. Phys. 123 (2005) 174503, doi:10.1063/1.2102867.

[56] Viscosity of ethanol. https://wiki.anton-paar.com/de-de/ethanol/ (accessed October 29, 2019).

[57] K. OGIWARA, Y. ARAI, S. SAITO, THERMAL conductivities of liquid alcohols and their binary mixtures, J. Chem. Eng. Japan 15 (1982) 335–342, doi:10.1252/jcej.15.335.

[58] M.M. Budeanu, V. Dumitrescu, Densities and viscosities for binary mixtures of n-heptane with alcohols at different temperatures, J. Serbian Chem. Soc. 82 (7–8) (2017), doi:10.2298/JSC151210051B.

[59] E. Jiménez, C. Franjo, L. Segade, J.L. Legido, M.I.P. Andrade, Viscosities and densities for the 1-Propanol + n-Heptane system at several temperatures, J. Solution Chem 27 (1998) 569–579, doi:10.1023/A:1022686707250.
[60] M.G. Bravo-Sánchez, G.A. Iglesias-Silva, A. Estrada-Baltazar, K.R. Hall, Densities and viscosities of binary mixtures of n-Butanol with 2-Butanol, isobutanol, and tert-Butanol from (303.15 to 343.15) K, J. Chem. Eng. Data 55 (2010) 2310–2315, doi:10.1021/je900722m.
[61] C. Wohlfarth, B. Wohlfahrt, Datasheet from landolt-börnstein - Group Iv physical chemistry volume 18B: "Pure organic liquids,". doi: 10.1007/10639283_6.
[62] D.R. Lide, CRC Handbook of Chemistry and Physics: A Ready-Reference Book of Chemical and Physical Data, CRC-Press, Boca Raton, USA, 1995.
[63] M.M. Bashirov, Y.M. Naziev, Investigation of the thermal conductivity of methanol–n-hexanol mutual solutions at high parameters of state, High Temp 41 (2003) 459–465, doi:10.1023/A:1025103630646.
[64] J. Gmehling, ed., Datasheet from "Thermophysical Properties Edition 2009" in SpringerMaterials. https://materials.springer.com/thermophysical/docs/tcn_c3 (accessed 05 Nov. 2019).
[65] C... Zhuo, C.H. Machielsen, Thermophysical properties of the trifluoroethanol-pyrrolidone system for absorption heat transformers, Int. J. Refrig. 16 (1993) 357–363, doi:10.1016/0140-7007(93)90009-W.
[66] M.L.V Ramires, F.J. Vieira dos Santos, U.V. M.ardolcar, C.A.N. de Castro, The thermal conductivity of benzene and toluene, Int. J. Thermophys. 10 (1989) 1005–1011, doi:10.1007/BF00503169.
[67] F.J.V Santos, C.A. Nieto de Castro, J.H. Dymond, N.K. Dalaouti, M.J. Assael, A. Nagashima, Standard reference data for the viscosity of toluene, J. Phys. Chem. Ref. Data 35 (2005) 1–8, doi:10.1063/1.1928233.
[68] M.R. Rodríguez-Laguna, A. Castro-Alvarez, M. Sledzinska, J. Maire, F. Costanzo, B. Ensing, M. Pruneda, P. Ordejón, C.M. Sotomayor Torres, P. Gómez-Romero, E. Chávez-Ángel, Mechanisms behind the enhancement of thermal properties of graphene nanofluids, Nanoscale 10 (2018) 15402–15409, doi:10.1039/C8NR02762E.
[69] A.J. Teller, T.J. Walsh, Viscosities of benzene-methyl ethyl ketone systems., J. Chem. Eng. Data 4 (2002) 279–283, doi:10.1021/je60003a023.
[70] T.R. Kubendran, Viscosities and densities of binary mixtures of 1,4-Dioxane, carbon tetrachloride, and butanol at 303.15K, 308.15K, and 313.15K, J. Chem. Eng. Data 49 (2004) 421–425, doi:10.1021/je030133a.
[71] Y. Tanaka, Y. Itani, H. Kubota, T. Makita, Thermal conductivity of five normal alkanes in the temperature range 283–373 k at pressures up to 250MPa, Int. J. Thermophys. 9 (1988) 331–350, doi:10.1007/BF00513075.
[72] A.L. Lee, R.T. Ellington, Viscosity of n-Pentane, J. Chem. Eng. Data 10 (1965) 101–104, doi:10.1021/je60025a005.
[73] J.H. Dymond, H.A. O/ye, Viscosity of selected liquid n-Alkanes, J. Phys. Chem. Ref. Data. 23 (1994) 41–53, doi:10.1063/1.555943.
[74] F.P. Fleming, L. de Andrade Silva, G.dos S.V. Lima, I. Herzog, H.R.B. Orlande, J.-.L. Daridon, J. Pauly, L.F.A. Azevedo, Thermal conductivity of heavy, even-carbon number n-alkanes (C22 to C32), Fluid Phase Equilib 477 (2018) 78–86, doi:10.1016/J.FLUID.2018.08.016.
[75] D.L. Hogenboom, W. Webb, J.A. Dixon, Viscosity of several liquid hydrocarbons as a function of temperature, pressure, and free volume, J. Chem. Phys. 46 (1967) 2586–2598, doi:10.1063/1.1841088.
[76] K. Kurihara, M.E. Kandil, K.N. Marsh, A.R.H. Goodwin, Measurement of the viscosity of liquid cyclopentane obtained with a vibrating wire viscometer at temperatures between (273 and 353) K and pressures below 45MPa, J. Chem. Eng. Data 52 (2007) 803–807, doi:10.1021/je060416d.
[77] R.-.F. Ma, L. Shi, Y.-.Y. Duan, L.-.Z. Han, N.-.X. Liu, Saturated liquid viscosity of cyclopentane and isopentane, J. Chem. Eng. Data 48 (2003) 1418–1421, doi:10.1021/je0202174.
[78] M.J. Assael, H. Bauer, N.K. Dalaouti, K.R. Harris, Reference correlation for the viscosity of liquid cyclopentane from 220 to 310K at pressures to 25MPa, Int. J. Thermophys. 25 (2004) 13–20, doi:10.1023/B:IJOT.0000022326.17098.50.
[79] H. Watanabe, H. Kato, Thermal conductivity and thermal diffusivity of twenty-nine liquids: alkenes, cyclic (Alkanes, alkenes, alkadienes, aromatics), and deuterated hydrocarbons, J. Chem. Eng. Data 49 (2004) 809–825, doi:10.1021/je034162x.
[80] M.J. Assael, N.K. Dalaouti, Thermal conductivity of toluene+cyclopentane mixtures: measurements and prediction, Int. J. Thermophys. 22 (2001) 659–678, doi:10.1023/A:1010759629398.
[81] C.A. Nieto De Castro, M. Dix, J.M.N.A. Fareleira, S.F.Y. Li, W.A. Wakeham, Thermal conductivity of chlorobenzene at pressures up to 430MPa, Phys. A 156 (1989) 534–546, doi:10.1016/0378-4371(89)90139-8.
[82] M. Kleiber, R. Joh, R. Span, D3 properties of pure fluid substances: datasheet from VDI-Buch • volume : "VDI heat atlas" in springermaterials (doi: 10.1007/978-3-540-77877-6_18). https://materials.springer.com/lb/docs/sm_nlb_978-3-540-77877-6_18.
[83] C.L. Yaws, X. Lin, L. Bu, S. Nijhawan, Appendix a coefficients for liquid thermal conductivity equation, Handb. Therm. Conduct. 2 (1995) 326–330, doi:10.1016/S1874-8783(06)80007-3.
[84] D.K.H. Briggs, Thermal conductivity of liquids, Ind. Eng. Chem. 49 (1957) 418–421, doi:10.1021/ie51392a039.
[85] R.A. Perkins, E.D. Sloan, Experimental study of the thermal conductivity of coal liquefaction products and some constituent pure compounds, Ind. Eng. Chem. Process Des. Dev. 25 (1986) 1016–1022, doi:10.1021/i200035a028.
[86] Y. Oshmyansky, H.J.M. Hanley, J.F. Ely, A.J. Kidnay, The viscosities and densities of selected organic compounds and mixtures of interest in coal liquefaction studies, Int. J. Thermophys. 7 (1986) 599–608, doi:10.1007/BF00502393.
[87] R. Bachmann, Messung der wärmeleitfähigkeit flüssiger benzolderivate mit einem instationären hitzdrahtverfahren, Wärme- Und Stoffübertragung 2 (1969) 129–134, doi:10.1007/BF00751158.
[88] M.S. Hossain, S. Akhtar, F. Verpoort, Densities and dynamic viscosities of alicyclic cyclohexane with toluene, o -Xylene, and mesitylene at t = (303.15 to 323.15) k and atmospheric pressure, J. Chem. Eng. Data 63 (2018) 1885–1895, doi:10.1021/acs.jced.7b01003.
[89] J.A. Al-Kandary, A.S. Al-Jimaz, A.H.M. Abdul-Latif, densities Viscosities, and speeds of sound of binary mixtures of benzene, toluene, o-xylene, m-xylene, p-xylene, and mesitylene with anisole at (288.15, 293.15, 298.15, and 303.15) K, J. Chem. Eng. Data 51 (2006) 2074–2082, doi:10.1021/je060170c.
[90] J.C. Zhou, Y.Y. Che, K.J. Wu, J. Shen, C.H. He, Thermal conductivity of DMSO + C_2H_5OH, DMSO + H_2O, and DMSO + C_2H_5OH + H_2O mixtures at T = (278.15 to 338.15) K, J. Chem. Eng. Data 58 (2013) 663–670, doi:10.1021/je301171y.
[91] F.P. Incropera, D.P. DeWitt, Fundamentals of Heat and Mass Transfer, John Wiley & Sons, Inc., New York, USA, 1996.
[92] J. Wu, H. Zheng, X. Qian, X. Li, M.J. Assael, Thermal conductivity of liquid 1,2-dimethoxyethane from 243K to 353K at pressures up to 30MPa, Int. J. Thermophys. 30 (2009) 385–396, doi:10.1007/s10765-008-0549-z.
[93] P. Zheng, X. Meng, J. Wu, Z. Liu, Density and viscosity measurements of dimethoxymethane and 1,2-dimethoxyethane from 243K to 373K up to 20MPa, Int. J. Thermophys. 29 (2008) 1244–1256, doi:10.1007/s10765-008-0503-0.
[94] H. Mensah-Brown, W.A. Wakeham, Thermal conductivity of water and 2-n-butoxyethanol and their mixtures in the temperature range 305-350K at pressures up to 150MPa, Int. J. Thermophys. 16 (1995) 237–244, doi:10.1007/BF01438974.
[95] H. Mensah-Brown, W.A. Wakeham, Thermal conductivity of aqueous mixtures of 2-n-Butoxyethanol at pressures up to 150MPa, J. Chem. Eng. Data 55 (2010) 4499–4506, doi:10.1021/je1007197.
[96] A.M. Cases, A.C. Gómez Marigliano, C.M. Bonatti, H.N. Sólimo, viscosity Density, and refractive index of formamide, three carboxylic acids, and formamide + carboxylic acid binary mixtures, J. Chem. Eng. Data 46 (2001) 712–715, doi:10.1021/je000327f.
[97] H.S. Gill, V.K. Rattan, Thermophysical properties of binary mixtures of dimethylsulfoxide with 1-phenylethanone and 1,4-dimethylbenzene at various temperatures, J. Thermodyn. 1 (2014), doi:10.1155/2014/607052.
[98] M. Shokouhi, A.H. Jalili, M. Hosseini-Jenab, Thermo physical properties of some physical and chemical solvents at atmospheric pressure, Iran. J. Chem. Eng. 10 (2013) 43–54 http://www.ijche.com/article_11673.html.
[99] C. Yang, W. Yu, D. Tang, Densities and viscosities of binary mixtures of m-cresol with ethylene glycol or methanol over several temperatures, J. Chem. Eng. Data 51 (2006) 935–939, doi:10.1007/s00396-005-1441-z.
[100] T.E.V Prasad, A. Phanibhushan, D.H.L. Prasad, Densities and viscosities of binary mixtures of m-cresol with some chlorohydrocarbons, J. Solution Chem 34 (2005) 1263–1272, doi:10.1007/s10953-005-8017-x.
[101] N.B. Vargaftik, Handbook of Thermal Conductivity of Liquids and Gases, CRC press, Boca Raton, USA, 1993.
[102] H. Kashiwagi, M. Oishi, Y. Tanaka, H. Kubota, T. Makita, Thermal conductivity of fourteen liquids in the temperature range 298–373K, Int. J. Thermophys. 3 (1982) 101–116, doi:10.1007/BF00503634.
[103] C. Yang, L. Zhao, C. Zhong, Correlation of liquid thermal conductivity using molecular connectivity indices, Int. J. Thermophys. 24 (2003) 1651–1665, doi:10.1023/B:IJOT.0000004097.46622.1a.
[104] R.S. Porter, J.F. Johnson, Thermal conductivities of aviation hydraulic fluids, Preprints 2 (1957) 87–96, doi:10.1021/i460004a021.
[105] M. Shokouhi, A.H. Jalili, A.H. Mohammadian, M. Hosseini-Jenab, S.S. Nouri, Heat capacity, thermal conductivity and thermal diffusivity of aqueous sulfolane solutions, Thermochim. Acta 560 (2013) 63–70, doi:10.1016/j.tca.2013.03.017.
[106] J. Fischer, A. Weiss, Transport properties of liquids. V. self diffusion, viscosity, and mass density of ellipsoidal shaped molecules in the pure liquid phase, Berichte Der Bunsengesellschaft/Physical Chem. Chem. Phys. 90 (1986) 896–905, doi:10.1002/bbpc.19860901013.
[107] F.A. Gonçalves, K. Hamano, J.V. Sengers, Density and viscosity of tetralin and trans-decalin, Int. J. Thermophys. 10 (1989) 845–856, doi:10.1007/BF00514480.
[108] D.J. Luning Prak, J.S. Cowart, P.C. Trulove, D.J. Luning Prak, J.S. Cowart, P.C. Trulove, Density and viscosity from 293.15 to 373.15K, speed of sound and bulk modulus from 293.15 to 343.15K, surface tension, and flash point of binary mixtures of bicyclohexyl and 1,2,3,4-Tetrahydronaphthalene or trans-decahydronaphthalene at 0.1MPa, J. Chem. Eng. Data 61 (2016) 650–661, doi:10.1021/acs.jced.5b00790.
[109] W.F. Seyer, J.D. Leslie, The viscosity of cis and trans decahydronaphthalene, J. Am. Chem. Soc. 64 (2002) 1912–1916, doi:10.1021/ja01260a046.
[110] A.A. Silva, R.A. Reis, M.L.L. Paredes, Density and viscosity of decalin, cyclohexane, and toluene binary mixtures at (283.15, 293.15, 303.15, 313.15, and 323.15) k, J. Chem. Eng. Data 54 (2009) 2067–2072, doi:10.1021/je800940j.
[111] C.K. Zéberg-Mikkelsen, A. Baylaucq, M. Barrouhou, C. Boned, The effect of stereoisomerism on dynamic viscosity: a study of cis-decalin and trans-decalin versus pressure and temperature, Phys. Chem. Chem. Phys. 5 (2003) 1547–1551, doi:10.1039/b301202f.
[112] R.M. Sisson, J.C. Giddings, Effects of solvent composition on polymer retention in thermal field-flow fractionation: retention enhancement in binary solvent mixtures, Anal. Chem. 66 (1994) 4043–4053, doi:10.1021/ac00094a029.
[113] C.A. Rue, M.E. Schimpf, Thermal diffusion in liquid mixtures and its effect on

polymer retention in thermal field-flow fractionation, Anal. Chem. 66 (1994) 4054–4062, doi:10.1021/ac00094a030.
[114] J. Kendall, K.P. Monroe, The viscosity of liquids. III. ideal solutions of solids in liquids, J. Am. Chem. Soc. 39 (1917) 1802–1806, doi:10.1021/ja02254a002.
[115] L. Grunberg, A.H. Nissan, Mixture law for viscosity, Nature 164 (1949) 799–800, doi:10.1038/164799b0.
[116] A.J.A. Van Der Wyk, Viscosity of binary mixtures, Nature 138 (1936) 845–846, doi:10.1038/138845b0.
[117] R.A. McAllister, The viscosity of liquid mixtures, AIChE J 6 (1960) 427–431, doi:10.1002/aic.690060316.

8.2. The Role of Solubility in Thermal Field Flow Fractionation – A Revisited Theoretical Approach for Tuning the Separation of Chain Walking Polymerized Polyethylene

analytical chemistry

pubs.acs.org/ac Article

The Role of Solubility in Thermal Field-Flow Fractionation: A Revisited Theoretical Approach for Tuning the Separation of Chain Walking Polymerized Polyethylene

Martin Geisler, Laura Plüschke, Jan Merna, and Albena Lederer*

Cite This: *Anal. Chem.* 2020, 92, 14822−14829 Read Online

ACCESS | Metrics & More | Article Recommendations | Supporting Information

ABSTRACT: The influence of the polymer solubility on the separation efficiency in thermal field-flow fractionation (ThFFF) was investigated for a polymer model system of differently branched chain walking polyethylenes in five different solvents, which were selected depending on their physical parameters. The understanding of polymer thermal diffusion has been elucidated using a revisited approach based on the latest thermal diffusion prediction model by Mes, Kok, and Tijssen combined with the Hansen solubility theory. Thereby, a significant improvement in the precision of the thermal diffusion prediction and the separation efficiency has been achieved by implementation of the temperature dependency on Hansen solubility parameters. In addition, we demonstrate a method for validation of the segmental size of polymer chains with varying topology by using the revisited thermal diffusion prediction approach in inverse mode and experimental thermal diffusion data.

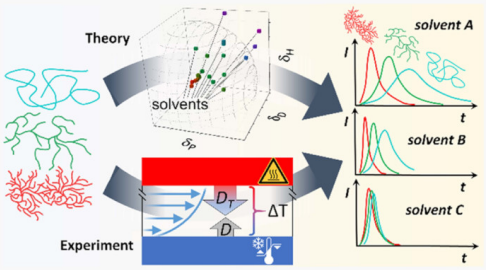

Topology characterization of polymers still represents a challenge using classical approaches such as size exclusion chromatography due to co-elution of differently branched polymers leading to low separation efficiency.[1] To overcome these problems, field-flow fractionation (FFF) as a complementary separation and analysis method, which does not rely on a stationary phase, has been established.[2] FFF separations are realized by an external separation force field applied perpendicular to a parabolic laminar flow in a thin ribbon-like separation channel. The principle of FFF is generic for all derived subtechniques and is explained in detail elsewhere.[3,4] Depending on the FFF subtype, a separation of analytes according to different intrinsic physicochemical properties can be realized.[5] For polymers in organic solvents, thermal field-flow fractionation (ThFFF) has been established to characterize polymers in their copolymer content[6−9] and recently in their topological differences.[10,11] In ThFFF, the separation force field is given by a temperature gradient ΔT, where one channel wall is heated and the opposite one is actively cooled (hereinafter referred as hot and cold wall, respectively). The retention in ThFFF is described in eq 1:

$$R = \frac{t_0}{t_R} = 6\lambda\left[\nu + (1 - 6\lambda\nu)\left(\coth\left(\frac{1}{2\lambda}\right) - 2\lambda\right)\right] \quad (1)$$

where the retention ratio of the void time t_0 to the retention time t_R is defined by the dimensionless FFF parameter λ representing the relative mean layer thickness and uniquely for this FFF subtype, with correction of the flow profile by the non-parabolicity parameter ν due to the non-constant viscosity of the carrier liquid. ν can be calculated in dependency to ΔT and the cold wall temperature by a polynomial approach with polynomial coefficients tabulated for a large choice of solvents.[12,13] The FFF parameter λ is defined by a physicochemical property of the analyte, which describes the response to the separation force field. In ThFFF, λ is described as given in eq 2:

$$\lambda = \frac{1}{S_T \Delta T} = \frac{D_T}{D\Delta T} \quad (2)$$

and depends on the ratio of the thermal diffusion coefficient D_T to the translational diffusion coefficient D, also named Soret coefficient S_T, and ΔT. For most of the FFF subtypes, the basic underlying principle is well understood. However, a fundamental theory to describe the phenomenon of thermophoresis in particular for liquid systems is still missing.

Received: August 31, 2020
Accepted: October 4, 2020
Published: October 16, 2020

https://dx.doi.org/10.1021/acs.analchem.0c03686
Anal. Chem. 2020, 92, 14822−14829

THEORETICAL BACKGROUND

Since the first observations on thermophoresis in the mid 1800's,[14,15] several theories have been developed with varying success to describe this mass transport phenomenon. Meanwhile, since thermophoresis is of technical relevance for ThFFF separations, the interest in the prediction of D_T has increased. The latest prediction model for D_T was reported by Mes, Kok, and Tjissen[16] (hereinafter coined the Mes D_T model) and describes D_T in dependence on the polymer−solvent interaction using the following relationship:

$$D_T = \phi_S^2 \left(\frac{k_B T}{6\pi\eta_S(T) r_m}\right)\left(2\frac{\partial\chi}{\partial T} + T\frac{\partial^2\chi}{\partial T^2}\right) \tag{3}$$

with the Boltzmann constant k_B, the solvent's dynamic viscosity $\eta_S(T)$, the volume fraction ϕ_S, and the first and second partial derivative of the polymer solvent interaction parameter χ differentiated to the (absolute) temperature T (in K). χ is defined by the Flory−Huggins solution theory.[17,18] For dilute polymer solutions as used in this work, ϕ_S is set to a value of 1. r_m represents the radius of a local segment of the polymer chain in the size region of a monomer, which is given based on approximations as discussed below. χ is the sum of the enthalpic χ_H and entropic contribution χ_S. As defined by the Flory−Huggins model, χ_S is not temperature-dependent and is therefore neglected for the calculation of χ.[16] Yet, χ_H can be calculated as given in eq 4:

$$\chi_H(T) = \frac{V_m(T)(Ra(T))^2}{RT} \tag{4}$$

with the molar volume $V_m(T)$ of the solvent, the universal gas constant R, and the distance of the solubility parameters Ra. $V_m(T)$ is thereby calculated as the ratio of the molar mass M to the temperature dependent mass density $\rho(T)$, given in eq 5:

$$V_m(T) = \frac{M}{\rho(T)} \tag{5}$$

Originally, the distance of the Hildebrandt solubility parameters[19] has been used, as given in eq 6:

$$(Ra(T))^2_{\text{Hildebrand}} = (\delta_{Po}(T) - \delta_S(T))^2 \tag{6}$$

with the Hildebrandt solubility parameters of the polymer δ_{Po} and of the solvent δ_S. This parameter represents the cohesive energy density and is used in its squared form to avoid negative values because an energy density cannot be negative in this context. The prediction of D_T on the basis of the Hildebrandt solubility parameters may result in a medium accurate match with D_T measured experimentally by ThFFF or other batch techniques such as thermogravitational column[20,21] or thermal diffusion forced Rayleigh scattering (TDFRS),[22] which are closest to the theoretical definition of thermal diffusion. Yet, the aim of this study is to improve the prediction power of the Mes D_T model by the means of the Hansen solubility theory, given in eq 7:

$$\delta^2 = \delta_D^2 + \delta_P^2 + \delta_H^2 \tag{7}$$

where the total solubility parameter δ is represented by a three-dimensional model with contributions from dispersion (δ_D), polar (δ_P), and hydrogen bonding (δ_H) interactions. Note that reported Hildebrandt solubility parameters do not necessarily match the total Hansen solubility parameters (HSPs). In many cases, they only represent the dispersion interactions. Though, in both solubility theories, the total δ is related to the cohesive energy density. The distance Ra from eq 4 is defined as shown in eq 8:

$$(Ra(T))^2 = (\Delta\delta_D(T))^2 + \frac{1}{4}(\Delta\delta_P(T))^2 + \frac{1}{4}(\Delta\delta_H(T))^2 \tag{8}$$

with the differences of the three contributions between the polymer and solvent, as given in eq 9:

$$\Delta\delta_{X=D,P,H}(T) = \delta_{X,Po}(T) - \delta_{X,S}(T) \tag{9}$$

The 1/4 fractions in eq 8 reflect the different impact quantity on the HSP distance.[23] Note that eq 8 has been divided by 4 from its original definition, thus corresponding to the quantity of $(Ra(T))^2_{\text{Hildebrandt}}$. The calculation of χ_H using the modified definition of Ra (eq 8) was initially proposed by Lindvig and co-workers.[24] However, in contrast to our work, they used constant HSP. Temperature-dependent δ_D, δ_P, and δ_H to be applied in $(Ra(T))^2_{\text{Hansen}}$ for the prediction of D_T can be approximated on the basis of the volumetric thermal expansion coefficient α_V or based on the ratio of the temperature-dependent mass density $\rho(T)$ to ρ of the regarded reference temperature $T_{ref.}$ (in this study 298.15 K), as given in eqs 10−12:[25]

$$\frac{\delta_{D,ref.}}{\delta_D(T)} = \left(\frac{V_{ref.}}{V(T)}\right)^{-1.25} \tag{10}$$

$$\frac{\delta_{P,ref.}}{\delta_P(T)} = \left(\frac{V_{ref.}}{V(T)}\right)^{-0.5} \tag{11}$$

$$\frac{\delta_{P,ref.}}{\delta_P(T)} = \exp\left[-0.00122\,(T_{ref.} - T) - \ln\left(\frac{V_{ref.}}{V(T)}\right)^{0.5}\right] \tag{12}$$

with the ratio of the reference volume $V_{ref.}$, typically at the reference temperature $T_{ref.}$ to the volume at the regarded temperature $V(T)$, defined in eq 13:

$$\frac{V_{ref.}}{V(T)} = \frac{1}{\alpha_V\,(T_{ref.} - T) + 1} = \frac{\rho(T)}{\rho_{ref.}} \tag{13}$$

Several influences affecting the prediction need to be considered. On the one hand, the HSP reported in the literature may differ depending on the method they were determined (e.g., by group contribution models[26−28] or on the basis of correlated experimental results[29]). On the other hand, α_V also varies with the temperature and it has to correspond to the physicochemical state of the polymer (glassy or liquid), which fits its behavior in solution (see discussion below). The temperature-dependent HSP of the solvents were calculated solely with comprehensive density data reported in the literature.[30] In this study, only the Mes D_T prediction model is considered. Other prediction theories reported or tested earlier, e.g., by Bender,[31] Schimpf and Giddings,[32] or Schimpf and Semenov,[33−35] were found to be less accurate[32,36] and are not considered in this work.

Branching characterization of regular polyolefins typically done by high temperature column-based chromatography[37,38] still represents a challenge, e.g., due to the abnormal elution behavior of branched polymers when separated in size exclusion mode.[39] Thus, ThFFF turns to be a good alternative

https://dx.doi.org/10.1021/acs.analchem.0c03686
Anal. Chem. 2020, 92, 14822−14829

Table 1. HSPs, V_m, and Its Temperature Dependency at 25 °C (in cm^3 (mol K)$^{-1}$) and α_V in the Temperature Range Used for Predictions in This Study

solvents	HSP[23] δ_D	[MPa$^{0.5}$] δ_P	δ_H	V_m [cm^3 mol^{-1}][30]	$\frac{dV_m}{dT}$ [cm^3 (mol K)$^{-1}$][30]
cyclohexane (CHX)	16.7	0.0	0.2	108.63	0.1322
mesitylene (MST)	18.0	0.6	0.6	139.83	0.1335
n-decane (DEC)	15.7	0.0	0.0	195.91	0.2121
paraffin oil[a] (ALK)	16.0[a]	0.0[a]	0.1[a]	212.40	0.2086
decalin (DHN)	17.8	0.0	0.0	157.22	0.1370
toluene (TOL)	18.3	1.4	2.0	106.95	0.1039
ethylbenzene (EB)	17.8	0.6	1.4	123.08	0.1234
perchloroethylene (TCE)	18.3	5.7	0.0	102.81	0.1068
o-dichlorobenzene (ODBC)	19.2	6.3	3.3	113.04	0.1039
chloroform (CLF)	17.8	3.1	5.7	81.64	0.1054
tetrahydrofuran (THF)	16.8	5.7	8.0	81.66	0.0962
1,4-dioxane (DOX)	17.5	1.8	9.0	85.70	0.0915
2-butanone (MEK)	16.0	9.0	5.1	90.10	0.1166
acetone (ACT)	16.0	9.0	5.1	73.96	0.1076
ethyl acetate (ETA)	15.8	5.3	7.2	98.52	0.1328
N,*N*-dimethylacetamide (DMA)	16.8	11.5	9.4	93.05	0.0918
acetonitrile (ACN)	15.3	18.0	6.1	52.85	0.0729

polymers		HSP[23] δ_D	[MPa$^{0.5}$] δ_P	δ_H	C_∞	α_V [10^{-4} K^{-1}] (at T in °C)
HDPE		18.0	0.0	0.0	8.3[43]	8.63[44] (≈120)
LDPE		17.6	0.0	0.0	8.3[43]	5.3[44] (≈100)
cwPE					8.3[43]	3.6[44,45] (20−60)
polystyrene (PS)		18.6	10.5	7.5	9.5[46]	2.6[47] (20−80)
						5.47[45] (≈100)
						8.64[48] (≈120)
poly(methyl acrylate) (PMA)		19.6[b]	12.1[b]	5.9[b]	7.9[49]	6.45[50] (25)
poly(methyl methacrylate) (PMMA)	iso	18.8	10.5	5.7	10.3[c]	2.85[51] (25−60)
	syndio				8.1[c]	2.2[51] (25−60)
	a-tactic				8.2[c]	2.48[d] (25−60)
poly(*n*-butyl acrylate) (PBA)		19.9[a]	11.9[a]	4.2[a]	9.6[49]	6.33[52] (25)
polyisoprene (PI)		16.9	1.1	−0.4	8.1[49]	7.06[53] (25)

[a]Extrapolated and weighted by the HSP from *n*-alkanes and isoalkanes, content determined by GC-MS and ^{1}H NMR (given in the Supporting Information).[23] [b]Approximated by monomer-HSP and polymer-HSP from by related derivates and prediction by ref 28. [c]Averaged values from ref 54 weighted to stereoregular content reported in ref 55. [d]Weighted according to ref 56 with the experimental α_V.[51]

for (branching) characterization.[9−11,40] ThFFF in high temperature mode has been already successfully applied for regular polyethylene separation.[41,42] However, an extension of the analysis scope toward polymer topology has not been tried yet. One aim in this study is to predict suitable separation conditions for a branching characterization of regular polyolefins by HT-ThFFF.

■ EXPERIMENTAL DETAILS

ThFFF experiments were carried out with a setup and with the same cwPE samples of different topologies than reported previously.[11] Details to the synthesis and characteristic average data of the samples are reported in the Supporting Information. ThFFF separations were carried out with a constant flow rate of 0.3 and a constant temperature gradient of ΔT = 40 K (ALK and DEC) or 0.2 mL min^{-1} and 100 K (all other separations). Solvents and carrier fluids were purchased by Merck KGaA, Fisher Scientific GmbH (both Germany) and Honeywell Int. Inc. USA. The void time in the separations with 0.2 mL min^{-1} flow was 11.04 min (no stop-flow) or 12.36 min (5 min stop-flow) and in the separations with 0.3 mL min^{-1} flow 7.36 min (5 min stop-flow). A channel pressure of about 0.6−1.5 MPa was adjusted for the used flow rate by a back pressure tubing (inner Ø 0.001″) between the ThFFF channel and the multi-angle light scattering detector in order to maintain the stability of the dRI baseline and to avoid possible accumulation of gas bubbles due to residual dissolved gas in the carrier fluid or solvent boiling. The samples dissolved the used carrier fluid in a concentration of ca. 4.3 mg mL^{-1}, and the injection volume for all separations was 49 μL. The data recording and analysis was carried out with the TF2000 software. Due to the limited sample amount, the retention experiments in THF could not be repeated with application of stop-flow. The influence of insufficient relaxation is respected in calculations of the following section.

■ RESULTS AND DISCUSSION

Revisiting the Prediction of Polymer Thermal Diffusion. Predictions of D_T were reported previously by Mes et al. for polystyrene[16] (PS) as well as for polyacrylates by Runyon and Williams,[36] both matching experimentally measured D_T reported in the literature with more or less fair

https://dx.doi.org/10.1021/acs.analchem.0c03686
Anal. Chem. 2020. 92. 14822−14829

accuracy. In previous studies, D_T values were calculated with theoretically approximated r_m values of 0.201 nm[16,31] or 0.29 nm[36] for PS and 0.153 nm[31] or 0.27 nm[36] for poly(methyl methacrylate) (PMMA),using liquid thermal expansion coefficients of the these polymers in melt. The question appears: are these small length scales thermodynamically meaningful? An initial reverse test calculation of r_m based on experimental D_T for PS and PMMA with χ_H and its temperature derivatives calculated by the means of HSP (eqs 4, 8−13) led in fact to larger r_m values of about 0.6 nm for PS and 0.5 for PMMA, respectively, using the thermal expansion of the polymers in the glassy state at the temperatures corresponding to the reported D_T values. For PS, this length is in close agreement to reported Kuhn lengths l_K (1.2−1.8 nm).[57−59] For PMMA instead, a slight underestimation compared to the reported l_K (1.4−1.7 nm)[49,60] is found. The determination of l_K, e.g., by scattering experiments, depends on the fitting model and the experimental conditions (in melt or in solution and for polymer solutions on the solvent quality). An approximation of the Kuhn length independent on experimental factors used for the D_T prediction can be done by using tabulated characteristic ratios C_∞ of the polymers together with the bond length l_b and bond angle θ[61,62] (e.g., from rotational isomeric state modeling)[63] in the polymer chain, as given in eq 14:

$$l_K = l_b C_\infty \cos\left(\frac{\theta}{2}\right) \approx 2r_m \tag{14}$$

The idea that D_T may be dependent on the Kuhn length or a related segment length was described previously[64,65] and may set a physiochemical basis for the Mes D_T prediction model.[16] The HSPs and α_V used in this study are reported in Table 1, and the references for the reported experimental D_T are given below.

For all C−C bonded polymers $\theta = 112°$, $l_b = 0.154$ nm, and for polyisoprene $\theta = 111°$, $l_b = 0.151$ nm was used.[63] The prediction of D_T for various polymer solvent systems based on the data given in Table 1 allow for an accurate match of the experimental values reported in the literature (see Figure 1) than predicted previously.[16,36] For PS, data for room temperature and as well for elevated temperatures were calculated. Thereby, D_T predictions were found to display D_T in better agreement to reported experimental values when D_T for temperatures above the glass transition temperature of PS were calculated with α_V for the molten state. Calculation data for the D_T predictions with the approach presented in this study and the numerical data presented in Figure 1 are given in Table S1 in the Supporting Information. The necessity to include phase transitions of amorphous polymers in solubility parameter calculations was also reported previously.[66] Furthermore, in the D_T prediction of PMMA, the tacticity influences the calculation of α_V. The experimental D_T for PMMA in different tacticities[67] were recalculated from the reported ThFFF retention times using the calculation procedure and coefficients for ν reported elsewhere[13] because the reported D_T were derived without non-parabolicity correction of the flow profile[55] and differ relatively from the corrected D_T by up to 130%. The necessity of this correction has been stated previously[12,13,68] and was confirmed by comparison of experimental D_T from ThFFF and D_T from other methods.[16,36]

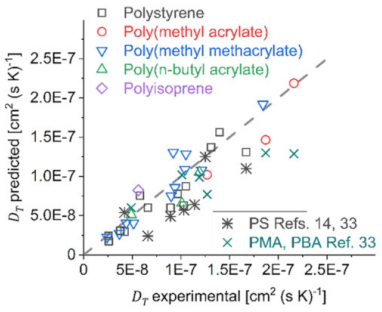

Figure 1. Comparison of the D_T prediction by the procedure with eqs 3−5, 8−13 to the experimental values reported in the literature (PS in CHX,[32] CLF,[64] THF,[36,64,69] DOX,[70,71] TOL,[71−73] MEK,[71,74] ETA,[64,70] ODBC,[42] DMA (own experiments, see the Supporting Information), DHN,[75] EB;[71,76,77] PMA and PBA in THF, MEK, ACT;[36] PMMA in THF,[69] DOX, ACN;[55] PI in THF[69]) and in comparison to the predicted D_T reported previously.[16,36] The dashed line is guide for the eye at $D_{T,\,exp.} = D_{T,\,predict.}$. The abbreviations are listed with their full name in Table 1.

As indicated in Figure 1, the predictive power of the Mes D_T model is significantly increased when the solubility is modeled by the Hansen solubility theory and the segmental mobility of the polymer is approximated in correspondence to the Kuhn length. We therefore hypothesize that this revised model enables to characterize polymers on the local scale based on experimentally found D_T. However, the application of this approach for scaling predictions of monomeric and oligomeric analytes showing thermophilic behavior and hence, negative D_T, has to be evaluated in a future work.

ThFFF of Chain Walk Polyethylene in Different Solvents. So far, finding solvents that yield sufficiently high D_T for a good retention in ThFFF analysis was performed in a trial-and-error process. The latest D_T prediction theories proved to shorten this process tremendously. However, up to this study, they have not reached a prediction level yet accurately matching experimentally found D_T.[36] Furthermore, predictions with the Mes D_T model with the approach given in the Theoretical Background section require elaborate calculations. Trends may not directly be derived from eq 3. Hence, we present exemplarily for a library of chain walking polyethylenes (cwPE) with different amounts of calculated long-chain branching (LCB) and molar masses,[11] an alternative approach to find an optimal solvent for ThFFF separations yielding high retention and topological selectivity. A good solvent matching these properties was already intuitively found in CHX. Details are reported in previous studies on these polymers[78] and their topological analysis by ThFFF.[11] These polymers remain thoroughly amorphous with liquid to waxy consistence due to their unique structure with a high amount of short-chain branches and a controllable topology in terms of long-chain branching. In contrast to HDPE or LDPE, they are readily soluble at room temperature in a variety of solvents and are thus perfect candidates for an investigation by ThFFF as a model system.

In order to trace possible correlations between the solvent quality and the ThFFF retention behavior, the solubility sphere for cwPE was modeled with the HSPs given in Table 1, as illustrated in Figure 2. The radius of the sphere Ro indicates the border between solvency (inside) and nonsolvency (outside). The ratio $Ra\ Ro^{-1}$ is called the relative energy difference (RED). Ro was estimated by experimental solubility tests to $Ro = 10.4$ MPa$^{0.5}$: cwPE is found to be soluble in THF

https://dx.doi.org/10.1021/acs.analchem.0c03686
Anal. Chem. 2020, 92, 14822−14829

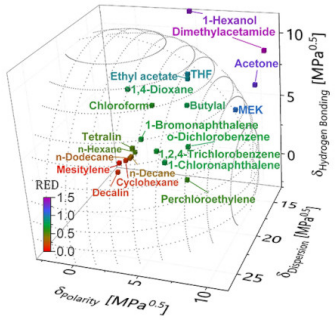

Figure 2. Hansen solubility sphere modeled for cwPE with the HSP given in Table 1 and further solvents. The sphere radius was approximated to Ro = 10.4 $MPa^{0.5}$ based on experimentally observed solubilities. The center of the sphere is in between the coordinates of CHX and *n*-dodecane. The color scale indicates the relative energy distance (RED) of the solvent to the sphere center.

(RED = 0.96) but insoluble in MEK (RED = 1.04). It is immediately clear that no protic polar solvent is found inside the sphere. Furthermore, most of the aprotic polar solvents are outside, near the surface of the sphere. Thereby, dioxane is found in the region of a theta solvent equal to cyclohexane for polystyrene[79] (RED ≈ 0.9).[23] The medium polar chlorinated solvents used in polyolefin analysis[37,38,78,80−82] are found in between the center and the surface of the sphere. In the center, solely hydrocarbons are located. Based on the good and selective retention behavior found for cwPE in CHX and the lack of retention in THF (Figure 3),[11] we set the hypothesis: The retention behavior correlates with Ra and becomes optimal for solvent candidates with the HSP located closer to the center of the sphere. The verification of this hypothesis was investigated by ThFFF retention experiments with a library of seven cwPE samples of different molar masses and varying

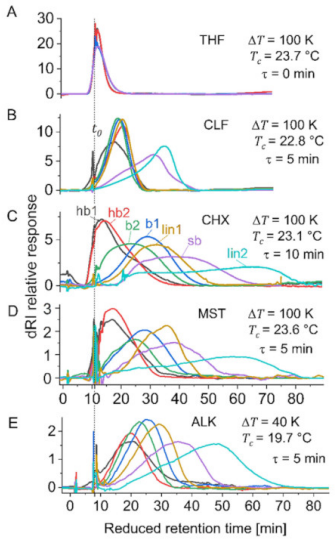

Figure 3. ThFFF fractograms (dRI) of seven cwPE samples with different molar masses and topologies, shown in dependency to the reduced retention time (stop-flow time subtracted). The separations shown in (A) to (D) were performed with a flow rate of 0.2 mL min^{-1} and the separations shown in (E) with 0.3 mL min^{-1}.

topology ranging from highly branched (hb), branched (b), slightly branched (sb) to linear (lin) topology taking into account the LCB calculation. Further details on the polymer properties are reported in a previous study[11] and in the Supporting Information.

The outcome of this investigation is illustrated in Figure 3 and confirms our hypothesis. The highest retention is found for *n*-decane (DEC), which is believed to be located closest to the center of the solubility sphere. Figure S5 in the Supporting Information demonstrates the improved quality of separation with DEC even in comparison to ALK. Thereby, the HSP of cwPE are probably close to DEC HSPs. A similar but slightly less effective separation is found for paraffin oil (*n*-alkanes C9 to C13 from redistilled lamp oil). This confirms that, for effective separation, not necessarily pure solvents need to be used. In the case of alkane mixtures, significant solvent effects observed in other solvent mixtures are not expected. In fact, such mixture effects can be also used to improve ThFFF separations.[83,84]

The retention in ThFFF is a result of the interplay between D_T and D. In particular, D is strongly dependent on the mean layer temperature, which corresponds to the retention time measured in ThFFF. Hence, the question arises: to which extent does the solubility influences D_T? Average D_T values were calculated from differential refractometry (dRI) peak apex retention times with the help of $D(T)$ measured in batch by temperature-dependent dynamic light scattering (data are given in Table S5, Supporting Information). The overview of D_T (multiplied by the solvent viscosity for comparison) superimposed in Figure 4 in dependency on RED shows

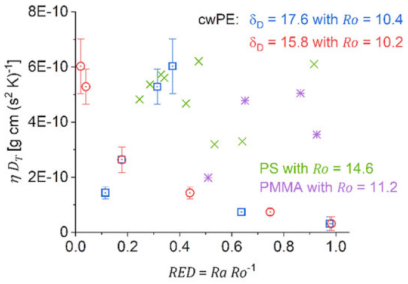

Figure 4. Experimental D_T (normalized with $\eta_S(T)$ at mean layer temperature) of the linear cwPE sample lin2 in dependency to RED for δ_D = 17.6 $MPa^{0.5}$ (blue) from the initial approximation and for δ_D = 15.8 $MPa^{0.5}$ (red) after empirical adjustment (see text) in comparison to normalized experimental D_T of PS (green) and PMMA (purple) from data reported in the literature (refs. see Figure 1).

significantly different D_T values depending on the solvent. However, with the initially applied HSP (LDPE) with δ_D = 17.6 $MPa^{0.5}$ for cwPE, the dependency appears not to be consistent. With the boundary condition of DEC having the closest HSP to cwPE on one hand and the insolubility in MEK on the other hand, an empirical adjustment of the HSP for cwPE to δ_D = 15.8 $MPa^{0.5}$ with Ro = 10.2 $MPa^{0.5}$ by keeping δ_P, δ_H = 0 $MPa^{0.5}$ yields in a meaningful correlation of D_T to RED. The question appears: why δ_D for this cwPE appears to be significantly lower than reported for regular types of PE (δ_D = 18 $MPa^{0.5}$ for HDPE or LDPE δ_D = 17.6 $MPa^{0.5}$)?[85]

The trend to lower δ_D is also found for isoalkanes in comparison to their *n*-derivates. Hence, for a highly short-chain

https://dx.doi.org/10.1021/acs.analchem.0c03686
Anal. Chem. 2020, 92, 14822−14829

branched material such as cwPE, the same trend is assumed. A shift of δ_P and δ_H, away from 0 $MPa^{0.5}$, does not yield a better correlation. Some hydrocarbon materials such as polyisobutylene (PIB) are in fact reported with δ_P and δ_H deviating from 0 $MPa^{0.5}$. However, in contrast to PIB, cwPE does not contain quaternary carbon atoms and therefore a deviation of δ_P and δ_H from 0 is not justified. In this context, discrepancies are to be considered if HSP values are used to describe either solubility or chemical resistance (in terms of permeation).[23]

Considering the validity of the empirical adjustment of *Ro* for cwPE as justified above, the hypothesis appears to be correct for PE. However, correlations of reported experimental data for PS and PMMA indicate no distinct trend of normalized D_T to RED and show that the hypothesis stated above may not be generic. Additional studies have to be performed in the future to understand the correlation between D_T and solubility in general. Among other potential contributions, the influence of intramolecular chemical heterogeneity should be investigated. The impact of such contributions is indicated in a previous study by Smith et al., who reported similar high thermal diffusion for silylated aromatic-aliphatic polyesters despite different physicochemical solvent properties.[10]

Evaluation of Polymer Segmental Blob Size from Experimental D_T. In the previous section, we indicated that the Mes D_T model is suitable to predict D_T in high and improved accuracy with the help of HSP and segmental sizes for a particular polymer from the Kuhn length or related segment size. Based on our theoretical reconsiderations, we aim to validate the D_T for the prediction of polymer segment length as indicators for the molecular chain stiffness or branching density directly from thermophoretic data. In this context, the juxtaposition of the segmental dimensions defined by various polymer models needs to be evaluated. Depending on the polymer model, this could either be the Kuhn length or a related segment length as stated earlier[64] or a blob size like a thermal blob as defined by de Gennes[86] with the Flory theory.[59] The thermal blob in a polymer chain may become theoretically equal to the Kuhn segment length for a polymer depending on the solvent conditions. So far, we consider this local size information as a thermophoretically effective blob size.

The reverse application of the Mes D_T model reveals in fact on one hand a dependency of the polymer blob size to the solvent quality as illustrated in Figure 5 and on the other hand a dependency on the polymer topology since branching influences strongly the chain stiffness,[78] which is expressed here in the number of long-chain branches per 1000 monomers (LCB).

Increasing blob diameters were found in good solvents such as CHX, MST, and ALK, whereas in CLF, the blob diameter remains almost constant. This is in agreement with the theory because, with increasing branching (i.e., LCB), the stiffness of the polymer should increase due to an increasing steric hindrance. In a thermodynamically good solvent, the solvent is freely draining into the polymer coil. Contrarily, in a poor solvent, the polymer coil is in a collapsed state with reduced interaction with the solvent and thus the blob diameter does not significantly change with LCB. A similar or even reverse trend may be observed for THF. Yet, the yielded blob diameter for THF may represent here only a lower limit of its actual size because D_T data from ThFFF are not fully resolved due to the poor retention. The blob diameter found for cwPE in ALK and

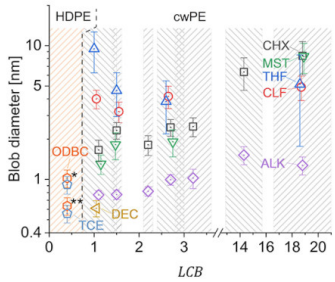

Figure 5. Calculated thermophoretically effective blob diameters from experimental D_T by reverse application of the Mes D_T model combined with the Hansen solubility theory. The values for HDPE (NIST SRM 1484) were calculated based on reported literature ThFFF retention data[41,42] and literature radii data for the estimation of D.[87,88] *, calculated with D_T at the mean layer temperature; **, calculated to 25 °C with the help of $\eta_S(T)$. The hashed regions indicate the error bars of the LCB values. The abbreviations of the solvents are listed with their full name in Table 1.

DEC as well as the retraced values for HDPE from literature retention[41,42] and scaling data[87,88] (transformed to 25 °C for comparison) in ODBC and TCE are in close agreement to the segment lengths reported for short-chain branched (SCB) PE. For SCB-PE, a persistence length ranging from 0.9 nm for high numbers of SCB to 0.6 nm for non-branched PE chains is reported.[89] Furthermore, the blob diameter of the cwPE with higher LCB is in agreement to the blob size of cwPE material originated from the same synthesis approach of about 8−10 nm found by atomic force microscopy (AFM) and SANS and corresponding to a bottlebrush-like conformation with a large thickness.[78]

With regard to HT-ThFFF of regular polyolefins, a separation according to branching may most efficiently be performed in solutions of higher *n*-alkanes. Previously reported HT-ThFFF separations were carried out in medium solvents for PE at higher temperatures with ODBC (RED = 0.65 at 102 °C) and TCE (RED = 0.54 at 114 °C), which is in comparable distance like CLF (RED = 0.63 and 0.64 at 102 and 114 °C). Therefore, the branching selectivity in the separation may be similarly low like in CLF, as shown in Figure 3 due to the hindered drainage as stated in Figure 5. A branching separation is not reported in these investigations, and in early reports, branching was assumed to have no effect on D_T.[90] With the latest investigations in this regard,[9−11] it can be concluded that this is only true for specific polymer solvent pairings and only the independence of M on D_T is found to be generic.

The correlation of thermal diffusion to the thermodynamic solvent quality discussed above is in certain aspects in agreement to Köhler et al. They concluded that mainly the Kuhn segments from the thin draining outer layer take part in the thermophoretic motion.[91] However, with regard to the found variety of blob sizes depending on polymer architecture and solvent quality, their conclusion may be reevaluated to which the depth of the polymer coil its segments contributes to the polymer's D_T.

■ CONCLUSIONS

In this study, we show that, on the basis of the Hansen solubility theory, the predictive power of thermophoretic behavior by the Mes D_T prediction model is improved when the temperature dependency of the solubility is derived from

https://dx.doi.org/10.1021/acs.analchem.0c03686
Anal. Chem. 2020, 92, 14822−14829

physical data and the segmental radius of the polymer is approximated by polymer chain models. However, uncertainties remain in the Mes D_T model since it is based on solubility and polymer scaling models with intrinsic generalizations and assumptions. In future studies, the influence of i.a. nonconstant χ_S or electrostatic interactions[92] on the accuracy of predicted D_T can be tested. For concentrated polymer solutions, in fact a significant dependency of χ_S to temperature was experimentally found.[93]

Taking the improved D_T prediction as a basis, a direct correlation of the thermal diffusion to the solvent quality has been found for a polymer model system of chain walking polyethylene (cwPE) in different topologies. By reverse application of the Mes D_T model, we calculated polymer segmental or blob sizes from experimental D_T. These thermophoretically effective blob sizes are found to be in reasonable agreement with the persistence length of short-chain branched polyethylenes[89] for linear samples and maximum blob sizes for higher branched samples in the range of blob sizes estimated in previous studies.[78] With this approach, thus we demonstrate that the local stiffness of a polymer can be approximated by D_T measurements.

In addition, we demonstrated for cwPE that the Hansen solubility theory can be also applied empirically without elaborate calculations to find suitable solvents for ThFFF separations. However, future studies are needed to find a valid approach for polymers in general and to understand the effects governing their ThFFF separation behavior. With regard to the application of ThFFF as a branching characterization method of regular polyolefins, i.e., in high-temperature regime, higher alkanes are found as preferential candidates for highly selective separations yielding superior retention.

■ ASSOCIATED CONTENT

Supporting Information

The Supporting Information is available free of charge at https://pubs.acs.org/doi/10.1021/acs.analchem.0c03686.

Calculation details, characteristics, und preparation of materials; $D(T)$ data measured by temperature-dependent DLS; and numeric values of Figures 4 and 5 (PDF)

■ AUTHOR INFORMATION

Corresponding Author

Albena Lederer − *Leibniz-Institut für Polymerforschung Dresden e.V., 01069 Dresden, Germany; Faculty of Chemistry and Food Chemistry, Technische Universität Dresden, 01162 Dresden, Germany; Department of Chemistry and Polymer Science, Stellenbosch University, Matieland 7602, South Africa;* orcid.org/0000-0002-1760-6426; Email: lederer@ipfdd.de

Authors

Martin Geisler − *Leibniz-Institut für Polymerforschung Dresden e.V., 01069 Dresden, Germany; Faculty of Chemistry and Food Chemistry, Technische Universität Dresden, 01162 Dresden, Germany*

Laura Plüschke − *Leibniz-Institut für Polymerforschung Dresden e.V., 01069 Dresden, Germany; Faculty of Chemistry and Food Chemistry, Technische Universität Dresden, 01162 Dresden, Germany*

Jan Merna − *Department of Polymers, University of Chemistry and Technology Prague, 166 28 Prague 6, Czech Republic;* orcid.org/0000-0002-6508-0844

Complete contact information is available at: https://pubs.acs.org/10.1021/acs.analchem.0c03686

Author Contributions

The manuscript was written through contributions of all authors. All authors have given approval to the final version of the manuscript.

Notes

The authors declare no competing financial interest.

■ ACKNOWLEDGMENTS

This work was supported by the Deutsche Forschungsgemeinschaft (DFG, German Research Foundation) [grant number DFG LE 1424/7] and Czech Science Foundation (grant number 18-22059S). Robert Mundil is greatly acknowledged for the synthesis of the polyethylene samples used in this study. We thank Christina Harnisch for the Pyrolysis GC-MS analysis of the paraffin oil used in this work and Petra Treppe for technical assistance.

■ REFERENCES

(1) Podzimek, S.; Vlcek, T. *J. Appl. Polym. Sci.* **2001**, *82*, 454−460.
(2) Malik, M. I.; Pasch, H. *Prog. Polym. Sci.* **2016**, *63*, 42−85.
(3) Martin, M.; Williams, P. S. In *Theoretical Advancement in Chromatography and Related Separation Techniques*; Dondi, F., Guiochon, G., Eds.; Springer: Dordrecht, 1992; pp 513−580, DOI: 10.1007/978-94-011-2686-1_18.
(4) Schure, M. R.; Schimpf, M. E.; Schettler, P. D. *Field-Flow Fractionation Handbook*; Schimpf, M. E., Caldwell, K. D., Giddings, J. C., Eds.; John Wiley & Sons: New York, USA, 2000; pp 31−48.
(5) Dondi, F.; Martin, M. *Field Flow Fractionation Handbook*; Schimpf, M., Caldwell, K., Giddings, J., Ed.; John Wiley & Sons: New York, USA, 2000; pp 103−132.
(6) Ponyik, C. A.; Wu, D. T.; Williams, S. K. R. *Anal. Bioanal. Chem.* **2013**, *405*, 9033−9040.
(7) Schimpf, M. E.; Wheeler, L. M.; Romeo, P. F. *Chromatography of Polymers*; American Chemical Society, 1993; Vol. *521*, pp. 63−76.
(8) Radebe, N. W.; Beskers, T.; Greyling, G.; Pasch, H. *J. Chromatogr. A* **2019**, *1587*, 180−188.
(9) Runyon, J. R.; Williams, S. K. R. *J. Chromatogr. A* **2011**, *1218*, 6774−6779.
(10) Smith, W. C.; Geisler, M.; Lederer, A.; Williams, S. K. R. *Anal. Chem.* **2019**, *91*, 12344−12351.
(11) Geisler, M.; Smith, W. C.; Plüschke, L.; Mundil, R.; Merna, J.; Williams, S. K. R.; Lederer, A. *Macromolecules* **2019**, *52*, 8662−8671.
(12) Belgaied, J. E.; Hoyos, M.; Martin, M. *J. Chromatogr. A* **1994**, *678*, 85−96.
(13) Geisler, M.; Lederer, A. *J. Chromatogr. A* **1621**, *1621*, 461082.
(14) Ludwig, C. *Sitzungber. Bayer. Akad. Wiss. Wien Math.-Naturwiss. Kl.* **1856**, *20*, 539.
(15) Soret, C. *J. Phys. Theor. Appl.* **1880**, *9*, 331−332.
(16) Mes, E. P. C.; Kok, W. T.; Tijssen, R. *Int. J. Polym. Anal. Charact.* **2003**, *8*, 133−153.
(17) Flory, P. J. *J. Chem. Phys.* **1942**, *10*, 51−61.
(18) Huggins, M. L. *J. Chem. Phys.* **1941**, *9*, 440.
(19) Hildebrand, J. H.; Prausnitz, J. M.; Scott, R. L. *Regular and Related Solutions: The Solubility of Gases, Liquids, and Solids*; Van Nostrand Reinhold Company, 1970, p 190.
(20) Clusius, K.; Dickel, G. *Naturwissenschaften* **1938**, *26*, 546.
(21) Washall, T. A.; Melpolder, F. W. *Ind. Eng. Chem. Process Des. Dev.* **1962**, *1*, 26−28.
(22) Köhler, W. *J. Chem. Phys.* **1993**, *98*, 660−668.

(23) Hansen, C. M.; Durkee, J.; Kontogeorgis, G.; Panayiotou, C.; Willliams, L. L.; Poulsen, T. S.; Priebe, H.; Redelius, P. *Hansen Solubility Parameters: A User's Handbook*; 2nd ed.; CRC Press, 2007.
(24) Lindvig, T.; Michelsen, M. L.; Kontogeorgis, G. M. *Fluid Phase Equilib.* **2002**, *203*, 247−260.
(25) Hansen, C. M.; Beerbower, A. In *Kirk-Othmer Encyclopedia of Chemical Technology*; Mark, H. F., McKetta, J. J., Othmer, D. F., Eds.; John Wiley & Sons: New York, 1971; Vol. 2, pp 889−910.
(26) Van Krevelen, D. W.; Te Nijenhuis, K. In *Properties of Polymers*; 4th E., Eds.; Elsevier: Amsterdam, 2009; pp 189−227, DOI: 10.1016/B978-0-08-054819-7.00007-8.
(27) Hoy, K. L. *J. Ind. Text.* **1989**, *19*, 53−67.
(28) Stefanis, E.; Panayiotou, C. *Int. J. Thermophys.* **2008**, *29*, 568−585.
(29) Adamska, K.; Voelkel, A. *J. Chromatogr. A* **2006**, *1132*, 260−267.
(30) Data extracted from the SpringerMaterials database.
(31) Bender, M. *Macromolecules* **1995**, *28*, 1309−1311.
(32) Schimpf, M. E.; Giddings, J. C. *J. Polym. Sci. Part B Polym. Phys.* **1989**, *27*, 1317−1332.
(33) Schimpf, M. E.; Semenov, S. N. *J. Phys. Chem. B* **2000**, *104*, 9935−9942.
(34) Schimpf, M. E.; Semenov, S. N. *Philos. Mag.* **2003**, *83*, 2185−2198.
(35) Semenov, S.; Schimpf, M. *Phys. Rev. E - Stat. Physics, Plasmas, Fluids, Relat. Interdiscip. Top.* **2004**, *69*, 8.
(36) Runyon, J. R.; Williams, S. K. R. *J. Chromatogr. A* **2011**, *1218*, 7016−7022.
(37) Plüschke, L.; Mundil, R.; Sokolohorskyj, A.; Merna, J.; Sommer, J.-U.; Lederer, A. *Anal. Chem.* **2018**, *90*, 6178−6186.
(38) Plüschke, L.; Ndiripo, A.; Mundil, R.; Merna, J.; Pasch, H.; Lederer, A. *Macromolecules* **2020**, *53*, 3765−3777.
(39) Podzimek, S.; Vlcek, T.; Johann, C. *J. Appl. Polym. Sci.* **2001**, *81*, 1588−1594.
(40) Greyling, G.; Lederer, A.; Pasch, H. *Macromol. Chem. Phys.* **2018**, *219*, 1800417.
(41) Brimhall, S. L.; Myers, M. N.; Caldwell, K. D.; Giddings, J. C. *Sep. Sci. Technol.* **1981**, *16*, 671−689.
(42) Pasti, L.; Roccasalvo, S.; Dondi, F.; Reschiglian, P. *J. Polym. Sci., Part B Polym. Phys.* **1995**, *33*, 1225−1234.
(43) Fetters, L. J.; Graessley, W. W.; Krishnamoorti, R.; Lohse, D. J. *Macromolecules* **1997**, *30*, 4973−4977.
(44) Boyer, R. F. *Macromolecules* **1973**, *6*, 288−299.
(45) Orwoll, R. A. *Physical Properties of Polymers Handbook*; Mark, J. E., Ed.; Springer: New York, USA, 2007; pp 93−101.
(46) Boothroyd, A. T.; Rennie, A. R.; Wignall, G. D. *J. Chem. Phys.* **1993**, *99*, 9135−9144.
(47) Patnode, W.; Scheiber, W. J. *J. Am. Chem. Soc.* **1939**, *61*, 3449−3451.
(48) Alsewailem, F. D. *J. Thermoplast. Compos. Mater.* **2009**, *22*, 585−604.
(49) Fetters, L. J.; Lohse, D. J.; Colby, R. H. *Physical Properties of Polymers Handbook*; Mark, J. E., Ed.; Springer: New York, USA, 2007; pp 447−454.
(50) Brunacci, A.; Pedemonte, E.; Turturro, A. *Polymer* **1992**, *33*, 4428−4431.
(51) Soldera, A. *Macromol. Symp.* **1998**, *133*, 21−32.
(52) Song, K. H.; Kwon, K. W.; Cho, J. *Macromol. Res.* **2009**, *17*, 721−724.
(53) Akiyama, S.; Kawahara, S.; Akiba, I.; Iio, S.; Li, H. L.; Ujihira, Y. *Polym. Bull.* **2000**, *45*, 275−279.
(54) O'Reilly, J. M.; Teegarden, D. M.; Wignall, G. D. *Macromolecules* **1985**, *18*, 2747−2752.
(55) Greyling, G.; Pasch, H. *Anal. Chem.* **2015**, *87*, 3011−3018.
(56) Behbahani, A. F.; Allaei, S. M. V.; Motlagh, G. H.; Eslami, H.; Harmandaris, V. A. *Soft Matter* **2018**, *14*, 1449−1464.
(57) Jones, R. L.; Kumar, S. K.; Ho, D. L.; Briber, R. M.; Russell, T. P. *Nature* **1999**, *400*, 146−149.
(58) Jones, R. L.; Kumar, S. K.; Ho, D. L.; Briber, R. M.; Russell, T. P. *Macromolecules* **2001**, *34*, 559−567.
(59) Rubinstein, M.; Colby, R. H. *Polymer Physics*; Oxford University Press: New York, 2003; Vol. *100*, pp. 97−133.
(60) Kirste, R. G. *Makromol Chem.* **1967**, *101*, 91−103.
(61) Kuhn, W. *Kolloid-Z.* **1934**, *68*, 2−15.
(62) Kuhn, W.; Kuhn, H. *Helv. Chim. Acta* **1943**, *26*, 1394−1465.
(63) Rehahn, M.; Mattice, W. L.; Suter, U. W. *Rotational Isomeric State Models in Macromolecular Systems*; Rehahn, M., Mattice, W. L., Suter, U. W., Eds.; Springer: Berlin, Heidelberg, 1997; pp 19−476, DOI: 10.1007/BFb0050961.
(64) Stadelmaier, D.; Köhler, W. *Macromolecules* **2009**, *42*, 9147−9152.
(65) Pur, B.; Schock, F.; Köhler, W.; Morozov, K. I. *J. Phys. Chem. Lett.* **2020**, *11*, 4498−4502.
(66) Chen, X.; Yuan, C.; Wong, C. K. Y.; Zhang, G. *J. Mol. Model.* **2012**, *18*, 2333−2341.
(67) Muza, U. L.; Greyling, G.; Pasch, H. *Anal. Chem.* **2018**, *90*, 13987−13995.
(68) Martin, M.; Reynaud, R. *Anal. Chem.* **1980**, *52*, 2293−2298.
(69) Cao, W.; Williams, P. S.; Myers, M. N.; Giddings, J. C. *Anal. Chem.* **1999**, *71*, 1597−1609.
(70) Van Asten, A. C.; Kok, W. T.; Tijssen, R.; Poppe, H. *J. Polym. Sci., Part B Polym. Phys.* **1996**, *34*, 297−308.
(71) Giddings, J. C.; Caldwell, K. D.; Myers, M. N. *Macromolecules* **1976**, *9*, 106−112.
(72) Köhler, W.; Rosenauer, C.; Rossmanith, P. *Int. J. Thermophys.* **1995**, *16*, 11−21.
(73) Rauch, J.; Köhler, W. *Macromolecules* **2005**, *38*, 3571−3573.
(74) Stadelmaier, D.; Köhler, W. *Macromolecules* **2008**, *41*, 6205−6209.
(75) Melucci, D.; Contado, C.; Mingozzi, I.; Reschiglian, P.; Dondi, F. *Chromatographia* **1999**, *49*, 131−136.
(76) Myers, M. N.; Caldwell, K. D.; Giddings, J. C. *Sep. Sci.* **1974**, *9*, 47−70.
(77) Brimhall, S. L.; Myers, M. N.; Caldwell, K. D.; Giddings, J. C. *J. Polym. Sci., Part A* **1984**, *23*, 2443−2456.
(78) Dockhorn, R.; Plüschke, L.; Geisler, M.; Zessin, J.; Lindner, P.; Mundil, R.; Merna, J.; Sommer, J.-U.; Lederer, A. *J. Am. Chem. Soc.* **2019**, *141*, 15586−15596.
(79) Krigbaum, W. R.; Geymer, D. O. *J. Am. Chem. Soc.* **1959**, *81*, 1859−1868.
(80) Otte, T.; Pasch, H.; Macko, T.; Brüll, R.; Stadler, F. J.; Kaschta, J.; Becker, F.; Buback, M. *J. Chromatogr. A* **2011**, *1218*, 4257−4267.
(81) Mekap, D.; Macko, T.; Brüll, R.; Cong, R.; Degroot, A. W.; Parrott, A.; Cools, P. J. C. H.; Yau, W. *Polymer* **2013**, *54*, 5518−5524.
(82) Grinshpun, V.; O'Driscoll, K. F.; Rudin, A. In *ACS Symposium Series*; American Chemical Society, 1984; Vol. *245*, pp 273−280.
(83) Rue, C. A.; Schimpf, M. E. *Anal. Chem.* **1994**, *66*, 4054−4062.
(84) Greyling, G.; Pasch, H. *Macromolecules* **2017**, *50*, 569−579.
(85) Zhao, L.; Capt, L.; Kamal, M. R.; Choi, P. *Polym. Eng. Sci.* **2004**, *44*, 853−860.
(86) de Gennes, P. G. *Scaling Concepts in Polymer Physics*; Cornell University Press, 1979; Vol. 33.
(87) Wagner, H. L.; Verdier, P. H. *J. Res. Natl. Bur. Stand.* **1978**, *83*, 195−201.
(88) Han, C. C.; Verdier, P. H.; Wagner, H. L. *J. Res. Natl. Bur. Stand.* **1978**, *83*, 185−193.
(89) Ramachandran, R.; Beaucage, G.; Kulkarni, A. S.; McFaddin, D.; Merrick-Mack, J.; Galiatsatos, V. *Macromolecules* **2008**, *41*, 9802−9806.
(90) Schimpf, M. E.; Giddings, J. C. *Macromolecules* **1987**, *20*, 1561−1563.
(91) Morozov, K. I.; Köhler, W. *Langmuir* **2014**, *30*, 6571−6576.
(92) Niether, D.; Wiegand, S. *J. Phys. Condens. Matter* **2019**, *31*, 503003.
(93) Etxabarren, C.; Iriarte, M.; Uriarte, C.; Etxeberría, A.; Iruin, J. J. *J. Chromatogr. A* **2002**, *969*, 245−254.

https://dx.doi.org/10.1021/acs.analchem.0c03686
Anal. Chem. 2020, 92, 14822−14829

Supporting Information for

The Role of Solubility in Thermal Field-Flow Fractionation – A Revisited Theoretical Approach for Tuning the Separation of Chain-Walking Polymerized Polyethylene

Martin Geisler[†‡], Laura Plüschke[†‡], Jan Merna[§] and Albena Lederer[†‡,&*]

[†] Leibniz-Institut für Polymerforschung Dresden e.V., Hohe Str. 6, 01069 Dresden, Germany
[‡] Faculty of Chemistry and Food Chemistry, Technische Universität Dresden, 01162 Dresden, Germany
[§] Department of Polymers, University of Chemistry and Technology Prague, Technická 5, 166 28, Prague 6, Czech Republic
[&] Department of Chemistry and Polymer Science, Stellenbosch University, Private Bag X1, Matieland 7602, South Africa

Table of Content:

1.) Calculation details to section 2.1. in the main article S2
2.) Summary to the cwPE model library S4
3.) Purification and analysis of paraffin oil used as eluent (ALK) S5
4.) Translational diffusion coefficients measured by temperature dependent DLS S7
5.) ThFFF separation of the linear cwPE sample in ALK and DEC S8
6.) Numeric values of Figure 4 and 5 illustrated in the main article S8
References S9

1. Calculation details to section 2.1. in the main article

Table S1 Calculation details to section 2.1. in the main article with numerical values of D_T illustrated in Figure 1 of the main article. The calculation was done with the data values given in Table 1 in the main article.

Polymer	Solvent	η(T) [mPa s]	T [°C]	V_m (T) [cm³ mol⁻¹]	χ_H	$\frac{d\chi_H}{dT}$	$\frac{d^2\chi_H}{dT^2}$	$D_{T,\,exp}$ [cm² (s K)⁻¹]	Ref.	$D_{T,\,predict.}$ [cm² (s K)⁻¹]	Δ $D_{T,\,pred.}$ to $D_{T,\,exp}$ [%]
PS	CLF	0.551	23.0	81.61	0.503	3.088E-04	3.799E-05	5.800E-08	1	7.549E-08	30
	CHX	0.925	23.0	108.60	1.964	-2.785E-03	7.249E-05	6.600E-08	2	6.028E-08	-9
	THF	0.446	30.0	82.15	0.304	1.725E-03	2.440E-05	1.050E-07	1,3,4	8.739E-08	-17
	DOX	1.149	27.0	85.70	0.721	-4.917E-04	3.507E-05	4.200E-08	5,6	2.950E-08	-30
	TOL	0.521	30.0	106.95	1.230	-3.310E-03	5.190E-05	1.030E-07	6–8	6.276E-08	-39
	MEK	0.372	30.0	90.10	0.326	3.217E-03	2.350E-05	1.670E-07	6,9	1.309E-07	-22
	ETA	0.437	23.0	98.52	0.593	3.765E-03	3.235E-05	1.310E-07	1,5	1.372E-07	5
	DMA	0.878	30.0	93.51	0.176	1.343E-03	1.584E-05	3.760E-08	*	3.061E-08	-19
	ODBC	0.573	102.0	121.52	0.316	-7.709E-04	1.240E-05	2.560E-08	10	2.410E-08	-6
	DHN	1.142	89.8	166.12	2.201	-5.841E-03	4.491E-05	2.590E-08	11	1.738E-08	-33
	EB	0.628	25.8	123.17	1.717	-4.047E-03	6.271E-05	8.935E-08	12	6.006E-08	-33
		0.545	37.7	124.68	1.673	-3.325E-03	5.838E-05	9.655E-08	6	7.763E-08	-20
		0.257	122.1	137.26	1.308	-2.423E-03	3.401E-05	1.396E-07	13	1.564E-07	12
PMA	THF	0.425	35.0	81.66	0.632	1.413E-05	2.397E-05	1.270E-07	3	7.642E-08	-40
	MEK	0.354	35.0	90.10	0.557	1.583E-03	1.799E-05	1.870E-07	3	1.078E-07	-42
	ACT	0.281	35.0	73.96	0.457	2.088E-03	2.222E-05	2.160E-07	3	1.716E-07	-21
PMMA	THF	0.435	32.5	82.40	0.378	1.671E-03	2.579E-05	9.388E-08	4	9.338E-08	-1
syndio.	THF	0.461	26.5	81.81	0.368	1.523E-03	3.185E-05	1.212E-07	14	1.141E-07	-6
atactic		0.459	27.0	81.81	0.368	1.645E-03	2.707E-05	1.042E-07	14	1.021E-07	-2
isotactic		0.457	27.3	81.86	0.368	1.530E-03	2.562E-05	9.001E-08	14	7.724E-08	-14
syndio.	DOX	1.162	26.4	85.80	0.806	-1.008E-03	4.481E-05	5.131E-08	14	4.094E-08	-20
atactic		1.154	26.8	85.89	0.805	-7.231E-04	3.864E-05	4.379E-08	14	3.606E-08	-18
isotactic		1.144	27.3	85.98	0.805	-8.082E-04	3.698E-05	3.679E-08	14	2.721E-08	-26
syndio.	ACN	0.341	26.3	52.96	0.563	1.149E-03	2.719E-05	1.842E-07	14	1.277E-07	-31
atactic		0.338	27.5	53.03	0.564	1.102E-03	2.599E-05	1.051E-07	14	1.220E-07	16
isotactic		0.336	27.9	53.07	0.564	9.993E-04	2.541E-05	9.211E-08	14	9.429E-08	2
	DMA	0.821	35.4	94.01	0.298	9.638E-04	8.076E-06	2.421E-08	14	2.273E-08	-6
PBA	THF	0.468	25.0	81.66	0.458	4.651E-04	1.980E-05	4.900E-08	3	5.107E-08	4
	MEK	0.391	25.0	90.10	0.307	1.676E-03	1.345E-05	1.010E-07	3	6.575E-08	-35
	ACT	0.309	25.0	73.96	0.252	1.966E-03	1.806E-05	1.190E-07	3	1.052E-07	-12
PI	THF	0.407	39.8	83.13	0.442	4.183E-04	1.92627E-05	5.625E-08	4	7.276E-08	29

*own experiments, from ThFFF data given below

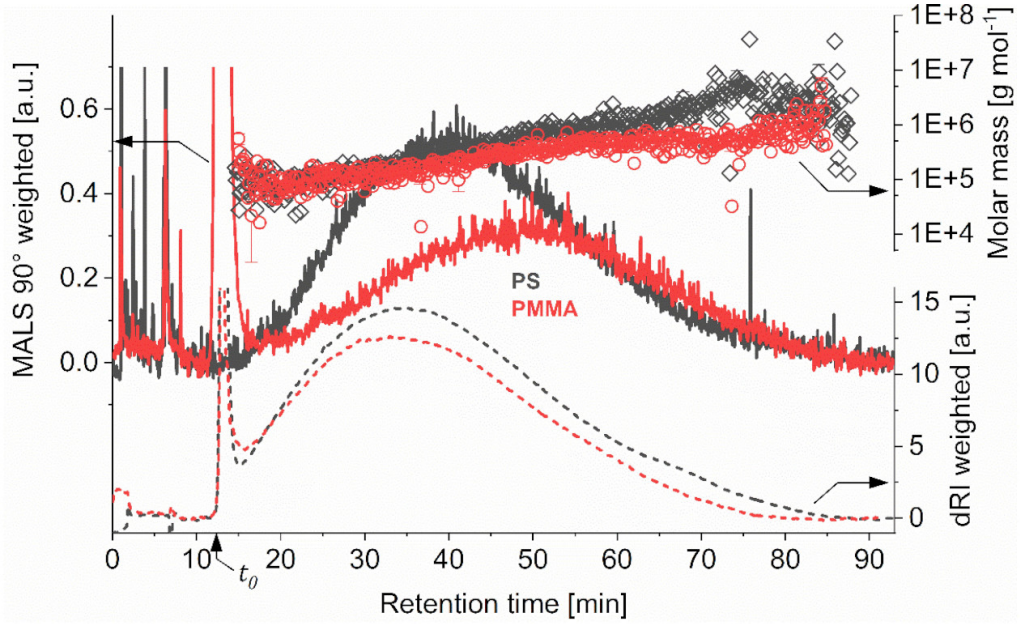

Figure S1 ThFFF fractogram of NIST 706a broad polystyrene (PS) standard and an industrial poly(methyl methacrylate) (PMMA) sample from extruded Plexiglas® by Röhm GmbH, Germany, both measured in *N,N*-dimethylacetamide (DMAc) at constant $\Delta T = 85$ K ($T_c = 23.5$ °C) and with a stop-flow time of 5 min. The void time (incl. stop-flow) is 12.36 min.

Table S2 Summary of the ThFFF-MALS-dRI analysis given in Fig. S1

	PS	PMMA
M_n [10^5 g mol^{-1}]	1.43 ± 0.04	1.36 ± 0.04
M_w [10^5 g mol^{-1}]	2.85 ± 0.1	2.37 ± 0.07
M_z [10^5 g mol^{-1}]	4.9 ± 0.3	3.7 ± 0.2
$Đ$	1.99 ± 0.04	1.74 ± 0.05

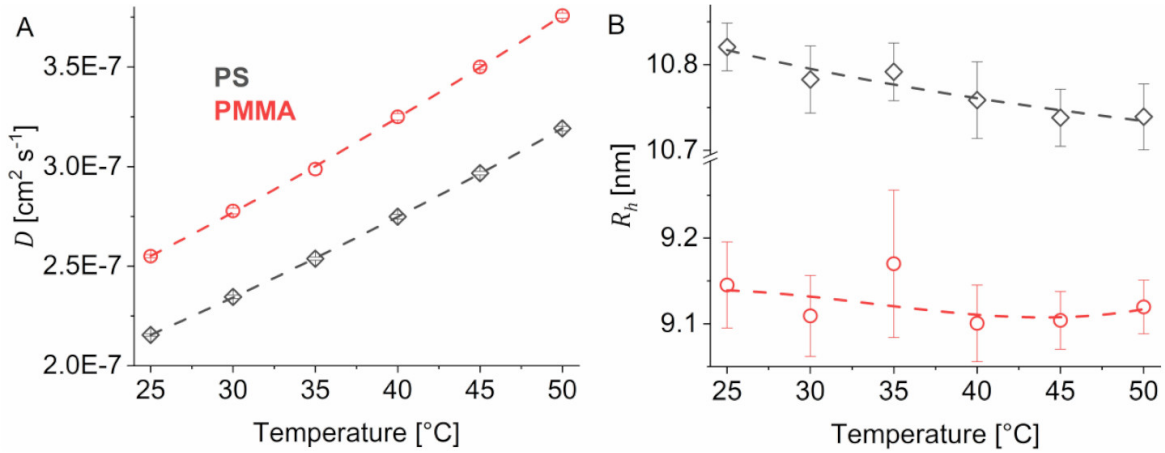

Figure S2 Translational diffusion coefficients (A) and hydrodynamic radii (B) of PS and PMMA, both measured in DMAc in a concentration of ca. 2 g L^{-1} by dynamic light scattering in batch. The measurements were done with a DynaPro® Nanostar® DLS by Wyatt Technology Corp., USA.

2. Summary to the cwPE polymer model library

The chain walking polymerized polyethylenes used in this work were synthesized with α-diimine palladium catalyst ([(N, N'-bis(2,6-diisopropylphenyl)-2,3-dimethyl-1,4-diazabutane)Pd$(CH_2)_3COOCH_3]^+$ $[BAr^F{}_4]^-$ (Ar^F=3,5-bis-(trifluoromethyl)phenyl)) as described previously[15–17] based on the synthesis approach of Brookhart *et al.*[18] with the conditions shown in Table S2. All samples contain ~ 200 branches per 1000 ethylene monomers according to ^{1}H NMR analysis but differ in topology mainly influenced by ethene pressure[19].

Table S3 Synthesis conditions and main average characteristics of the investigated short chain branched cwPEs found by high temperature size exclusion chromatography with a four-fold online detection system: multi-angle light scattering, DLS, viscometry and dRI (HT-SEC-D4) in 1,2,4-trichlorobenzene at 150 °C. The experimental details to the HT-SEC-D4 analysis is reported elsewhere.[16,17,20] ν_R is the scaling exponent from the double logarithmic R_G - M conformation plot, g is the gyration radius contraction factor, indices: w weight average moment, z centrifugal average moment.

Synthesis conditions				Average results found by HT-SEC-D4				
Sample	p / bar [a]	T / °C	Reaction time / h	M_w / kg mol^{-1}	$R_{G,z}$ / nm	ν_R	g_z	LCB_w
hb1	0.14	35	24	230 ± 6	15.8 ± 0.3	0.56 ± 0.3	0.22 ± 0.01	18.8 ± 2.2
hb2	0.09	0	24	161 ± 2	12.9 ± 0.2	0.45 to 1.15*	0.27 ± 0.01	14.3 ± 1.4
b1	4	0	20	140 ± 3	16.6 ± 0.4	0.60 ± 0.09	0.55 ± 0.03	2.7 ± 0.3
b2	2	0	20	136 ± 2	16.3 ± 0.2	0.65 ± 0.08	0.55 ± 0.01	3.2 ± 0.4
sb	2	10	20	313 ± 8	25.4 ± 0.5	0.47 to 0.73*	0.49 ± 0.02	1.5 ± 0.1
lin1	8	0	20	175.4 ± 0.5	18.5 ± 0.2	0.53 ± 0.02	0.53 ± 0.01	2.2 ± 0.1
lin2	8	10	20	384 ± 7	30.4 ± 0.3	0.35 to 0.74*	0.54 ± 0.01	1.1 ± 0.4

Pd catalyst 10 µmol, chlorobenzene 30 mL, [a]absolute ethene pressure

*) dependent on the molar mass

3. Purification and analysis of paraffin oil used as eluent (ALK)

Table S4 Report of the GC-MS analysis given in Figure S1.

Peak	t_R [min]	Amount [%]	Identified compound
1	5.18	0.39	n-Nonane
2	5.30	0.22	1,2,3-Trimethylcyclohexane
3	5.70	0.85	2,6-Dimethyloctane
4	5.81	0.70	1-ethyl-2,3-dimethylcyclohexane
5	6.02	0.85	1.2-Dimethylcyclooctane
6	6.13	2.57	4-Methylnonane
7	6.26	1.34	3-Methylnonane
8	6.36	1.69	2-methylnonane
9	6.41	0.73	1-Ethyl-2,3-dimethylcyclohexane
10	6.48	3.79	1-Methyl-2-propylcyclohexane
11	**6.79**	**20.8**	**n-Decane**
12	6.91	2.09	pentylcyclopentane
13	7.04	2.87	4-Methyldecane
14	7.11	1.37	1-Methylpropylcyclohexane
15	7.20	2.50	Butylcyclohexane
16	7.26	2.11	3-Methyldecane
17	7.33	0.91	1-Butylcyclohexane
18	7.39	1.41	1-Ethyl-2,2,6-trimethylcyclohexane
19	7.44	0.93	Trimethylcyclohexanes (mix)
20	7.51	1.14	5-Methyldecane
21	7.56	2.34	trans-Decalin
22	7.61	1.81	2-Methyldecane
23	7.64	0.94	1,2-Dipropylcyclopentane
24	7.70	1.76	Cyclodecane
25	7.74	0.79	1-Ethyl-2-propylcyclohexane
26	7.82	1.32	2-Methylbutylcyclohexane
27	7.84	0.71	1,2-Diethyl-3-methylcyclohexane
28	7.92	1.56	1-Ethyl-3-methylcyclohexane
29	7.98	1.20	1-Methyl-2-pentylcyclohexane
30	8.01	1.57	Trimethylcyclohexanes (mixture)
31	**8.17**	**13.1**	**n-Undecane**
32	8.27	0.86	1-Pentylcyclohexene
33	8.34	1.95	2,6-Dimethyldecane
34	8.46	1.02	3,7-Dimethyldecane
35	8.57	1.53	2-Methyldecalin (cis/trans mixture)
36	8.61	0.80	Pentylcyclohexane
37	8.65	1.04	Heptylcyclopentane
38	8.82	1.01	2,7-Dimethylundecane
39	8.87	0.81	4-Methylundecane
40	8.92	0.95	2-Methylundecane
41	9.01	0.70	3-Methylundecane
42	**9.40**	**3.21**	**n-Dodecane**
43	9.55	0.32	2,6-Dimethylundecane
44	10.58	0.28	n-Tridecane

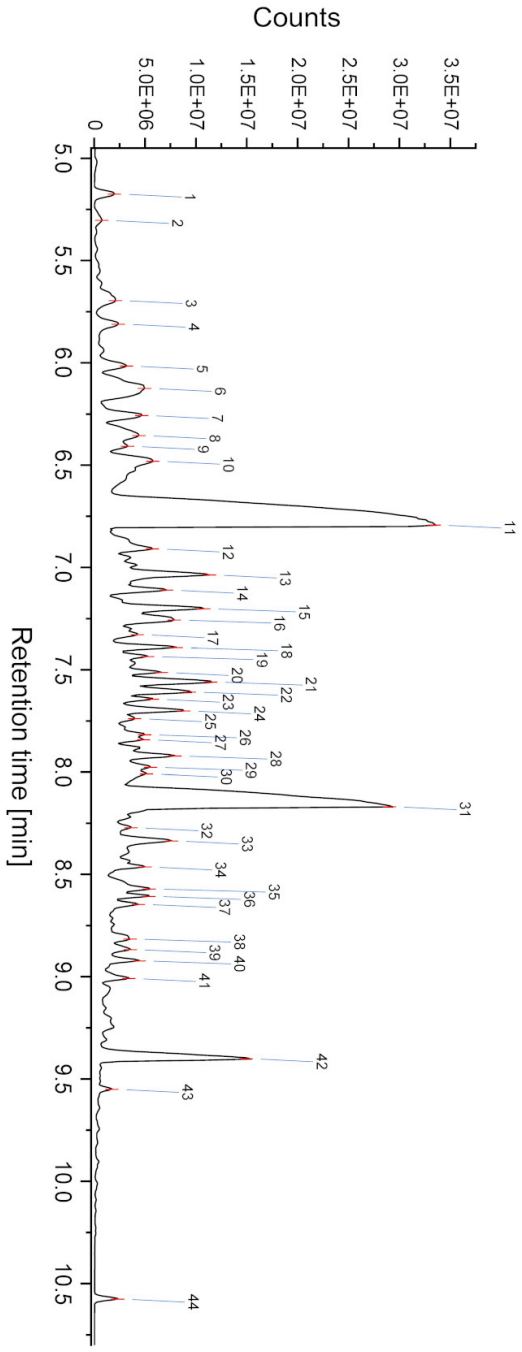

Figure S3 Py-GC/MS chromatogram of redistilled paraffin oil used for ThFFF separations in this study.

Py-GC/MS was performed with a modular system composed of a pyrolyzer Pyroprobe 5000 (CDS Analytical Inc., USA) with a platinum filament, a gas chromatograph GC7890A (Agilent Technologies, USA) with a HP-5MS-clumn (nonpolar, 30 m × 250 µm × 0.25 µm) and a mass spectrometer MSD 5975 CD inert XL EI/CD (EI at 70 eV, mass scan range 15–550 m/z, Agilent Technologies, USA). 0.2 mL paraffin oil were injected. For the flash pyrolysis, the interface CDS1500 at 280 °C and a pyrolysis temperature at 600 °C (isotherm for 10 s) was used. The inlet temperature during gas chromatography was 280 °C and the oven temperature was first maintained isothermally at 50 °C for 2 min, increased to 280 °C with a gradient of 12 K min^{-1} and finally isothermally held at 280 °C for 10 min.

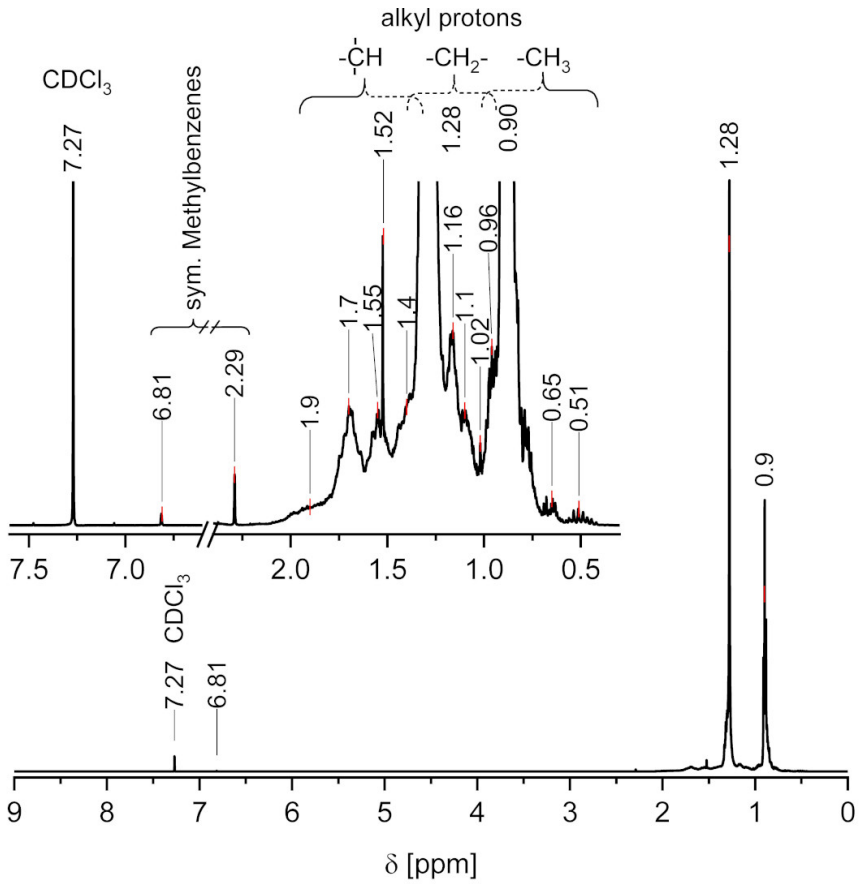

Figure S4 ^{1}H NMR spectrum of the paraffin oil (ALK) used as eluent in ThFFF separations. Signals of the n-, iso, and alkyl-cycloalkanes are found. The content of aromatic compounds (e.g., Mesitylene) is found to be less than 0.2 mol-%. The spectrum was recorded with a Bruker Avance III spectrometer operating at 500.13 MHz using the standard pulse programs included in the Bruker Topspin 3.2 software package. Deuterated chloroform was used as solvent, lock, and internal standard [δ(^{1}H) 7.27 ppm].

Purification

Two liter of Paraffin-based lamp oil (favorit® Lampenöl klar) as purchased from Alschu-Chemie GmbH, Germany and fractionated via column distillation over a thermally insulated Vigreux fractional column (length 40 cm) and with partial reflux under vacuum (8 mbar). About 250 mL were first fractionated from the raw lamp oil in the pot as foreshots, before about 600 mL of the main (body) fraction was collected, which was used then as the eluent ALK in the ThFFF separations. The main fraction condensed at a temperature of 57-64 °C at about 8 mbar (corresponds to a boiling point of 187 - 196 °C at 1 atm).

Further characterization

Viscosity measurements were performed with a LOVIS 2000 M rolling-ball viscometer (capillary ∅ 1.59 mm, ball ∅ 1.5 mm, calibrated with toluene) in the temperature range between 20 and 60 °C. Densities for the calculation of dynamic viscosities were measured in the same capillary by thermal expansion measurements of an exactly balanced amount of purified ALK. The determined dynamic viscosities for ALK within 20 – 60 °C are found to closely match $\eta(T)$ literature data of n-undecane.[21]

4. Translational diffusion coefficients measured by temperature dependent DLS

Table S5 Summarized translational diffusion coefficients measured by temperature-dependent DLS

T [°C]	D [10^7 cm^2 s^{-1}] hb1	hb2	b1	b2	sb	lin1	lin2
				Tetrahydrofuran			
20	4.51±0.06	4.02±0.06	4.36±0.16		3.60±0.08		2.27±0.03
25	4.88±0.10	4.50±0.06	4.77±0.47		3.88±0.07		2.41±0.02
30	5.26±0.09	5.03±0.22	5.35±0.25		4.31±0.10		2.57±0.02
35	5.63±0.09	5.51±0.09	6.00±0.37		4.78±0.07		2.72±0.02
40	6.03±0.07	5.93±0.08	6.64±0.30		5.12±0.10		2.89±0.02
45	6.43±0.04	6.07±0.09	7.17±0.40		5.74±0.11		3.05±0.03
				Chloroform			
20	2.67±0.10		2.71±0.14		1.94±0.08		1.45±0.10
25	2.78±0.14		2.95±0.26		2.15±0.09		1.54±0.12
30	3.14±0.09		3.22±0.44		2.34±0.05		1.64±0.11
35	3.29±0.06		3.29±0.57		2.56±0.03		1.77±0.12
40	3.58±0.10		3.72±0.22		2.67±0.15		1.93±0.09
45							2.08±0.11
50							2.27±0.16
60	4.56±0.09		4.50±0.49		3.41±0.10		
				Cyclohexane[20]			
20	1.73±0.02	1.89±0.03	1.77±0.01	1.80±0.01	1.28±0.00	1.60±0.02	1.16±0.00
25	1.80±0.03	2.06±0.03	1.97±0.02	1.99±0.04	1.41±0.02	1.76±0.03	1.28±0.01
30	2.03±0.03	2.27±0.04	2.18±0.02	2.22±0.01	1.58±0.00	1.95±0.03	1.41±0.01
35	2.25±0.03	2.52±0.04	2.40±0.02	2.44±0.01	1.73±0.01	2.15±0.03	1.55±0.01
40	2.49±0.03	2.73±0.04	2.63±0.01	2.68±0.01	1.89±0.01	2.36±0.03	1.69±0.01
45	2.73±0.02	3.01±0.03	2.88±0.02	2.93±0.01	2.06±0.01	2.59±0.02	1.83±0.02
50	3.00±0.02	3.30±0.05	3.14±0.02	3.19±0.02	2.25±0.01	2.83±0.02	2.02±0.01
60	3.59±0.01	3.90±0.03	3.72±0.02	3.75±0.01	2.65±0.02	3.34±0.03	2.38±0.02
				Mesitylene			
20	2.64±0.12		2.45±0.19		1.82±0.05		1.66±0.07
25	2.91±0.20		2.66±0.53		1.97±0.10		1.79±0.07
30	3.19±0.26		2.88±0.56		2.13±0.29		1.92±0.07
35	3.48±0.31		3.10±0.05		2.27±0.31		2.06±0.09
40	3.74±0.30		3.33±0.30		2.44±0.27		2.18±0.10
60	4.94±0.85				2.62±0.37		2.32±0.22
				Paraffin oil			
20	1.40±0.05	1.17±0.10	1.38±0.09	1.48±0.05	1.23±0.01	1.58±0.01	0.94±0.01
25	1.53±0.05	1.30±0.08	1.54±0.04	1.63±0.14	1.36±0.02	1.71±0.02	1.03±0.02
30	1.66±0.11	1.45±0.17	1.71±0.07	1.79±0.21	1.49±0.01	1.85±0.01	1.13±0.01
35	1.80±0.09	1.59±0.14	1.89±0.06	1.96±0.11	1.62±0.01	2.04±0.02	1.23±0.01
40	1.95±0.11	1.75±0.16	2.07±0.04	2.14±0.08	1.76±0.01	2.22±0.03	1.34±0.03
45	2.11±0.06	1.93±0.16	2.27±0.11	2.34±0.07	1.92±0.01	2.40±0.01	1.44±0.04

Temperature dependent dynamic light scattering (DLS) experiments were performed in batch mode with a DynaPro® NanoStar® instrument (Laser λ = 658 nm) by Wyatt Technology Corporation, USA using a 1.25 µl quartz cuvette (total volume approximately 1 mL). In all experiments, the cuvette was completely filled with ca. 0.8 mL sample solution to avoid cavities, containing 1 mg mL^{-1} of polymer and filtered through a 0.45 µm PTFE syringe filter (Carl Roth, Germany). The cuvette was sealed with an affiliated PTFE lid to prevent evaporation of solvent. The data analysis was done with the software Dynamics® by Wyatt Technology Corporation, USA, version 7.9.0.5.

5. ThFFF separation of the linear cwPE sample in ALK and DEC

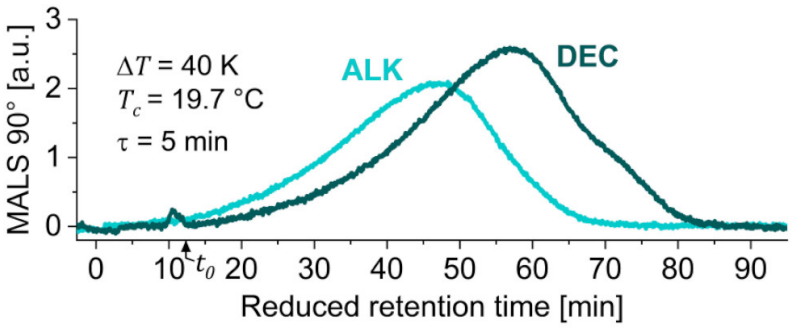

Figure S5 ThFFF fractograms of the linear cwPE sample lin2 shown in dependency to the reduced retention time (stop-flow time subtracted). The separations were performed in equal conditions (see section 3, SI) for n-decane (DEC) and to paraffin oil (ALK) at a flow rate of 0.3 ml min^{-1} and with a stop-flow time of $\tau = 5$ min.

6. Numeric values of Figure 4 and 5 illustrated in the main article

Table S6 Numeric values for the plot given in Figure 4 of the main article.

Solvent	*RED* calculated with $\delta_D = 17.6$ MPa$^{0.5}$ *Ro* = 10.4 MPa$^{0.5}$	*RED* calculated with $\delta_D = 15.8$ MPa$^{0.5}$ *Ro* = 10.2 MPa$^{0.5}$	$\eta(T)\ D_T$ [10^{10} g cm (s^2 K)$^{-1}$]
Cyclohexane	0.178	0.178	2.63 ± 0.46
Mesitylene	0.114	0.439	1.44 ± 0.22
n-Decane	0.373	0.020	6.03 ± 0.99
Paraffin oil	0.314	0.040	5.29 ± 0.64
Chloroform	0.637	0.747	0.74 ± 0.11
Tetrahydrofuran	0.976	0.983	0.32 ± 0.25

Table S7 Numeric values for the plot given in Figure 5 of the main article.

	LCB	blob diameter [nm]							
		CLF	CHX	THF	MST	ALK	DEC	ODBC	TCE
hb1	18.8 ± 2.2	4.9 ± 1.0	8.4 ± 2.3	5 ± 3	8.3 ± 2.1	1.27 ± 0.20			
hb2	14.3 ± 1.4		6.4 ± 1.7	9 ± 9		1.52 ± 0.23			
b1	2.7 ± 0.3	4.2 ± 0.8	2.4 ± 0.3	4 ± 2	1.9 ± 0.4	0.99 ± 0.09			
b2	3.2 ± 0.4		2.5 ± 0.4			1.02 ± 0.17			
sb	1.5 ± 0.1	3.2 ± 0.6	2.3 ± 0.3	5 ± 2	1.8 ± 0.4	0.77 ± 0.06			
lin1	2.2 ± 0.1		1.8 ± 0.3			0.82 ± 0.06			
lin2	1.1 ± 0.4	4.0 ± 0.6	1.7 ± 0.3	9 ± 3	1.3 ± 0.2	0.77 ± 0.06	0.61 ± 0.08		
HDPE	0.4 ± 0.3 [a]	at mean layer temperature (102 °C; 114 °C)						1.02 ± 0.15	0.91 ± 0.14
		transformed to 25 °C						0.64 ± 0.10	0.56 ± 0.08

[a] measured by HT-SEC-D4 in 1,2,4-trichlorobenzene, experimental conditions as reported earlier[16]

References

(1) Stadelmaier, D.; Köhler, W. Thermal Diffusion of Dilute Polymer Solutions: The Role of Chain Flexibility and the Effective Segment Size. *Macromolecules* **2009**, *42* (22), 9147–9152. DOI: 10.1021/ma901794k.

(2) Schimpf, M. E.; Giddings, J. C. Characterization of Thermal Diffusion in Polymer Solutions by Thermal Field-flow Fractionation: Dependence on Polymer and Solvent Parameters. *J. Polym. Sci. Part B Polym. Phys.* **1989**, *27* (6), 1317–1332. DOI: 10.1002/polb.1989.090270610.

(3) Runyon, J. R.; Williams, S. K. R. A Theory-Based Approach to Thermal Field-Flow Fractionation of Polyacrylates. *J. Chromatogr. A* **2011**, *1218* (39), 7016–7022. DOI: 10.1016/J.CHROMA.2011.08.007.

(4) Cao, W.; Williams, P. S.; Myers, M. N.; Giddings, J. C. Thermal Field-Flow Fractionation Universal Calibration: Extension for Consideration of Variation of Cold Wall Temperature. *Anal. Chem.* **1999**, *71* (8), 1597–1609. DOI: 10.1021/ac981094m.

(5) Van Asten, A. C.; Kok, W. T.; Tijssen, R.; Poppe, H. Study of Thermal Diffusion of Polybutadiene and Polytetrahydrofuran in Various Organic Solvents. *J. Polym. Sci. Part B Polym. Phys.* **1996**, *34* (2), 297–308. DOI: 10.1002/(SICI)1099-0488(19960130)34:2<297::AID-POLB10>3.0.CO;2-E.

(6) Giddings, J. C.; Caldwell, K. D.; Myers, M. N. Thermal Diffusion of Polystyrene in Eight Solvents by an Improved Thermal Field-Flow Fractionation Methodology. *Macromolecules* **1976**, *9* (1), 106–112. DOI: 10.1021/ma60049a021.

(7) Köhler, W.; Rosenauer, C.; Rossmanith, P. Holographic Grating Study of Mass and Thermal Diffusion of Polystyrene/Toluene Solutions. *Int. J. Thermophys.* **1995**, *16* (1), 11–21. DOI: 10.1007/BF01438953.

(8) Rauch, J.; Köhler, W. On the Molar Mass Dependence of the Thermal Diffusion Coefficient of Polymer Solutions. *Macromolecules* **2005**, *38* (9), 3571–3573. DOI: 10.1021/ma050231w.

(9) Stadelmaier, D.; Köhler, W. From Small Molecules to High Polymers: Investigation of the Crossover of Thermal Diffusion in Dilute Polystyrene Solutions. *Macromolecules* **2008**, *41* (16), 6205–6209. DOI: 10.1021/ma800891p.

(10) Pasti, L.; Roccasalvo, S.; Dondi, F.; Reschiglian, P. High Temperature Thermal Field-flow Fractionation of Polyethylene and Polystyrene. *J. Polym. Sci. Part B Polym. Phys.* **1995**, *33* (8), 1225–1234. DOI: 10.1002/polb.1995.090330808.

(11) Melucci, D.; Contado, C.; Mingozzi, I.; Reschiglian, P.; Dondi, F. Properties of Decalin as a Solvent in Thermal Field-Flow Fractionation. *Chromatographia* **1999**, *49* (3–4), 131–136. DOI: 10.1007/BF02575274.

(12) Myers, M. N.; Caldwell, K. D.; Calvin Giddings, J.; Giddings, J. C. A Study of Retention in Thermal Field-Flow Fractionation. *Sep. Sci.* **1974**, *9* (1), 47–70. DOI: 10.1080/01496397408080043.

(13) Brimhall, S. L.; Myers, M. N.; Caldwell, K. D.; Giddings, J. C. Study of Temperature Dependence of Thermal Diffusion in Polystyrene/Ethylbenzene By Thermal Field-Flow Fractionation. *J. Polym. Sci. Part A-2, Polym. Phys.* **1984**, *23* (12), 2443–2456. DOI: 10.1002/pol.1985.180231203.

(14) Greyling, G.; Pasch, H. Tacticity Separation of Poly(Methyl Methacrylate) by Multidetector Thermal Field-Flow Fractionation. *Anal. Chem.* **2015**, *87* (5), 3011–3018. DOI: 10.1021/ac504651p.

(15) Mundil, R.; Hermanová, S.; Peschel, M.; Lederer, A.; Merna, J. On the Topology of Highly Branched Polyethylenes Prepared by Amine−Imine Nickel and Palladium Complexes: The Effect of Ortho-Aryl Substituents. *Polym. Int.* **2018**, *67* (7), 946–956. DOI: 10.1002/pi.5593.

(16) Plüschke, L.; Mundil, R.; Sokolohorskyj, A.; Merna, J.; Sommer, J.-U.; Lederer, A. High Temperature Quadruple-Detector Size Exclusion Chromatography for Topological Characterization of Polyethylene. *Anal. Chem.* **2018**, *90* (10), 6178–6186. DOI: 10.1021/acs.analchem.8b00619.

(17) Dockhorn, R.; Plüschke, L.; Geisler, M.; Zessin, J.; Lindner, P.; Mundil, R.; Merna, J.; Sommer, J.-U.; Lederer, A. Polyolefins Formed by Chain Walking Catalysis - A Matter of Branching Density Only? *J. Am. Chem. Soc.* **2019**, *141* (39), 15586–15596. DOI: 10.1021/jacs.9b06785.

(18) Johnson, L. K.; Killian, C. M.; Brookhart, M. New Pd(II)- and Ni(II)-Based Catalysts for Polymerization of Ethylene and α-Olefins. *J. Am. Chem. Soc.* **1995**, *117* (23), 6414–6415. DOI: 10.1021/ja00128a054.

(19) Guan, Z.; Cotts, P. M.; McCord, E. F.; McLain, S. J. Chain Walking: A New Strategy to Control Polymer Topology. *Science* **1999**, *283* (5410), 2059–2062. DOI: 10.1126/science.283.5410.2059.

(20) Geisler, M.; Smith, W. C.; Plüschke, L.; Mundil, R.; Merna, J.; Williams, S. K. R.; Lederer, A. Topology Analysis of Chain Walking Polymerized Polyethylene: An Alternative Approach for the Branching Characterization by Thermal FFF. *Macromolecules* **2019**, *52* (22), 8662–8671. DOI: 10.1021/acs.macromol.9b01410.

(21) Data Extracted from the Landolt-Börnstein book series and associated databases. *SpringerMaterials database*. Springer: Berlin Heidelberg, Germany 2017.

8.3. Thermal Field-Flow Fractionation for Characterization of Architecture in Hyperbranched Aromatic-Aliphatic Polyesters with Controlled Branching

analytical chemistry

Article

Cite This: *Anal. Chem.* 2019, 91, 12344−12351

pubs.acs.org/ac

Thermal Field-Flow Fractionation for Characterization of Architecture in Hyperbranched Aromatic-Aliphatic Polyesters with Controlled Branching

William C. Smith,[†] Martin Geisler,[‡,§] Albena Lederer,[‡,§] and S. Kim Ratanathanawongs Williams*[,†]

[†]Department of Chemistry, Colorado School of Mines, Golden, Colorado 80401, United States

[‡]Leibniz-Institut für Polymerforschung Dresden e.V., Hohe Strasse 6, 01069 Dresden, Germany

[§]School of Science, Faculty of Chemistry and Food Chemistry, Technische Universität Dresden, 01062 Dresden, Germany

Supporting Information

ABSTRACT: Thermal field-flow fractionation (ThFFF) was used to characterize the architecture of aromatic−aliphatic polyesters with varying degrees of branching. Thermal diffusion and Soret coefficients (D_T and S_T, respectively) provide a novel route to polymer architecture analysis. This paper demonstrates an innovative strategy to extract architecture information from the physicochemical separation parameters embedded in ThFFF retention times without explicit separation of linear and branched samples. A Soret contraction factor (g''), defined as the ratio of the S_T of a branched polymer to the S_T of a molecular weight equivalent linear analogue, is introduced as a metric to indicate degree of branching (DB). This approach circumvents several challenges associated with the analysis of high molar mass polymers with a high degree of branching. The g'' value is shown to be proportional to the degree of branching for linear (DB, 0%), gradually branched (DB, <50%), hyperbranched (DB, 50%), and pseudodendritic (DB, 100%) polyesters allowing the establishment of architecture calibration curves. Furthermore, positive log(g'') values (~0.2) at low molar mass are attributed to cyclic subpopulations. This work demonstrates the usefulness of the Soret contraction factor for statistically and hyperbranched polymer systems and its sensitivity to cyclic polymers.

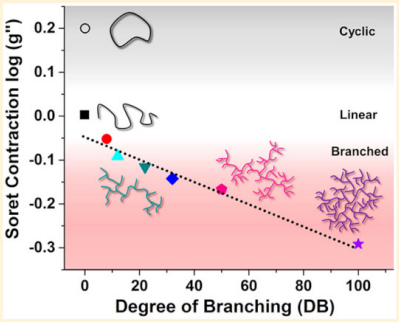

Hyperbranched (hb) polymers are a class of branched polymers where the branching repeat units have a possibility of secondary branching leading to random and highly dense polymer structures. The commercialization of hb polyesters is driven by the low production cost, the industrial scalability, and relatively easy "one-pot" synthesis.[1] However, this process often leads to polymers which have distributions both in molecular weight (M_w) and degree of branching (DB), both of which strongly influence the polymer's rheological and solution behavior, processability, and end product performance.[2−4] Measurement of hb polymer molecular weight is typically done by a combination of size exclusion chromatography (SEC) with online viscometry or multiangle light scattering (MALS) detection.[5] While this approach works for low M_w hb polymers, in some cases, hb polymers with high M_w can experience enthalpic and physical interactions with the stationary phase that may cause abnormal elution behavior leading to inaccuracy in the measured M_w and dispersity.[6] Ideal separations in SEC are based solely on entropic considerations; therefore, the solvent and column chemistries are chosen explicitly to mitigate any complications from undesirable analyte−column interactions. Adsorption phenomena have however been exploited for branching characterization and separations using solvent gradient interaction chromatography (SGIC), liquid chromatography at critical conditions (LCCC), and temperature gradient interaction chromatography (TGIC),[7] where conditions and columns are chosen specifically to tune the strength of analyte−column interactions. In this regard, LCCC has proven to be useful in the separation of branched, linear, and cyclic polymers, though there is some discrepancy between theoretical prediction and experimental retention behavior.[8] High-resolution 2D-SGIC-SEC has also been used to determine both branching and molar mass for linear and branched polymer blends.[9] However, strong enthalpic interactions of hyperbranched polyesters with high molar masses (>50 kDa) can lead to significant adsorption causing poor sample recovery and can convolute retention volume branching correlations.[10] The average degree of branching is commonly determined using ensemble techniques like NMR.[11] Similarly, the rheological properties of polymers can be correlated to the overall average branching in a polymer sample allowing linear and branched architectures to be differentiated.[12,13] While these ensemble techniques provide an average value for the degree of branching, they do

Received: June 11, 2019
Accepted: September 6, 2019
Published: September 6, 2019

DOI: 10.1021/acs.analchem.9b02664
Anal. Chem. 2019, 91, 12344−12351

not yield the distribution.[14] A method able to identify the degree of branching, number of branches or chain ends, and their distributions is imperative to understanding the structure−function relationships and behavior of these complex polymers.

Typical analyses of macromolecules emphasize the measurement of properties like molar mass and "size", and the latter is given by an equivalent spherical radius. Correlation of the volume a polymer occupies in dilute solution with the mass and/or geometric radius can provide valuable information on polymer conformation. Further comparison of the conformational state with that of a molar mass equivalent linear analogue helps to illuminate polymer architecture. One of the foremost of these relations is the light scattering contraction factor (g) whose definition is shown in eq 1:

$$g = \frac{(R_{g\,\mathrm{Branched}})^2}{(R_{g\,\mathrm{Linear}})^2} \quad (1)$$

where R_g is the radius of gyration.[15] From this proportion, a reasonable estimate of branching can be made using the Zimm−Stockmayer formalism.[16] Determination of g requires a polymer to have a sufficiently large size (larger than $\frac{\mathrm{MALS\ wavelength}}{\sim 50}$) so that R_g can be determined from the light scattering angular dependence with reasonable accuracy.[17] For this reason, hb polymers of low molar mass have been carried out via the coupling of separations methods to viscometry.[18] Following a similar process as above, a viscometric contraction factor (g') can be determined and has been shown to be effective for determining branching in polymers with regular architecture.[19] Recent studies have looked into the universality of the relation[20,21] between g' and g in order to understand the difficulty of this method for quantifying random or statistical branching.[22] In order to address the problems associated with column-based chromatography techniques and light scattering detection limits, an additional technique for branching analysis must be introduced.

Thermal field-flow fractionation (ThFFF) is a separation technique that has been developed for the characterization of both polymer molar mass and composition.[23] Thermal FFF utilizes a temperature gradient to induce the migration of molecules (usually) toward regions of lower temperature. The magnitude of this thermal diffusion is dependent on the chemistry of the polymer−solvent interface; this flux is balanced by molecules undergoing translational diffusion in the opposite direction. The ratio of the thermal diffusion coefficient D_T to the translational diffusion coefficient D is termed the Soret coefficient or S_T.[24] The S_T is conveniently directly proportional to the measured ThFFF retention time (as discussed further in the Experimental Section). As an alternative to traditional chromatography, ThFFF provides several benefits due to its open channel design and absence of packing material. These benefits include a high molar mass range as well as limited sample loss and degradation. These problems are especially relevant in the architecture characterization of high molar mass polymer where chromatography stationary-phase induced shear degradation and adsorption are commonplace. Recently, a new approach to architecture characterization has been introduced based on first-principles of the ThFFF separation mechanism.[25] This work compared experimentally measured Soret coefficients (S_T) for regularly branched star and miktoarm star polymers with theoretical Soret coefficients of the corresponding linear polymer based on a predictive model of thermal diffusion. A ratio of S_T values defines the Soret contraction factor (g'').[25]

$$g'' = \frac{S_{T\,\mathrm{Branched}}}{S_{T\,\mathrm{Linear}}} \quad (2)$$

As S_T contains information about the hydrodynamic size of a polymer, via D, a ratio of branched and linear polymer S_T values can perform a similar function to viscometric- and light scattering-based contraction factors. The original work investigated polymers with regular branching (linear, star, pom-pom) and demonstrated that the number of chain ends could be determined via the construction of a calibration curve which was independent of polymer chemical composition. This principle was later applied to investigate bottle-brush polymers with variations in backbone and side-chain lengths.[26] Recent application of this analysis to linear and star polystyrene illustrated how the thermodynamic quality of the solvent may cause deviation in the estimation of chain ends.[27] It should be noted that g'' is an empirical relationship and a fully quantitative relation to various types of branching has yet to be established. To the best of our knowledge, this approach has only been applied to polymers with regular branching topologies.

The objective of this current study is to investigate the potential of the Soret contraction (g'') to characterize hyperbranched polymers with random or statistical branching and not to develop an architecture-based separation. This study focuses on the determination of S_T values from ThFFF retention times and their use in conjunction with MALS and dynamic light scattering (DLS) to simultaneously determine distributions in M_w and DB for hyperbranched and pseudodendrimeric polymers. Accordingly, the ThFFF retention behavior of a series of aromatic-aliphatic polyesters with controlled DB of 100, 50, 32, 22, 12, 8, and 0% was investigated. Three approaches that utilized thermal diffusion coefficients D_T, hydrodynamic conformation plots, and Soret contraction factors for architecture characterization were evaluated and compared.

EXPERIMENTAL SECTION

Materials. Polyesters with DB from 0 to 50% were prepared via an ABB*/AB_2 polycondensation of 4,4-bis(4′-hydroxyphenyl) valeric acid (AB_2) with a *tert*-butyldimethylsilyl protected version of the monomer (ABB*) as previously described.[28] The ABB*/AB_2 ratio dictates the degree of branching of the resultant polymer. These samples are referred to as SY-0, -8, -12, -22, -32, and -50 to denote the presence of the silyl group (SY) and the nominal DB. The SY-100 sample was produced following a postmodification process where the OH-50 (analogue to SY-50 but with OH end groups for further modification) sample was reacted with additional AB^*_2 monomer with two silyl groups.[29] This replaced any remaining linear regions that are statistically present in the hyperbranched sample with an AB^*_2 terminal chain creating a pseudodendrimer. The final structure had two distinct chemistries, polar ester groups providing linear or dendritic linkage and nonpolar silyl pendant groups (Scheme 1). Molecular weights and PDI from SEC-MALS analysis are summarized in Table 1. Experimental details to the SEC analysis are given in the Supporting Information. Solubility of the polymers was investigated in several solvents. Tetrahydrofuran (THF) and

DOI: 10.1021/acs.analchem.9b02664
Anal. Chem. 2019, 91, 12344−12351

Scheme 1. Scheme of Polyester Synthesis Following ABB*/AB_2 Condensation Process for DB 0−50%[a]

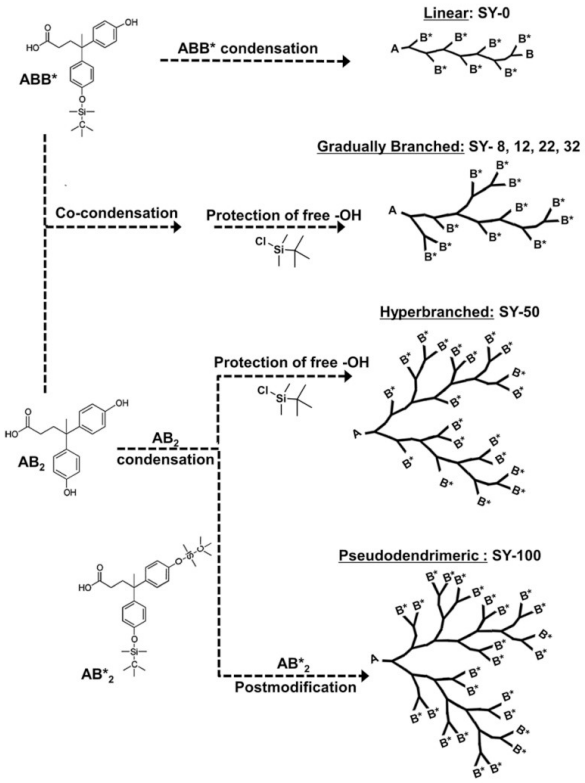

[a]The DB 100% is produced by postmodification of linear units on the SY-50 hyperbranched sample with AB^*_2 monomers producing a pseudodendrimer.

Table 1. Degree of Branching, Molecular Mass, and $Đ = M_w/M_n$ for Aliphatic-Aromatic Polyester Samples

sample	topology	degree of branching (%)[a]	M_w (g/mol)[b]	$Đ$
SY-0	linear	0	73300 ± 200	2.28
SY-8	gradually branched	8	30300 ± 200	2.42
SY-12	gradually branched	12	53700 ± 100	2.14
SY-22	gradually branched	22	60700 ± 300	2.56
SY-32	gradually branched	32	44700 ± 200	2.38
SY-50	hyperbranched	50	42400 ± 200	1.86
SY-100	pseudodendritic	100	153100 ± 300	2.42

[a]Determined by ^{13}C NMR according to ref 28. [b]Uncertainties represent one standard deviation.

cyclohexane (CH) (Sigma-Aldrich, St. Louis, MO) were used in the subsequent study representing polar and nonpolar solvents, respectively.

Thermal Field-Flow Fractionation (ThFFF) and Light Scattering. Fractionation was conducted using a TF2000 model ThFFF system coupled online to a model PN 3621 multiangle light scattering (MALS) and a PN 3150 dRI (Postnova Analytics, Salt Lake City, UT). The refractive index increment (dn/dc) for the polyester samples was determined to be 0.1550 mL/g in THF (in agreement to previous studies[20,28]) and 0.1435 in CH following a standard batch method (Figure S1). No significant dependence of dn/dc on degree of branching had been observed; therefore, average values were used for all samples. The ThFFF channel had dimensions of 250 μm in thickness, 2.0 cm in breadth, and 45.6 cm in length. The carrier liquid in all experiments was CH or THF pumped through the channel at 0.2 mL/min. Samples were introduced into the system by a PN 5300 autosampler (Postnova Analytics) with a 102.5 μL sample loop. All SY samples were prepared at ∼3−5 mg/mL, and the injected volume was ∼50 μL; the total mass of sample was below the average sample overloading mass of 400 μg as determined by an overloading study.[30] The void time was 11.04 min. Temperature dependent dynamic light scattering (DLS) studies were performed using a Wyatt DynaPro Nanostar (Wyatt Technology Corporation, Santa Barbara, CA) at 5 °C intervals from 20 to 50 °C for THF and from 20 to 60 °C in CH (Figure S2). Each temperature step was 17 min to ensure adequate equilibration time; data was taken for a 5 min period after the temperature stabilized with an acquisition time interval of 5 s. Attenuation and laser power were automatically adjusted for each sample. All samples were filtered through a 0.2 μm PTFE filter prior to analysis, and 1 mL was added and the cuvette sealed securely. Values were calculated with the Dynamics software version 7.6.0.48 using the cumulant autocorrelation fit method.

Calculation of S_T and D_T. In a normal mode separation, ThFFF analytes elute according to the balance of thermal (D_T) and translational diffusion (D) coefficients also known as the Soret coefficient (S_T). An approximation of the ThFFF retention equation is given in eq 3:

$$t_r \cong \frac{D_T \Delta T t^0}{6D} \quad \text{or} \quad \frac{S_T \Delta T t^0}{6} \tag{3}$$

where t^0 is the void time (the travel time through the ThFFF channel of an unretained solute) and ΔT is the temperature drop across the spacer. The value of ΔT is known, D is measured by batch and/or online DLS, and t^0 and t_r (the retention time at peak maximum) are determined from ThFFF fractograms. Therefore, S_T and D_T can be calculated for any given ThFFF retention time resulting in continuous values across a sample peak. Equation 3 holds only for highly retained analytes ($t_r \geq 5$ times the void time).[31] A deeper look at ThFFF retention theory at high temperatures and considerations for D values and actual equations used in calculation of D_T values from retention time can be found in the Supporting Information section 2.

■ RESULTS AND DISCUSSION

The ThFFF retention behavior of a series of linear, gradually branched, hyperbranched, and pseudodendrimeric polyester was investigated, and the fractograms obtained in THF and CH are shown in Figure 1a−g. All samples exhibited higher retention in THF due to a larger hydrodynamic size (Figure S3). The thermal diffusion coefficient (D_T) can also impact retention time and these values were calculated according to eqs S1 and S2 and plotted in Figure 2. Two distinct trends are observed in CH and THF. Branching did not influence the D_T of polymers dissolved in CH with all values falling within one standard deviation about the mean. In THF, a different behavior is observed with polymer D_T decreasing with

DOI: 10.1021/acs.analchem.9b02664
Anal. Chem. 2019, 91, 12344−12351

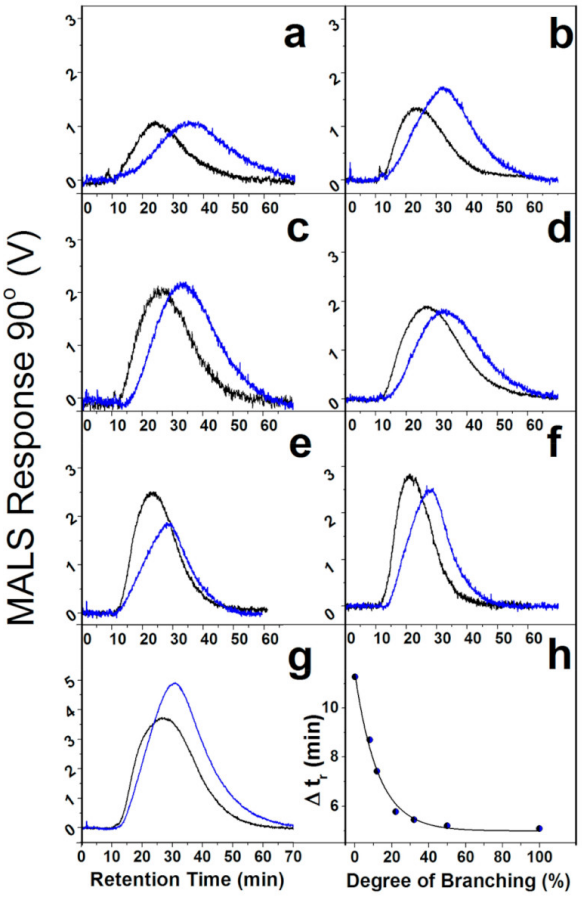

Figure 1. Overlay of MALS fractograms of polyester samples in THF (blue) and CH (black) for (a) SY-0, (b) SY-8, (c) SY-12, (d) SY-22, (e) SY-32, (f) SY-50, (g) SY-100, and (h) the difference in retention time for each sample between solvents.

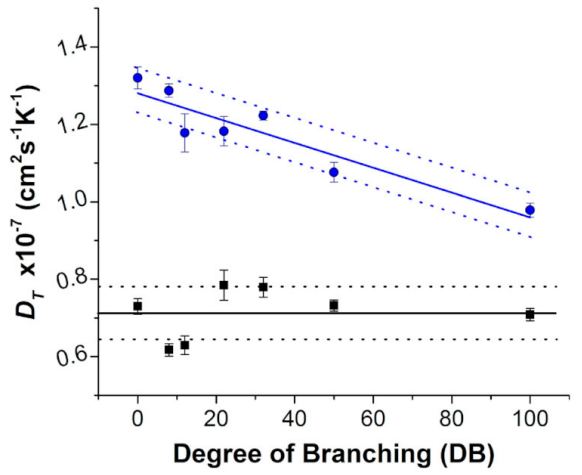

Figure 2. Polymer D_T dependence on DB and solvent (THF blue, CH black). The solid line represents the fit for trend in THF and mean value in CH. Dotted lines represents one standard deviation.

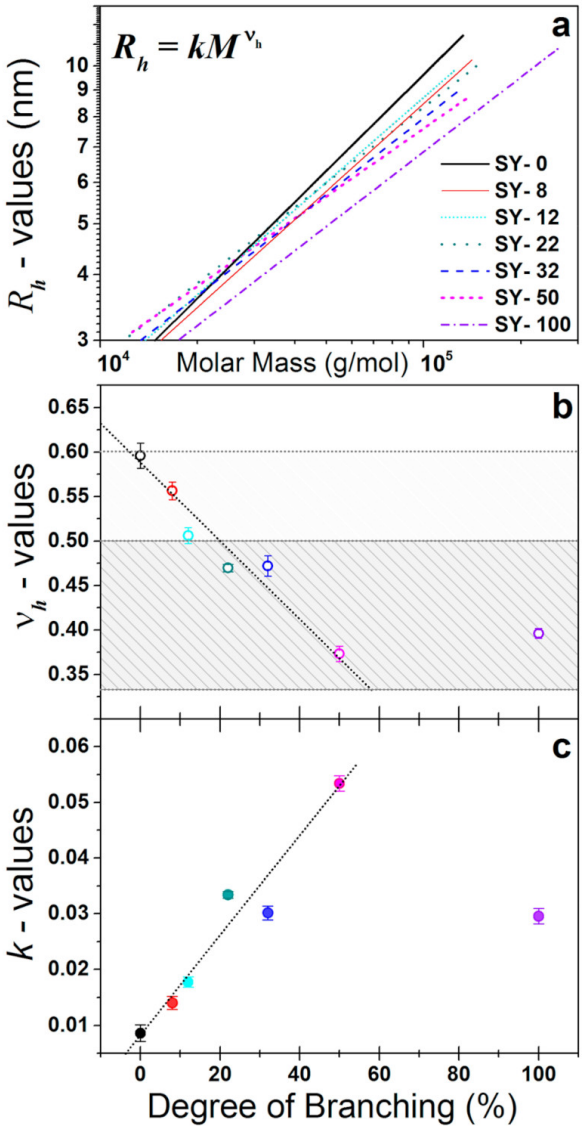

Figure 3. (a) Conformation plots of R_h and M_w from ThFFF-DLS for all samples in THF, (b) plot of conformation slope (ν_h), and (c) conformation plot intercept (k) with respect to the degree of branching.

increasing DB. D_T has been shown to be sensitive to the polymer chemistry, and this sensitivity was exploited for determining composition distributions.[32] Furthermore, architecture and branching is not expected to influence the D_T of a homopolymer in a good solvent.[33] The observed trend in THF could be due to copolymer-like thermal diffusion behavior. As polymer D_T is based on polymer−solvent interactions at the interface, copolymer D_T will be a combination of the behavior of both blocks.[34] The presence of the silyl and ester groups present two distinct chemistries at the polymer−solvent interface. The D_T in THF decreases as the ratio of terminal silyl-groups to dendritic ester groups at the solvent interface increases. Conversely, a copolymer in a selective solvent for one of the blocks exhibits D_T behavior that is dominated by the solvated block.[35] In CH, polar ester sites are sequestered in the

DOI: 10.1021/acs.analchem.9b02664
Anal. Chem. 2019, 91, 12344−12351

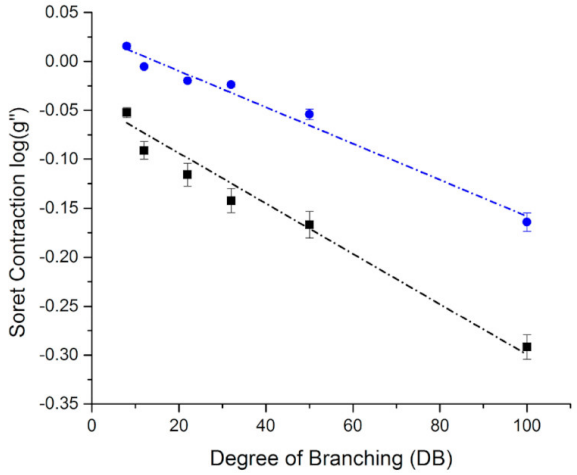

Figure 4. Dependence of Soret contraction (g'') on degree of branching in THF (blue) and CH (black).

polymer excluded volume with the silyl groups in the solvent accessible region. Therefore, the D_T of the polyesters in CH is driven by silyl−CH interactions at the interface. Thus, no trend in D_T with respect to DB is observed in CH. The absence of a trend in D_T with respect to DB prevents determination of branching based on thermal diffusion when using CH as a carrier fluid. Although D_T can readily differentiate SY-0 and SY-50 in THF, discerning the gradually branched (SY-8 to SY-32) from the linear SY-0 is difficult, as the error bars for these points do not show a significant difference.

A second method by which architecture information can be obtained is through the construction of conformation plots. The scaling of the polymers size with respect to the molar mass is expressed in eq 4:

$$R_h = kM^{\nu_h} \tag{4}$$

where R_h is the hydrodynamic radius, M is the molar mass, and k and ν_h are scaling parameters. In Figure 3a, fits for hydrodynamic radius (R_h) versus molar mass from online ThFFF-MALS-DLS for each of the SY samples are overlaid. Overlays of R_h vs M_w raw data can be seen in Figure S4. The linear SY-0 displays the highest slope with the hyperbranched SY-100 exhibiting the lowest slope. The other SY samples fits fall in an expected manner between these bounds. The slopes (ν_h) of these Figure 3 plots offer an indication of both, polymer architecture and the thermodynamic quality of the solvent system.[19] In Figure 3b, the slope of the conformation plots (ν_h) is seen to decrease with increased DB. Branched species therefore exhibit smaller changes in size with respect to changes in molar mass, suggestive of an increase in apparent density of the polymer with increased DB. A decrease in ν_h is indicative of the presence of long chain branching in the polymer.[36] Alternately, fits that are shifted to higher molar masses while maintaining similar slopes can reveal the presence of both short-chain branching[37] and changes in monomer functionality.[38] This trend is easily visualized as a decrease in the conformation plot intercept (k). This is illustrated by comparing SY-50 and SY-100 in Figure 3c. Although both samples exhibit similar ν_h values, the fit of SY-100 is shifted to higher molar masses and lower k value compared to SY-50 indicating additional "short chain" branching. This is expected as the SY-100 sample is produced via the addition of monomer to the statistically branched OH-50 sample producing terminal short chains at any of the remaining linear positions (see Scheme 1).

As mentioned above, ν_h also provides a means to describe solvent quality. In Figure 3b, the upper shaded region represents slope values for a linear random coil in a "good" solvent ($\nu_h \approx 0.6$) to theta solvent ($\nu_h \approx 0.5$), while the lower region represents more compact polymer conformations approaching the slope value for a hard sphere ($\nu_h \approx 0.33$). THF is believed to be a good solvent for both chemistries present in the SY polyesters, which is confirmed from the conformation slope of the linear SY-0 ($\nu_h = 0.59 \pm 0.01$). Solvent quality was also investigated via measurement of the second virial coefficient (A_2) from MALS (data not shown) and SANS which was positive in both solvents, with A_2 in THF being greater than in CH.[20,39] Because of poor light scattering in CH, a comparative conformation analysis was not possible with MALS online. Although the construction of conformation plots yields useful complementary information about the polymer architecture, it does not provide a quantitative method for distinguishing the degree of branching for hyperbranched (SY-50) and pseudodendrimer species (SY-100).

We are therefore introducing a third method to extract architecture information from ThFFF retention data. Treatment of ThFFF data to create Soret contraction relations is possible if the S_T of a compositionally analogous linear polymer can be determined either theoretically or via experiment. In the initial work on Soret contraction,[25] a predictive model of thermal diffusion developed by Mes et al.[40] was used to calculate the Soret coefficient of a linear polymer (polystyrene and polyacrylates) at any molar mass. This enabled determination of architecture from g'' without the

Table 2. Summary of Hydrodynamic Radius and Translational and Thermal Diffusion Coefficients[a]

	tetrahydrofuran			cyclohexane		
sample	R_h (nm)	$D \times 10^{-7}$ (cm^2 s^{-1})	$D_T \times 10^{-8}$ (cm^2 K^{-1} s^{-1})	R_h (nm)	$D \times 10^{-7}$ (cm^2 s^{-1})	$D_T \times 10^{-8}$ (cm^2 K^{-1} s^{-1})
SY-0	6.9 ± 0.1	7.9 ± 0.2	13.2 ± 0.3	4.9 ± 0.2	6.5 ± 0.2	7.3 ± 0.2
SY-8	5.5 ± 0.1	10.1 ± 0.1	12.8 ± 0.2	5.5 ± 0.2	5.7 ± 0.2	6.2 ± 0.2
SY-12	6.8 ± 0.4	8.1 ± 0.3	11.7 ± 0.5	5.9 ± 0.2	5.3 ± 0.2	6.3 ± 0.2
SY-22	6.5 ± 0.1	8.4 ± 0.3	11.8 ± 0.4	5.0 ± 0.3	6.2 ± 0.3	7.8 ± 0.4
SY-32	5.3 ± 0.1	10.6 ± 0.1	12.2 ± 0.1	4.3 ± 0.1	7.5 ± 0.3	7.8 ± 0.3
SY-50	5.4 ± 0.1	10.3 ± 0.2	10.8 ± 0.3	4.1 ± 0.1	7.9 ± 0.2	7.3 ± 0.1
SY-100	7.4 ± 0.2	7.4 ± 0.1	9.8 ± 0.2	5.4 ± 0.1	5.9 ± 0.1	7.1 ± 0.2

[a]Uncertainties represent one standard deviation (instrumental).

DOI: 10.1021/acs.analchem.9b02664
Anal. Chem. 2019, 91, 12344−12351

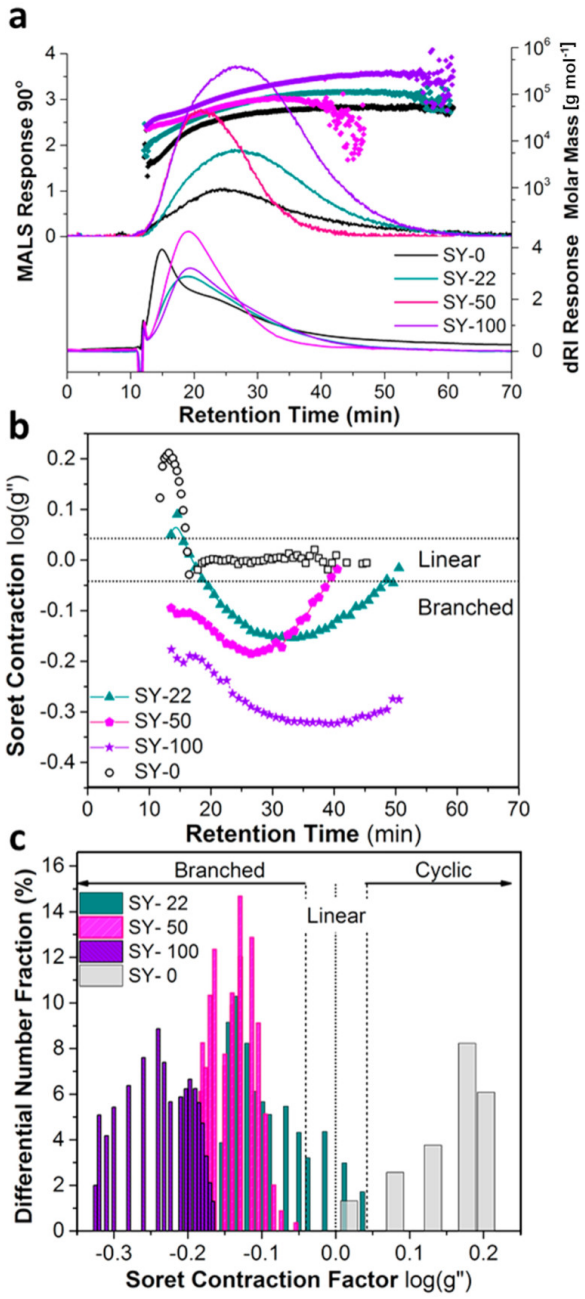

Figure 5. (a) Fractograms of linear SY-0 (black), SY-22 (green), SY-50 (pink), and SY-100 (purple) in CH. MALS and molar mass (top) overlaid with dRI signal (bottom). (b) Overlay of log (g'') calculated at 1 min intervals. (c) Distribution of g'' within each sample. For parts b and c, the linear region (log (g'') = 0 is bounded by dotted lines based on error of fit from Figure S4.

need to experimentally measure a linear analogue. This method is effective for common polymers, where tables of solution properties are readily available. For novel polymers, the temperature dependence of solubility and interaction parameters in the necessary solvents systems would need to be determined. Alternatively, a linear analogue can be used if one exists. Ideally a linear analogue with the equivalent M_w of each DB sample would be analyzed when calculating g''. If this is not possible, the ThFFF can be calibrated with either a series of narrowly distributed M_w of linear standards or a single high dispersity standard.[41] In this work, the chemically analogous linear polyester (SY-0) was used for this purpose. The resulting calibration plot of S_T versus molecular weight is shown in Figure S5b. Values of g'' are then calculated according to eq 2 using M_w equivalent $S_{T\ Linear}$ values from the calibration plot and average values of $S_{T\ Branched}$ from the retention times of the peak maximum in Figure 1a−g. The relation of Soret contraction g'' and DB in both CH and THF is shown in Figure 4. This relation enables the construction of architecture-based calibration curves. The magnitude of contraction is higher in CH than in THF, and this translates to the difference in R_h as seen by DLS (Table 2). The sensitivity of the g'' calibration is greater in CH than in THF by ∼30%. The lower sensitivity in THF can be attributed to the inverse relation of DB and D_T shown in Figure 2. The relation of DB to log(g'') provides a metric to determine the distribution of DB within a polymer sample based on ThFFF retention time. Fractograms of SY-0, -22, -50, and -100 in cyclohexane are shown in Figure 5a. Soret contraction factors are calculated from M_w and $S_{T\ Branched}$ as a continuous function of retention time, following the same process for calculating the average g'' in Figure 3. This is shown in Figure 5b where the SY-0 linear region is bounded by the dotted lines and the branched samples falling below (in the region where log(g'') is negative). Within a sample, the higher DB subpopulations are expected to elute earlier while the more "linear-like" polymers elute at higher retention times. This is indeed observed for the SY-22 and SY-50 (Figure 5b), which showed an initial decrease in g'' followed by an increase toward the linear region. Using the dRI (Figure 5a) to determine the concentration of each g'' subpopulation (Figure 5b) within a sample, a corresponding differential distribution can be constructed. The three branched samples SY-22, -50, -100 exhibited different amounts of dispersity with respect to g'' and thus to DB. Figure 5c shows three distinct regions where (i) log(g'') < 0 represents polymers in a "contracted" state with lower S_T when compared to a linear polymer of analogous molecular weight; (ii) log(g'') ≅ 0 ± 0.04 signifies the presence of linear polymers; and (iii) a region with positive log(g'') values, discussed below.

Interestingly, the linear polyester SY-0 showed the presence of a low M_w subpopulation eluting at ∼14 min (Figure 5a). This subpopulation exhibited a Soret contraction factor above unity (Figure 5b), which means it is more retained than the M_w equivalent linear polymer. A low M_w subpopulation was also noted in SEC-MALS of the as-synthesized samples (Figure S6) and was identified as 2−5 kDa cyclic polyesters by MALDI-TOF MS.[28] The low M_w subpopulation in SY-0 was collected as it eluted from ThFFF and further analyzed by MALDI-TOF MS (Figure S8). The presence of subpopulations with positive log(g'') were also identified in both the SY-8 and SY-12 samples. These subpopulations were also collected for analysis by MALDI-TOF and confirmed the presence of cyclic polyester (Figure S8a,b). The Soret contraction methodology suggests the presence of a different architecture, e.g., the cyclic subpopulation, (Figure 5) as compared to SEC (Figure S6) that only indicates the presence of a low-molecular weight population. The Soret contraction ($g'' > 1$) for cyclic polymers is in opposition to traditional g-values from light scattering which have contracted conformations ($g \cong 0.5$).[42] We hypothesize that these cyclic oligomeric species exhibit

DOI: 10.1021/acs.analchem.9b02664
Anal. Chem. 2019, 91, 12344−12351

different thermal diffusion than the corresponding linear species leading to higher retention than expected at this molecular weight. This first report of the thermal diffusion behavior of cyclic polymers is an exciting development and could lead to advancements in their analyses, particularly in mixtures.

CONCLUSIONS

An innovative approach founded in Soret contraction factors derived from ThFFF retention times is shown to provide insights into distributions in the degree of branching in complex random and statistical branched polymer systems. This analysis was possible despite separations based on size and composition (as evidenced by MALS M_w measurements and changes in D_T as a function of retention time when THF was used as the separation solvent). Aromatic-aliphatic polyesters with controlled DB of 100, 50, 32, 22, 12, 8, and 0% were used as a model system. The extension of the Soret contraction to statistically and randomly branched systems showed that $\log(g'')$ is linearly correlated to the degree of branching enabling identification of the average polymer DB as well as online determination of architecture distributions. Care must be taken when using this method for copolymers and functionalized polymers as the solvent quality may influence the selectivity of the architecture calibration. The unexpected enhanced retention of cyclic subpopulations requires further study; their distinct thermophoretic behavior opens a new avenue of analysis for these difficult polymeric species.

ASSOCIATED CONTENT

Supporting Information

The Supporting Information is available free of charge on the ACS Publications website at DOI: 10.1021/acs.analchem.9b02664.

Increment of refraction (dn/dc) determination, temperature-programmed dynamic light scattering, R_h versus M_w conformation plots data and fits, molecular weight versus Soret calibration using ThFFF-MALS, polyester room temperature SEC, isolation and characterization of cyclic polyester subpopulations, and thermal FFF multiangle light scattering overlays (PDF)

AUTHOR INFORMATION

Corresponding Author

*E-mail: krwillia@mines.edu.

ORCID

Albena Lederer: 0000-0002-1760-6426

S. Kim Ratanathanawongs Williams: 0000-0003-3894-478X

Notes

The authors declare no competing financial interest.

ACKNOWLEDGMENTS

This material is based upon work primarily supported by the National Science Foundation (NSF) under NSF Awards CHE-150882 and CHE-1808805 (W.C.S. and S.K.R.W.). We also acknowledge a Fulbright Award (S.K.R.W.) and the German Research Foundation (DFG) as part of Project LE1424/7 (M.G. and A.L.). Christina Harnisch is gratefully acknowledged for SEC measurements and Dr. Anna Sharmak for the synthesis of the polyesters. Any opinions, findings and conclusions, or recommendations expressed in this material are those of the author(s) and do not necessarily reflect those of the NSF.

REFERENCES

(1) Voit, B.; Komber, H.; Lederer, A. Hyperbranched Polymers: Synthesis and Characterization Aspects. In *Materials Science and Technology*; Wiley-VCH Verlag GmbH & Co. KGaA: Weinheim, Germany, 2012; p 701, .

(2) Khalyavina, A.; Häußler, L.; Lederer, A. *Polymer* **2012**, *53* (5), 1049−1053.

(3) Zhu, X.; Zhou, Y.; Yan, D. *J. Polym. Sci., Part B: Polym. Phys.* **2011**, *49*, 1277−1286.

(4) McLeish, T. *Curr. Opin. Solid State Mater. Sci.* **1997**, *2* (6), 678−682.

(5) Podzimek, S.; Vlcek, T. *J. Appl. Polym. Sci.* **2001**, *82* (2), 454−460.

(6) Erber, M.; Boye, S.; Hartmann, T.; Voit, B. I.; Lederer, A. *J. Polym. Sci., Part A: Polym. Chem.* **2009**, *47* (19), 5158−5168.

(7) Hutchings, L. R. *Macromolecules* **2012**, *45* (14), 5621−5639.

(8) Lee, H. C.; Lee, H.; Lee, W.; Chang, T.; Roovers, J. *Macromolecules* **2000**, *33*, 8119−8121.

(9) Al Samman, M.; Radke, W. *Polymer* **2016**, *99*, 734−740.

(10) Al Samman, M.; Radke, W.; Khalyavina, A.; Lederer, A. *Macromolecules* **2010**, *43* (7), 3215−3220.

(11) Maniego, A. R.; Sutton, A. T.; Gaborieau, M.; Castignolles, P. *Macromolecules* **2017**, *50* (22), 9032−9041.

(12) Wood-Adams, P. M.; Dealy, J. M. *Macromolecules* **2000**, *33* (20), 7481−7488.

(13) Magnusson, H.; Malmström, E.; Hult, A.; Johansson, M. *Polymer* **2002**, *43* (2), 301−306.

(14) Hölter, D.; Burgath, A.; Frey, H. *Acta Polym.* **1997**, *48* (1), 30−35.

(15) Grcev, S.; Schoenmakers, P.; Iedema, P. *Polymer* **2004**, *45* (1), 39−48.

(16) Burchard, W.; Schmidt, M.; Stockmayer, W. H. *Macromolecules* **1980**, *13* (5), 1265−1272.

(17) Andersson, M.; Wittgren, B.; Wahlund, K.-G. *Anal. Chem.* **2003**, *75* (16), 4279−4291.

(18) Boye, S.; Ennen, F.; Scharfenberg, L.; Appelhans, D.; Nilsson, L.; Lederer, A. *Macromolecules* **2015**, *48* (13), 4607−4619.

(19) Burchard, W. Solution Properties of Branched Macromolecules. In *Branched Polymers II*; Roovers, J., Ed.; Springer Berlin Heidelberg: Berlin, Heidelberg, Germany, 1999; pp 113−194.

(20) Lederer, A.; Burchard, W.; Khalyavina, A.; Lindner, P.; Schweins, R. *Angew. Chem., Int. Ed.* **2013**, *52* (17), 4659−4663.

(21) Lederer, A.; Burchard, W.; Hartmann, T.; Haataja, J. S.; Houbenov, N.; Janke, A.; Friedel, P.; Schweins, R.; Lindner, P. *Angew. Chem., Int. Ed.* **2015**, *54* (43), 12578−12583.

(22) Radke, W.; Müller, A. H. E. *Macromolecules* **2005**, *38* (9), 3949−3690.

(23) Williams, S. K. R.; Smith, W. C.; Oliver, J. D.; Benincasa, M.-A. Field-Flow Fractionation in the Analysis of Polymers and Rubbers. In *Encyclopedia of Analytical Chemistry*; Meyers, R. A., Ed.; John Wiley & Sons, Ltd.: Chichester, U.K., 2016.

(24) Köhler, W.; Morozov, K. I. *J. Non-Equilib. Thermodyn.* **2016**, *41* (3), 151−197.

(25) Runyon, J. R. *Thermal Field-Flow Fractionation of Polymers with High Molecular Weight and Complex Architectures*. Ph.D. Thesis, Colorado School of Mines, Golden, CO, 2009.

(26) Ponyik, C. A. *Characterization of Complex Polymers of Poly(Styrene) and Poly(Acrylate) by Thermal Field-Flow Fractionation with Light Scattering and Other Detection*. Master Thesis, Colorado School of Mines, Golden, CO, 2016.

(27) Greyling, G.; Lederer, A.; Pasch, H. *Macromol. Chem. Phys.* **2018**, *219* (24), 1800417.

(28) Khalyavina, A.; Schallausky, F.; Komber, H.; Al Samman, M.; Radke, W.; Lederer, A. *Macromolecules* **2010**, *43* (7), 3268−3276.

(29) Lederer, A.; Hartmann, T.; Komber, H. *Macromol. Rapid Commun.* **2012**, *33* (17), 1440−1444.

DOI: 10.1021/acs.analchem.9b02664
Anal. Chem. 2019, 91, 12344−12351

(30) Caldwell, K. D.; Brimhall, S. L.; Gao, Y.; Giddings, J. C. *J. Appl. Polym. Sci.* **1988**, *36* (3), 703−719.
(31) *Field Flow Fractionation Handbook*, 1st ed.; Schimpf, M., Caldwell, K., Giddings, J., Eds.; John Wiley & Sons: New York, NY, 2000.
(32) Runyon, J. R.; Williams, S. K. R. *J. Chromatogr. A* **2011**, *1218*, 6774−6779.
(33) Schimpf, M. E.; Giddings, J. C. *Macromolecules* **1987**, *20* (7), 1561−1563.
(34) Schimpf, M. E.; Giddings, J. C. *J. Polym. Sci., Part B: Polym. Phys.* **1990**, *28* (13), 2673−2680.
(35) Morozov, K. I.; Köhler, W. *Langmuir* **2014**, *30* (22), 6571−6576.
(36) Yu, Y.; DesLauriers, P. J.; Rohlfing, D. C. *Polymer* **2005**, *46* (14), 5165−5182.
(37) Sun, T.; Brant, P.; Chance, R. R.; Graessley, W. W. *Macromolecules* **2001**, *34* (19), 6812−6820.
(38) Haidar Ahmad, I. A.; Striegel, A. M. *Anal. Bioanal. Chem.* **2011**, *399* (4), 1515−1521.
(39) Burchard, W.; Khalyavina, A.; Lindner, P.; Schweins, R.; Friedel, P.; Wiemann, M.; Lederer, A. *Macromolecules* **2012**, *45* (7), 3177−3187.
(40) Mes, E. P. C.; Kok, W. T.; Tijssen, R. *Int. J. Polym. Anal. Charact.* **2003**, *8* (2), 133−153.
(41) Nguyen, M. T.; Beckett, R. *Polym. Int.* **1993**, *30* (3), 337−343.
(42) Burchard, W. Theory of Cyclic Macromolecules. In *Cyclic Polymers*; Springer Netherlands: Dordrecht, The Netherlands, 1986; pp 43−84.

DOI: 10.1021/acs.analchem.9b02664
Anal. Chem. 2019, 91, 12344−12351

Supporting Information for:

Thermal field-flow fractionation for characterization of architecture in hyperbranched aromatic-aliphatic polyesters with controlled branching

William C. Smith,[†] Martin Geisler,[‡,§] Albena Lederer,[‡,§,] S. Kim Ratanathanawongs Williams,*[,†]

[†]Department of Chemistry, Colorado School of Mines, Golden, USA
[‡]Leibniz-Institut für Polymerforschung Dresden e.V., Germany
[§]School of Science, Faculty of Chemistry and Food Chemistry, Technische Universität Dresden, 01062 Dresden, Germany

Table of content for the supporting information:

1. Increment of Refraction (*dn/dc*) Determination S-2
2. Temperature Programmed Dynamic Light Scattering S-3
3. Online ThFFF-MAL-DLS (R_h versus M_w Conformation Plots Data and Fits) S-5
4. Molecular Weight versus Soret Calibration using ThFFF-MALS S-6
5. Polyester Room Temperature SEC S-7
6. Isolation and Characterization of Cyclic Polyester Subpopulations S-8
7. Thermal FFF Multiangle Light Scattering Overlays S-10
8. References S-11

1. Determination of Specific Refractive Index Increment for Polyester Samples

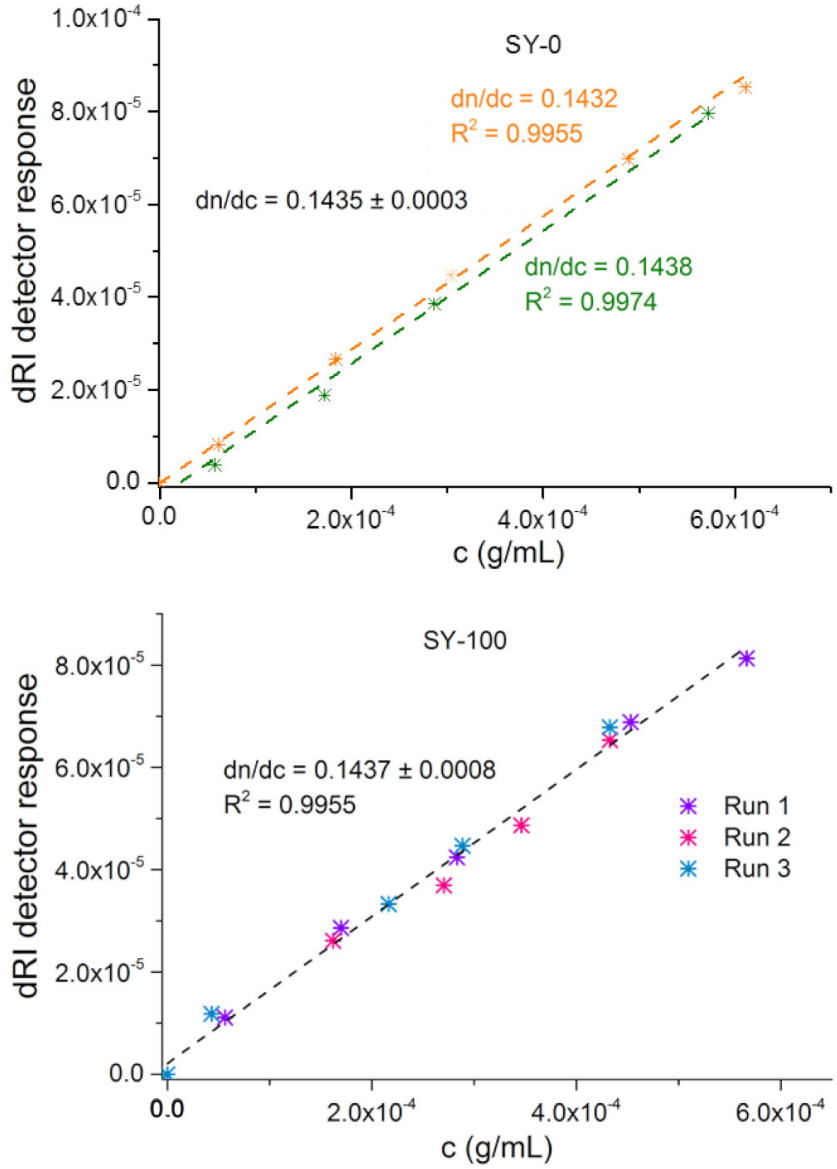

Figure S1. Representative data for determination of increments of refraction (*dn/dc*) for linear (SY-0) and pseudo-dendrimer (SY-100) polyester in cyclohexane. SY- 0 and SY-100 exhibit the same *dn/dc* within experimental error. The dn/dc is independent of branching for these aliphatic-aromatic polyesters. An average *dn/dc* value of 0.1435 mL/g was used in subsequent analyses in cyclohexane.

2. Temperature Programmed Batch-Mode Dynamic Light Scattering

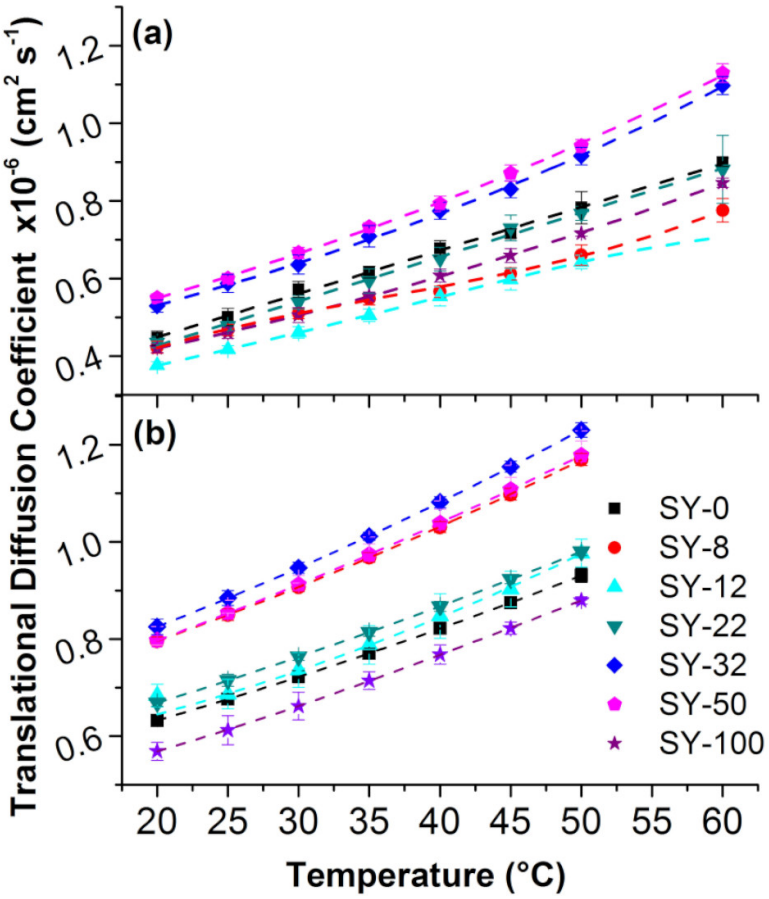

Figure S2. Translational diffusion coefficients versus temperature for all DB Polyester samples in a) cyclohexane and b) tetrahydrofuran. Regression lines have been added for ease in examining trends with respect to temperature. For the calculation of D_T from ThFFF experiments at high temperature ($\Delta T \geq 65$ K) the values of D used must be determined based on the temperature at the mean layer thickness (or height in the channel, 'l') from the average sample retention time (t_r). Values of D for all samples are listed in Tables 2. For all samples in both solvents, the temperature at the mean layer thickness was between 36 – 40 °C. Determining the temperature profile in the ThFFF channel is covered by Belgaied *et al.*[1] Mean layer thickness is related to t_r and void time t^0 via Equation (S1):

$$R = \frac{t^0}{t_r} = 6\lambda\{v + (1 - 6\lambda v)[\coth(1/2\lambda) - 2\lambda]\} \quad \text{(S1)}$$

where the retention parameter λ is a ratio between 'l' and the channel's thickness (w). The λ is also directly related to the physicochemical properties of the analyte based on the field driven transport (thermal diffusion 'D_T' in ThFFF), diffusional transport (D), and the magnitude of the field (temperature difference across the channel 'ΔT') as given by Equation (S2):

$$\lambda = (S_T \Delta T)^{-1} = \frac{D}{D_T \Delta T} \quad \text{(S2)}$$

Equation (S1) is an adjusted form of the generalized FFF retention equation. The factor (v) is used to correct for distortion of the parabolic flow based on the temperature dependence of the solvent viscosity. Values for v can be found in existing literature.[2]

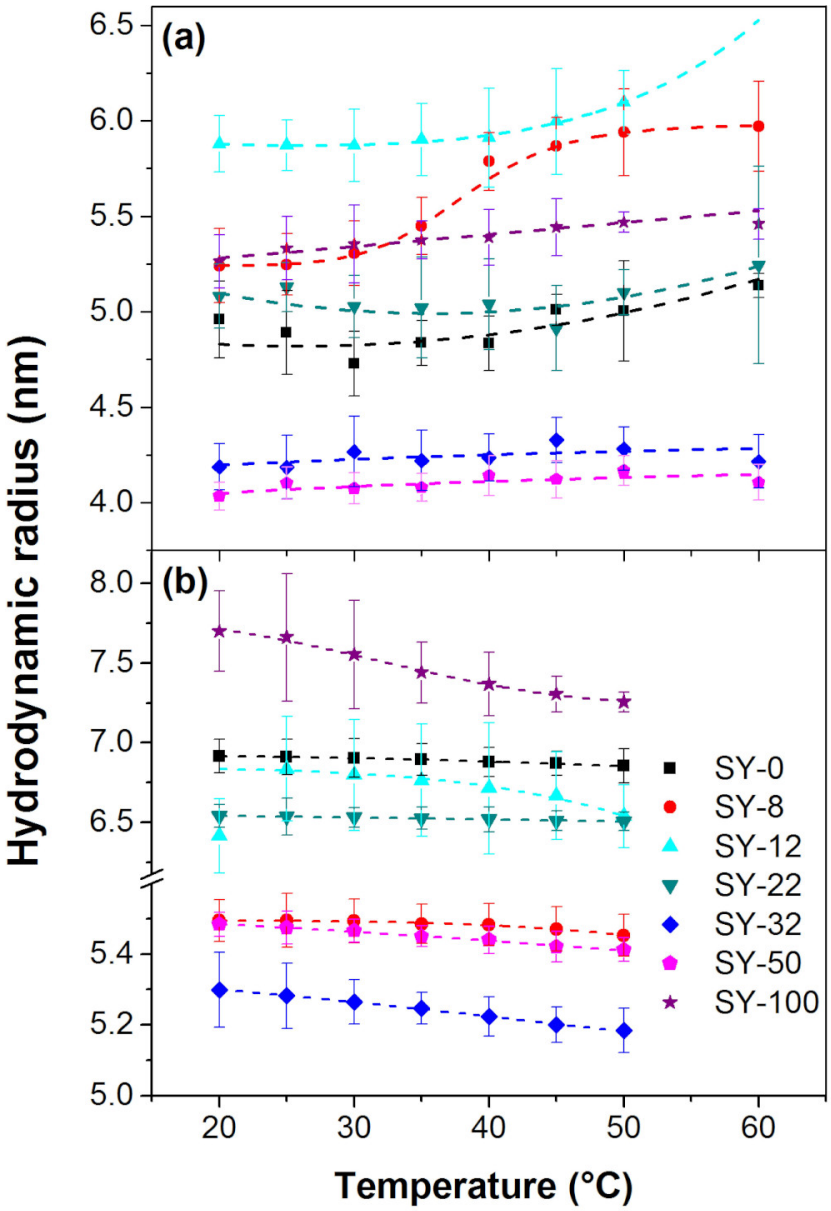

Figure S3. Temperature dependence of hydrodynamic radius (R_h) for all DB polyester samples in a) cyclohexane and b) tetrahydrofuran. Regression lines have been added for ease in examining trends with respect to temperature. Error bars represent measurement standard deviations.

3. R_h versus M_w Conformation Plots Data and Fits

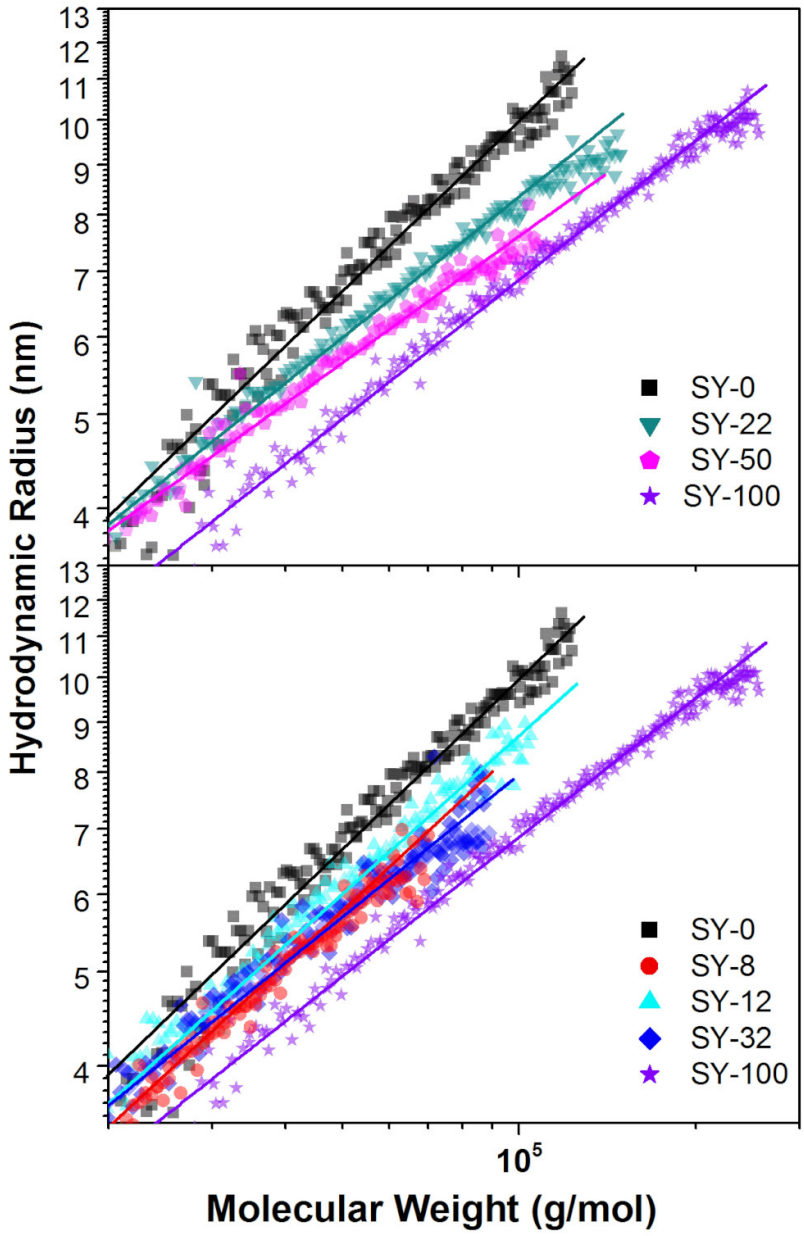

Figure S4. Conformation plots from ThFFF-DLS-MALS for all samples in THF. The allometric fits (solid lines) are overlaid on R_h and M_w (symbols) from DLS and MALS. Scaling parameter values can be found in Figure 3b and c.

Fractionation was performed using a TF2000 model ThFFF channel (Postnova Analytics, Salt Lake City, UT, USA) coupled online to a Dawn Heleos II multiangle light scattering (MALS)-dynamic light scattering (DLS) detector (Wyatt Technology Corporation, Santa Barbara, CA, USA), and an Optilab T-rEX differential refractive index detector (Wyatt Technology Corporation, Santa Barbara, CA). The ThFFF channel was made from a 127 µm polyimide spacer with a ribbon-like section removed that was 2.0 cm in breadth and 45.6 cm in length from inlet to outlet. The carrier liquid was tetrahydrofuran (THF) pumped through the channel at 0.2 mL/min. A 20 µL sample loop was used to introduce the sample into the channel. For all experiments, the cold wall, MALS-DLS, and dRI flow cells were maintained at 30 ± 1 °C. DLS data was collected with 2 second acquisition times.

4. Soret Coefficient versus Molecular Weight Calibration using ThFFF-MALS

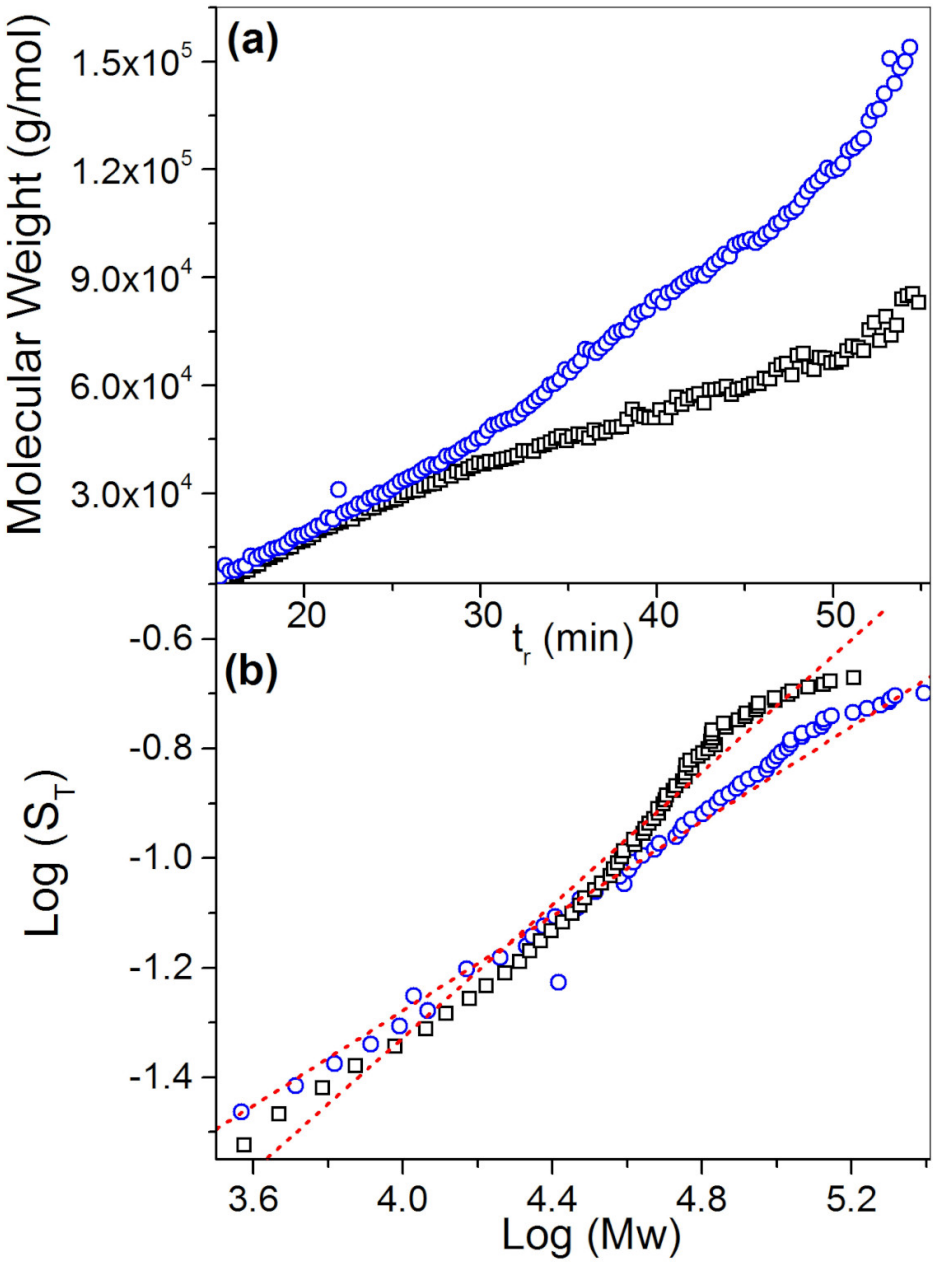

Figure S5. a) Molecular weight versus retention time for the linear SY-0 polyester in cyclohexane (black) and tetrahydrofuran (blue) at ΔT: ~100 °C and T_c: ~23 °C for both solvent systems. For the same retention time, *Mw* and S_T are higher in THF. However, at equivalent M_w both retention time and S_T are higher in cyclohexane. This indicates that the M_w-based selectivity is higher in cyclohexane than THF. b) Molecular weight calibration with the linear SY-0 polyester in cyclohexane (black) and tetrahydrofuran (blue) at ΔT: ~100 °C and T_c: ~23 °C for both solvent systems. Soret coefficients are calculated using Equation (S1)-(S2) and compared to M_w from MALS at the corresponding retention times. Correlation of log(M_w) and log(S_T) allows prediction of the Soret coefficient of a linear analogue for use in Equation (2) of the main article to produce *g"* values at a given measured molecular weight for each branched sample.

5. Polymer Size Exclusion Chromatography with MALS and dRI

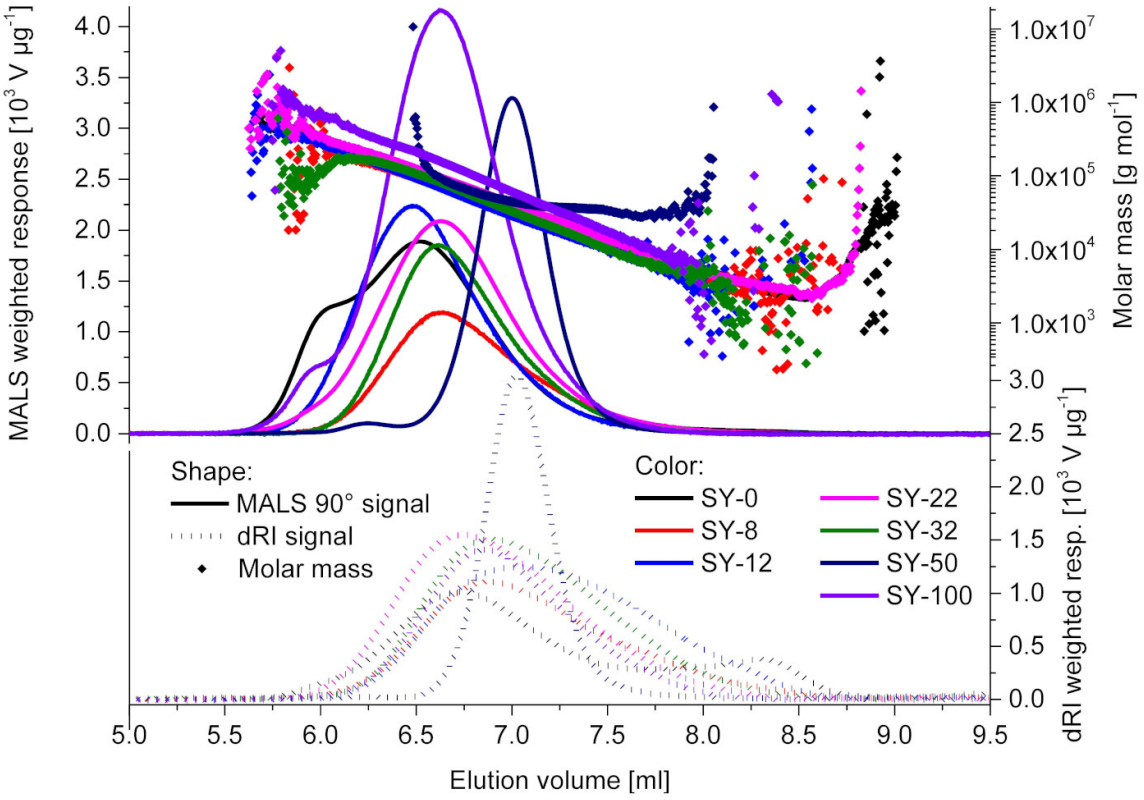

Figure S6. Overlay of SEC-MALS fractograms of linear (SY-0), gradually branched (SY-8, SY-12, SY-22, SY-32), hyperbranched (SY-50), and pseudodendrimeric (SY-100) polyesters from Figure 5 in the main article. Solid lines for MALS response and *Mw* (top half), dotted lines for dRI response (bottom half), both weighted by the detected mass. Presence of a low molecular weight subpopulation in the SY-0 can be seen at 8.3 mL.

The determination of the molecular weights given in Table 1 were performed by SEC-MALS using a flow rate of 1 mL/min. The SEC was equipped with an HPLC system (pump, degasser and manual control unit, Series 1200 by Agilent Technologies Inc., Santa Clara, CA, USA), a manual injection valve with a fixed injection volume of 53 µl, a PLgel 5 µm Mixed C chromatography column (300 mm × 7.5 mm, Agilent Technologies Inc.) and was coupled to a viscosity/differential refractive index (dRI) dual detector (ETA-2020, WGE Dr. Bures, Germany) and a multiangle laser light scattering detector (MALS) Tristar® miniDawn (Wyatt Technology Corporation, USA, $\lambda = 632$ nm). The carrier fluid was THF (Acros, Germany) and the analyte concentrations were about 1.5 to 2 mg/mL. All evaluations were done with the software ASTRA 4.9 and 6.1.2 (Wyatt Technology Corporation). The molecular weight calculations were done using the Zimm formalism and d*n*/d*c* values of 0.1550 mL/g as used previously.[3,4]

6. Isolation and Characterization of Cyclic Polyester Subpopulations

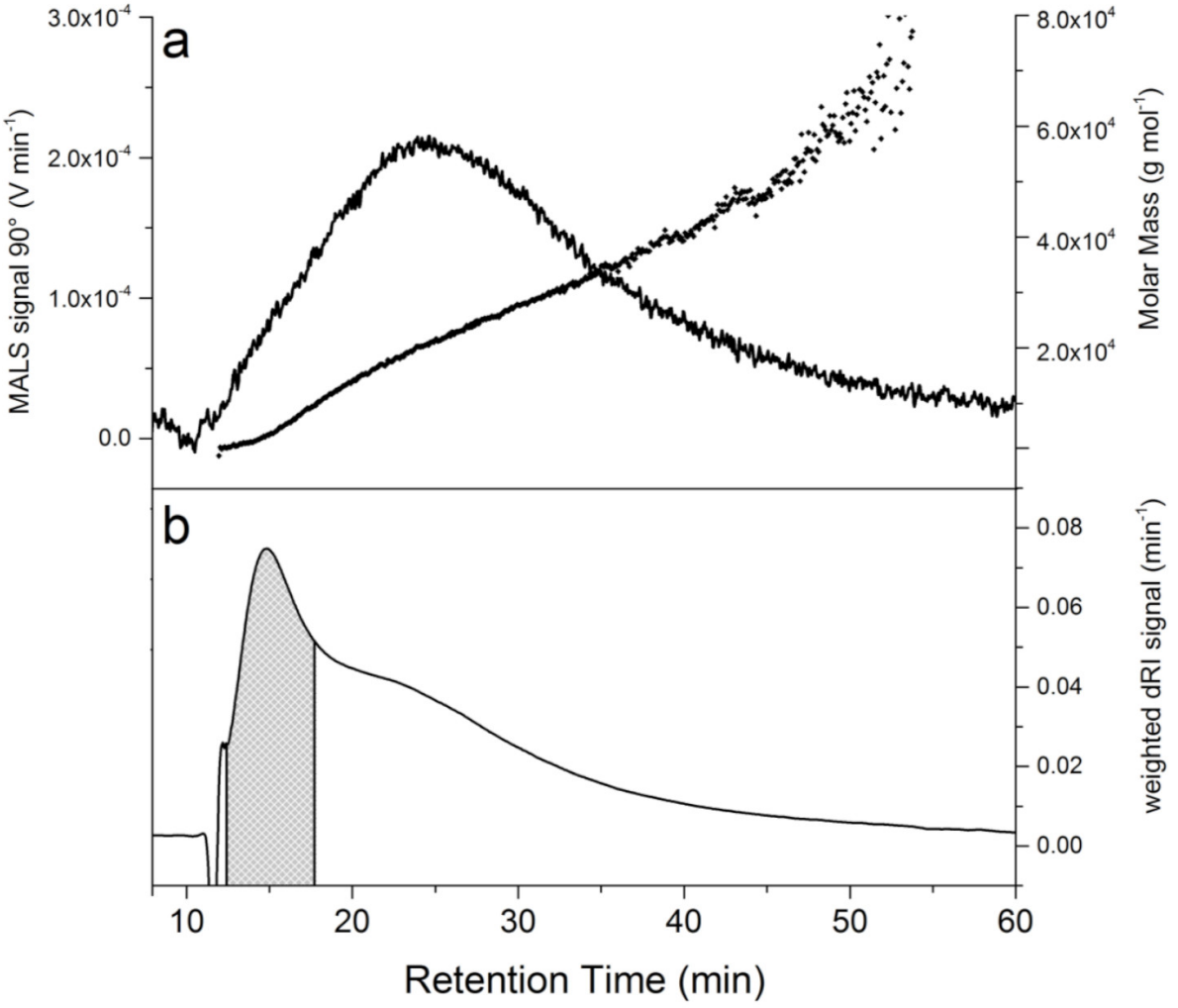

Figure S7. Fractogram of the linear SY-0 polyester in CH with a) MALS detector response and overlaid M_w and b) dRI response. Fraction collection interval from 12.5 to 17.5 minutes indicated by the shaded grey region.

Matrix assisted laser desorption time of flight mass spectrometry (MALDI-TOF-MS)

MALDI-TOF mass spectrometry is used to distinguish cyclized structures from their linear analogues.[5] Mass spectra were recorded using a Bruker UltrafleXtreme (Bruker Daltronics, Billerica, MA, USA) time-of-flight mass spectrometer. Low molecular weight fractions from SY-0 and SY-8 were prepared following a published method using dithranol as the matrix and lithium chloride as the cationization agent[3], a 2400 Da polystyrene (Polymer Source, Dorval, Quebec, Canada) was used for calibration. The irradiation was provided by a nitrogen pulse laser at 337 nm with the 'minimum' spot size, pulses at 1000 Hz and 80% power. The measurement conditions were as follows: reflectron-mode, positive polarity, 25 kV, detector gain at 10x, and pulsed ion extraction at 100 ns.

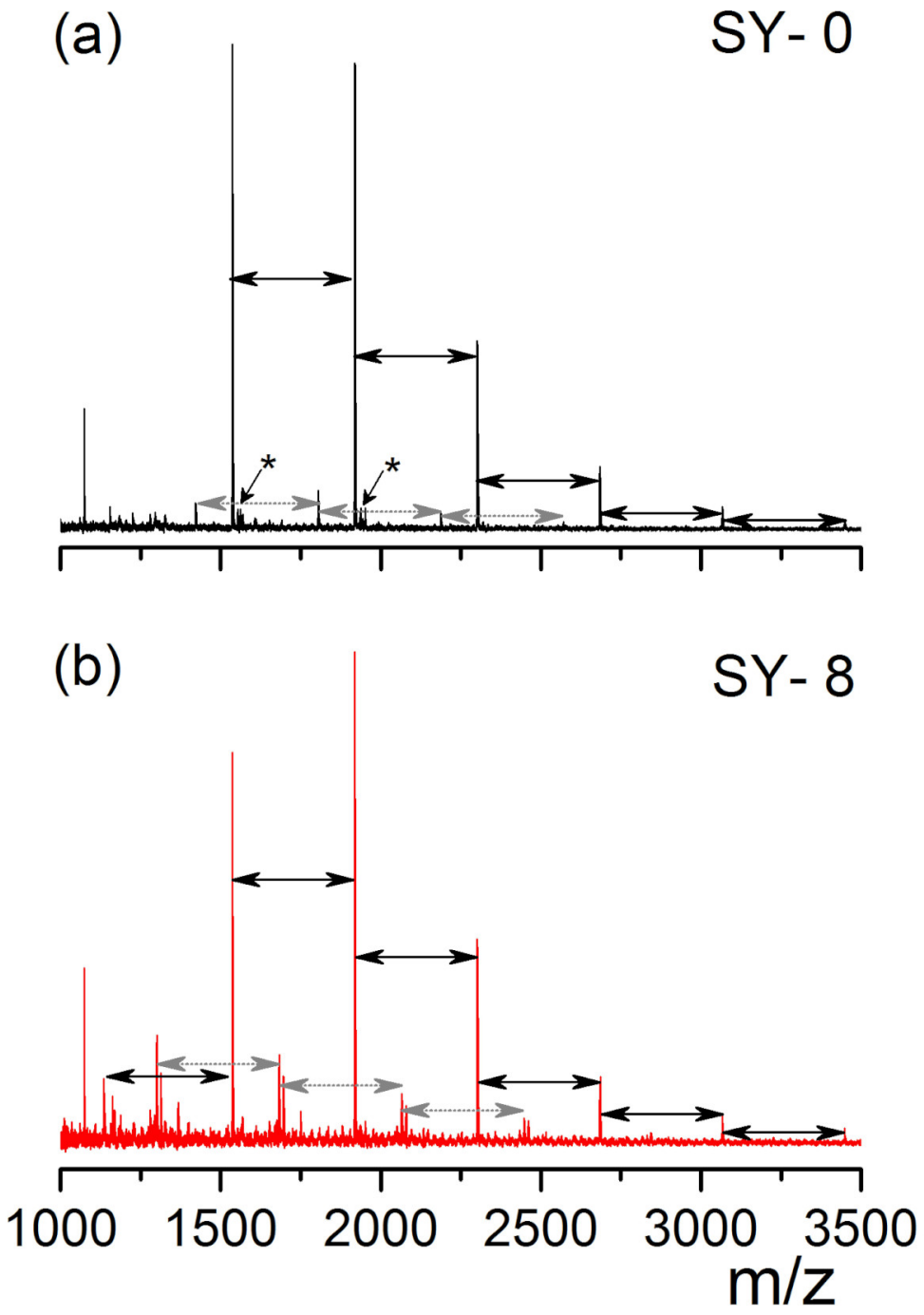

Figure S8. MALDI-TOF MS spectrum of a) SY-0 cyclic ThFFF fraction and b) SY-8 cyclic fractions collected according to the positive g" regions in Figure 5b. Spacing between peaks (indicated by dual arrows) represents the addition of single monomer units of 382.5 amu (arbitrary mass units). A low intensity population of with identical spacing (dual grey arrows) may be due to fragmentation during fly through the reflectron. The mass difference between the two populations is ~140 amu and may be due to loss of a tert-butyldimethylsilyl group.
* Indicates the presence of a linear analogue to the polymer cycle at 18 amu greater mass.

7. Thermal FFF with Multiangle Light Scattering Overlays

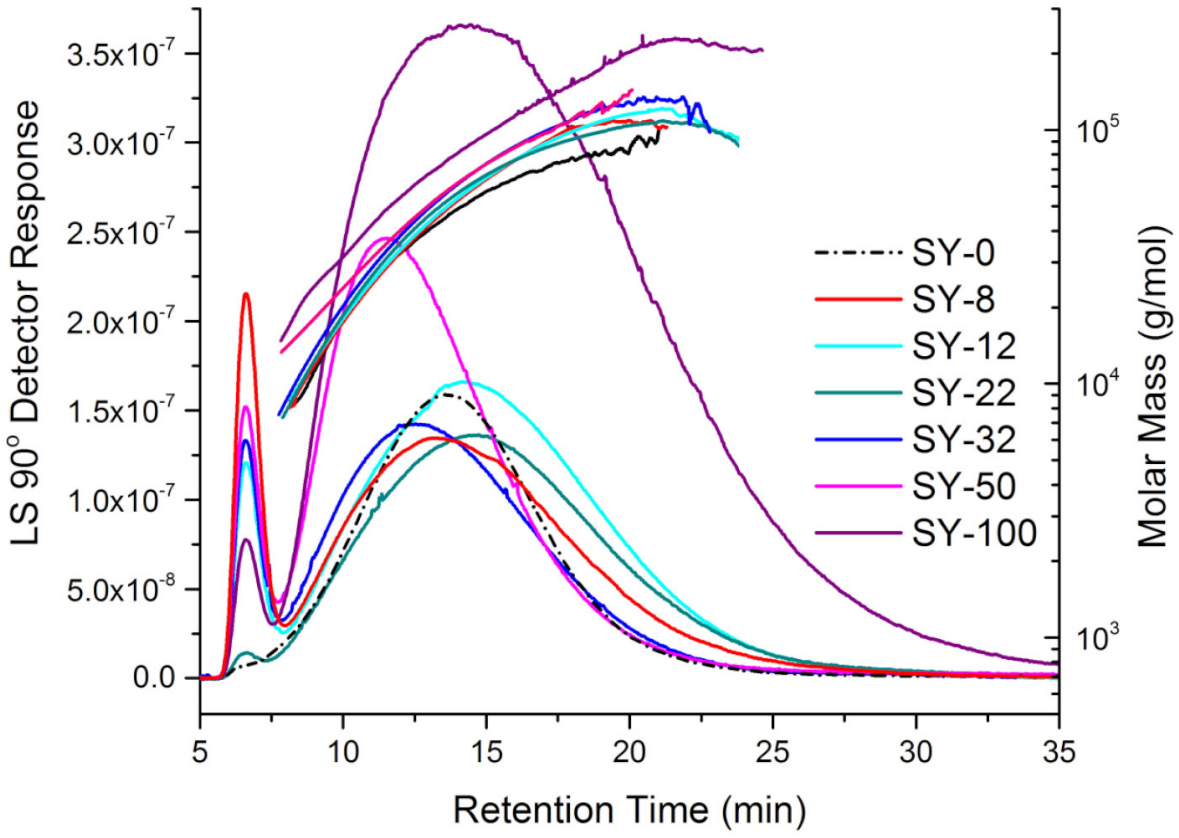

Figure S9. MALS fractograms with overlaid molar mass for all polyester samples in CH. Conditions: ΔT:100 °C, T_C: 30 °C; channel thickness 127 μm.

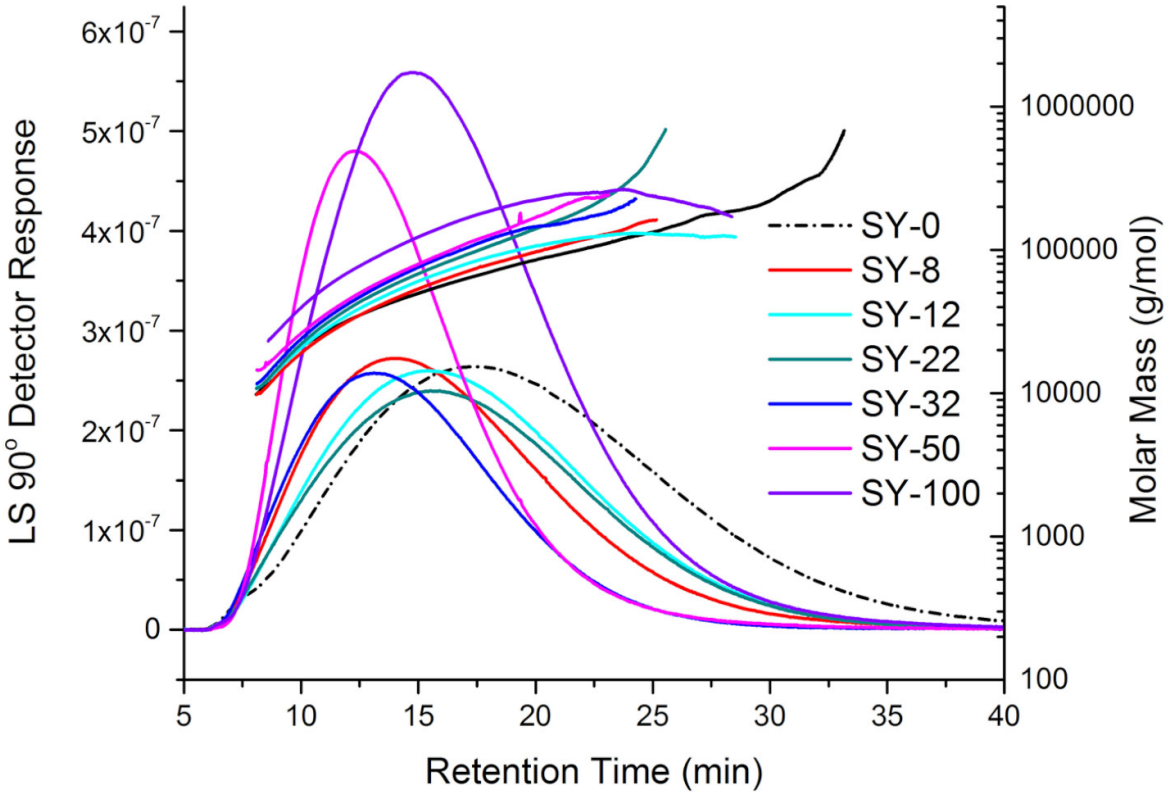

Figure S10. MALS fractograms with overlaid molar mass for all polyester samples in THF. Conditions: ΔT:100 °C, T_C: 30 °C, channel spacer 127 µm.

References:

(1) Belgaied, J. E.; Hoyos, M.; Martin, M. Velocity Profiles in Thermal Field-Flow Fractionation. *J. Chromatogr. A* **1994**, *678* (1), 85–96. https://doi.org/10.1016/0021-9673(94)87077-2.

(2) Gunderson, J. J.; Caldwell, K. D.; Giddings, J. C. Influence of Temperature Gradients on Velocity Profiles and Separation Parameters in Thermal Field-Flow Fractionation. *Sep. Sci. Technol.* **1984**, *19* (10), 667–683. https://doi.org/10.1080/01496398408060668.

(3) Khalyavina, A.; Schallausky, F.; Komber, H.; Al Samman, M.; Radke, W.; Lederer, A. Aromatic–Aliphatic Polyesters with Tailored Degree of Branching Based on AB/AB $_2$ and ABB*/AB $_2$ Monomers. *Macromolecules* **2010**, *43* (7), 3268–3276. https://doi.org/10.1021/ma100037n.

(4) Lederer, A.; Burchard, W.; Khalyavina, A.; Lindner, P.; Schweins, R. Is the Universal Law Valid for Branched Polymers? *Angew. Chemie Int. Ed.* **2013**, *52* (17), 4659–4663. https://doi.org/10.1002/anie.201209228.

(5) Sepulchre, M.; Sepulchre, M.-O.; Belleney, J. Aliphatic-Aromatic Hyperbranched Polyesters by Polycondensation of Potassium 3,5-Bis(Bromomethyl)Benzoate: Formation of Cyclic Structures. *Macromol. Chem. Phys.* **2003**, *204* (14), 1679–1705. https://doi.org/10.1002/macp.200350023.

8.4. Topology Analysis of Chain Walking Polymerized Polyethylene: An Alternative Approach for the Branching Characterization by Thermal FFF

Macromolecules

Article

Cite This: *Macromolecules* 2019, 52, 8662−8671

pubs.acs.org/Macromolecules

Topology Analysis of Chain Walking Polymerized Polyethylene: An Alternative Approach for the Branching Characterization by Thermal FFF

Martin Geisler,[†,‡] William C. Smith,[§] Laura Plüschke,[†,‡] Robert Mundil,[∥] Jan Merna,[∥] S. Kim Ratanathanawongs Williams,[§] and Albena Lederer*[,†,‡]

[†]Polymer Separation Group, Leibniz-Institut für Polymerforschung Dresden e. V., Hohe Str. 6, 01069 Dresden, Germany

[‡]Faculty of Chemistry and Food Chemistry, Technische Universität Dresden, 01062 Dresden, Germany

[§]Department of Chemistry, Colorado School of Mines, Golden, Colorado 80401, United States

[∥]Department of Polymers, University of Chemistry and Technology Prague, Technická 5, 166 28 Praha 6, Czech Republic

Supporting Information

ABSTRACT: Thermal field-flow fractionation (ThFFF) was designed to investigate the retention behavior of a series of dendritic polyethylenes synthesized using a chain walking catalyst (cwPE) with variations in the branching architecture. The retention behavior of these macromolecules correlates with their branching. Based on differences in the Soret coefficient, a new model has been developed for the application of ThFFF as an alternative to the branching calculation approach based on light scattering or viscosity for the branching analysis of novel short-chain branched PEs.

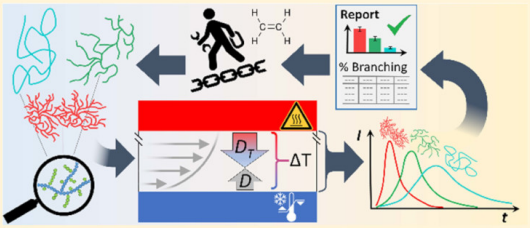

INTRODUCTION

Polyethylene (PE) represents a multibillion dollar industry[1,2] each year as a polymer widely used in multiple applications. Fine-tuning of the molar mass and molecular topology enables control over processing and mechanical properties. These optimized materials are nowadays readily accessible due to the progress in catalyst development since Ziegler−Natta in the 1950s.[3] However, an in-depth understanding of the molecular size and topology in relation to the bulk properties of the polymers still needs to be developed. The often semicrystalline structure of polyolefins requires an analysis at elevated temperatures to enable sufficient solubility.[4] This solution behavior is the reason for time-consuming analytical approaches for the characterization of molecular topology, for example, fractionation according to the crystallization of PE such as temperature rising elution fractionation[5] and crystallization analysis fractionation.[6] Currently, the established characterization method of polyolefins is high-temperature size exclusion chromatography (HT-SEC), most commonly performed in chlorinated aromatic solvents such as 1,2,4-trichlorobenzene (TCB)[7,8] or in its recently introduced green substitute butylal.[9] Coupled to absolute molar mass detection methods, like multiangle light scattering (MALS), online viscometry, and dynamic light scattering (DLS) with concentration detectors,[10] a comprehensive characterization of the molar mass and branching is possible. The branching analysis introduced by Zimm and Stockmayer[11] proposes the definition of a contraction factor g, as shown in eq 1[11]

$$g = \left(\frac{R_{G,BRA}^{\ 2}}{R_{G,LIN}^{\ 2}}\right)_M = \left[\left(\frac{[\eta]}{[\eta]_{LIN}}\right)_M\right]^{1/\varepsilon} \quad (1)$$

where R_G is the radius of gyration or mathematically the root-mean-square radius (RMS) of the branched polymer and $R_{G,LIN}$ is the RMS radius of a linear polymer chain of the same molar mass and chemical structure. An alternative definition for a contraction factor g' defined as the quotient of the intrinsic viscosities of the sample $[\eta]$ and the linear analogue $[\eta]_{LIN}$ has been introduced later,[12] in that the drainage exponent ε has been found to be dependent on the branching type.[13−15] g can be expressed as a function of the number of branches per molecule (B). For a randomly branched monodisperse trifunctional polymer, g (index 3 for trifunctional) is described as given in eq 2[11]

$$g_3 = \left[\left(1 + \frac{B}{7}\right)^{0.5} + \frac{4B}{9\pi}\right]^{-0.5} \quad (2)$$

Several parameters have been defined to enable an easy comparison between macromolecules of the same chemical origin, but different topologies. One parameter is the number of long-chain branches per 1000 monomers (LCB) as defined in eq 3

Received: July 8, 2019
Revised: September 19, 2019
Published: November 5, 2019

DOI: 10.1021/acs.macromol.9b01410
Macromolecules 2019, 52, 8662−8671

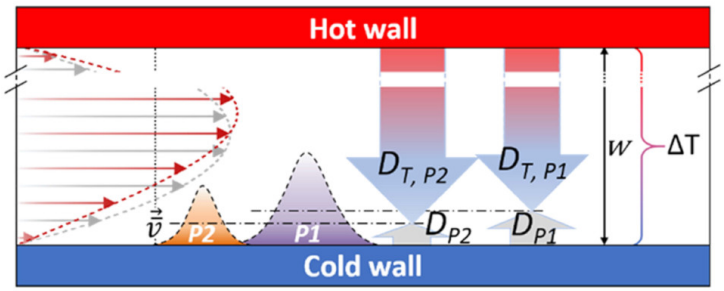

Figure 1. Schematic separation of two analytes *P*1 and *P*2 in the laminar flow of a thin ThFFF channel with thickness *w*, separated by a difference in their counteracting mass transports described by D_T and D in the separation force field ΔT. The flow profile in gray shows a laminar profile without field; the distorted flow profile with the applied field is shown in red.

$$\mathrm{LCB} = 1000 \times B \times \frac{M_{\mathrm{RU}}}{M} \tag{3}$$

where M is the molecule molar mass and M_{RU} is the molar mass of a repeat unit. In this work, a value of M_{RU} = 28.05 g mol^{-1} has been chosen for polyethylene referring to one ethylene monomer as the repeat unit within the polymer chain.

Additionally, the theoretical molar mass of a long-chain branch segment eq 4 can be used as an alternative branching expression of a polymer molecule

$$M_{\mathrm{Seg}} = \frac{M}{(B+2)+(B-1)} = \frac{M}{2B+1} \tag{4}$$

where the term $(B + 2)$ represents segments at a terminal position and $(B - 1)$ segments in between two branching points.[16,17] The number of branches B for the calculation of M_{Seg} in eq 4 is accessible by the transformation of eq 2.

The introduction of late transition metal catalysts opened a novel route for the synthesis of short-chain branched polyolefins via the chain walking mechanism with precisely defined macroscopic topologies.[18,19] These polyolefins have special local structural characteristics containing a constant amount of branches of about 50−60 per 1000 monomers. This specific structure defines the bulk and solution properties of these polymers.[20] However, the structure−property relationship of this entirely different polyethylene is not yet comprehensively understood. Nevertheless, it opens an opportunity to investigate alternative ways for the branching analysis due to their very low crystallinity or even amorphous structure and their good solubility in a variety of rather untypical PE solvents, such as cyclohexane (CHX), chloroform, and tetrahydrofuran (THF), even at low temperatures.[10,18,21,22] Furthermore, the absence of functionalities at the branch ends and the variation of branching[23,24] makes a straightforward investigation possible, based only on the branching architecture.

■ THERMAL FIELD-FLOW FRACTIONATION (THFFF)

In SEC, the separation is based on entropically driven diffusivity of the analytes and depends on their hydrodynamic volume.[25] However, SEC may become challenging if the samples are far beyond the separation range and if interactions with the column packing material or, typically for highly branched structures, anchoring effects may occur, which lead to a co-elution of linear and less-branched fractions with highly branched fractions of different hydrodynamic sizes.[26] Unlike SEC, field-flow fractionation (FFF) provides a variety of advantages for the separation of branched and hyperbranched structures due to the absence of a column packing material.[27] Depending on the FFF method, different separation mechanisms have been explored.[28] In all FFF techniques, the principle of the separation is based on a laminar flow through a thin ribbon-like channel. Perpendicular to the flow direction, a separation force field is applied, causing retention of an analyte due to its response to the field. This response induces mass transport, which is counterbalanced by the translational diffusion caused by the Brownian motion.[28]

In ThFFF, the separation force is provided by a temperature gradient between a heated and actively cooled wall of the channel. The basic separation principle is illustrated in Figure 1. The process describing the response of molecules or particles to a temperature gradient is called thermophoresis and has been described by Ludwig and Soret in the late 19th century.[29,30] A variety of different theoretical approaches have been developed to describe this phenomenon. However, thermal diffusion in liquids is sensitive to many different contributions, making an in-depth understanding still challenging.[31] For polymers in solution, the dependence of the thermophoretic mobility on the length of the Kuhn segment has been indicated recently.[32,33]

To express the strength of the response to the temperature field, the Soret coefficient S_T is defined as the ratio of the thermal diffusion coefficient D_T causing the accumulation of objects in solution/dispersion on either the hot (thermophilic) or the cold site (thermophobic) to the translational diffusion coefficient D caused by the Brownian motion. The dimensionless retention parameter λ in the FFF theory describes the ratio between the distance of the center of gravity of the analyte concentration distribution from the accumulation wall (mean layer thickness) and the channel thickness w for ThFFF and is defined in eq 6 by S_T and ΔT.

$$\lambda = \frac{1}{S_T \Delta T} = \frac{D_T}{D\,\Delta T} \tag{6}$$

With the parameters containing the field strength and the description of the analyte mass transport, the retention in ThFFF is then defined as given in eq 7

$$R = \frac{t_0}{t_R} = 6\lambda\left[\nu + (1 - 6\lambda\nu)\left(\coth\left(\frac{1}{2\lambda}\right) - 2\lambda\right)\right] \tag{7}$$

with R being the retention ratio, t_0 the void time describing the average flow time of the solvent or an unretained analyte, and t_R the retention time of a retained analyte. For careful work and in particular for less retained analytes, the general retention equation for ThFFF is modified by introducing a non-

DOI: 10.1021/acs.macromol.9b01410
Macromolecules 2019, 52, 8662−8671

Table 1. Summary of the Mean Results Obtained by HT-SEC−D4 and ThFFF (ΔT = 100.9 ± 0.7 K, τ = 10 min)[a]

	HT-SEC−D4					ThFFF				
	M_w/kg mol^{-1}	$Đ$	g_z	LCB$_w$	M_{Seg}/kg mol^{-1}	M_w /kg mol^{-1}	$Đ$	t_R/min	$S_T/10^1$ K^{-1}	$D_T/10^8$ cm^2 s^{-1} K^{-1}
hb1	230 ± 6	1.32	0.22 ± 0.01	18.8 ± 2.2	0.85 ± 0.04	205 ± 10	1.07	14.1 ± 0.7	0.32 ± 0.06	0.9 ± 0.2
hb2	161 ± 3	1.12	0.27 ± 0.01	14.3 ± 1.4	0.91 ± 0.05	166 ± 9	1.06	14.9 ± 0.9	0.37 ± 0.07	1.1 ± 0.2
b1	140 ± 3	1.02	0.55 ± 0.03	2.7 ± 0.3	4.35 ± 0.02	136 ± 7	1.06	30.2 ± 0.4	0.96 ± 0.08	2.2 ± 0.2
b2	136 ± 2	1.03	0.55 ± 0.01	3.2 ± 0.4	2.97 ± 0.21	131 ± 5	1.03	24.5 ± 0.1	0.77 ± 0.07	1.9 ± 0.2
sb	313 ± 9	1.08	0.49 ± 0.02	1.5 ± 0.1	8.61 ± 0.40	307 ± 16	1.08	39.2 ± 1.0	1.33 ± 0.11	2.1 ± 0.2
lin1	175 ± 1	1.06	0.53 ± 0.01	2.2 ± 0.1	6.36 ± 0.20	167 ± 11	1.04	36.8 ± 0.4	1.14 ± 0.11	2.3 ± 0.3
lin2	384 ± 7	1.11	0.54 ± 0.01	1.1 ± 0.4	17.5 ± 2.0	373 ± 14	1.07	56.6 ± 0.4	1.8 ± 0.2	2.5 ± 0.3

[a]All averages are calculated from n = 3; uncertainties represent overall deviation-inclusive systematic errors (see SI).

parabolicity factor ν describing the deformation of the flow profile depending on the field strength due to the changing viscosity of the carrier fluid eq 7.[34,35]

In contrast to the flow field-flow fractionation (FlFFF),[36−38] the separation of ThFFF is driven by thermophoresis and is mainly dependent on the chemical composition of analytes.[39] This dependence was already shown by Schimpf and Giddings using ThFFF[40] and by Köhler and Rauch by thermal diffusion-forced Rayleigh scattering (TDFRS) for polymers.[41] These properties depend only weakly on the size or molar mass and become even independent of them above a certain size.[41] Although thermal diffusion was assumed to be independent of the molar mass and branching,[42] in later reports, it was demonstrated that ThFFF can be used for the separation and analysis of differently branched polymers even if they are of the same size or molar mass.[43−46] However, due to the need of elevated temperatures, for polyolefins, only a few investigations with ThFFF have been performed in the past showing the potential of this method,[47,48] but without focusing on the influence of branching on the thermal diffusion behavior.

EXPERIMENTAL SECTION

Detailed information about the synthesis, the ThFFF instrumentation, and experimental conditions for ThFFF separations is given in the Supporting Information (SI).

RESULTS AND DISCUSSION

Characterization by HT-SEC−D4. Prior to the ThFFF experiments, the short-chain branched cwPE samples have been comprehensively analyzed by high-temperature size exclusion chromatography coupled to a fourfold detection system (HT-SEC−D4)[10] to obtain reliable molecular parameters and to validate the expected topology according to the conditions used for their synthesis. The results obtained by HT-SEC−D4 are summarized in Table 1. Molar mass calculations were carried out using a refractive index increment for PE in TCB at 150 °C of dn/dc^{-1} = −0.104 mL g^{-1} taken from the literature.[49,50] Due to the unavailability of an entirely soluble, absolutely linear sample without short-chain branches or an absolutely well-defined sample without any long-chain branches and to retain the comparability to previous works, well-established theoretical models with $R_{G,LIN}$ = 0.023 M$^{0.58}$ and $[\eta]_{G,LIN}$ = 0.053 M$^{0.70}$ have been used for the branching calculations.[10,51,52] The samples have been named according to their expected topology with hb for hyperbranched, b for branched, sb for slightly branched, and lin for rather linear structures.

The influence of the synthesis conditions on the molecular topology was confirmed by HT-SEC−D4 in this investigation. Thus, a low pressure leads to highly branched samples while a

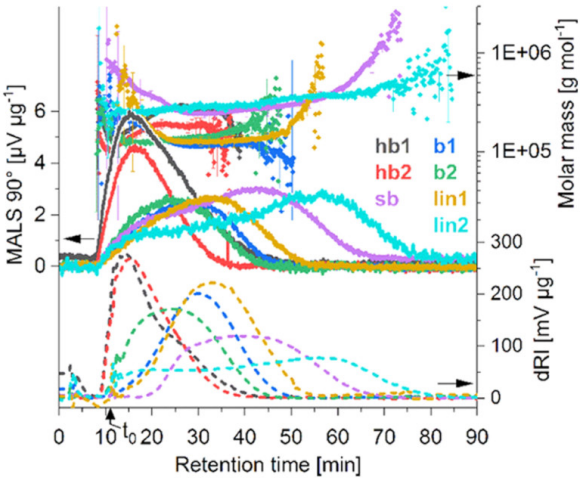

Figure 2. Superimposed fractograms of seven cwPEs with different topologies ranging from linear to dendritic, separated in a field of ΔT = 100.9 ± 0.7 K with a stop-flow of τ = 10 min. The temperature of the cold wall was kept at T_c = 23.0 ± 0.04 °C.

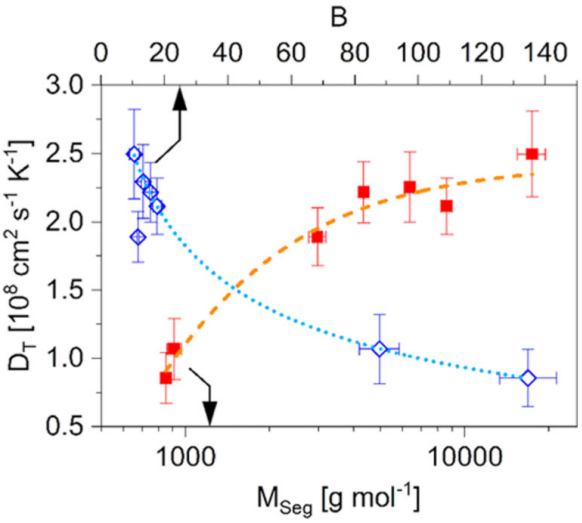

Figure 3. Dependence of D_T on the polymer topology: D_T vs B and vs M_{Seg}. B and M_{Seg} were calculated from HT-SEC−D4 data and temperature-dependent DLS data (measured in batch). The dotted and dashed red lines are for guiding the eye. The shown D_T are measured at ΔT = 100.9 K and τ = 10 min.

DOI: 10.1021/acs.macromol.9b01410
Macromolecules 2019, 52, 8662−8671

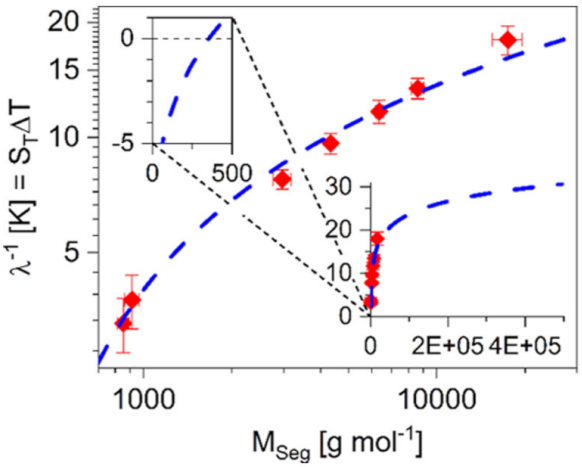

Figure 4. Double logarithmic plot of λ^{-1} against M_{Seg} from the data measured at ΔT = 100.9 K and τ = 10 min, fitted with a natural logarithmic function $y = a \ln(x) + b$. The inset shows the continuation of the fits to M_w, and the enlarged view of the inset indicates the trend toward negative S_T values for M_{Seg}, as shown previously for *n*-alkanes.[32]

Table 2. Branching Analysis Results Obtained by eqs 8−10 from ThFFF at ΔT = 100.9 ± 0.7 K and τ = 10 min and HT-SEC−D4 Weight Average g_w for Comparison with the g'' Estimated from ThFFF dRI Peak Apexes[a]

	ThFFF			HT-SEC−D4
	g''	$g = f(g'')$	LCB = $[g(g'')]$	g_w
hb1	0.11 ± 0.02	0.21 ± 0.03	18 ± 4	0.21 ± 0.01
hb2	0.13 ± 0.02	0.25 ± 0.04	17 ± 4	0.25 ± 0.01
b1	0.39 ± 0.03	0.50 ± 0.01	3.6 ± 0.5	0.50 ± 0.01
b2	0.30 ± 0.03	0.45 ± 0.01	4.4 ± 0.3	0.46 ± 0.02
sb	0.44 ± 0.04	0.52 ± 0.02	1.4 ± 0.2	0.48 ± 0.02
lin1	0.46 ± 0.04	0.54 ± 0.01	2.6 ± 0.3	0.53 ± 0.01
lin2	0.62 ± 0.07	0.57 ± 0.01	0.9 ± 0.1	0.57 ± 0.03

[a]See footnote of Table 1.

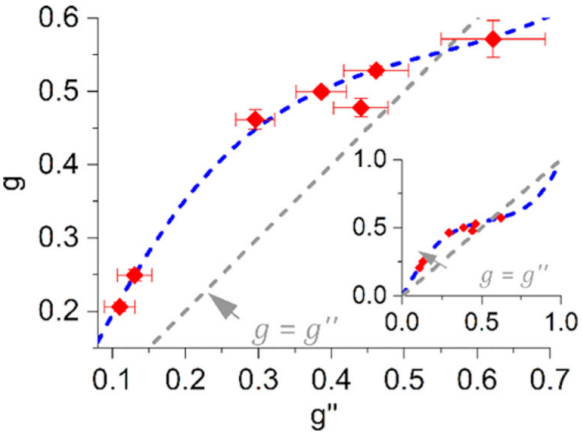

Figure 5. Comparison of g and g'' (data given in Table 2) and the fit to transform g'' into g for further calculations, shown for ΔT = 100.9 K and τ = 10 min. The inset shows the plot in the full scale within the limits of 0 and 1 for the fit in eq 10.

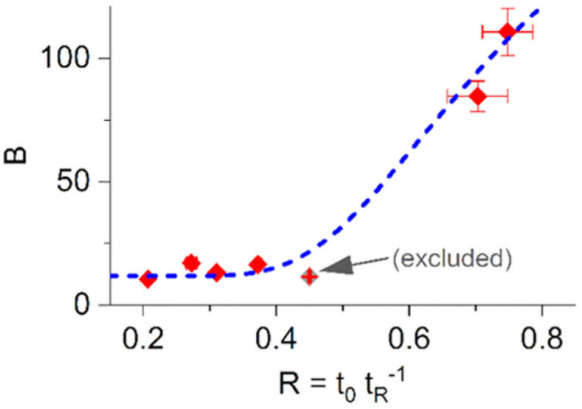

Figure 6. Dependence of $t_{R,\ dRI\ apex}$ on the number of branches per molecule B for ΔT = 100.9 K and τ = 10 min. The dashed lines indicate the fit by eq 13. The comparison of the data and fit parameters between the relaxed/unrelaxed systems and different field strengths is given in Figure S10, SI.

high pressure leads to almost entirely linear structures. Instead, higher reaction temperatures lead to generally higher molar masses than lower ones, but their influence on the resulting topology is not significant.[10,22,53] The chromatograms and detailed results of the branching analysis can be found in the SI.

Characterization by ThFFF. In our previous investigations, we successfully used THF as the carrier fluid in SEC under ambient conditions to characterize the molecular properties of the cwPE,[10,22] which needs much lesser technical effort than HT-SEC−D4. Therefore, our first attempt was to use THF as an eluent in ThFFF; however, under these conditions, no significant retention was observed even at increasing ΔT. Assumptions by the Hansen solubility theory using the solubility parameters of commercial PE indicated CHX as a thermodynamically good, nonhygroscopic solvent.[54] Retention experiments at two different isocratic ΔT values confirmed the suitability of CHX as a carrier liquid enabling reasonable retention for all PE samples, as shown in Figure 2. A significant difference in retention was observed depending on the molecular topology found by HT-SEC−D4. Furthermore, a dependence of the relaxation time on the length of the linear chain has been found indirectly (Figure S6, SI). For the presented differential refractive index (dRI) signals as the concentration source, a subtraction of separately recorded blank-baselines has been applied.

The narrow molar mass dispersity[55,56] $Đ = M_w M_n^{-1}$ of the samples allows for the investigation of the relation between the polymer topology and thermal diffusivity as a model system. Generally and in this work, the index n refers to the number-average, w to the weight-average, and z to the z-average moments of the regarded quantity.[55,57] The Soret coefficients S_T in Table 1 were calculated based on the mean retention times t_R's of the MALS and dRI peak apexes merged using a numerically derived polynomial solution given in the SI with respect to the distortion of the flow profile even for poorly retained analytes. The ΔT value used in the calculations is the cumulative average of the recorded $\Delta T(t_{R,i})$ from t_0 to the considered t_R. The given thermal diffusion coefficients D_T were calculated from S_T with translational diffusion coefficients D, which were determined at the corresponding mean layer

DOI: 10.1021/acs.macromol.9b01410
Macromolecules 2019, 52, 8662−8671

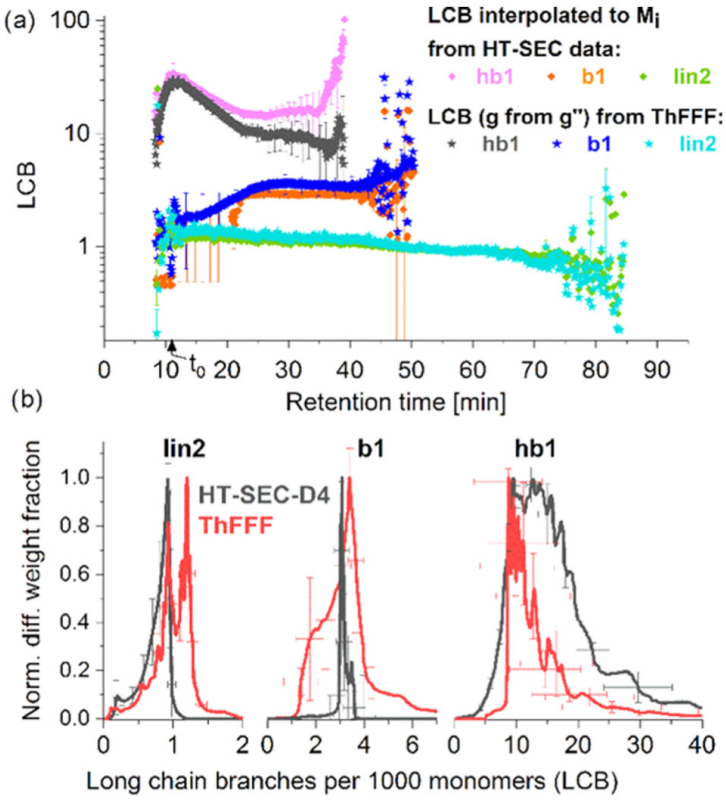

Figure 7. (a) Superimposed LCB$_i$ from the ThFFF data (shown for ΔT = 100.9 K and τ = 10 min) and LCB$_i$ from HT-SEC−D4, interpolated to M_i from the ThFFF experiments as a fractogram for three different topologies. (b) Normalized differential weight distributions of the ThFFF data given in (a), superimposed by the normalized differential weight distributions generated directly from the HT-SEC−D4 data.

temperature (calculated with the exact temperature profile as that reported in ref 35) of t_R by batch DLS experiments (DLS data are given in the SI). The molar masses, measured by MALS coupled to the ThFFF, were calculated with a $dndc^{-1}$ = 0.075 ± 0.002 mL g^{-1} for cwPE in CHX, measured in batch (see Figure S3, SI). The results obtained from the ThFFF separation, given in Figure 2 and summarized in Table 1, show for all polymer topologies a lower thermal diffusion compared to that of other polymers of a similar molar mass such as polystyrene (PS) in CHX,[43] but a retention behavior very similar to that of commercial PEs as obtained by high-temperature ThFFF investigations.[48]

At a first glance, no obvious relation between M_w and S_T or D_T could be found. However, a strong correlation of molecular parameters like the molar apparent density ρ_{app} and LCB$_w$ (from HT-SEC−D4) to S_T has been found (see Figures 3 and S7, SI). Furthermore, the dependence of D_T on M_{Seg} given in Figure 3b indicates the independence of the molar mass for large linear polymers, which is in agreement with Giddings et al.[42]

The same report also shows the lack of dependence of D_T on the branching,[42] which was also noted for a linear block and mikto-arm star copolymers pair of the same composition.[44,46] Both findings are in contradiction to our results. The dependence on branching, however, has instead been observed in other studies, for example, for linear and star PSs[43] and for dendritic polyesters.[45] It has been posited that this discrepancy in behavior may be driven by the thermodynamic quality of the solvent, similar to the nonideal scaling behavior in thermal diffusion observed for copolymers in selective solvents.[58]

We observe a significant influence of the polymer topology on the thermal diffusion behavior in our polymer−solvent system. The calculated thermal diffusion coefficients given in Table 1 directly correlate to the contraction factor g and the number of branches per molecule, calculated by eq 2 from HT-SEC−D4 data, respectively. The data shown in Figure 3c indicate the trend that D_T may become independent of the molar mass for larger linear segments. Furthermore, it also shows a clear dependence of the decreasing M_{Seg} with a trend toward decreasing D_T values, which would describe a thermophilic behavior for short linear segments. Both findings are in agreement with those of Köhler and Stadelmaier, who found a thermophilic behavior for *n*-alkanes and other mono-/oligomers in various solvents and a thermophobic behavior of their analogue polymers[32] by thermal-diffusion-forced Rayleigh scattering.[32,33,41,59] However, the trend of D_T for hydrocarbons to higher molar masses was not investigated due to the lack of polymers being readily soluble in the same solvent. It can be concluded that the thermal diffusion may be dependent on the effective size of a polymer segment where $M_{Seg} \ll M_w$.

Branching Analysis by ThFFF. The clearly found dependence of S_T and D_T on the polymer topology allows the development of a branching characterization approach by ThFFF. Similar to g and g', Runyon proposed the introduction of a Soret contraction factor g'',[46] defined as follows

DOI: 10.1021/acs.macromol.9b01410
Macromolecules 2019, 52, 8662−8671

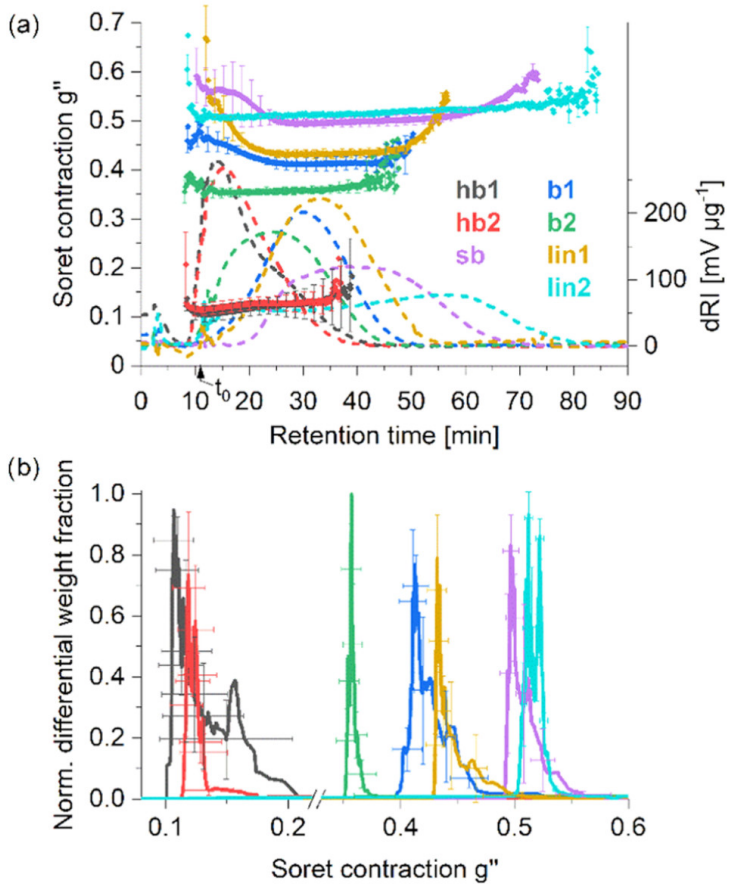

Figure 8. Superimposed generated data of g'' (a) as fractograms and (b) the derived normalized differential weight distributions for the fully relaxed system at a high field strength (ΔT = 100.9 K, τ = 10 min).

$$g'' = \left(\frac{S_{T,BRA}}{S_{T,LIN}}\right)_M \tag{8}$$

where $S_{T,BRA}$ is the Soret coefficient of the branched analyte and $S_{T,LIN}$ of the linear analogue with the same molar mass. For polymers with branching units, such as star-like structures or polymers consisting of an AB_2-type monomer,[60] a direct comparison with a linear analogue is applicable.[45] However, for cwPE, thermal diffusion properties of an entirely linear analogue soluble under the same conditions are not directly accessible. Furthermore, the previously used approach to calculate $S_{T,LIN}$ from a calibration of the molar mass versus retention time[61] of an almost linear sample in this case was not applicable due to the very narrow dispersity of the cwPE samples as a result of the synthesis conditions and the reaction mechanism.[22,53,62] Thus, a linear model has to be developed. Based on the observed direct dependence of S_T on the segmental molar mass (Figure S7d), a temperature-dependent model using the reciprocal of λ has been developed, as exemplarily shown in Figure 4 for the fully relaxed system, measured at a high field strength. The model parameters for the partially relaxed system without stop-flow (τ = 0 min) and for the fully relaxed system (τ = 10 min), measured at two different field strengths, are given in the SI. Due to deviation of the dRI data, the average retention time of the dRI and MALS peak apexes were used.

The fit parameters of λ^{-1} vs M_{Seg} were assumed to correspond to a linear dependence. Thus, a general model for the Soret coefficient of the linear analogue by extrapolation of M_{Seg} to M_w was developed, leading to a relation between $S_{T,LIN}$ and M_w, as given in eq 12.

$$S_{T,LIN} = \frac{(a_1 \cdot \Delta T + a_2) \cdot \ln M_w - (a_3 \cdot \Delta T + a_4)}{\Delta T} \tag{9}$$

The coefficients of eq 9 are given in Table S2 in the SI. According to the model described in eq 9, S_T reaches a plateau at a very high M_w and shows negative values in the oligomeric region of M_w, describing a thermophilic behavior. The tendency of S_T in the log (S_T) to log (M_w) plot to level-off for high molar masses has been described for PS in various solvents[63] over a wide range of M_w values,[64] but is less pronounced as we observed here. Consequently, it is considered to be dependent on the polymer−solvent system.

The obtained Soret contraction factors $g''(t_{R,dRI\ apex})$ summarized in Table 2 contain branching information analogous to the radius contraction factor determined by HT-SEC−D4. To calculate LCB from the ThFFF data as directly comparable to those from SEC-MALS, g'' needs to be transformed into g. As can be seen in Figure 5, g and g'' show a

DOI: 10.1021/acs.macromol.9b01410
Macromolecules 2019, 52, 8662−8671

correlation similar to the relation $g' = g^{\varepsilon}$. The concept with a single exponent could be also applied in $g'' = g^{\xi}$ by the introduction of a thermal drainage parameter ξ. The ξ from $g''(t_{R,dRI\ apex}) = (g_{HT\text{-}SEC-D4})^{\xi}$ yields values between 0.8 and 1.6, which is comparable to the typical range of ε between 0.5 and 1.5.[14] However, similar to ε, ξ seems to also depend on branching, which then would need to be described by a second independent variable related to branching, such as t_R or R. This may lead to a lower precision of the predicted g values due to the additional uncertainty contribution from the fit to the second variable. Therefore, a relation $g(g'')$ with only one variable has been developed, as described in eq 10. The transformation of g'' to g needs to fulfill the boundary condition of $g(g''= 1) = 1$. Thus, the fit of $g(g'')$ had to be realized by a more complex double Boltzmann fit.

$$g(g'') = K_1 + (K_2 - K_1)\left[\frac{K_3}{1 + 10^{(K_4 - g'')K_5}} + \frac{1 - K_3}{1 + 10^{(K_6 - g'')K_7}}\right] \quad (10)$$

The calculation of the values of the coefficient $K_x(\Delta T)$ is given in Tables S3−1 and S3−2 in the SI. The results found using eqs 8−10, summarized in Table 2 as average results from $t_{R,dRI\ apex}$, show a very good agreement between the calculated LCB$[g(g'')]$ and LCB$_w$ from HT-SEC−D4 as given in Table 1.

More information is expected to be gained by analyzing the entire ThFFF fractograms of the cwPE system. However, a determination of $S_{T,i}$ and g''_i for each slice at a certain retention time t_R or R was not directly accessible due to the unavailability of a sufficiently sensitive instrument to measure D online. This is also expected to be challenging due to the low $dndc^{-1}$ of the polymers to the solvent and the low analyte concentration. Furthermore, the reverse application of the ThFFF approach given in eq 7 does not include the broadening of the analyte peak and can only display a discrete S_T value, for example, at the peak apex. Therefore, an indirect way has been developed to calculate $g''_i(R)$ eq 11 by application of the concept for $S_{T,LIN}$ eq 9 with a calculated molar mass of a segment for each slice, $M_{Seg,i}(R)$.

$$g''_i(R) = \left[\frac{S_{T,BRA}(M_{Seg,i})}{S_{T,LIN}(M_i)}\right]_{M_i} \quad (11)$$

For well-retained analytes, the calculation of LCB$_i(R)$ (calculated from $g''_i(R)$) with $M_{Seg} = M_i(R)\ (2B_{apex} + 1)^{-1}$ according to eq 4 was found to be in good agreement with LCB$_i(M_i)$ determined by HT-SEC−D4, which were numerically interpolated to M_i measured in the ThFFF fractionations. Here, the number average of B found by SEC was accounted to be the main fraction of the analyte at the peak apex (B_{apex}). However, LCB$_i(R)$ of poorly retained analytes could not be sufficiently described with the original definition of M_{Seg}. By implementing an empirically found correction in the definition of $M_{Seg,i}(R)$ eq 12, a satisfactory calculation of LCB$_i(R)$ in the entire retention range was achieved, resembling the values of LCB$_i(M_i)$ from HT-SEC−D4 interpolated to M_i of the ThFFF fractograms. The detailed development of eq 12 is described in the SI.

$$M_{Seg,i}(R) = \frac{R_{apex} \cdot M_{apex} + (1 - R_{apex})M_i(R)}{\left(2 - \frac{R^2}{e^R}\right)B_{apex} + 1} \quad (12)$$

To enable the calculation of LCB$_i(R)$ also for unknown analytes, a substitution for B_{apex} is required. Analogous to the previously shown dependence of D_T on B in Figure 3, a fit of B directly to the average of R_{MALS} and R_{dRI} was performed.

The data of B_{apex} shown in Figure 6 were found to resemble LCB$_{i,\ ThFFF}(R)$ on LCB$_{i,\ HT\text{-}SEC-D4}(M_{i,\ ThFFF})$ in good accuracy after fitting by a five-parameter logistic function (see eq 13).

$$B_{apex}(R_{apex}) = K_1 + \frac{K_2 - K_1}{\left[1 + \left(\frac{K_3}{R}\right)^{K_4}\right]^{K_5}} \quad (13)$$

The values of the coefficient $K_x(\Delta T)$ of eq 13 for the partially relaxed and fully relaxed systems are given in Tables S4−1 and S4−2 in the SI.

The application of the concept for the branching analysis, given by eqs 9−13, on the recorded data in the ThFFF separations shown in Figure 2 with $M_i(t_R)$, ΔT, and the cold wall temperature T_c is able to generate "online" data for LCB in correlation to t_R and is in reasonably good agreement to the LCB data from HT-SEC−D4, interpolated to $M_{i,\ ThFFF}$, as indicated in Figure 7a. The comparison of the normalized differential weight distribution indicates a good performance of the concept to analyze LCB for cwPEs of a more linear topology and a reasonable performance for highly branched topologies of analytes with a narrow and slightly broader dispersity. It also takes into account the effect of band broadening in an indirect way. Due to the non-Gaussian shape of the fractogram peak especially for poorly retained analytes, a band-broadening correction as described earlier[65,66] was considered not to be applicable for all analytes of this system; therefore, a mathematical consideration of band broadening is beyond the scope of this work. Furthermore, the molar mass dispersities $Đ$ reported in Table 1 were found to be marginally narrower compared to those obtained by SEC since SEC is discussed in the literature to slightly overestimate narrowly dispersed polymers,[66−68] and this also indicates that the band broadening may not have negatively affected the analysis. An improvement of the concept by a deeper understanding of the relation found between g and g'' is believed to deliver results with a higher accuracy.

Based on the output for LCB$_{i,\ ThFFF}(t_R)$ being in good agreement with the interpolated data of the HT-SEC−D4 analysis as illustrated in Figure, the reliability of the predictive generation of online data in correlation to t_R was considered to be accurate enough for the fractogram and distribution analysis of g''. As illustrated in Figure 8, the Soret contraction factor g'' shown together with the fractograms could be displayed with respect to the dispersities of the analytes. The generation of online data by application of the developed solution given in eqs 11−13 was found to be certainly accurate for an online branching analysis of the cwPE samples as a model in this investigation. It is also able to generate sufficiently correct data for unknown samples, which have not been part of the fitting process in the model development (see Figure S16 and Table S6). However, for broadly distributed systems in terms of M_w and branching, only an online determination by a separate detection is believed to generate reliable data for a true online branching analysis. For that, the temperature dependence of D needs to be determined either by heating the detector flow cell to the expected mean layer temperature or by the calculation of D measured at a fixed temperature. If the analyte concentration is too low for a reliable measurement of D by online-DLS, an

DOI: 10.1021/acs.macromol.9b01410
Macromolecules 2019, 52, 8662−8671

indirect determination by online viscometry could be an alternative. However, a systematic error needs to be taken into account, because R_h and the viscometric radius R_η, both sphere-equivalent radii, may differ for various polymers and topologies.[10,69]

CONCLUSIONS

Based on a model system of seven PE samples with varied molecular architectures (topologies) being produced by chain walking catalysis, an alternative approach for a branching analysis by ThFFF coupled to MALS and dRI detection has been developed in the context of the recently proposed concept of the Soret contraction. For this, a model to predict S_T for linear analogues of the same M_w has been introduced. The evaluation of this approach, either based on the mean retention time or with the help of an indirect method for the analysis of fractograms of narrowly dispersed samples, was found to be in good agreement with the reference data determined by HT-SEC−D4, representing the established approach for the branching analysis of polyolefins in general. It is believed that the new approach generally holds for commercial PEs as well as for similar polymers soluble only at elevated temperatures. However, this may need re-evaluations of the relationship of S_T vs M_{Seg} and g vs g'', and additionally, the analysis of broadly dispersed samples requires an online detection of D.

ASSOCIATED CONTENT

Supporting Information

The Supporting Information is available free of charge on the ACS Publications website at DOI: 10.1021/acs.macromol.9b01410.

Experimental details; HT-SEC−D4 results; temperature-dependent DLS experiments in batch; ThFFF data from different ΔT and τ; numerical solution of eq 7 for λ; development of eq 12; and cumulative and differential weight distributions of LCB and g'' (PDF)

AUTHOR INFORMATION

Corresponding Author

*E-mail: lederer@ipfdd.de.

ORCID

S. Kim Ratanathanawongs Williams: 0000-0003-3894-478X

Albena Lederer: 0000-0002-1760-6426

Author Contributions

The manuscript was written through contributions of all authors. All authors have given approval to the final version of the manuscript.

Notes

The authors declare no competing financial interest.

ACKNOWLEDGMENTS

This work was supported by the Deutsche Forschungsgemeinschaft (DFG, German Research Foundation) [grant number DFG LE 1424/7], the Czech Science Foundation [15-15887J and 18-22059S], the National Science Foundation (NSF) [CHE-150882, CHE-1808805], and Fulbright (SKRW). We thank Petra Treppe and Christina Harnisch for their technical assistance.

REFERENCES

(1) Thayer, A. M. Metallocene Catalysts Initiate New Era In Polymer Synthesis. *Chem. Eng. News* **1995**, *73*, 15−20.

(2) Ittel, S. D.; Johnson, L. K.; Brookhart, M. Late-Metal Catalysts for Ethylene Homo- and Copolymerization. *Chem. Rev.* **2000**, *100*, 1169−1204.

(3) Knuuttila, H.; Lehtinen, A.; Nummila-Pakarinen, A. Advanced Polyethylene Technologies---Controlled Material Properties. In *Long Term Properties of Polyolefins*; Albertsson, A.-C., Ed.; Springer: Berlin, Heidelberg, 2004; pp 13−28.

(4) Macko, T.; Brüll, R.; Zhu, Y.; Wang, Y. A Review on the Development of Liquid Chromatography Systems for Polyolefins. *J. Sep. Sci.* **2010**, *33*, 3446−3454.

(5) Wild, L.; Glöckner, G. In*Temperature Rising Elution Fractionation BT - Separation Techniques Thermodynamics Liquid Crystal Polymers*; Springer: Berlin, Heidelberg, 1991; pp 1−47.

(6) Monrabal, B. Crystallization Analysis Fractionation: A New Technique for the Analysis of Branching Distribution in Polyolefins. *J. Appl. Polym. Sci.* **1994**, *52*, 491−499.

(7) Wild, L.; Guliana, R. Gel Permeation Chromatography of Polyethylene: Effect of Long-Chain Branching. *J. Polym. Sci., Part A-2.* **1967**, *5*, 1087−1101.

(8) Crouzet, P.; Fine, F.; Mangin, P. Comparaison Des Méthodes de Fractionnement Par Chromatographie de Perméation et Par Gradient d'elution Pour La Détermination Des Répartitions Moléculaires Des Polypropylénes. *J. Appl. Polym. Sci.* **1969**, *13*, 205−213.

(9) Boborodea, A.; Collignon, F.; Brookes, A. Characterization of Polyethylene in Dibutoxymethane by High-Temperature Gel Permeation Chromatography with Triple Detection. *Int. J. Polym. Anal. Charact.* **2015**, *20*, 316−322.

(10) Plüschke, L.; Mundil, R.; Sokolohorskyj, A.; Merna, J.; Sommer, J.-U.; Lederer, A. High Temperature Quadruple-Detector Size Exclusion Chromatography for Topological Characterization of Polyethylene. *Anal. Chem.* **2018**, *90*, 6178−6186.

(11) Zimm, B. H.; Stockmayer, W. H. The Dimensions of Chain Molecules Containing Branches and Rings. *J. Chem. Phys.* **1949**, *17*, 1301−1314.

(12) Stockmayer, W. H.; Fixman, M. DILUTE SOLUTIONS OF BRANCHED POLYMERS. *Ann. N. Y. Acad. Sci.* **1953**, *57*, 334−352.

(13) Zimm, B. H.; Kilb, R. W. Dynamics of Branched Polymer Molecules in Dilute Solution. *J. Polym. Sci.* **1959**, *37*, 19−42.

(14) Lederer, A.; Burchard, W.; Khalyavina, A.; Lindner, P.; Schweins, R. Is the Universal Law Valid for Branched Polymers? *Angew. Chem., Int. Ed.* 2013, *52* (17), 4659−4663. DOI: 10.1002/anie.201209228

(15) Lederer, A.; Burchard, W.; Hartmann, T.; Haataja, J. S.; Houbenov, N.; Janke, A.; Friedel, P.; Schweins, R.; Lindner, P. Dendronized Hyperbranched Macromolecules: Soft Matter with a Novel Type of Segmental Distribution. *Angew. Chem., Int. Ed.* 2015, *54* (43), 12578−12583. DOI: 10.1002/anie.201504059

(16) Gabriel, C.; Münstedt, H. Influence of Long-Chain Branches in Polyethylenes on Linear Viscoelastic Flow Properties in Shear. *Rheol. Acta* **2002**, *41*, 232−244.

(17) Krause, B.; Voigt, D.; Häußler, L.; Auhl, D.; Münstedt, H. Characterization of Electron Beam Irradiated Polypropylene: Influence of Irradiation Temperature on Molecular and Rheological Properties. *J. Appl. Polym. Sci.* **2006**, *100*, 2770−2780.

(18) Guan, Z. Chain Walking: A New Strategy to Control Polymer Topology. *Science* **1999**, *283*, 2059−2062.

(19) Johnson, L. K.; Killian, C. M.; Brookhart, M. New Pd(II)- and Ni(II)-Based Catalysts for Polymerization of Ethylene and.Alpha.-Olefins. *J. Am. Chem. Soc.* **1995**, *117*, 6414−6415.

(20) Patil, R.; Colby, R. H.; Read, D. J.; Chen, G.; Guan, Z. Rheology of Polyethylenes with Novel Branching Topology Synthesized by a Chain-Walking Catalyst. *Macromolecules* **2005**, *38*, 10571−10579.

(21) Cotts, P. M.; Guan, Z.; McCord, E.; McLain, S. Novel Branching Topology in Polyethylenes As Revealed by Light Scattering and 13C NMR. *Macromolecules* **2000**, *33*, 6945−6952.

DOI: 10.1021/acs.macromol.9b01410
Macromolecules 2019, 52, 8662−8671

(22) Dockhorn, R.; Plüschke, L.; Geisler, M.; Zessin, J.; Lindner, P.; Mundil, R.; Merna, J.; Sommer, J.-U.; Lederer, A. Polyolefins Formed by Chain Walking Catalysis—A Matter of Branching Density Only? *J. Am. Chem. Soc.* **2019**, *141*, 15586−15596.
(23) Schallausky, F.; Erber, M.; Komber, H.; Lederer, A. An Easy Strategy for the Synthesis of Well-Defined Aliphatic-Aromatic Hyperbranched Polyesters. *Macromol. Chem. Phys.* **2008**, *209*, 2331−2338.
(24) Khalyavina, A.; Häußler, L.; Lederer, A. Effect of the Degree of Branching on the Glass Transition Temperature of Polyesters. *Polymer* **2012**, *53*, 1049−1053.
(25) Striegel, A. M.; Yau, W. W.; Kirkland, J. J.; Bly, D. D. Retention. In *Modern Size-Exclusion Liquid Chromatography*; Wiley Online Books: 2009; p 496.
(26) Podzimek, S.; Vlcek, T.; Johann, C. Characterization of Branched Polymers by Size Exclusion Chromatography Coupled with Multiangle Light Scattering Detector. I. Size Exclusion Chromatography Elution Behavior of Branched Polymers. *J. Appl. Polym. Sci.* **2001**, *81*, 1588−1594.
(27) Erber, M.; Boye, S.; Hartmann, T.; Voit, B. I.; Lederer, A. A Convenient Room Temperature Polycondensation toward Hyperbranched AB2-Type All-Aromatic Polyesters with Phenol Terminal Groups. *J. Polym. Sci., Part A: Polym. Chem.* **2009**, *47*, 5158−5168.
(28) Schimpf, M. E.; Caldwell, K.; Giddings, J. C. *Field-Flow Fractionation Handbook*; John Wiley & Sons, Inc., 2000; pp 3−48.
(29) Ludwig, C. Diffusion Zwischen Ungleich Erwärmten Orten Gleich Zusammengesetzter Lösungen *Sitzungber Bayer Akad Wiss Wien Math-Naturwiss Kl* 1856, *20*, 539.
(30) Soret, C. Sur l'état d'équilibre Que Prend, Au Point de Vue de Sa Concentration, Une Dissolution Saline Primitivement Homogène, Dont Deux Parties Sont Portées à Des Températures Différentes. *J. Phys. Theor. Appl.* **1880**, *9*, 331−332.
(31) Eslamian, M.; Ziad, S. M. A Critical Review of Thermodiffusion Models: Role and Significance of the Heat of Transport and the Activation Energy of Viscous Flow. *J. Non-Equilib. Thermodyn.* **2009**, *34*, 97.
(32) Stadelmaier, D.; Köhler, W. Thermal Diffusion of Dilute Polymer Solutions: The Role of Chain Flexibility and the Effective Segment Size. *Macromolecules* **2009**, *42*, 9147−9152.
(33) Morozov, K. I.; Köhler, W. Thermophoresis of Polymers: Nondraining vs Draining Coil. *Langmuir* **2014**, *30*, 6571−6576.
(34) Van Asten, A. C.; Boelens, H. F. M.; Kok, W. T.; Poppe, H.; Williams, P. S.; Giddings, J. C. Temperature Dependence of Solvent Viscosity, Solvent Thermal Conductivity, and Soret Coefficient in Thermal Field-Flow Fractionation. *Sep. Sci. Technol.* **1994**, *29*, 513−533.
(35) Belgaied, J. E.; Hoyos, M.; Martin, M. Velocity Profiles in Thermal Field-Flow Fractionation. *J. Chromatogr. A* **1994**, *678*, 85−96.
(36) Williams, S. K. R.; Lee, D. Field-Flow Fractionation of Proteins, Polysaccharides, Synthetic Polymers, and Supramolecular Assemblies. *J. Sep. Sci.* **2006**, *29*, 1720−1732.
(37) Williams, S. K. R.; Runyon, J. R.; Ashames, A. A. Field-Flow Fractionation: Addressing the Nano Challenge. *Anal. Chem.* **2011**, *83*, 634−642.
(38) Qureshi, R. N.; Kok, W. T. Application of Flow Field-Flow Fractionation for the Characterization of Macromolecules of Biological Interest: A Review. *Anal. Bioanal. Chem.* **2011**, *399*, 1401−1411.
(39) Gunderson, J. J.; Giddings, J. C. Field-Flow Fractionation. In *Comprehensive Polymer Science*; Allen, G.; Bevington, J., Eds.; Pergamon Press: Oxford, 1989; p 279.
(40) Schimpf, M. E. Characterization of Polymers by Thermal Field-Flow Fractionation. *J. Chromatogr. A* **1990**, *517*, 405−421.
(41) Rauch, J.; Köhler, W. On the Molar Mass Dependence of the Thermal Diffusion Coefficient of Polymer Solutions. *Macromolecules* **2005**, *38*, 3571−3573.
(42) Schimpf, M. E.; Giddings, J. C. Characterization of Thermal Diffusion in Polymer Solutions by Thermal Field-Flow Fractionation: Effects of Molecular Weight and Branching. *Macromolecules* **1987**, *20*, 1561−1563.
(43) Greyling, G.; Lederer, A.; Pasch, H. Thermal Field-Flow Fractionation for the Investigation of the Thermoresponsive Nature of Star and Linear Polystyrene. *Macromol. Chem. Phys.* **2018**, *219*, No. 1800417.
(44) Runyon, J. R.; Williams, S. K. R. Composition and Molecular Weight Analysis of Styrene-Acrylic Copolymers Using Thermal Field-Flow Fractionation. *J. Chromatogr. A* **2011**, *1218*, 6774−6779.
(45) Smith, W. C.; Geisler, M.; Lederer, A.; Williams, S. K. R. Thermal Field-Flow Fractionation for Characterization of Architecture in Hyperbranched Aromatic-Aliphatic Polyesters with Controlled Branching. *Anal. Chem.* **2019**, *91*, 12344−12351.
(46) Runyon, J. R. *Thermal Field-Flow Fractionation of Polymers with High Molecular Weight and Complex Architectures*; Colorado School of Mines: Golden, CO, 2009.
(47) Brimhall, S. L.; Myers, M. N.; Caldwell, K. D.; Giddings, J. C. High Temperature Thermal Field-Flow Fractionation for the Characterization of Polyethylene. *Sep. Sci. Technol.* **1981**, *16*, 671−689.
(48) Pasti, L.; Roccasalvo, S.; Dondi, F.; Reschiglian, P. High Temperature Thermal Field-Flow Fractionation of Polyethylene and Polystyrene. *J. Polym. Sci., Part B: Polym. Phys.* **1995**, *33*, 1225−1234.
(49) Horská, J.; Stejskal, J.; Kratochvíl, P. Refractive Index Increments of Polyethylene. *J. Appl. Polym. Sci.* **1979**, *24*, 1845−1855.
(50) MacRury, T. B.; McConnell, M. L. Measurement of the Absolute Molecular Weight and Molecular Weight Distribution of Polyolefins Using Low-Angle Laser Light Scattering. *J. Appl. Polym. Sci.* **1979**, *24*, 651−662.
(51) Sun, T.; Brant, P.; Chance, R. R.; Graessley, W. W. Effect of Short Chain Branching on the Coil Dimensions of Polyolefins in Dilute Solution. *Macromolecules* **2001**, *34*, 6812−6820.
(52) Wood-Adams, P. M.; Dealy, J. M.; deGroot, A. W.; Redwine, O. D. Effect of Molecular Structure on the Linear Viscoelastic Behavior of Polyethylene. *Macromolecules* **2000**, *33*, 7489−7499.
(53) Mundil, R.; Hermanová, S.; Peschel, M.; Lederer, A.; Merna, J. On the Topology of Highly Branched Polyethylenes Prepared by Amine−imine Nickel and Palladium Complexes: The Effect of Ortho-Aryl Substituents. *Polym. Int.* **2018**, *67*, 946−956.
(54) Hansen, C. M.; Durkee, J.; Kontogeorgis, G.; Panayiotou, C.; Willliams, L. L.; Poulsen, T. S.; Priebe, H.; Redelius, P. *Hansen Solubility Parameters: A User's Handbook, Second Edition*, 2nd ed.; CRC Press: 2007; pp 75−110 and 345−507
(55) Stepto, R. F. T. Dispersity in Polymer Science (IUPAC Recommendations 2009). *Pure Appl. Chem.* **2009**, *81*, 351.
(56) Stepto, R. F. T. Erratum. *Pure Appl. Chem.* **2009**, *81*, 351−353.
(57) Lansing, W. D.; Kraemer, E. O. Molecular Weight Analysis of Mixtures by Sedimentation Equilibrium in the Svedberg Ultracentrifuge. *J. Am. Chem. Soc.* **1935**, *57*, 1369−1377.
(58) Schimpf, M. E.; Giddings, J. C. Characterization of Thermal Diffusion of Copolymers in Solution by Thermal Field-Flow Fractionation. *J. Polym. Sci., Part B: Polym. Phys.* **1990**, *28*, 2673−2680.
(59) Köhler, W. Thermodiffusion in Polymer Solutions as Observed by Forced Rayleigh Scattering. *J. Chem. Phys.* **1993**, *98*, 660−668.
(60) Khalyavina, A.; Schallausky, F.; Komber, H.; Al Samman, M.; Radke, W.; Lederer, A. Aromatic−Aliphatic Polyesters with Tailored Degree of Branching Based on AB/AB2 and ABB*/AB2 Monomers. *Macromolecules* **2010**, *43*, 3268−3276.
(61) Nguyen, M.; Beckett, R. Calibration Methods for Field-Flow Fractionation Using Broad Standards. I. Thermal Field-Flow Fractionation. *Sep. Sci. Technol.* **1996**, *31*, 291−317.
(62) Gottfried, A. C.; Brookhart, M. Living Polymerization of Ethylene Using Pd(II) α-Diimine Catalysts. *Macromolecules* **2001**, *34*, 1140−1142.
(63) Giddings, J. C.; Caldwell, K. D.; Myers, M. N. Thermal Diffusion of Polystyrene in Eight Solvents by an Improved Thermal Field-Flow Fractionation Methodology. *Macromolecules* **1976**, *9*, 106−112.

DOI: 10.1021/acs.macromol.9b01410
Macromolecules 2019, 52, 8662−8671

(64) Gao, Y. S.; Caldwell, K. D.; Myers, M. N.; Giddings, J. C. Extension of Thermal Field-Flow Fractionation to Ultra-High (20.Times. 106) Molecular Weight Polystyrenes. *Macromolecules* **1985**, *18*, 1272−1277.
(65) Schimpf, M. E.; Williams, P. S.; Giddings, J. C. Accurate Molecular Weight Distribution of Polymers Using Thermal Field-Flow Fractionation with Deconvolution to Remove System Dispersion. *J. Appl. Polym. Sci.* **1989**, *37*, 2059−2076.
(66) Schimpf, M. E.; Myers, M. N.; Giddings, J. C. Measurement of Polydispersity of Ultra-Narrow Polymer Fractions by Thermal Field-Flow Fractionation. *J. Appl. Polym. Sci.* **1987**, *33*, 117−135.
(67) Lee, W.; Lee, H.; Cha, J.; Chang, T.; Hanley, K. J.; Lodge, T. P. Molecular Weight Distribution of Polystyrene Made by Anionic Polymerization. *Macromolecules* **2000**, *33*, 5111−5115.
(68) Lee, H. C.; Chang, T. Polymer Molecular Weight Characterization by Temperature Gradient High Performance Liquid Chromatography. *Polymer* **1996**, *37*, 5747−5749.
(69) Brewer, A. K.; Striegel, A. M. Particle Size Characterization by Quadruple-Detector Hydrodynamic Chromatography. *Anal. Bioanal. Chem.* **2009**, *393*, 295.

DOI: 10.1021/acs.macromol.9b01410
Macromolecules 2019, 52, 8662−8671

Supporting Information for

Topology Analysis of Chain Walking Polymerized Polyethylene: An Alternative Approach for the Branching Characterization by Thermal FFF

Martin Geisler,[†,‡] William C. Smith,[§] Laura Plüschke, [†,‡] Robert Mundil,[⊥] Jan Merna,[⊥] S. Kim Ratanathanawongs Williams,[§] and Albena Lederer*[,†,‡]

[†]Polymer Separation Group, Leibniz-Institut für Polymerforschung Dresden e. V., Hohe Str. 6, 01069 Germany

[‡]Faculty of Chemistry and Food Chemistry, Technische Universität Dresden, 01062 Dresden, Germany

[§]Department of Chemistry, Colorado School of Mines, Golden, Colorado 80401, USA

[⊥] Department of Polymers, University of Chemistry and Technology Prague, Technická 5, 166 28 Praha 6, Czech Republic

*Email of corresponding author: lederer@ipfdd.de

Table of content for the Supplementary data:

1.	Experimental Details	S-2
2.	HT-SEC-D4 chromatograms and topological analysis	S-3
3.	Determination of the refractive index increment $dn\ dc^{-1}$ for cwPE	S-4
4.	Temperature dependent Dynamic Light scattering (DLS) experiments in batch	S-4
5.	ThFFF fractograms with online MALS, dRI and molar mass	S-5
6.	Dependency of S_T and D_T on the polymer topology (Fig. 3) from different ΔT and τ	S-6
7.	Coefficients of the equations (9), (10) and (13)	S-6
8.	λ^{-1} to M_{Seg}, g versus g'' and the dependency of t_R on B, each from different ΔT and τ	S-8
9.	Numerical solution of Equation (7) to λ	S-9
10.	Development of equation (12) to be applied in equation (11) from the main article	S-10
11.	Cumulative and differential weight distributions of LCB and g''	S-11
12.	Uncertainties and errors	S-12
13.	References	S-14

1. Experimental details

1.1. Materials

The polyethylenes used in this work were synthesized with α-diimine palladium catalyst ([(N, N'-bis(2,6-diisopropylphenyl)-2,3-dimethyl-1,4-diazabutane)Pd(CH_2)$_3$COOCH_3]$^+$ [BAr$^F{}_4$]$^-$ (Ar^F=3,5-bis-(trifluoro-methyl)phenyl)) as described elsewhere[1–3] based on the synthesis approach of Brookhart *et al.*[4] with the conditions shown in Table S1. All samples contain ~ 100 branches per 1000 total carbon atoms according to ^{1}H NMR analysis but differ in topology mainly influenced by ethene pressure.[5]

Table S1. Synthesis conditions, expected topology and the characterization average results of the investigated short chain branched cwPEs found by HT-SEC-D4.

Synthesis conditions					Average results found by HT-SEC-D4		
Sample	p / bar [a]	T / °C	Reaction time / h	Expected topology	M_w / kg mol^{-1}	$R_{G,z}$ / nm	ν_R
hb1	0.14	35	24	highly branched, medium M_w	230 ± 6	15.8 ± 0.3	0.56 ± 0.3
hb2	0.09	0	24	highly branched, lower M_w	161.3 ± 2.2	12.9 ± 0.2	0.45 to 1.15*
b1	4	0	20	linear, lower M_w	140 ± 3	16.6 ± 0.4	0.60 ± 0.09
b2	2	0	20	branched, lower M_w	136 ± 2	16.3 ± 0.2	0.65 ± 0.08
sb	2	10	20	slightly branched, higher M_w	313 ± 8	25.4 ± 0.5	0.47 to 0.73*
lin1	8	0	20	linear, lower M_w	175.4 ± 0.5	18.5 ± 0.2	0.53 ± 0.02
lin2	8	10	20	linear, higher M_w	384 ± 7	30.4 ± 0.3	0.35 to 0.74*

Pd catalyst 10 µmol, chlorobenzene 30 mL, [a]absolute ethene pressure

*) dependent on the molar mass, see Fig. S2

1.2. Instrumentation

1.2.1. High temperature size exclusion chromatography

High temperature quadruple-detector size exclusion chromatography (HT-SEC-D4) experiments were done with a PL-GPC220 (Polymer Laboratories Ltd., U. K.) setup, connected to a MALS detector (Wyatt Technology Corporation, USA), a dRI detector and an online viscometer (both Agilent Technologies, Inc., USA) as described in our previous report.[2] The carrier fluid 1,2,4-trichlorobenzene was purchased from Sigma Aldrich with a purity of ≥ 99 % and stabilized with 1 g L^{-1} 2,6-di-tert-butyl-4-methylphenol (Carl Roth, Germany, purity ≥ 98 %) to prevent thermo-oxidative decomposition. Data recording and analysis was done with the Astra® software, version 6.1.2.84 (Wyatt Technology Corporation, USA).

1.2.2. Temperature dependent dynamic light scattering

Temperature dependent dynamic light scattering (DLS) experiments were performed with a DynaPro® NanoStar® instrument (Laser λ = 658 nm) by Wyatt Technology Corporation, USA using a 1.25 µl quartz cuvette (total volume approximately 1 mL). In all experiments, the cuvette was completely filled with ca. 0.8 mL sample solution to avoid cavities, containing 1 mg mL^{-1} of polymer, dissolved in cyclohexane (EMSURE®, Merck KGaA, Germany, purity ≥ 99.5 %) and filtered through a 0.45 µm PTFE syringe filter (Carl Roth, Germany). The cuvette was closed with an affiliated PTFE lid and sealed with Parafilm® wax foil to prevent evaporation of solvent. The data recording and analysis was done with the software Dynamics® by Wyatt Technology Corporation, USA, versions 7.6.0.48 and 7.8.0.26 using the cumulant fit method.[6] During the run of all experiments (T = 20 to 60 °C in stages of 5 K, total time ca. 6 h) no solvent lost due to evaporation or leakage of the sealing was observed.

1.2.3. ThFFF

ThFFF experiments were carried out with a TF2000 set up, consisting of an isocratic pump, degasser, auto-sampler, actively heated and cooled ThFFF channel, PN3621 multi-angle light scattering (MALS) detector with a laser of the wavelength 532 nm and PN3150 differential refractive index (dRI) detector (all by Postnova Analytics GmbH, Germany). The channel dimensions were 45.6 cm tip-to-tip length, width 2 cm and a thickness of 250 µm, realized by spacers made of Mylar A® and Teonex®. All separations were done with a constant flow rate of 0.2 mL min^{-1} and CHX (EMSURE®, Merck KGaA, Germany, purity ≥99.5 %) as carrier fluid. The void time in all separations was 11.04 min. A channel pressure of about 1 MPa to avoid boiling of the carrier fluid at the hot wall was adjusted for the used flow rate by a sufficient long back pressure tubing (inner diameter 0.001“) between the ThFFF channel and the MALS detector. The data recording and analysis was carried out with the Postnova software.

2. HT-SEC-D4 chromatograms and topological analysis

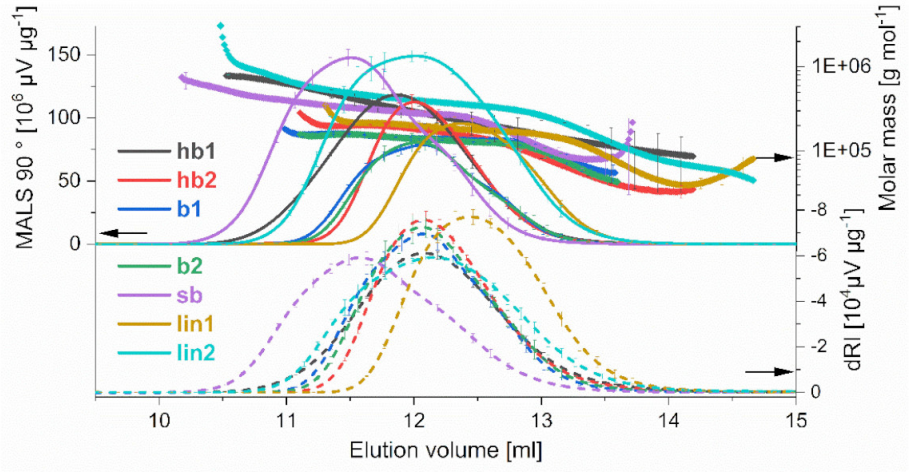

Figure S1. Superimposed HT-SEC-D4 chromatograms of 7 short chain branched chain walk polyethylenes (cwPE) with different topologies ranging from linear up to hyperbranched macrostructure, measured at 150 °C in 1,2,4-trichlorobenzene as eluent. The flow rate was 1 mL min^{-1}.

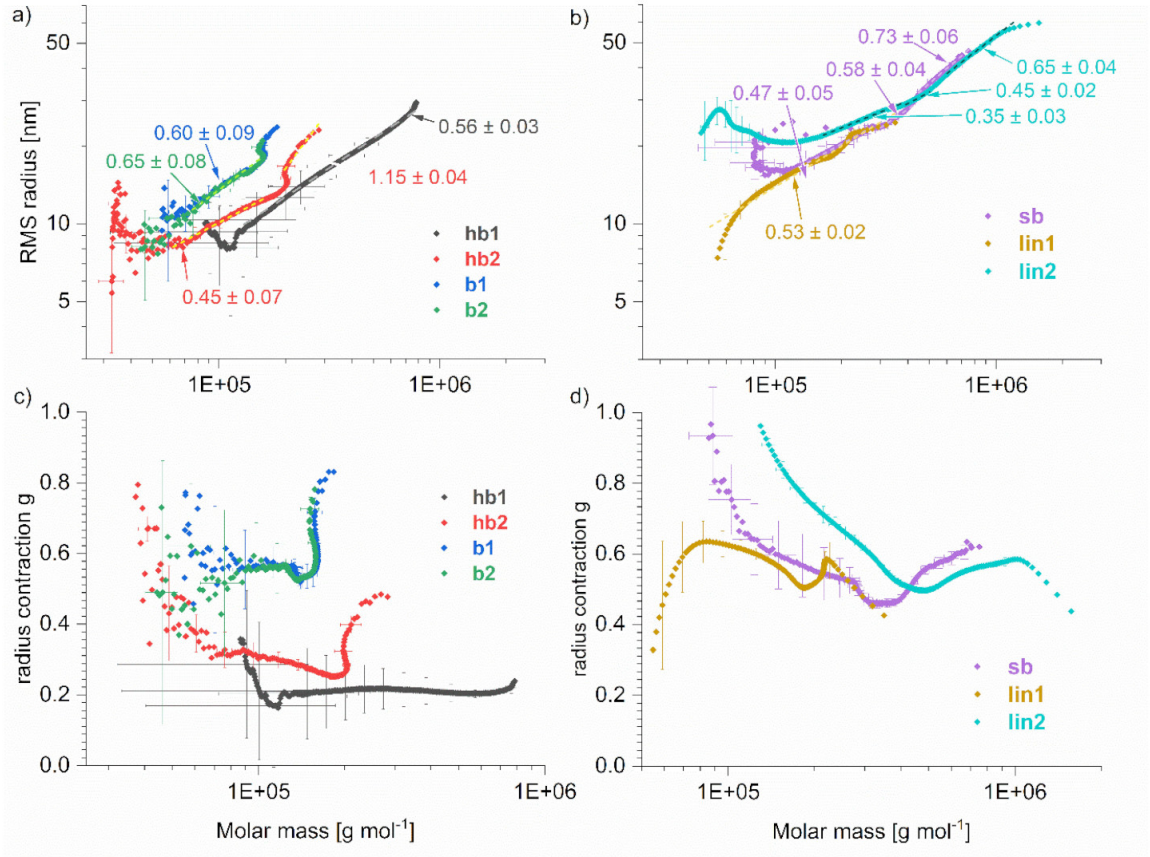

Figure S2. Superimposed conformation plots (a and b) of the cwPE from Fig. S1 and the radius contraction factors (c and d), calculated with the linear model $R_{G,LIN} = 0.023\ M^{0.58}$.

Generally, polymers of the same topology show a scaling behavior described by the relation $R_G = K \cdot M^{\nu_R}$ where K is a polymer specific constant and ν_R is the scaling exponent describing the conformation of the polymer. Analogue to this, the so-called *Kuhn-Mark-Houwink-Sakurada Equation* $[\eta] = K \cdot M^{\alpha}$ can be used. Theoretical values for ν are in the range from 0.33 representing a compact sphere passing through 0.59 for a random linear coil in a thermodynamically good solvent up to 1 for rigid rods.[7–9] For α instead, the value range is broader starting from 0 for very compact object, passing 1.0 for linear coils in a good solvent up to 2 for rod-like objects.[8–10]

3. Determination of the Refractive Index Increment for cwPE

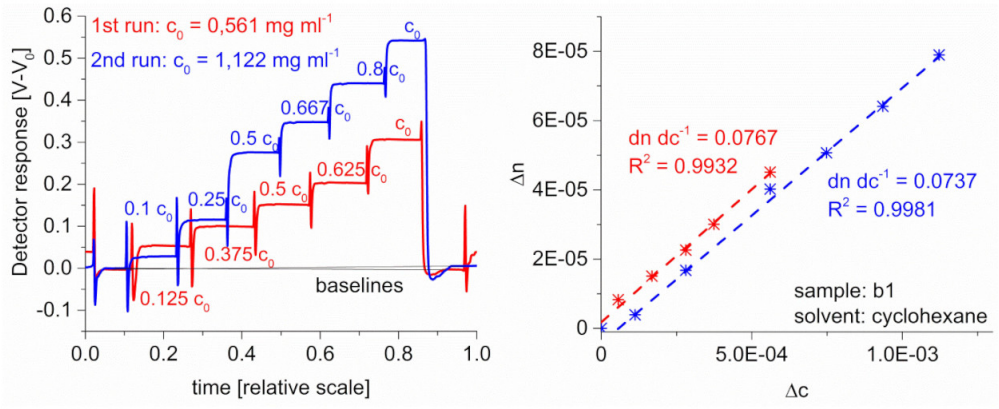

Figure S3. The determination of the refractive index increment $dn\ dc^{-1}$ of cwPE, represented by sample b1, gave an average $dn\ dc^{-1} = 0.0752 \pm 0.0015$ mL g^{-1}. Changes in the $dn\ dc^{-1}$ caused by molar mass and topology differences are assumed to be negligible.

4. Temperature dependent Dynamic Light scattering (DLS) experiments in batch

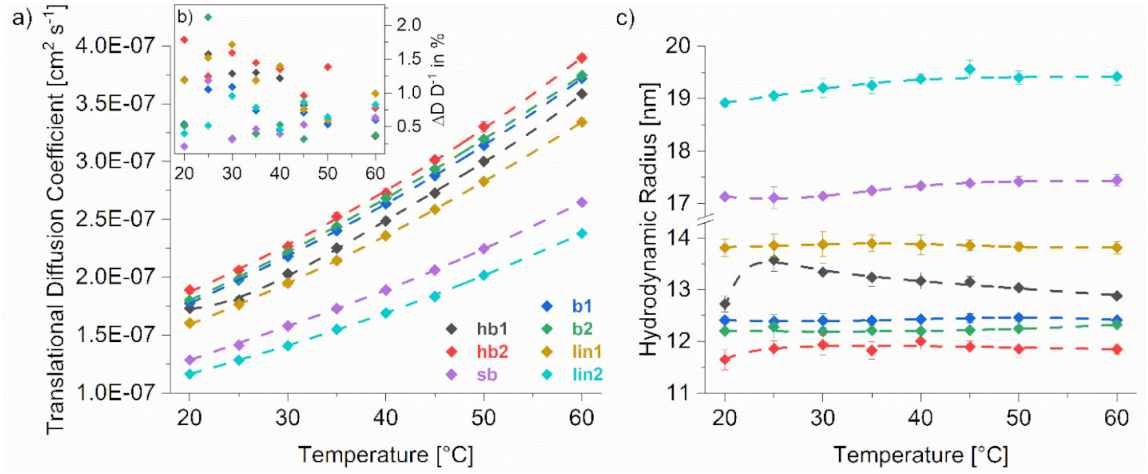

Figure S4. Superimposed translational diffusion coefficients (a) with their relative uncertainties in inset (b) and the hydrodynamic radii (c) of the cwPE with different topologies, dissolved in cyclohexane with a concentration of 1 g L^{-1}. The data were obtained by temperature dependent DLS experiments in batch.

The hydrodynamic radius R_h represents the radius of an equivalent hard sphere with the same diffusion rate. It can be calculated from the translational diffusion coefficient D by the Stokes-Einstein-relationship[9,11]

$$R_h = \frac{k_B \cdot T}{6\pi \cdot \eta \cdot D}$$

where k_B is the Boltzmann constant, T is here the absolute temperature in [K], η is the dynamic viscosity of the solvent at the same temperature.

D-fits as illustrated in Fig. S4; used in this work for the calculation of D_T [T in °C]:

hb1 $D(T) = 1.06649E\text{-}6 - 1.28921E\text{-}07T + 6.97223E\text{-}9T^2 - 1.781493E\text{-}10T^3 + 2.22371E\text{-}12T^4 - 1.081756E\text{-}14T^5$

hb2 $D(T) = (T + 59.60459)\ (741276848.6 - 4651875.866\ (T + 59.60459) + 8505.683494\ (T + 59.60459)^2)^{-1}$

b1 $D(T) = 1.00763E\text{-}7 + 3.80828E\text{-}9T - 4.38586E\text{-}12T^2 + 2.70737E\text{-}13T^3$

b2 $D(T) = 1.14866E\text{-}7 + 2.6256E\text{-}9T + 3.38488E\text{-}11T^2 - 9.12468E\text{-}14T^3$

sb $D(T) = 5.37556E\text{-}8 + 4.9977E\text{-}9T - 9.36631E\text{-}11T^2 + 1.68986E\text{-}12T^3 - 8.99452E\text{-}15T^4$

lin1 $D(T) = 1.16877E\text{-}7 + 1.16418E\text{-}9T + 5.59629E\text{-}11T^2 - 2.97754E\text{-}13T^3 + 7.96575E\text{-}16T^4$

lin2 $D(T) = 6.85707E\text{-}8 + 2.67579E\text{-}9T - 2.86986E\text{-}11T^2 + 8.11968E\text{-}13T^3 - 4.88957E\text{-}15T^4$

5. ThFFF fractograms with online MALS, dRI and molar mass

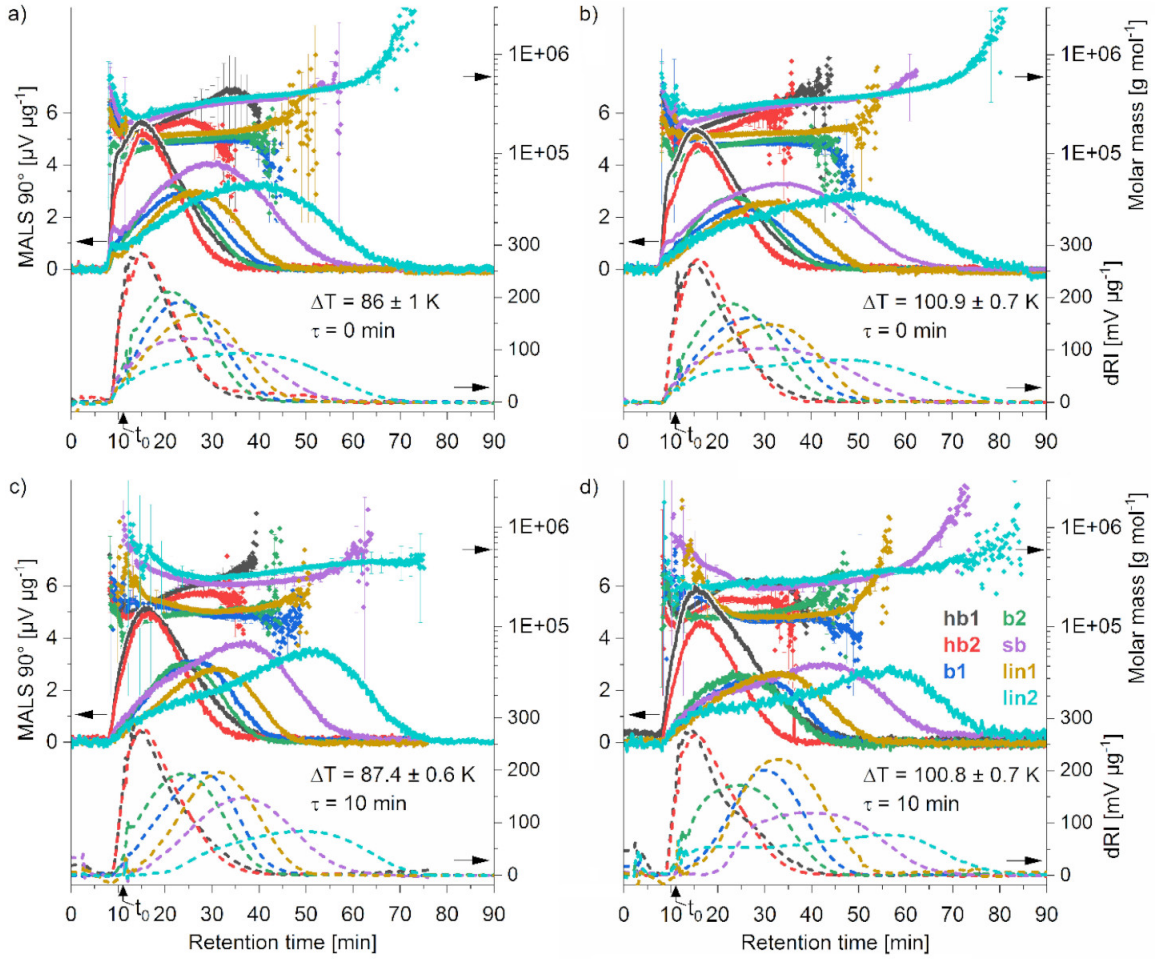

Figure S5. Superimposed fractograms of seven short chain branched chain walk polyethylenes (cwPE) with different topologies ranging from linear up to hyperbranched macrostructure, separated without stop-flow (a and b) and with stop-flow of τ = 10 min (c and d), each with 2 different field strengths of $\Delta T \approx 85$ K and $\Delta T \approx 100$ K. The void time corresponding to the used flow rate of 0.2 ml min^{-1} was t_0 = 11.035 min.

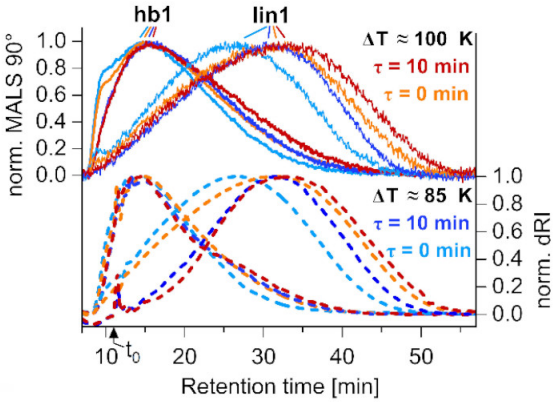

Figure S6. Different topologies of about the same molar mass showed differences in their mean retention time, indicating a different duration to reach their relaxation equilibrium: The found mean retention times between $\Delta T \approx 85$ K and $\Delta T \approx 100$ K measured without stop-flow show a significantly larger difference than the experiments with a stop-flow of τ = 10 min.

6. Dependency of S_T and D_T on the polymer topology (Fig. 3) from different ΔT and τ

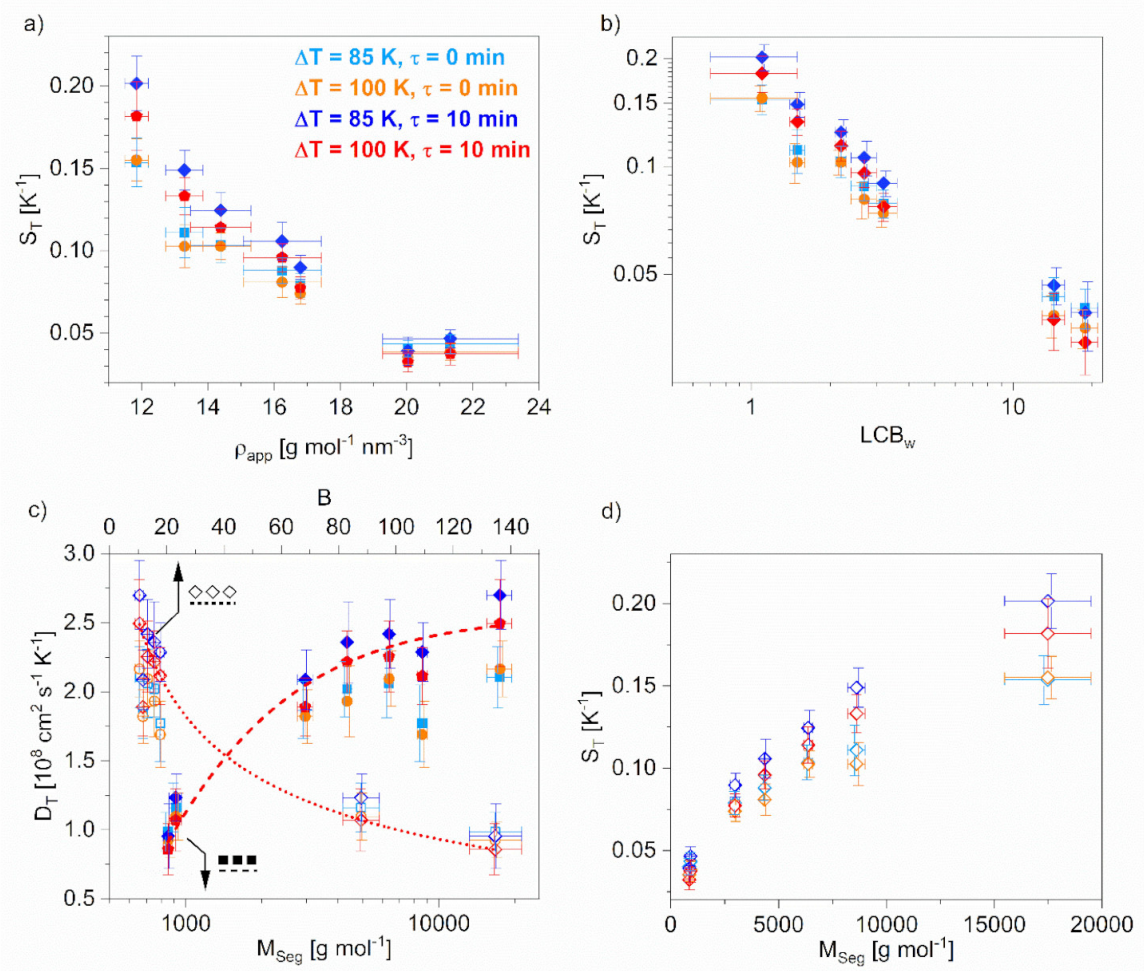

Figure S7. The dependency of S_T and D_T on the polymer topology: a) S_T vs. ρ_{app}; b) S_T vs. LCB_w; c) D_T vs. B, M_{Seg} and d) S_T vs. M_{Seg}. All branching parameters were calculated from HT-SEC-D4 data and temperature-dependent DLS data (measured in batch). The dotted and dashed red lines are fits for guiding the eye for ΔT = 100 K, τ = 10 min.

The molecular apparent density ρ_{app},[12] shown in (a) was calculated by the definition

$$\rho_{app} = \frac{3M}{4\pi R^3}$$

where R is the equivalent sphere radius, for the original definition derived from its dependence to $[\eta]$.[13] Here, we used the hydrodynamic radius R_h derived from DLS experiments calculated from D by the Stokes-Einstein equation.[9,11]

7. Coefficients of the equations (9), (10) and (13) in the main article

Equation (9):

$$S_{T,LIN} = \frac{(a_1 \cdot \Delta T + a_2) \cdot lnM_w - (a_3 \cdot \Delta T + a_4)}{\Delta T} \; [K^{-1}] \qquad (9)$$

Table S2 The coefficients used in equation (9)

	τ = 0 min	τ = 10 min
a_1	0.04365228	0.02443976
a_2	-0.75990437	2.16415169
a_3	0.29717323	0.17378145
a_4	-8.55297743	10.8069849

Equation (10):

$$g(g'') = K_1 + (K_2 - K_1)\left[\frac{K_3}{1 + 10^{(K_4 - g'')K_5}} + \frac{1 - K_3}{1 + 10^{(K_6 - g'')K_7}}\right] \quad (10)$$

Table S3-1 K-coefficients of equation (10)(13):

K coefficients	τ = 0 min	τ = 10 min
K_1	$c_1 \cdot \Delta T^2 + c_2 \cdot \Delta T + c_3$	$c_1 \cdot \Delta T^2 + c_2 \cdot \Delta T + c_3$
K_2	$c_4 \cdot \Delta T + c_5$	$c_4 \cdot \Delta T^2 + c_5 \cdot \Delta T + c_6$
K_3	$c_6 \cdot \Delta T + c_7$	$c_7 \cdot \Delta T^2 + c_8 \cdot \Delta T + c_9$
K_4	$c_8 \cdot \Delta T + c_9$	$c_{10} \cdot \Delta T^2 + c_{11} \cdot \Delta T + c_{12}$
K_5	$c_{10} + c_{11} \cdot c_{12}{}^{\Delta T}$	$c_{13} \cdot \Delta T^2 + c_{14} \cdot \Delta T + c_{15}$
K_6	$c_{13} \cdot \Delta T^2 + c_{14} \cdot \Delta T + c_{15}$	$c_{16} \cdot \Delta T^2 + c_{17} \cdot \Delta T + c_{18}$
K_7	$c_{16} + c_{17} \cdot e^{c_{18} \cdot \Delta T}$	$c_{19} \cdot \Delta T^2 + c_{20} \cdot \Delta T + c_{21}$

Table S3-2 c-coefficients of equation (10)(13):

c coefficients	τ = 0 min	τ = 10 min	*c* coefficients	τ = 0 min	τ = 10 min
c_1	1.03514E-04	3.56288E-03	c_{12}	0.734959533	9.208338
c_2	-0.02400594	-0.6782382	c_{13}	-3.517549E-05	5.636435E-03
c_3	1.195496	31.64408	c_{14}	4.30501E-03	-1.05332
c_4	-0.01279948	-1.030309E-03	c_{15}	1.023378	52.2233
c_5	3.278437	0.1894345	c_{16}	3.136567757	-1.070268E-04
c_6	3.314146E-03	-6.636798	c_{17}	6.00572485E-06	0.01883061
c_7	8.183203E-03	-5.771928E-04	c_{18}	0.109717763	0.2853224
c_8	-3.215138E-03	0.1110859	c_{19}		1.408593E-03
c_9	0.4663463	-4.904675	c_{20}		-0.2466364
c_{10}	3.578675501	1.013327E-03	c_{21}		14.08777
c_{11}	8.19243552E+10	-0.1934036			

Equation (13):(13)

$$B_{apex}(R_{apex}) = K_1 + \frac{K_2 - K_1}{\left[1 + \left({}^{K_3}/_{R}\right)^{K_4}\right]^{K_5}} \quad (13)$$

Table S4-1 K-coefficients of equation (13)(13):

K coefficients	τ = 0 min	τ = 10 min
K_1	$c_1 \cdot \Delta T^2 + c_2 \cdot \Delta T + c_3$	$c_1 \cdot \Delta T + c_2$
K_2	$c_4 \cdot \Delta T^2 + c_5 \cdot \Delta T + c_6$	$c_3 \cdot \Delta T + c_4$
K_3	$c_7 \cdot \Delta T + c_8$	$c_5 \cdot \Delta T^2 + c_6 \cdot \Delta T + c_7$
K_4	$c_9 \cdot \Delta T^2 + c_{10} \cdot \Delta T + c_{11}$	$c_8 \cdot \Delta T^2 + c_9 \cdot \Delta T + c_{10}$
K_5	$c_{12} \cdot \Delta T^{c_{13}}$	$c_{11} + c_{12} \cdot e^{c_{13} \cdot \Delta T}$

Table S4-2 c-coefficients of equation (13)(13):

c coefficients	τ = 0 min	τ = 10 min	*c* coefficients	τ = 0 min	τ = 10 min
c_1	1.718121E-04	-0.02596673	c_8	-0.253226	1.99612E-04
c_2	0.03441019	14.37017	c_9	7.798888E-04	-0.04425696
c_3	10.60227	1.676767	c_{10}	-0.1723634	5.409786
c_4	0.9175371	45.63905	c_{11}	13.44938	10.00016233
c_5	-143.7393	3.764237E-05	c_{12}	236.6771	-2.23036533E-19
c_6	5886.537	-7.257181E-03	c_{13}	-1.056082	0.411955132
c_7	0.01120072	0.6693172			

8. λ^{-1} vs. M_{Seg}, g vs. g'' and the dependency of t_R on B, each from different ΔT and τ

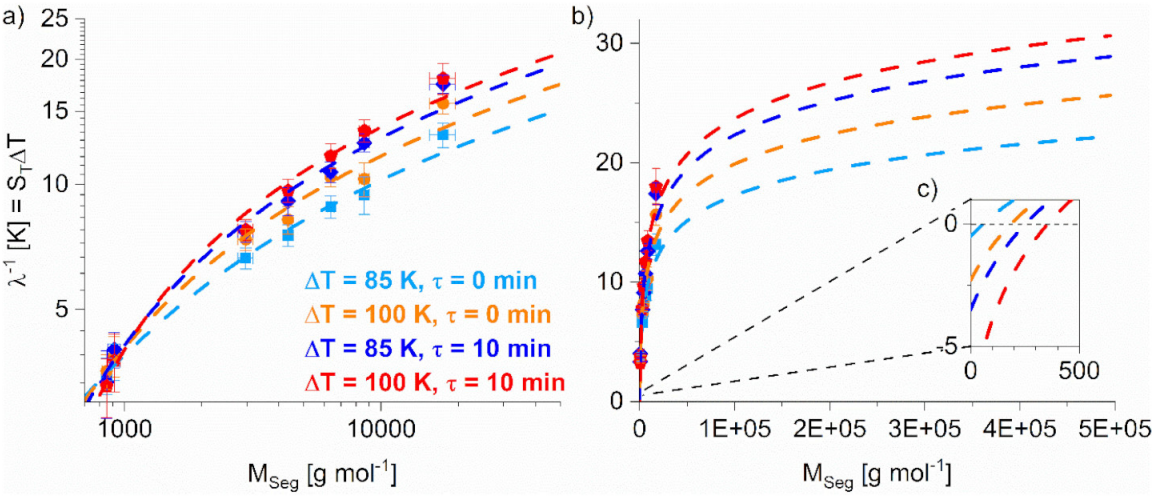

Figure S8. Double logarithmic plot of λ^{-1} against M_{Seg} in four different experimental conditions, fitted with a natural logarithmic function $y = a\ ln(x) + b$. b) shows the continuation of the fits to M_w and the inset in (b) indicates the trend to negative S_T values for M_{Seg} in the molar mass range of n-alkanes.

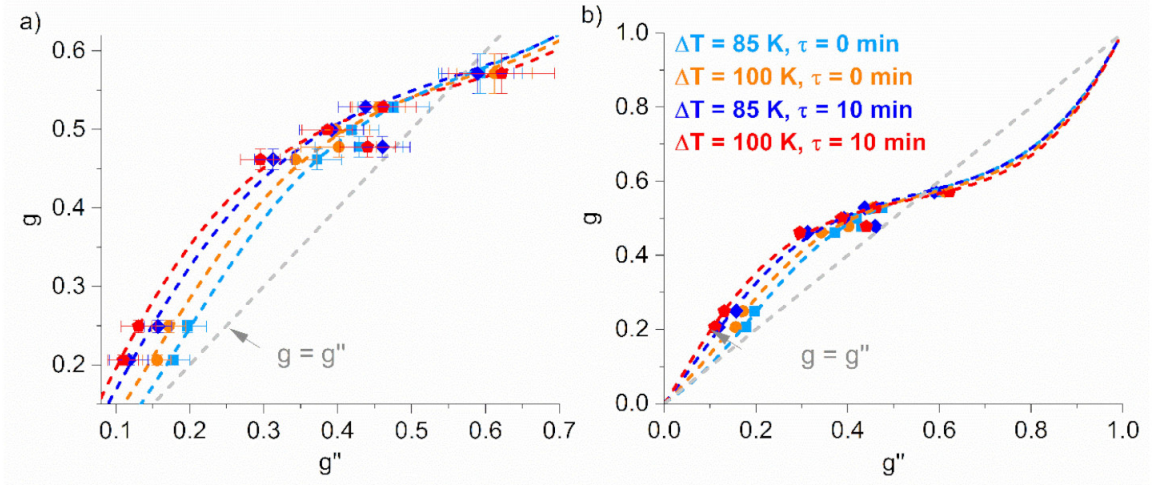

Figure S9. a) The comparison of g and g'' and the fit to transform g'' into g for further calculations for ΔT = 85 K and 100 K, each field strength un-/partially relaxed (τ = 0 min) and fully relaxed (τ = 10 min). The plot (b) shows the plot (a) in the full scale within the limits of 0 and 1 for the fit in Eq. (10) in the main article.

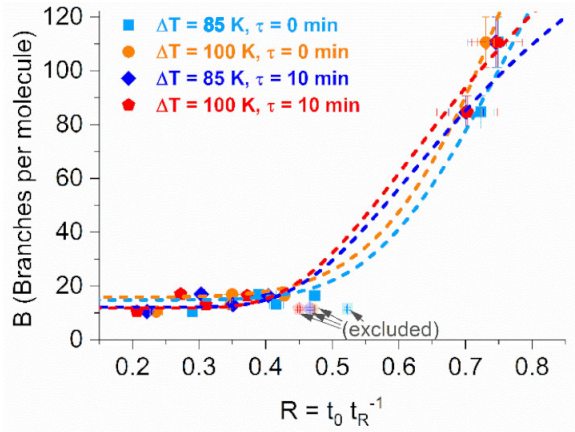

Figure S10. The dependency of the mean retention time t_R on the number of branches per molecule, measured with two different field strengths, each as un-/partially and as fully relaxed system. The dashed lines indicate the mathematical fit with Eq. (13) in the main article.

9. Numerical solution of Equation (7) from the main article for λ

$$R = 6\lambda\left[\nu + (1 - 6\lambda\nu)\left(coth\left(\frac{1}{2\lambda}\right) - 2\lambda\right)\right]$$

$$\lambda = \left(K_0 + K_1 \cdot \sqrt[3]{R} + K_2 \cdot \sqrt[3]{R}^2 + K_3 \cdot \sqrt[3]{R}^3 + K_4 \cdot \sqrt[3]{R}^4 + K_5 \cdot \sqrt[3]{R}^5 + K_6 \cdot \sqrt[3]{R}^6 + K_7 \cdot \sqrt[3]{R}^7\right)^{-1}$$

with $K_x = (\ldots)_0 + (\ldots)_1 \cdot \nu + (\ldots)_2 \cdot \nu^2 + (\ldots)_3 \cdot \nu^3 + (\ldots)_4 \cdot \nu^4$ $\quad (x = 1 \ldots 7)$

Non-parabolicity coefficient ν of the flow profile:[14] $\nu = (a_1 \cdot T_c + a_2) \cdot \Delta T + (a_3 \cdot T_c + a_4) \cdot \Delta T^2 + (a_5 \cdot T_c + a_6) \cdot \Delta T^3$

with a_1 to a_6 see Ref. [14]; T_c is the cold wall temperature

Coefficients:

K_0 with b_0 to b_4: $K_0 = b_0 + b_1 \cdot \nu + b_2 \cdot \nu^2 + b_3 \cdot \nu^3 + b_4 \cdot \nu^4$

K_1: c_0 to c_4; K_2: d_0 to d_4; K_3: e_0 to e_4; K_4: f_0 to f_4; K_5: g_0 to g_4; K_6: h_0 to h_4; K_7: i_0 to i_4

Table S5 coefficients for K_x

	$(\ldots)_0$	$(\ldots)_1$	$(\ldots)_2$	$(\ldots)_3$	$(\ldots)_4$
b_x	4228.278546	7408.974837	14058.75949	18774.62229	9786.035969
c_x	-38661.16221	-74509.45542	-153780.2465	-197891.3378	-100549.6353
d_x	158631.4997	328855.2611	709355.5714	879493.7253	436446.678
e_x	-369963.6997	-811709.8986	-1788451.305	-2136892.459	-1035884.973
f_x	523121.7591	1199855.428	2662459.885	3066184.996	1451155.933
g_x	-445233.8718	-1057390.797	-2341292.672	-2599225.546	-1199935.406
h_x	210269.538	513123.7367	1126627.035	1205908.256	542453.3103
i_x	-42392.08074	-105632.055	-228974.412	-236348.7758	-103470.0162

Ranges of precision:

ν	$\Delta R\,R^{-1}$		exemplary for Cyclohexane: ΔT	T_c
0 to -0.1343	100 % for $R < 1.2$	≤ 17 % for $R > 1.2$	0 to 25 K	17.47 to 18.84 °C
-0.1343 to -0.1937	≤ 26 % for $R < 1.2$	≤ 2 % for $R > 1.2$	25 to 40 K	18.84 to 21 °C
-0.1937 to -0.4583	**≤ 1 % for $R < 1.2$**	**≤ 0.5 % for $R > 1.2$**	**40 to 130 K**	**21 °C**
-0.4583 to -0.4821	≤ 10 % for $R < 1.2$	≤ 0.5 % for $R > 1.2$	130 to 140 K	21.3 °C
-0.4821 to -0.5247	≤ 65 % for $R < 1.2$	≤ 2.5 % for $R > 1.2$	140 to 160 K	21.3 to 25.3 °C

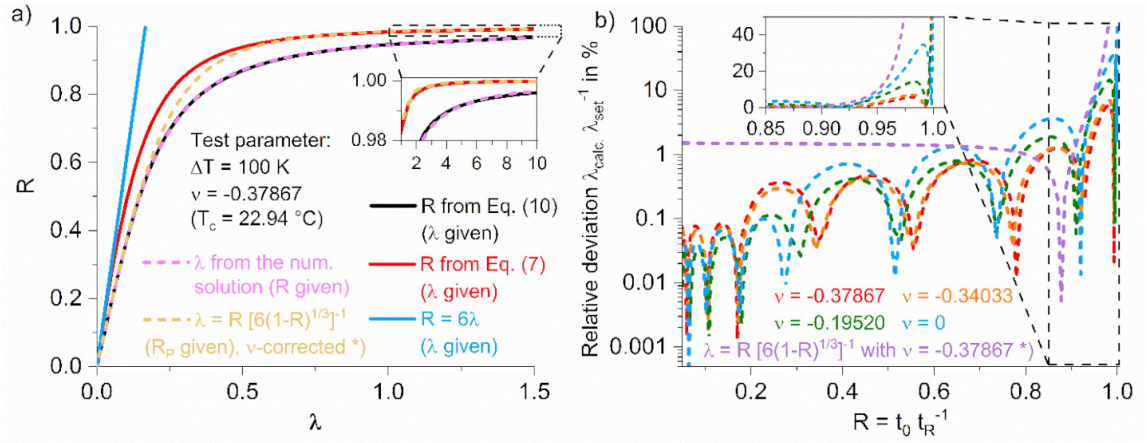

Figure S11. Recursive test of the numeric model (a) with the exact solution of R (black; λ solved by computation to exact match with a residual uncertainty of 1E-9); R recalculated by Equation (7) with the numerically calc. λ in in comparison to the simplified relations (red and blue) for R widely used in the literature. b) The residual deviation of R calc. by the numeric model for λ along the retention time exemplary for 4 different conditions within the range of validity for the model. Especially for poor retention with a certain field strength a more precise calculation of λ could be achieved, compared to the solution suggested by Schure, Schimpf and Schettler.[15]

*) corrected by ν with $R = 6\,\lambda\nu(1\text{-}R_{Parabolic}) + R_{Parabolic}$.[16] The average retention time (dRI peak apex) for all samples analysed in this work leads to R values below 0.8 representing less than 1.5% error in lambda, with error increasing as R approaches 1.

10. Development of equation (12) to be applied in equation (11) from the main article, g'' from peak apex to $g''(t_R)$ for the entire fractogram:

$$g''_i(R) = \left[\frac{S_{T,BRA}(M_{Seg,i})}{S_{T,LIN}(M_i)}\right]_{M_i} \qquad (11) \qquad \text{with} \quad M_{Seg,i}(R) \approx \frac{M_i(R)}{2B_{apex}+1}$$

$LCB_{i,\ ThFFF}$ [g_i from $g''_i(R)$] was found to be in good agreement for $R_{apex} << 1$. However, for poorly retained analytes a correction is needed.

Boundary conditions:

Empirically found for poor retention values

$$M_{Seg,i}(R_{apex} = 0.78) = \frac{0.8 \cdot M_{apex} + 0.2 \cdot M_i(R)}{1.6 \cdot B_{apex}+1}$$

and for good retention

$$M_{Seg,i}(R_{apex} \ll 1) = \frac{0 \cdot M_{apex} + 1 \cdot M_i(R)}{2 \cdot B_{apex}+1}$$

in good agreement to LCB_i ($M_{i,\ HT\text{-}SEC\text{-}D4}$), interpolated to $M_{i,\ ThFFF}$.

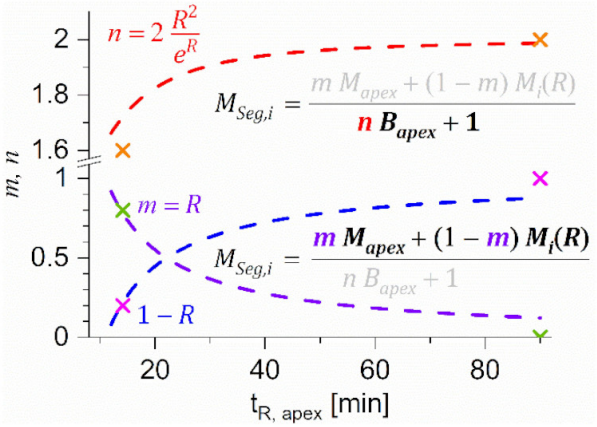

Figure S12. The development of a mathematical expression for the correction factor m in the numerator term and n in the denominator term. The dashed lines show the graphs of the equations for m and n matching the empirically found values as boundaries, symbolized by crosses.

Derived function containing the correction for low retention with R_{apex} as independent variable:

$$M_{Seg,i}(R) = \frac{R_{apex} \cdot M_{apex} + (1 - R_{apex}) M_i(R)}{\left(2 - \frac{R^2}{e^R}\right) B_{apex} + 1} \qquad (12)$$

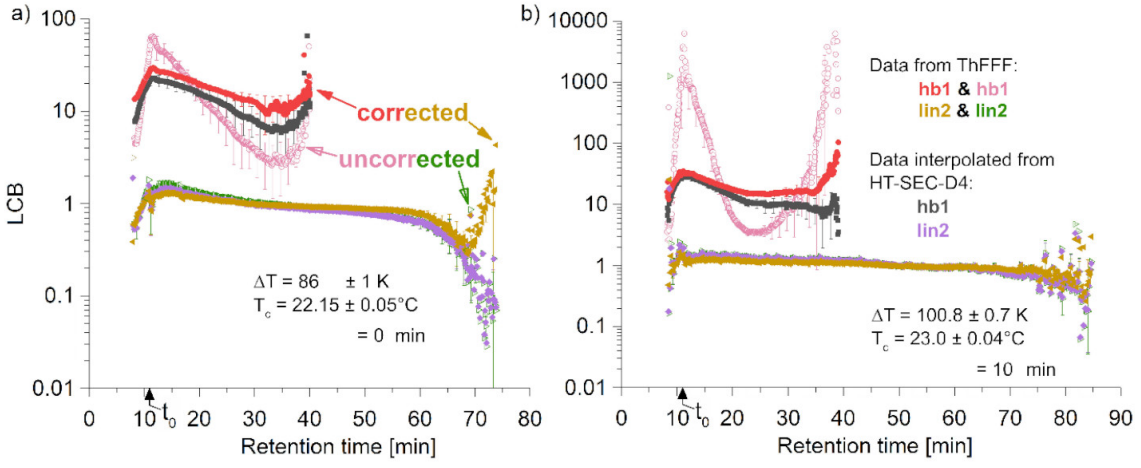

Figure S13. Superimposed data of $LCB_i[g(g'',t_R)]$, calculated for the entire fractogram of the hyperbranched sample and of the linear sample, separated without stop-flow and ΔT = 85 K (a) and with stop-flow of τ = 10 min ΔT = 100 K (b), calculated without correction of $M_{Seg,i}$ (pink and green) and with correction (red and yellow).

11. Cumulative and differential weight distributions of *LCB* and *g"*

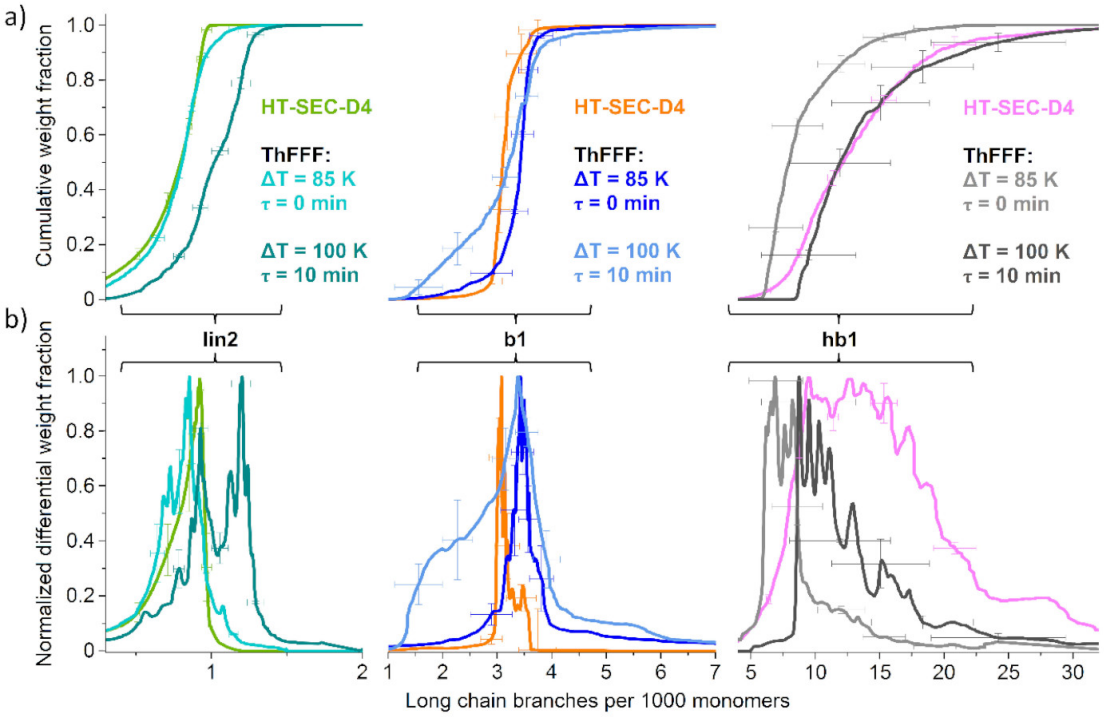

Figure S14. Superimposed cumulative weight (a) and normalized differential weight distributions (b) of *LCB* of three cwPE samples with different topology as shown in Fig. 7 in the main article.

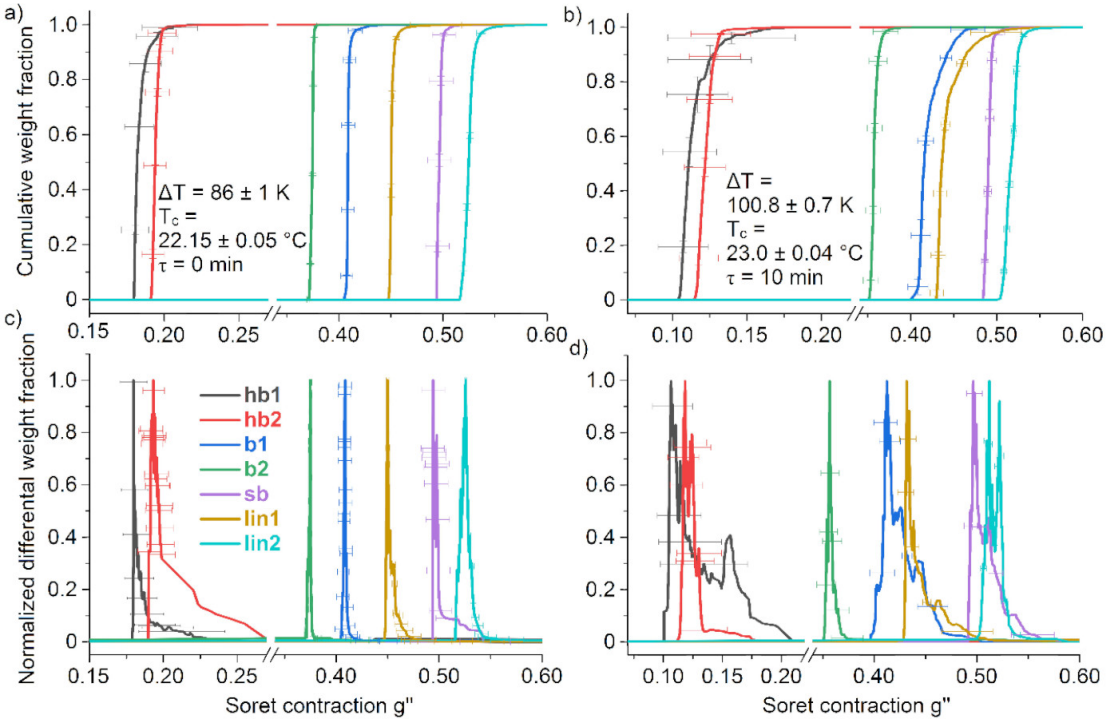

Figure S15. Superimposed cumulative weight (a) and normalized differential weight (b) distributions of *g"* calculated for all seven cwPE samples shown in Fig. 8 of the main article. The differential weight distribution analysis derived from the fractograms indicate, that stop-flow is not needed in order to improve the branching analysis. Avoiding stop-flow can even reduce other distorting influences,[17] which appear by a long stop-flow time.

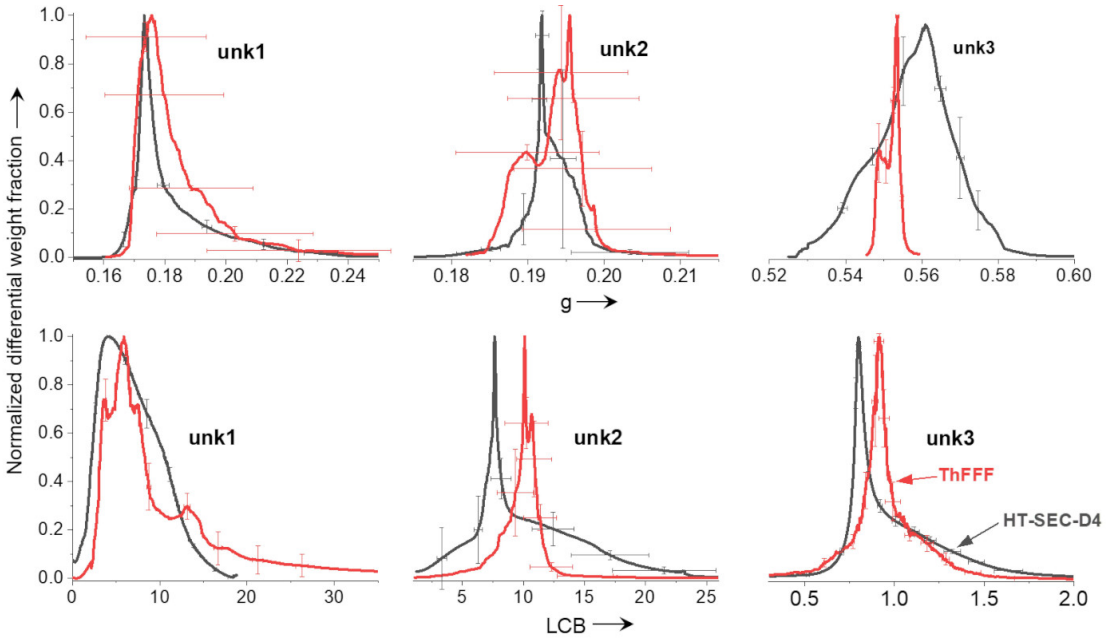

Figure S16. Superimposed normalized differential weight distributions of g and *LCB* of three different unknown cwPE samples, analyzed by HT-SEC-D4 (black color) and by ThFFF with the new approach (red color) as given in Eqs. (9) till (13) of the main article. The samples were synthesized with the same synthesis procedure and catalyst within the pressure and temperature limits like the samples hb1 to lin2 as described above. The ThFFF separation was done for unk1 and unk2 with ΔT = 100.9 ± 0.8 K, T_c = 22.98 ± 0.05 °C and for unk3 with ΔT = 84.2 ± 0.8 K, T_c = 22.07 ± 0.04 °C. The ThFFF experiments of all unknown samples were performed with a flow rate of 0.2 ml min^{-1} and τ = 0 min.

Table S6. Average characterization results of the unknown cwPE samples found by HT-SEC-D4 and ThFFF. The results of t_R, $g(g'')$ and $LCB[g(g'')]$ were generated from the dRI peak apex data.

	ThFFF					HT-SEC-D4			
Sample	M_w / kg mol^{-1}	$Đ$	t_R / min	$g(g'')$	$LCB[g(g'')]$	M_w / kg mol^{-1}	$Đ$	g_z	LCB_w
unk1	299 ± 11	1.13	13.9 ± 0.4	0.17 ± 0.02	9 ± 3	413 ± 3	1.63	0.20 ± 0.01	13.0 ± 0.7
unk2	263 ± 8	1.03	14.0 ± 0.2	0.19 ± 0.01	14 ± 4	394 ± 1	1.69	0.21 ± 0.01	13.7 ± 0.5
unk3	288 ± 16	1.07	32.8 ± 0.6	0.55 ± 0.01	1.1 ± 0.1	322 ± 2	1.08	0.560 ± 0.004	0.79 ± 0.03

12. Uncertainties and errors

Systematic errors

T, T_c	± (0.3 + 0.005 T) [T in °C]
Channel dimensions	height ± 4 µm, width ± 0.05 mm
Flow rate	± 1 %
Time	data collection interval 0.5 seconds
$\Delta\lambda$	≈ ± 0.1 % [Ref. [14]]

$$\frac{\Delta t_0}{t_0} = \left[\left(\frac{\Delta h}{h}\right)^2 + \left(\frac{\Delta w}{h}\right)^2 + \left(\frac{\Delta \dot{V}}{\dot{V}}\right)^2\right]^{0.5} + 0.83\ \% \approx 3\ \%$$

$$\lambda = \left(K_0 + K_1 \cdot \sqrt[3]{R} + K_2 \cdot \sqrt[3]{R}^2 + K_3 \cdot \sqrt[3]{R}^3 + K_4 \cdot \sqrt[3]{R}^4 + K_5 \cdot \sqrt[3]{R}^5 + K_6 \cdot \sqrt[3]{R}^6 + K_7 \cdot \sqrt[3]{R}^7\right)^{-1} = [f(R,\nu)]^{-1}$$

$$\Delta\lambda = \left|\left(\frac{\partial\lambda}{\partial R}\right)_\nu\right| |\Delta R| + \left|\left(\frac{\partial\lambda}{\partial \nu}\right)_R\right| |\Delta\nu| + 0.001\lambda = \frac{f^{-1}(R)_\nu}{[f(R,\nu)]^2}\Delta R + \frac{f^{-1}(\nu)_R}{[f(R,\nu)]^2}\Delta\nu + 0.001\lambda$$

$$\frac{f^{-1}(R)_\nu}{[f(R,\nu)]^2}\Delta R = \frac{K_1\cdot\frac{1}{3}R^{-\frac{2}{3}}+K_2\cdot\frac{2}{3}R^{-\frac{1}{3}}+K_3+\frac{4}{3}K_4\cdot R^{\frac{1}{3}}+\frac{5}{3}K_5\cdot R^{\frac{2}{3}}+2K_6\cdot R+\frac{7}{3}K_7\cdot R^{\frac{4}{3}}}{\left(K_0+K_1\cdot\sqrt[3]{R}+K_2\cdot\sqrt[3]{R}^2+K_3\cdot\sqrt[3]{R}^3+K_4\cdot\sqrt[3]{R}^4+K_5\cdot\sqrt[3]{R}^5+K_6\cdot\sqrt[3]{R}^6+K_7\cdot\sqrt[3]{R}^7\right)^2}\left\{\left[\left(\frac{\Delta t_R}{t_R}\right)^2+\left(\frac{\Delta t_0}{t_0}\right)^2\right]^{0.5}\cdot\frac{t_0}{t_R}\right\}$$

$$\frac{f^{-1}(\nu)_R}{[f(R,\nu)]^2}\Delta\nu = \frac{K_0'+K_1'\cdot\sqrt[3]{R}+K_2'\cdot\sqrt[3]{R}^2+K_3'\cdot R+K_4'\cdot\sqrt[3]{R}^4+K_5'\cdot\sqrt[3]{R}^5+K_6'\cdot R^2+K_7'\cdot\sqrt[3]{R}^7}{\left(K_0+K_1\cdot\sqrt[3]{R}+K_2\cdot\sqrt[3]{R}^2+K_3\cdot\sqrt[3]{R}^3+K_4\cdot\sqrt[3]{R}^4+K_5\cdot\sqrt[3]{R}^5+K_6\cdot\sqrt[3]{R}^6+K_7\cdot\sqrt[3]{R}^7\right)^2}\Delta\nu$$

with $K_x' = 0\ +(\ldots)_1+2(\ldots)_2\cdot\nu+3(\ldots)_3\cdot\nu^2+4(\ldots)_4\cdot\nu^3$; $\quad\frac{\Delta\nu}{\nu}=\left[\left(\frac{\Delta(\Delta\mathrm{T})}{\Delta\mathrm{T}}\right)^2+\left(\frac{\Delta\mathrm{T}_c}{\mathrm{T}_c}\right)^2\right]^{0.5}$

and $\frac{\Delta(\Delta T)}{\Delta T}=\frac{\Delta(\Delta\mathrm{T})_{random}}{\Delta T}+\left[\left(\frac{0.3+0.005T_{hot}}{T_{hot}}\right)^2+\left(\frac{0.3+0.005T_c}{T_c}\right)^2\right]^{0.5}$

Uncertainty calculations exemplarily for lin2 (see Table 1 in the main article):

$\frac{f^{-1}(R)_\nu}{[f(R,\nu)]^2}\Delta R = 0.00393381$ with t_R = 53.34 ± 3.3 min; t_0 = 11.035 ± 0.33 min

$\frac{f^{-1}(\nu)_R}{[f(R,\nu)]^2}\Delta\nu = 0.00077567$ with ν = -0.3762469

$$\frac{\Delta(\Delta T)}{\Delta T}=\frac{0.97\ K}{99.02\ K}+\left[\left(\frac{0.3+0.005\cdot 121.9\ °C}{121.9\ °C}\right)^2+\left(\frac{0.3+0.005\cdot 22.88\ °C}{22.88\ °C}\right)^2\right]^{0.5}=\underline{0.0294278}$$

$$\frac{\Delta\nu}{\nu}=[(0.0294278)^2+(0.002325)^2\ ]^{0.5}=\underline{0.0295195}$$

$$\Delta\lambda = 0.00393381+0.00077567+0.001\cdot 0.05557648 = \underline{0.00478181}$$

$$\frac{\Delta D}{D}=\left[\left(\frac{\Delta D}{D}\right)_{DLS}^{\ 2}+\left(\frac{\Delta D(T)}{D(T)}\right)_{Fit}^{\ 2}\right]^{0.5}=\left[(0.009562)_{DLS}{}^2+(0.0047242)_{Fit}{}^2\right]^{0.5}=\underline{0.010665}$$

$$S_T=\frac{1}{\lambda\Delta T}=\frac{1}{0.05557\cdot 99.02\ K}\qquad \Delta S_T=\left[\frac{\Delta\lambda}{\lambda}+\frac{\Delta(\Delta T)}{\Delta\mathrm{T}}\right]\cdot S_T=\left(\frac{0.00478181}{0.05557}+0.0294278\right)\cdot S_T=\underline{0.02098\ K^{-1}}$$

$$D_T=\frac{D}{\lambda\Delta T}=\frac{1.3738\cdot 10^{-7}\ \frac{cm^2}{s}}{0.0555765\cdot 99.02\ \mathrm{K}}$$

$$\Delta D_T=\left[\frac{\Delta D}{D}+\frac{\Delta\lambda}{\lambda}+\frac{\Delta(\Delta T)}{\Delta\mathrm{T}}\right]\cdot D_T=\underline{3.1488\times 10^{-9}\ \frac{cm^2}{s\ K}}$$

$$D_T=\underline{\underline{(2.5\pm 0.3)\times 10^{-8}\ \frac{cm^2}{s\ K}}}\qquad S_T=\underline{\underline{(0.18\pm 0.02)\ K^{-1}}}$$

13. References:

(1) Mundil, R.; Hermanová, S.; Peschel, M.; Lederer, A.; Merna, J. On the Topology of Highly Branched Polyethylenes Prepared by Amine−imine Nickel and Palladium Complexes: The Effect of Ortho-Aryl Substituents. *Polym. Int.* **2018**, *67* (7), 946–956.

(2) Plüschke, L.; Mundil, R.; Sokolohorskyj, A.; Merna, J.; Sommer, J.-U.; Lederer, A. High Temperature Quadruple-Detector Size Exclusion Chromatography for Topological Characterization of Polyethylene. *Anal. Chem.* **2018**, *90* (10), 6178–6186.

(3) Dockhorn, R.; Plüschke, L.; Geisler, M.; Zessin, J.; Lindner, P.; Mundil, R.; Merna, J.; Sommer, J.-U.; Lederer, A. Polyolefins Formed by Chain Walking Catalysis—A Matter of Branching Density Only? *J. Am. Chem. Soc.* **2019**, *141* (39), 15586–15596.

(4) Johnson, L. K.; Killian, C. M.; Brookhart, M. New Pd(II)- and Ni(II)-Based Catalysts for Polymerization of Ethylene and .Alpha.-Olefins. *J. Am. Chem. Soc.* **1995**, *117* (23), 6414–6415.

(5) Guan, Z. Chain Walking: A New Strategy to Control Polymer Topology. *Science* **1999**, *283*, (5410), 2059–2062.

(6) Koppel, D. E. Analysis of Macromolecular Polydispersity in Intensity Correlation Spectroscopy: The Method of Cumulants. *J. Chem. Phys.* **1972**, *57* (11), 4814–4820.

(7) Wyatt, P. J. Light Scattering and the Absolute Characterization of Macromolecules. *Anal. Chim. Acta* **1993**, *272* (1), 1–40.

(8) Müller, G.; Arndt, K. F. *Polymercharakterisierung*; Carl Hanser Verlag: München, Wien, Wien, 1996, 124–142.

(9) Lederer, A.; Burchard, W. *Hyperbranched Polymers*; Polymer Chemistry Series; The Royal Society of Chemistry, 2015.

(10) Flory, P. J. *Principles of Polymer Chemistry*; Cornell University Press: Ithaca, London, London, 1953, 283–303.

(11) Einstein, A. Über Die von Der Molekularkinetischen Theorie Der Wärme Geforderte Bewegung von in Ruhenden Flüssigkeiten Suspendierten Teilchen. *Ann. Phys.* **1905**, *322* (8), 549–560.

(12) Lederer, A.; Hartmann, T.; Komber, H. Sphere-Like Fourth Generation Pseudo-Dendrimers with a Hyperbranched Core. *Macromol. Rapid Commun.* **2012**, *33* (17), 1440–1444.

(13) Burchard, W. Solution Properties of Branched Macromolecules. In *Branched Polymers II*; Roovers, J., Ed.; Springer Berlin Heidelberg: Berlin, Heidelberg, Heidelberg, 1999; 113–194.

(14) Belgaied, J. E.; Hoyos, M.; Martin, M. Velocity Profiles in Thermal Field-Flow Fractionation. *J. Chromatogr. A* **1994**, *678* (1), 85–96.

(15) Schimpf, M. E.; Caldwell, K.; Giddings, J. C. *Field-Flow Fractionation Handbook*; John Wiley & Sons, Inc., 2000, 31–48.

(16) Martin, M.; Williams, P. S. Theoretical Basis of Field-Flow Fractionation. In *Theoretical Advancement in Chromatography and Related Separation Techniques*; Dondi, F., Guiochon, G., Eds.; Springer Netherlands: Dordrecht, 1992; 513–580.

(17) Smith, L. K.; Myers, M. N.; Giddings, J. C. Peak Broadening Factors in Thermal Field-Flow Fractionation. *Anal. Chem.* **1977**, *49* (12), 1750–1756.

8.5. Impact of Electron Beam Irradiation on Thermoplastic Polyurethanes Unraveled by Thermal Field-Flow Fractionation

Polymer Degradation and Stability 183 (2021) 109423

Contents lists available at ScienceDirect

Polymer Degradation and Stability

journal homepage: www.elsevier.com/locate/polymdegradstab

Impact of Electron Beam Irradiation on Thermoplastic Polyurethanes Unraveled by Thermal Field-Flow Fractionation

Martin Geisler[a,b], Tuhin Subhra Pal[c], Kerstin Arnhold[a], Mikhail Malanin[a], Michael Thomas Müller[a], Brigitte Voit[a,b], Jürgen Pionteck[a,*], Albena Lederer[a,b,d,*]

[a] Leibniz-Institut für Polymerforschung Dresden e. V., Hohe Str. 6, 01069 Germany
[b] Faculty of Chemistry and Food Chemistry, Technische Universität Dresden, 01062 Dresden, Germany
[c] Rubber Technology Centre, Indian Institute of Technology, Kharagpur, 721302 West Bengal, India
[d] Department of Chemistry and Polymer Science, Stellenbosch University, Private Bag X1, Matieland 7602, South Africa

ARTICLE INFO

Article history:
Received 16 September 2020
Revised 2 November 2020
Accepted 6 November 2020
Available online 8 November 2020

Keywords:
Electron beam irradiation
Thermoplastic polyurethane
Degradation
Crosslinking
Chain scission
Size-Exclusion Chromatography
Field-flow fractionation
Differential Scanning Calorimetry

ABSTRACT

The impact of electron beam irradiation on thermoplastic polyurethane material was studied for both an aliphatic and an aromatic polyurethane with approximately equal molar amount of hard and soft segments. Irradiation doses up to 300 kGy (kilogray) at room temperature and at 100 °C were applied. Changes in chemical structure, molar mass and size were assessed using infrared spectroscopy, differential scanning calorimetry, size-exclusion chromatography and thermal field-flow fractionation. Material alterations were correlated with trends regarding to degradation, crosslinking or branching changes. Thereby, limits of characterization by size exclusion chromatography are addressed and amended by thermal field-flow fractionation studies. In addition, a thermophoretic analysis has been carried out complementary to the portfolio of analytical methods applied in this work.

1. Introduction

The impact of irradiation on polymer materials has been widely studied in the past with the aim either to make materials more durable against environmental influences such as UV light [1,2] or to tailor material properties with regard to process engineering [3,4]. One polymer class being studied is thermoplastic polyurethane (TPU), which represents linear segmented block copolymers containing hard segments (adduct of di-isocyanate and small glycols as chain extender) and soft segments (polyester, polyether, etc.). These segments are connected by means of urethane linkages, which either mix or segregate depending on chemical composition and produce homogeneous or phase separated morphologies [5,6]. A comprehensive introduction into irradiation on polymers in general and with focus on TPU is given by Adem et al. [7].

So far, all studies dealing with irradiation of TPU focus on chemical alteration investigated by spectroscopy [2,8,9], crystallization changes monitored by diffraction techniques and thermal analysis [9–11] and property changes by mechanical analysis [12,13]. Only few studies take the changes in molar mass into account monitored by means of standard size exclusion chromatography (SEC) with standard calibration [14–17] or by absolute molar mass measurement using SEC coupling to multi-angle light scattering (MALS)[18]. However, using SEC, one has to be aware of some analytical challenges which may occur, like delayed elution behavior [19] or mixed elution due to branching or fraction of high molar masses beyond the separation range of SEC, which are generated by crosslinking [20]. In particular, for SEC with standard calibration used in this context, significant errors must be considered. Thus, our aim in this study is to apply thermal-field flow fractionation (ThFFF), a channel-based separation technique, as an alternative to SEC to get a comprehensive overview on changes in size and topology of the polymers causing different bulk, mechanical or thermodynamic properties, which cannot be followed in-depth by spectroscopic methods or thermal analysis only. This type of separation relies on the retention of analytes in an empty flat ribbon-like channel due to a response on a separation force field applied perpendicularly to the flow direction. Depending on the nature of the force field, a separation e.g. according to hydrodynamic size (AF4), effective mass (SdFFF), electrophoretic mobility (ElFFF) or thermal

* Corresponding authors.
E-mail addresses: pionteck@ipfdd.de (J. Pionteck), lederer@ipfdd.de (A. Lederer).

https://doi.org/10.1016/j.polymdegradstab.2020.109423
0141-3910/

diffusion (ThFFF) can be realized [21]. For this study we have chosen ThFFF since this separation technique can be highly selective for changes in the polymer topology [22–24] and/or chemical composition [25–29]. Details on the basic separation principle are given elsewhere [21,30] and in the supporting information (SI, Section 1). FFF is usually coupled to a series of detectors (MALS, dRI, UV, online dynamic light scattering or offline Fourier transform infrared spectroscopy (FTIR)) [31–35], though, the analysis of the separation itself contains already useful information. This is because the measurement of the retention ratio R (void time over retention time) at given field strength allows the determination of the physicochemical parameter describing the response to the force field. For ThFFF, this response is described by the Soret coefficient S_T, which is the ratio of thermal and translational diffusion [36,37]. Thermal diffusion is mainly influenced by the polymer-solvent interaction [38,39] and by the effective length of a linear polymer segment, respectively [23,40], whereas the translational diffusion at equal conditions depends to a great extent on the hydrodynamic size of the analyte [41]. Consequently, in combination with the associated analytical tools such as thermal analysis and FTIR spectroscopy, S_T is accounted to be a suitable parameter for structural characterization within this study.

2. Experimental

2.1. Sample preparation and treatment

The TPU samples used in this study were L780D10 (aliphatic polyester-TPU, assigned as Aliph-TPU) of the composition 4,4′-dicyclohexylmethane diisocyanate (H_{12}MDI) copolymerized with 1,4-butanediol (BD) and a segment of poly(1,6-hexylene adipate), and C74D50 (aromatic polyester-TPU, assigned as Ar-TPU) composed of diphenylmethane diisocyanate (MDI), BD and poly(1,4-butylene adipate). Both TPU are commercial products by BASF Polyurethanes GmbH. The structures are given in the SI (Fig. S9 and sect. 2). Rectangular samples of dimension approximately 40 mm x 10 mm were cut from a bulk polyurethane sheet and were irradiated in a special irradiation chamber [42] using an electron accelerator ELV-2 (manufactured by Budker Institute of Nuclear Physics, Novosibirsk, Russia; see Fig. S3, SI) [43]. Prior to irradiation the samples were dried at 40 °C for 4 h under vacuum in the vacuum oven. After the drying process the polyurethane sheets were placed into the irradiation chamber. Before irradiation, the temperature was firstly heated up to 80 °C and kept for 5 min under vacuum in order to remove the moisture and oxygen. Subsequently, the temperature was cooled down to the target irradiation temperatures in the nitrogen atmosphere. The irradiation was carried out with constant electron energy (1.5 MeV) and electron current (4 mA), the dose was applied by several steps of 25 kGy until the target dose had been reached.

2.2. Thermal analysis

Thermogravimetric Analysis was performed using a TA Instruments TGA Q 500 (V20.13 Build 39) in the range between 35 and 600 °C. The experiments were performed under constant nitrogen purge of 25 ml min^{-1} and a nominal heating ramp of 10 °C min^{-1}. DSC analysis was performed with a DSC 2500 differential scanning calorimeter by TA Instruments, Inc., USA, equipped with a liquid nitrogen accessory. For all analyses, a sample weight of approximately 10 mg per measurement was analyzed under a constant nitrogen purge in Tzero-Al hermetic with perforated lid. Aliph-TPU was analyzed by the following method: Isothermal equilibration at −90 °C for 5 min, followed by a preheating run to 80 °C. After a 30 s isothermal hold, the sample was cooled down again to −90 °C with another 5 min isothermal equilibration. Then the first heating scan was performed to 250 °C. After a 30 s isothermal hold the cooling scan was performed to −90 °C with an isothermal equilibration step for 5 min, before the second heating run up to 280 °C was done. All heating and cooling scans/runs in this method were carried out with a ramp of +/−10 °C min^{-1}. Ar-TPU was analyzed instead by the following method: Isothermal equilibration at −90 °C for 5 min, followed by the first heating scan to 250 °C. After a 30 s isothermal hold the cooling scan was performed down to −90 °C with an isothermal equilibration step for 5 min, before the second heating run up to 280 °C was done. The heating scans were performed with a ramp of +40 °C min^{-1} and the cooling scans a ramp of −10 °C min^{-1}. Melting (T_m) and crystallization temperatures ($T_{c,m}$) were taken as the maximum of the endothermic transition, whereas glass transition temperatures (T_g) were taken as onset and as midpoint at half of the step height in heat capacity Δc_p. Data recording and analysis of both, TGA and DSC analyses was done with the Software Universal V4.5A by TA Instruments, Inc., USA.

2.3. Spectroscopic methods

Attenuated total internal reflection-Fourier transform infrared analysis (ATR-FTIR) was carried out at room temperature using a TENSOR 27 infrared spectrometer (Bruker Optik GmbH, Germany) equipped with a MIRacle^{TM} diamond crystal ATR accessory (PIKE Technologies, Inc., USA). 32 scans were taken and averaged per spectrum in the spectral region 4000 to 400 cm^{-1} at a resolution of 4 cm^{-1} with a scan rate of 10 kHz. Data evaluation, including baseline correction and vector normalization [44,45] for valid comparison, was done with the spectroscopic software OPUS, version 7.5 (Bruker Optik GmbH).

^{1}H NMR spectra were recorded with a Bruker Avance III spectrometer operating at 500.13 MHz. DMSO–d6 was used as solvent, lock, and internal standard [$\delta(^1H)$ 2.50 ppm]. The spectra were recorded using the standard pulse programs included in the Bruker Topspin 3.2 software package.

2.4. Size-exclusion chromatography

SEC analysis was performed with a set up composed of an HPLC-Pump 1200, a Polar Gel-M separation column (300 × 7.5 mm; 8 µm) (both by Agilent Technologies, Inc.) coupled to a TREOS II 3-angle light scattering detector by Wyatt Technology, Corp. and a K-2301 dRI detector (generic) by KNAUER Wissenschaftliche Geräte GmbH, Germany. The samples were dissolved in 500 µl *N,N*-dimethylacetamide with 0.5% (di-n–butyl)amine and filled up to 1 mL with *N,N*-dimethylacetamide (with 3 g L^{-1} LiCl), which was also the eluent for the separation. For each run, a sample volume of 20 μL was injected and separated with a flowrate of 1.0 mL min^{-1}. Data recording and evaluation was done with the Astra® Software, Version 6.1.2 and 7.3.1.9.

2.5. Thermal field-flow fractionation

ThFFF experiments were carried out with a TF2000 set up, consisting of an isocratic pump, degasser, auto-sampler, actively heated and cooled ThFFF channel, PN3621 21-angle light scattering (MALS) detector with a laser of the wavelength 532 nm and PN3150 differential refractive index (dRI) detector (all by Postnova Analytics GmbH, Germany). The cold wall block was cooled by a liquid cooling circuit with a refrigeration unit Unichiller® 025-MPC (2.5 kW) by Peter Huber Kältemaschinenbau GmbH (now AG), Germany. The channel dimensions were 45.6 cm tip-to-tip length, width 2 cm and a thickness of 250 µm, realized by spacers made of Mylar A® and Teonex®. A constant flow rate of 0.3 mL min^{-1} was applied for all separations with the optimized temperature

drop program as given in Fig. S4, SI. As solvent and carrier fluid pure *N,N*-dimethylacetamide (ReagentPlus®, ≥ 99%, Sigma-Aldrich Chemie GmbH, Germany) was used. The void time in all separations was 12.36 min (incl. the stop-flow time of 5 min). A channel pressure of about 0.6 to 1 MPa was adjusted for the used flow rate by a back-pressure tubing (inner diameter 0.001“) between the ThFFF channel and the MALS detector in order to maintain the stability of the dRI baseline and to avoid possible accumulation of gas bubbles due to residual dissolved gas in the carrier fluid. The samples were dissolved in *N,N*-dimethylacetamide + 0.125% (v/v) (di-n–butyl)amine in a concentration ca. 4.3 mg mL^{-1} and the injection volume for all separations was 102.5 µL. The data recording and analysis was carried out with the TF2000 version of the NovaFFF software.

3. Results and discussion

We have chosen an aliphatic and an aromatic TPU with comparable hard- and soft segment composition (confirmed by ^{1}H- and ^{13}C NMR, see SI, Fig. S9). In the case of aliphatic TPU a temperature dependency during electron beam irradiation has been already investigated revealing an almost negligible effect of the irradiation temperature on the material alterations observed [7]. However, for aromatic TPU such an investigation has not been reported yet. Therefore, the irradiation studies of the aromatic TPU are performed for irradiation temperatures at room temperature (RT) and 100 °C, whereas the aliphatic TPU study is done solely for room temperature.

3.1. ATR-FTIR analysis

In the ATR-FTIR spectra of both materials, the typical bands of a regular TPU are found (see Fig. 1). Both specimen spectra contain the broad bands of N–H stretching vibrations at 3320 cm^{-1} (amide A), of the asymmetrical and symmetrical C–H stretching vibrations 2925 cm^{-1} and 2850 cm^{-1} of methylene groups of aliphatic chains, followed by the amide I band (around 1700 cm^{-1}), amide II (around 1530 cm^{-1}), amide III (1220 cm^{-1}) and amide IV (780 cm^{-1}). Ar-TPU shows additionally remarkable specific bands of C=C aromatic ring stretching vibrations (at 1595 cm^{-1} and 1410 cm^{-1}), of aromatic C–N stretching vibration at 1307 cm^{-1} [46], and at 815 and 751 cm^{-1} (C–H out of plane bending vibrations) [47–49]. There are also additional bands at 2960 and 2873 cm^{-1} assignable to methylene groups (asymmetrical and symmetrical C–H stretching vibrations) adjacent to butanediol-adipate functionality [50]. Both TPUs contain bands of C–O–C stretching vibrations in the range 1100–1000 cm^{-1} (as a part of urethane group [44,67] adjacent to the linear aliphatic chains of extenders in both hard and soft segments and simultaneously as stretching C–O–C vibration of ester group in soft segments) [42,49]. In contrast to Aliph-TPU, the spectrum of Ar-TPU irradiation exhibits two distinct bands in the region of amide I band, which are assigned to free carbonyl groups (1725 cm^{-1}) and hydrogen-bondings (1701 cm^{-1}) [51]. In the case of Aliph-TPU the band of free C=O groups appears as a shoulder reflecting higher amount of hydrogen bonding, i.e. lower amount of free urethane groups in the pristine materials. Generally, it can be stated that electron beam irradiation up to the maximum applied dose in this study only slightly impacts the TPU materials. Intensity changes for amide I/II/III and other bands of the urethane group as well as bands of methylene group can be observed, however, the degradation dynamics between both TPU materials differs depending on the chemical structure of the hard segments.

Already upon the lowest investigated irradiation dose (25 kGy) significant alterations in Aliph-TPU on the molecular level can be observed in the vibrational spectra: the amide I, II and III bands in the spectrum of Aliph-TPU decrease in intensity. Simultaneously, the bands of C–H and N–H stretching vibrations (Fig. 1, insets A1, B1 and A2, B2) become more intensive. This may be explained by induced chain scission/urethane group degradation in the hard segments and formation of primary amines [7]. Simultaneously, the broadening of amide I on the left band side at around 1800 cm^{-1} indicates presence of non-associated carboxylic acid groups [49]. Formation of primary amines and carboxylic acid as a result of irradiation degradation of TPU was reported previously [2,7,44] and may occur even under vacuum [48]. Elevated irradiation dose (50 kGy and higher) initiates an increase of the three aforementioned amide bands and at the same time a decrease with broadening of the N–H stretching vibration band(s) in the range 3400 – 3100 cm^{-1} with the most intensive one around 3300 cm^{-1} (Fig. 1, insets A1, A2). The stronger band at about 1700 cm^{-1} is explained on one hand by a stronger hydrogen bonding as stated above and on the other hand by associated carboxylic acids, which have strong bands around the same frequency regions (ca. 3300, 1700 and 1200 cm^{-1}; stretching vibration of OH, C=O and C–O groups, respectively) [49]. Surprisingly, the amide II band becomes more intensive too, regardless of urethane functionalities loss. This can be explained by an adjacent reaction between primary amines and carboxylic acids resulting in the formation of secondary amides as it may occur under harsh conditions without catalysts or coupling agent [52,53]. This hypothesis is supported by a subtle broadening of the amide I band on its right lower frequency slope (Fig. 1, inset C1) including contributions from secondary and primary amines (both absorb around 1650 cm^{-1}) [49]. Furthermore, the finding is explained by a non-linear behavior of N–H and $–CH_2–$ (methylene group) stretching vibration band intensities as a function of irradiation dose (≥ 50 kGy).

Similar to Aliph-TPU, also in Ar-TPU major noticeable changes in the material can be seen for the lowest investigated irradiation dose (25 kGy). Remarkable band intensity decreases of the methylene stretching vibration bands at 2920 and 2850 cm^{-1} were found, referring to aliphatic chain scissions. A slight band intensity drops of C–O–C urethane or ester group at 1065 cm^{-1} is observed, whereas other methylene group bands (e.g. in the vicinity to adipate carbonyls, soft segments) are found to remain almost constant. In addition, specific aromatic bands of the hard segments kept their intensity and profile or alter only marginally in comparison with other bands. This can be interpreted as a sign of chemical reactions starting at the hard- soft “interface” of the segments or within chain extender segments and in soft segments. Hence, contrary to the aliphatic material, in Ar-TPU the linear aliphatic chain extenders in the hard segments as well as the aliphatic part of the soft segments seem to degrade both. However, taking a certain crystallinity (discussed in Section 3.2) into account (signs of hydrogen bonding), we conclude that the soft segments are predominantly degraded. The amide bands of urethane increase in intensity, showing a probable formation of new groups (carboxylic acids, amides). With increasing of the irradiation dose (≥ 50 kGy) the amide I, II, III bands and N–H stretching vibration band become either more intensive and slightly broader (around 1640 and 1230 cm^{-1}) or change their intensity only negligibly. The intensity changes of methylene bands (at 2920, 2850 cm^{-1}) has no definite correlation with irradiation dose, which is an indication of multiple chain scission and recombination involving new functional groups (carboxylic acids, amides). The total non-linear band dynamics and the changes in the amide bands are similar to Aliph-TPU as discussed above.

From the findings by ATR-FTIR, we conclude that electron beam irradiation produces a cascade of similar parallel chemical reactions in the case of both TPUs including chain scission, chain recombination or branching as well as formation of new functionalities (amines, amides, carboxylic acids). The main irradiation response distinction between our systems is the location of the reac-

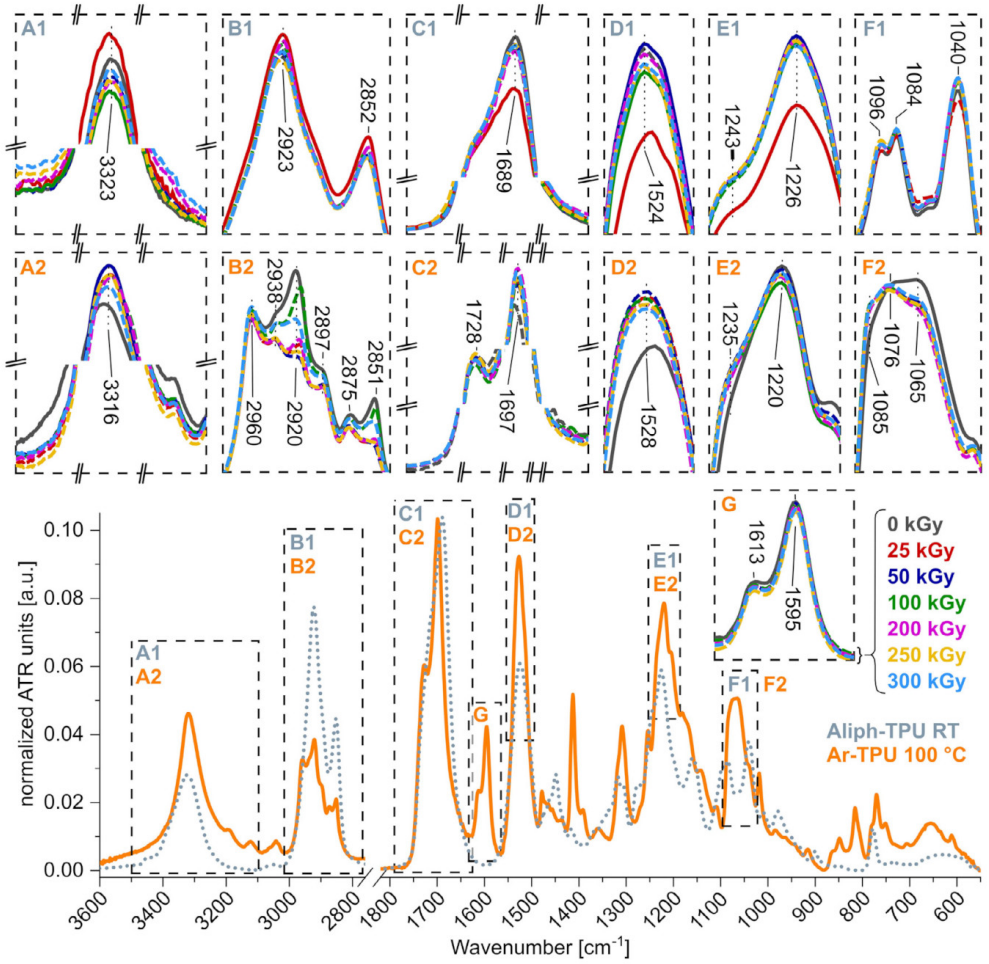

Fig. 1. The vector-normalized ATR-FTIR spectra of the aliphatic (insets with no. **1**) and the aromatic (insets with no. **2**) TPU irradiated with different effective doses. The full spectra are presented for the non-irradiated materials, whereas the insets illustrate superimposed bands with significant changes. **A1** and **A2** show enlarged plots of the band region for N–H stretching, **B1** and **B2** show the region of C–H stretching. The insets **C1** to **E1** and **C2** to **E2** display the Amide I, II and III bands, respectively. **F1** and **F2** indicate the bands of C–O–C stretching vibrations. Solely for Ar-TPU, the aromatic ring vibration band in is shown in inset **G**. Highly overlapping graphs in A to G are displayed in dashed lines.

tion/alternation onset. The hard segments (urethane functionality) undergo chemical alternations first in the case of Aliph-TPU and the spectra of Ar-TPU show the chain extender of both soft and hard segments and soft segments degrade faster than the hard segment cores (urethane and aromatic groups), but in general, in the case of TPUs it mainly depends on the formulation of the material. Earlier publications on aromatic TPUs [2,54] reported photo Fries rearrangement or oxidation of the central $-CH_2-$ unit in the MDI segments. There is also an example for moderately irradiated aromatic TPU, where significant changes in the soft segments may take place [55].

3.2. DSC-Analysis

Both TPU materials remain largely unaffected up to 270 °C as found by thermogravimetry (T = 285 °C at 2% weight loss; see SI, Fig. S5), although a slight mass loss of ca. 0.5% is detected in the first full heating scan for both materials starting above 120 °C regardless of the irradiation, which causes a low and broad endothermic peak in the DSC endotherms (see Fig. S6, SI). This can be accounted to the loss of water entrapped in the material.

The DSC analysis of Aliph-TPU shows in the first heating scan without pretreatment of the sample a relaxation peak superimposing the glass transition region. This phenomenon is well known for polymer glasses in general and originates from physical aging, e.g. by long storage of the material not far below the glass transition temperature [56,57]. Therefore the DSC analysis of Aliph-TPU was performed with a preheating step up to 80 °C prior to the first full heating scan in order to drive out relaxation effects. With preheating, the endothermic peak was not observable in the following heating scans anymore. Overall, no signs of melting or crystallization were found in the DSC thermograms, which indicates that Aliph-TPU is thoroughly amorphous.

Therefore, a clear glass transition was observed at around 45 °C (half step height), which shows a slightly decreasing trend in the glass transition temperature (T_g) in correlation to the irradiation dose from 0 kGy to 300 kGy (see Fig. 2). Thereby the step height of glass transition Δc_p does not show any significant trend,

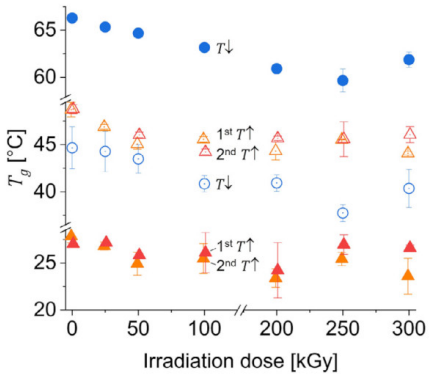

Fig. 2. Glass transition temperatures (T_g) of Aliph-TPU measured in the first heating scan (orange), in the cooling scan (blue) and in the second heating scan (red). Filled symbols display onset T_g and open symbols show mid-point T_g at half step height.

which indicates that the amorphous part of the material does not change significantly under impact of irradiation (see Fig. S8 A, SI). The slight decrease in T_g indicates isomerization or chain scission [58,59]. Furthermore, crosslinking cannot be excluded, because degraded molecules of lower molar mass may act additionally as plasticizer, which would induce a decrease of T_g, in contrast to the expected increase in T_g in case of crosslinking [60].

In contrast to Aliph-TPU, Ar-TPU shows in the first heating no glass transition and in the subsequent cooling as well as in the second heating thermograms only a weak, and much broader glass transition, which refers to the soft segments behavior (see Fig. S7, SI). A slight increase in T_g for both investigated irradiation temperatures is observed, which is accounted to crosslinking. In contrast to Aliph-TPU, Ar-TPU showed distinct melting and crystallization peaks, respectively, identifying it as material with higher crystallinity. As illustrated in Fig. 3B to D, melting and crystallization show both an intrinsically complex multiple phase transition behavior with superimposed effects that are enhanced by irradiation. The first heating scan showed in general only one higher melting peak at about 226 °C accompanied by one lower shoulder-like melting peak at about 207 °C. This corresponds somewhat to the bimodal crystallization peaks found in the cooling scans. However, the second heating scans indicate a multimodal melting behavior. The DSC heating scans were performed intentionally with a higher heating rate (40 K min^{-1}). In previous studies reorganization and superheating effects during melting could be sufficiently suppressed [61,62]. However, recent studies confirmed that reorganization effects may still occur also at higher heating rates [63]. Hence, we account this multimodal melting behavior in first instance as reorganization effects. The melting peak assigned with S at 130 - 135 °C in Fig. 3D possibly refers to a soft segment rich phase, whereas the following melting peak 1 at around 185 °C may represent the melting of a mixed phase with higher hard segment content near the interface of the hard domains. The mixing of hard and soft segments at the interface of crystallites is reported to originate from the molar mass dispersity of the hard segments, which causes a fraction-wise crystallization depending on their segment length [64,65]. Peak 2 corresponds to non-perfectly crystallized domains and peak 3, thus, refers to well-ordered crystallites. Microphase mixing, also superimposed to the observed melting behavior, can be discussed as an origin of the observed reorganization effects. This was also reported in previous studies for TPU with high hard segment content [63,66]. With increasing irradiation dose, the amount of imperfect crystallites as well as assumedly mixed-phase crystallites increases tremendously. At the same time, the number of well-ordered crystallites (Peak 3) with high hard segment content decreases (irradiation at RT) or almost disappears (irradiation at 100 °C), respectively, as indicated in Fig. 3D and confirmed by the enthalpy fractions from peak deconvolution (principle exemplarily shown in Fig. 3A) of the multiple melting peaks (Fig. 3J and K). The trend to form crystallites or domains of lower order is consistently found in the thermograms of the cooling scan with an increasing amount of material crystallizing at lower temperature (Peak 1, see Fig. 3H and J). However, the reverse image of the multimodal phase transition (Fig. 3D) cannot be observed in the cooling scans. Furthermore, no significant differences in the overall enthalpy is seen between melting and cooling scans as well as with regard to irradiation dose (see Fig. S8 B, SI). This confirms on the one hand that no significant chemical transformations occurred in the DSC scans and on the other hand that the multimodality found in the second heating is merged in the sharp crystallization peak, which can be explained by delayed crystallization far below the melting point(s) equilibrium due to absence of nuclei.

Next to the variation in fractions of melting and crystallization enthalpy stated above, all peaks, except in the first heating and peak 1 in the second heating show decreasing trends in the (peak apex) melting temperatures (T_m) and crystallization temperatures ($T_{c,m}$), respectively, correlating with the irradiation dose (see Fig. 3E, F, G). The constant T_m, peak 1 of the second heating scan (see Fig. 3D and Fig. S6, SI) originates most probably from a fraction in the outer part of domains containing a significant amount of soft segments. In that, the phase mixing and resulting crystallization seems not to be altered significantly by irradiation. Alternatively, changes could be disguised by other effects such as melting of different polymorphs like lamella or spherulite [67,68] and/or different discrete domain sizes, which possibly superimpose the observed overall melting behavior of the pristine or irradiated sample. However, an in-depth investigation of this issue would go beyond the scope of this work and needs to be addressed in a future study.

Meanwhile, the temperature shifts and the shifts from well-ordered to increasingly disordered crystallites and domains indicate that irradiation induces isomerization, branching or topology changes, degradation due to chain scission or, oppositely, crosslinking. Indications for chain scissions and possible recombination results in assumedly altered microstructure in agreement to the findings by ATR-FTIR.

With regard to the irradiation temperature, we found that the irradiation at elevated temperature leads to a stronger shift from well-ordered crystallites to disordered crystallizing domains in comparison to room temperature, where a certain high melting fraction remains (Fig. 3J and K). Interestingly, the decrease in Peak 3, which differs between the series at RT and 100 °C, correlates to the different behavior of peak 2, whereas the increase of peak 1 induced by irradiation is not significantly dependent on the temperature during irradiation. This supports the assumption that peak 1 refers to a not significantly affected by irradiation crystallite phase near the interface of the hard domains, which also contains soft segments. In contrast to the enthalpy fractions, the melting and crystallization temperatures do not show significant differences in dependence to the irradiation temperature. The observed differences allow the conclusion that the elevation of the irradiation temperature mainly increases the reaction rate of formed radicals leading to an increase in branching or crosslinking, but does not induce further changes e.g. in the chemical composition of the hard segments. In a recent study on electron beam irradiation of aromatic TPU chain scission or branching is reported to assumedly prevail over possible crosslinking reaction [69]. However, for thorough understanding of the observed effects in the material investigated in this work with regard to irradiation dose and temperature

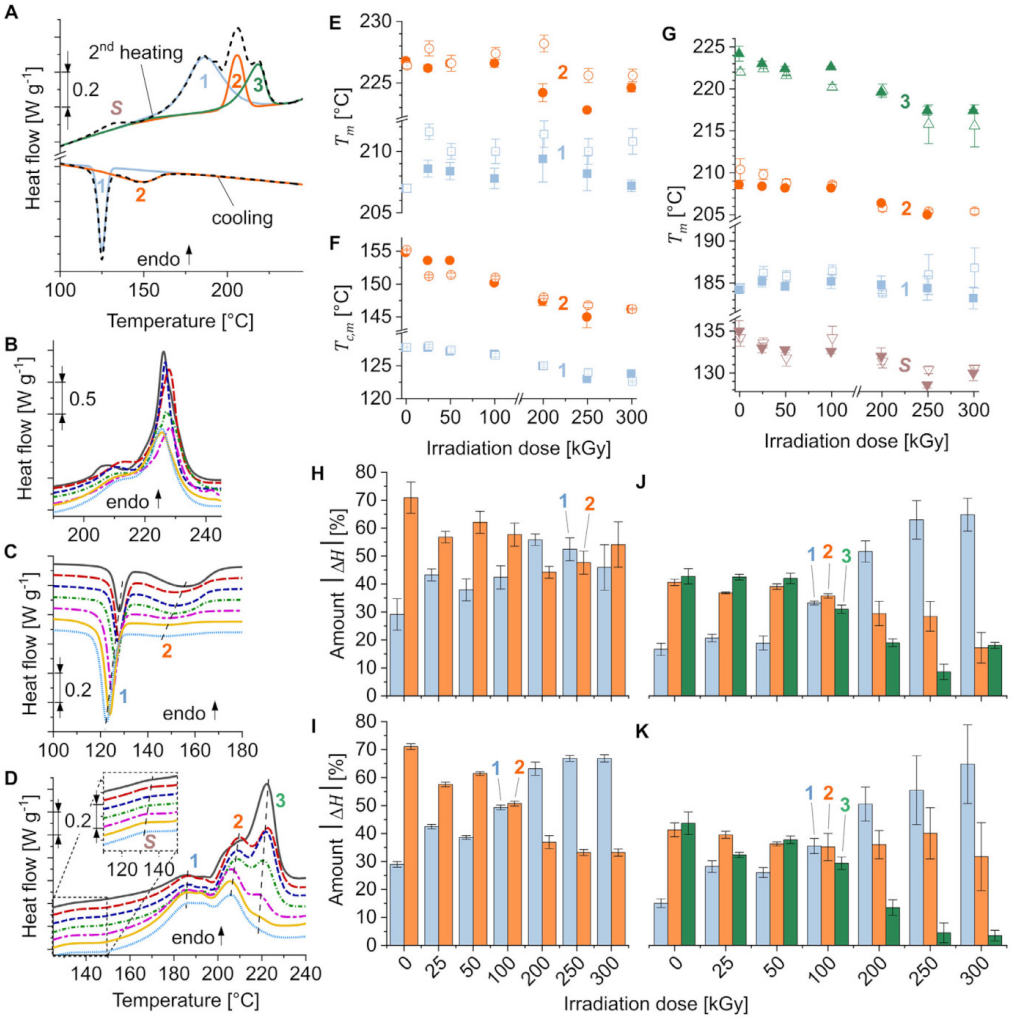

Fig. 3. Melting and crystallization analysis of Ar-TPU by peak deconvolution (exemplarily shown in **A**) of DSC-thermograms shown here for the series irradiated at 100 °C in **B** with the melting peaks of the first heating, in **C** the crystallization peaks of the cooling scan and in **D** melting peaks of the second heating scan. The corresponding full thermograms for both series irradiated a RT and 100 °C are given in the Fig. S6, SI. The dashed lines in C and D are for guiding the eyes. The thermograms were shifted in y-axis for better visibility. **E** indicates melting temperatures (all peak apexes) of the first heating and **G** of the second heating scan. **F** shows crystallization temperatures of the cooling scan. Open symbols in **E** to **G** represent the series irradiated at room temperature and filled symbols the series irradiated at 100 °C. The relative amount of the melting and crystallization enthalpy is displayed from the deconvolution of the series irradiated at room temperature (**H, J**) and at 100 °C (**I, K**) of the cooling (**H, I**) and the second heating scan (**J, K**).

a comprehensive, separation-based molar mass, size and conformation characterization is needed.

3.3. Size exclusion chromatography

Generally, when irradiation is applied to polymer material a vast number of different processes such as chain scission [70], crosslinking [71], branching [3,4], degradation [1,72,73], decomposition [74] or chemical transformations [70] e.g. oxidation [75] must be taken into account. For TPU materials irradiated under inert conditions mainly chain scission, increase of branching and crosslinking need to be considered [2,55]. Up to now, molar mass characterization of irradiated TPU is frequently carried out by SEC but mainly on the basis of relative calibration by polymer standards of narrow dispersity [16,69,76,77]. However, particular fractions of branched polymers tend to elute not just according to their size, as it is expected for entropy mode elution. Fractions containing long chain branches are hypothesized in the literature to elute delayed as a consequence of anchoring effects of branches with the column packing material [19]. Co-elution with less branched fractions of lower molar mass but of equal hydrodynamic size can result too [78,79]. Therefore, the comparability of the analyzed polymer species to the used calibration standards and consequently the accuracy of the reported molar masses may be affected. An absolute molar mass determination by means of SEC coupled with MALS and dRI (differential refractive index) detection is therefore recommended and was already used in previous irradiation studies of PU material [18]. In this study, we performed a comparison of different calculation methods. Molar mass calculation based on a calibration with polystyrene standards led clearly to erroneous molar mass moments in terms of number (M_n) and weight average

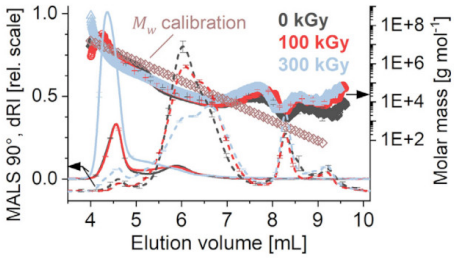

Fig. 4. SEC-MALS-dRI chromatogram of the aliphatic TPU measured in *N,N*-dimethylacetamide (+ LiCl, 3 g L^{-1}). The solid line indicates the MALS signal and the dashed line is the dRI response. The molar mass from calibration with narrow polystyrene standards is illustrated here for comparison.

(M_W) and an overestimation of the molar mass dispersity $Đ = M_W M_n^{-1}$ (see Fig. S19, SI).

SEC-MALS-dRI analyses of both TPU series show a broad range in molar mass and size and with regard to the impacted irradiation dose a decrease of the main fraction accompanied by an increase of both, fractions of lower and higher molar masses (see Fig. 4 and Fig. S11, SI). Thereby a good resolution is achieved in the lower and medium molar mass range up to 10^6 g mol^{-1}, whereas for molar masses beyond that the separation performance is significantly reduced. The SEC-analysis revealed that already the untreated version (0 kGy) of Aliph-TPU contains a certain fraction of higher molar mass, whereas for Ar-TPU this fraction shows very weak MALS response in an insignificantly low concentration. However, for both TPU series an abnormal elution behavior for both, the lower molar mass fraction as well as the ultra-high molar mass region (irradiated samples only) is observed, which also negatively affect the analysis of the polymer's conformation (see Fig. S11 and S12, SI). Non-ideal elution behavior in SEC for hyperbranched PU material was also reported previously [80]. This is one additional reason that molar mass determination based on relative calibration for a non-purely entropy-based separation leads to false interpretation and therefore methods for an absolute molar mass and size determination are definitely required.

3.4. ThFFF analysis

3.4.1. Molar mass, size and weight fraction analysis

To overcome the challenges in SEC a change of the separation mechanism to FFF with a much broader separation range may be a helpful alternative as it has been reported previously [19,81]. Among various FFF sub techniques, ThFFF may provide further information about intrinsic material properties such as differences in chemical composition [19,25,29] (with changed solvent interaction) or differences in topology[22–24,29] by means of thermophoresis. ThFFF is a valuable complementary technique to SEC as its separation range does not completely cover the range of SEC for low molar masses (see, Fig. S19, SI).

In fact, the fractograms of the ThFFF (see Fig. 5A) indicate that molar masses below 10^4 g mol^{-1} cannot be sufficiently resolved and elute together with the void peak at t_0 = 12.36 min. Included in this time is the stop-flow time of 5 min being applied to reach an equilibrium relaxation of the analytes (further details see Section 2.5 and Section 2.2, SI). Additionally, this fraction of unseparated analytes including also higher molar masses components may refer to densely compact objects with very low S_T. After the void peak, a good separation with high selectivity was observed. In order to keep the analysis time in a reasonable limit, a ThFFF method with a programmed temperature field has been optimized (see Fig. S4, SI) and two regions of interest (ROI) are defined: ROI 1 refers to poor and medium retained molecules in the retention region of about constant separation force field $\Delta T \approx 80$ K and ROI 2 contains all further retained species where the separation was performed with a ΔT of programmed decay approaching $\Delta T \rightarrow 0$ K.

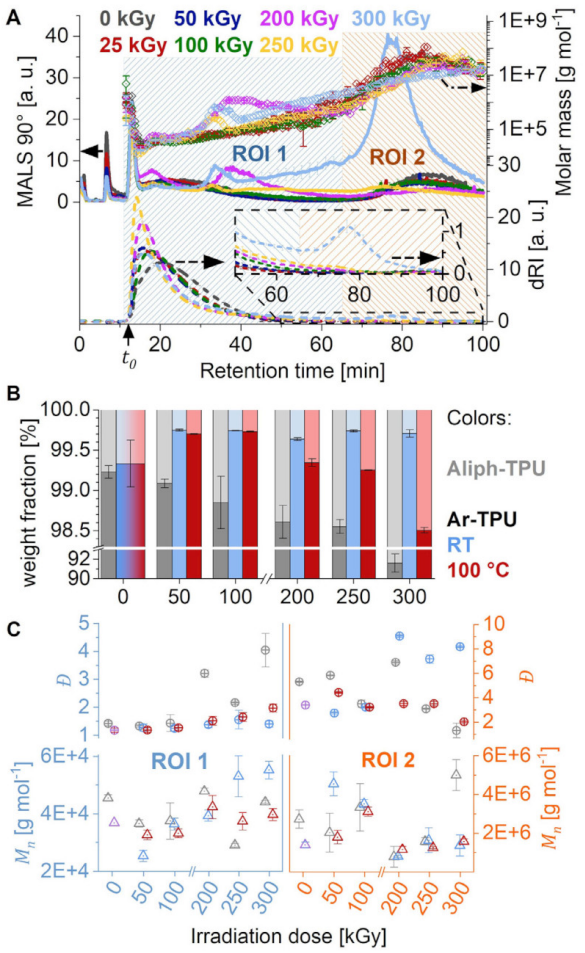

Fig. 5. Fractogram after ThFFF separation of the aliphatic TPU (**A**). Weight fraction (**B**) and mean molar mass with dispersity (**C**) evaluation per region of interest of the aliphatic TPU (grey) irradiated at RT and the aromatic TPU irradiated at RT (blue) and at 100 °C (red). The stout colors in A refer to ROI 1 and the pale colors correspond to ROI 2.

The evaluation of the fractograms per ROI in Fig. 5B and C shows for both TPU materials in ROI 2 first a slight decrease in weight fraction for low irradiation doses and thereafter an increase of the weight fraction containing ultra-high molar masses (UHMW) and possibly crosslinked species at high irradiation doses up to 300 kGy. For Aliph-TPU the increase of the weight fraction in ROI 2 ranged from originally less than 1% up to 9% and is much higher than for Ar-TPU 100 °C, for which ROI 2 increased by only 1%. In contrast, for Ar-TPU irradiated at RT the weight fraction in ROI 2 remained constantly low after first decrease at 50 kGy. Thus, the aliphatic TPU changes to a much greater extend under irradiation and forms a higher amount of crosslinked species. It can be concluded that for Aliph-TPU both, crosslinking and chain scission as competing mechanisms are reflected in M_n and $Đ$. In ROI 1 $Đ$ almost doubles, whereas M_n fluctuated around a constant average. At the same time in ROI 2 M_n rises for all samples, but $Đ$ decreases here under intense irradiation. The reason for this is found

in the differential molar mass distribution for the entire fractogram (see Fig. S15 A, SI). Here, an increase of the UHMW fraction and a shift of the weight distribution towards lower molar masses is depicted, indicating an increasing probability for chain scission of UHMW species once a certain (very high) molar mass is reached by crosslinking. In contrast to Aliph-TPU, the aromatic TPU Ar-TPU does not show significant changes in $Đ$ in ROI 1 when irradiated at RT, but an increase in M_n. Contrary, the irradiation at 100 °C leads to a slight increase in $Đ$, but only to fluctuation in M_n. In ROI 2, both series (RT and 100 °C) show a constant M_n, but for RT an increasing $Đ$ and for 100 °C a decreasing $Đ$ is observed. This can be also explained by the overall molar mass distribution (see Fig. S15 B and C, SI): During irradiation at room temperature crosslinked products with comparably low molar masses are formed while at 100 °C crosslinked products of higher molar masses are formed. The decreasing $Đ$ in ROI 2 for the 100 °C points at increasing chain scission during irradiation by the raised irradiation temperature.

As found by DSC, the irradiation influences in both TPU materials to some extend the phase transitions, indicating next to changing molar mass also topological changes such as increased branching. A suitable indicator for polymer topology is the scaling exponent ν_R, obtained as the slope from linear fitting of the gyration radius (RMS) and molar mass from MALS, for radii larger than approx. 12 nm (depending on the wavelength of the laser beam), enabling interpretation of the angular dependency of the scattered light [82,83]. This limits the applicability for this interpretation, since the main fraction for both TPU is below that limit. However, for the UHMW fractions conclusions about particle conformation can be drawn. In fact, the scaling exponents found by SEC-MALS-dRI for the first eluting fraction decrease from 0.62 (0 kGy) to about 0.48 (see Table S1, SI). Typical scaling exponents are 0.59 for a random coil in a good solvent decreasing to 0.33 for a dense sphere. The scaling exponents found by ThFFF-MALS-dRI show the same trend from 0.5 (Ar-TPU, 0 kGy) or slightly lower for Aliph-TPU down to about 0.3 indicating the formation of highly compact objects under irradiation (see Fig S16, SI) due to crosslinking and branching. The systematic difference of the scaling exponents between SEC and ThFFF is explained by differences in the solubility: For SEC the eluent *N,N*-dimethylacetamide was used with LiCl to enhance the solubility, disrupt possible intramolecular interactions like H-bonds and to decrease enthalpic interactions with the column material. In the ThFFF separations instead, the *N,N*-dimethylacetamide eluent had to be used without LiCl to avoid corrosion damage in the separation channel.

3.4.2. Thermophoretic analysis

Another indication for changes in topology, branching or changes in chemical composition is provided by the Soret coefficient S_T [22–24]. In this study changes in S_T are mainly ascribed to changes in the polymer topology, because in ATR-FTIR no significant changes accounting for transformations in chemical composition were found, even though they are supposed to be more likely seen by ATR as stated in sect. 3.1.

S_T calculations per slice (per retention time) were performed with correction of the flow profile distortion [84] and with an adapted approach to correct secondary relaxation [85]. Details are given in section 3.5.2 in the SI. The differential distributions of S_T (see Fig. 6) show a trend towards lower S_T with irradiation for the aliphatic TPU indicating a shortening of linear segments in the polymer chains [23]. The inconclusive S_T distribution of the 300 kGy-sample in Fig. 6A, which does not continue the trend observed up to an irradiation of 250 kGy, most probably originates from nonuniformities either in the material itself or in the irradiation impact, which is found to reflect in the chosen part of the bulk material from which the specimen originates. At a first glance, both series of Ar-TPU do not show significant alterations neither due to

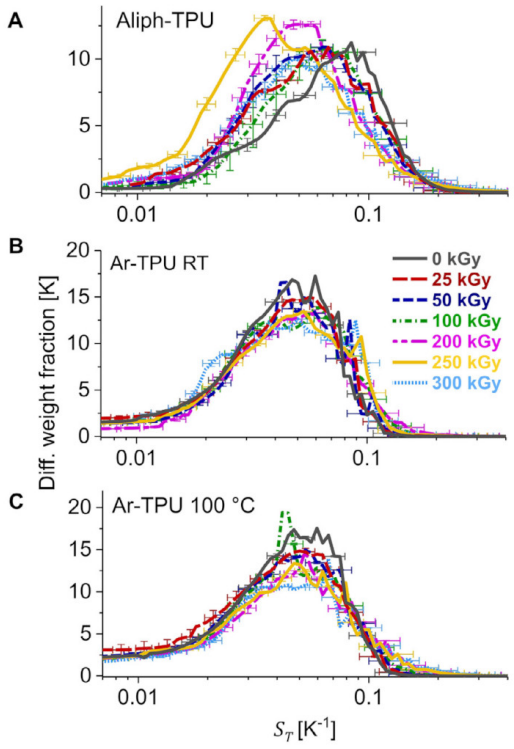

Fig. 6. Differential weight distributions of S_T calculated from the full ThFFF fractograms for Aliph-TPU (**A**), Ar-TPU irradiated at room temperature (**B**) and at 100 °C (C).

irradiation dose nor due to the irradiation temperature. The difference to Aliph-TPU in S_T as well as in the weight fraction analysis (see Fig. 5B and C) allows the conclusion that Ar-TPU is more resistant to irradiation, i.e. a higher energy is required to induce radical formation. This irradiation protection could originate from its crystalline nature.

A closer look at the cumulative S_T distributions shows on one hand the influence of the irradiation temperature for Ar-TPU, allowing visualization of small differences over a broad distribution range, in contrast to the differential distributions' representation. On the other hand, differences in cumulative distributions in their steep region are not as easy to differentiate, which are better visible in the differential distribution plots. The number and weight average values commonly used for reporting polymer molar masses are similarly insensitive to display deviations in the distribution. Therefore, alternative characteristic mean values with higher sensitivity for in particular narrow distributions have been introduced. For our study we have adapted the concept of the cumulative distribution angle [86] originally proposed for molar mass distributions to be used for the comparison of S_T distributions. The distribution angle is expected to display changes in the steep region of the cumulative S_T distribution. However, changes at the fronts and tails of the distribution may not be displayed by the distribution angle. Therefore additionally the width of the S_T distribution $\Delta S_{T,D}$ taken from a comparable confidence interval is used in this study. The corresponding cumulative distributions are given in Fig. S18, SI.

The analysis of the cumulative S_T distributions shows, as illustrated in Fig. 7, for Aliph-TPU a slight increase in the distribution angle at low irradiation dose, followed by a decrease at higher ir-

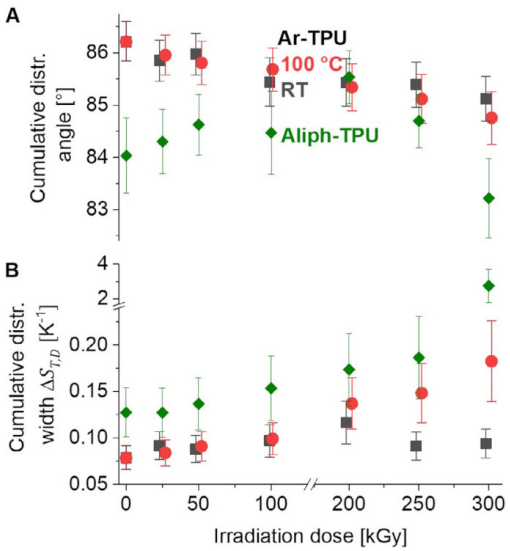

Fig. 7. The cumulative distribution angle from linear fit of the cumulative distributions given in Fig. S18, SI in between the distribution interval (y-axis, relative scale) 0.15 until 0.6 (**A**) and the distribution width $\Delta S_{T,D}$ (**B**) in between 0.05 until 0.95 of both TPU materials: Aliph-TPU irradiated at RT and Ar-TPU irradiated at RT and at 100 °C.

radiation doses. Meanwhile, $\Delta S_{T,D}$ shows only a steadily increasing width. This means, the main part of the S_T distribution shifts to lower S_T, but does not significantly broaden, whereas significant broadening occurs at the front and the tail of the distribution, which indicates that under influence of the irradiation small fractions (mainly at the tail) with a comparably high S_T are formed. As discussed above, crosslinking and branching have been found to be generated from irradiation, thus causing a decrease in thermal diffusion. Therefore, the increase in S_T can be explained with formation of large particles up to the microscale, which possess M_w in the UHMW range formed by crosslinking of already existing large macromolecular species.

The analysis for Ar-TPU shows different behavior for both irradiation temperature series: a constant decrease of the S_T distribution angle combined with a slightly increasing $\Delta S_{T,D}$ at lower irradiation doses is observed. However, at higher irradiation a significant difference with regard to the irradiation temperature is found. Irradiation at elevated temperature leads to further increase of $\Delta S_{T,D}$ similar to Aliph-TPU. In contrast to this, $\Delta S_{T,D}$ stays almost constant when the irradiation is carried out at room temperature. This observation is in accordance to the differences found in the molar mass distributions (see Fig. S15, SI) and the different weight fractions found in ROI 1, as stated in sect. 3.4.1., and supports the findings that crosslinking products of lower size and molar masses are formed at lower irradiation temperature, whereas additional architectures are formed at elevated temperatures in combination with higher irradiation dose. Under these conditions an increase of chain scission combined with crosslinking is competing, leading to broader molar mass range of the UHMW fraction for Ar-TPU 100 °C series. Consequently, the irradiation temperature changes the ratio between crosslinking and chain scission or degradation, while irradiation at lower temperature could suppress chain scission to some extent.

4. Conclusions

The influence of electron beam irradiation on commercially available aliphatic and aromatic thermoplastic polyurethane (TPU) material was thoroughly investigated on the molecular level by means of ATR-FTIR, DSC, SEC and complementary ThFFF separation, both separations coupled to absolute molar mass and size detection. Both materials are comparable in their hard and soft segment composition. ATR-FTIR investigations showed for both materials that electron beam irradiation produces a cascade of parallel chemical reactions including chain scission and chain recombination. These reactions lead to formation of branching, crosslinking as well to new functionalities (amines, amides, carboxylic acids), which are recognizable already in significant amount at low irradiation doses. Thereby, in the aliphatic TPU signs for urethane group degradation and secondary amine formation was indicated, which reveals a predominant degradation of hard segments, whereas in the aromatic TPU the soft segments were found to degrade earlier as indicated by of the isomerization in the polyol segments.

Complementary DSC studies reveal the aliphatic TPU as thoroughly amorphous material with a distinct glass transition, in which the slight decrease of the glass transition temperature supports the findings from the ATR-FTIR experiments, thus, indicating isomerization or branching. In contrast, the aromatic TPU showed highly crystalline character with a barely recognizable glass transition of its soft segments but a complex phase transition behavior with multiple melting and crystallization peaks. The multiple melting behavior caused by reorganization effects typical for TPU with high hard segment contents indicates an irradiation-induced transformation of the hard domains from well-ordered to increasingly disordered crystallites. Furthermore, the simultaneously found decrease in melting and crystallization temperatures supports the conclusion of irradiation induced isomerization, branching or topology changes found by ATR-FT-IR and DSC. The irradiation influence on the aromatic TPU was studied at room temperature and at 100 °C. The elevation of the irradiation temperature amplified the shift from well-ordered crystallites to disorderly crystallizing domains, but showed no effects on the phase transition temperatures.

The molar mass and size characterizations revealed for both materials the formation of a highly crosslinked fraction with ultra-high molar masses, compact conformation and an increased dispersity as a result of the irradiation. This study demonstrates the challenges arising from the limits of SEC and the possible deviations of the results generated by SEC with absolute molar mass determination from those obtained from SEC with relative calibration. Reliable determination of molar mass, size, and scaling with focus on the UHMW fraction was performed by ThFFF separation coupled to light scattering and dRI detection. Changes in topology were addressed by a thermophoretic analysis based on the ThFFF separation mechanism as a second independent investigation. These studies have revealed stronger tendency of the aliphatic TPU for crosslinking than the aromatic TPU, indicating a general high resistance of the aromatic TPU to irradiation. However, for the aliphatic TPU and for the aromatic TPU irradiated at 100 °C constant molar mass average in combination with a broadening in dispersity indicates that crosslinking is the main process competing with chain scission and degradation. For the aromatic TPU, lower irradiation temperature was found to significantly suppress chain scission and support crosslinking, although the crosslinking probability is also significantly reduced. Eventually, this study unravels that crosslinking is the dominating effect under irradiation influence prevailing chain scission and degradation. For this material, indications in agreement to our findings are reported for aliphatic [7] and aromatic TPU [55], but have not been yet verified by means of separation and absolute molar mass characterization. Depending on the material and irradiation conditions, degradation was also reported as main effect under irradiation [72,73].

Future studies in this field may address inhomogeneous alterations in the material due to irradiation (surface to bulk) by dif-

fuse reflexion spectroscopy (FTIR, Raman) of the material in powdered state. Furthermore, the existence of different polymorphs or discrete domain sizes superimposing the observed reorganization effects in the overall melting behavior found by DSC was not elucidated further and will be examined in detail with regard to irradiation in a future study. ThFFF investigations using light scattering are accounted to give further insights into the scaling behavior with irradiated TPU material of higher molar mass or fractionation combined with online viscometry for an indirect access to radius information of the polymers below the detection limit of MALS. Modulated DSC may further resolve reorganization effects seen in the multiple melting and crystallization behavior of the aromatic TPU.

Declaration of Competing Interest

The authors declare that they have no known competing financial interests or personal relationships that could have appeared to influence the work reported in this paper.

CRediT authorship contribution statement

Martin Geisler: Investigation, Conceptualization, Validation, Writing - original draft, Writing - review & editing, Visualization. **Tuhin Subhra Pal:** Investigation, Formal analysis. **Kerstin Arnhold:** Investigation, Formal analysis, Validation, Writing - review & editing. **Mikhail Malanin:** Investigation, Formal analysis, Validation, Writing - review & editing. **Michael Thomas Müller:** Resources, Writing - review & editing. **Brigitte Voit:** Supervision, Funding acquisition, Writing - review & editing. **Jürgen Pionteck:** Conceptualization, Validation, Supervision, Writing - review & editing. **Albena Lederer:** Validation, Supervision, Writing - review & editing.

Acknowledgements

This work was supported by the German Academic Exchange Service (DAAD) and the Ministry of Human Resource Development India. Hartmut Komber from IPF Dresden is greatly acknowledged for the NMR investigations of the materials. We thank Christina Harnisch from IPF Dresden for technical assistance in the SEC analysis. Lothar Jakisch is acknowledged for guidance in the ATR-FIR analysis and Sabine Krause (both from IPF Dresden) for help in thermal analyses. We thank Mr. Nikhil Kumar Singha, Prasanta Kumar Behera (IIT Kharagpur) and Susanne Boye (IPF Dresden) for valuable discussions regarding the interpretation of the results.

Supplementary materials

Supplementary material associated with this article can be found, in the online version, at doi:10.1016/j.polymdegradstab.2020.109423.

References

[1] E. Yousif, R. Haddad, Photodegradation and photostabilization of polymers, especially polystyrene: Review, Springerplus 2 (2013) 398.
[2] C. Wilhelm, A. Rivaton, J.L. Gardette, Infrared analysis of the photochemical behaviour of segmented polyurethanes: 3. Aromatic diisocyanate based polymers, Polymer 39 (1998) 1223–1232.
[3] B. Krause, D. Voigt, L. Häußler, D. Auhl, H. Münstedt, Characterization of electron beam irradiated polypropylene: Influence of irradiation temperature on molecular and rheological properties, J. Appl. Polym. Sci. 100 (2006) 2770–2780.
[4] B. Krause, D. Voigt, A. Lederer, D. Auhl, H. Münstedt, Determination of low amounts of long-chain branches in polypropylene using a combination of chromatographic and rheological methods, J. Chromatogr. A. 1056 (2004) 217–222.
[5] M. Szycher, Basic concepts in polyurethane chemistry and technology, in: Szychers Handb. Polyurethanes, Second Ed., 2012, pp. 13–36.
[6] T. Thomson, Polyurethane Chemistry, in: Polyurethane Immobil. Cells Biomol., 2017, pp. 1–27.
[7] E. Adem, E. Angulo-Cervera, A. González-Jiménez, J.L. Valentín, A. Marcos-Fernández, Effect of dose and temperature on the physical properties of an aliphatic thermoplastic polyurethane irradiated with an electron beam, Radiat. Phys. Chem. 112 (2015) 61–70.
[8] C. Wilhelm, J.L. Gardette, Infrared analysis of the photochemical behaviour of segmented polyurethanes: Aliphatic poly(ether-urethane)s, Polymer 39 (1998) 5973–5980.
[9] H. Sui, X. Ju, X. Liu, K. Cheng, Y. Luo, F. Zhong, Primary thermal degradation effects on the polyurethane film, Polym. Degrad. Stab. 101 (2014) 109–113.
[10] H.L. Sui, X.Y. Liu, F.C. Zhong, X.Y. Li, X. Ju, A study of radiation effects on polyester urethane using two-dimensional correlation analysis based on thermogravimetric data, Polym. Degrad. Stab. 98 (2013) 255–260.
[11] M.M. Ghobashy, Z.I. Abdeen, Radiation Crosslinking of Polyurethanes: Characterization by FTIR, TGA, SEM, XRD, and Raman Spectroscopy, J. Polym. 2016 (2016) 1–9.
[12] F. Dong, S. Maganty, S.J. Meschter, S. Nozaki, T. Ohshima, T. Makino, J. Cho, Electron beam irradiation effect on the mechanical properties of nanosilica–filled polyurethane films, Polym. Degrad. Stab. 141 (2017) 45–53.
[13] J. Dutta, T. Chatterjee, G. Dhara, K. Naskar, Exploring the influence of electron beam irradiation on the morphology, physico-mechanical, thermal behaviour and performance properties of EVA and TPU blends, RSC Adv. 5 (2015) 41563–41575.
[14] B. Ravat, M. Grivet, Y. Grohens, A. Chambaudet, Electron irradiation of polyesterurethane: Study of chemical and structural modifications using FTIR, UV spectroscopy and GPC, Radiat. Meas. 34 (2001) 31–36.
[15] B. Ravat, B. Oudot, M. Grivet, Y. Grohens, A. Chambaudet, Electron irradiation of polyurethane using UV spectroscopy, GPC and swelling analyses, Radiat. Phys. Chem. 63 (2002) 93–99.
[16] Q. Tian, E. Takács, I. Krakovský, Z.E. Horváth, L. Rosta, L. Almásy, Study on the microstructure of polyester polyurethane irradiated in air and water, Polymers 7 (2015) 1755–1766.
[17] Y.W. Deng, T.L. Yu, C.H. Ho, Effect of aging under strain on the physical properties of polyester–urethane elastomer, Polym. J. 26 (1994) 1368–1376.
[18] S.L. Cooke, A.R. Whittington, Investigation into Polyurethane at Varying Dose Rates of Ionizing Radiation for Clinical Application, J. Chem. 2018 (2018) 7312147.
[19] S. Podzimek, T. Vlcek, C. Johann, Characterization of branched polymers by size exclusion chromatography coupled with multiangle light scattering detector. I. Size exclusion chromatography elution behavior of branched polymers, J. Appl. Polym. Sci. 81 (2001) 1588–1594.
[20] J. Brandt, J. Lenz, K. Pahnke, F.G. Schmidt, C. Barner-Kowollik, A. Lederer, Investigation of thermoreversible polymer networks by temperature dependent size exclusion chromatography, Polym. Chem. 8 (2017) 6598–6605.
[21] M.E. Schimpf, K. Caldwell, J.C. Giddings, Field-Flow Fractionation Handbook, John Wiley & Sons, Inc., New York, USA, 2000.
[22] W.C. Smith, M. Geisler, A. Lederer, S.K.R. Williams, Thermal Field-Flow Fractionation for Characterization of Architecture in Hyperbranched Aromatic-Aliphatic Polyesters with Controlled Branching, Anal. Chem. 91 (2019) 12344–12351.
[23] M. Geisler, W.C. Smith, L. Plüschke, R. Mundil, J. Merna, S.K.R. Williams, A. Lederer, Topology Analysis of Chain Walking Polymerized Polyethylene: An Alternative Approach for the Branching Characterization by Thermal FFF, Macromolecules 52 (2019) 8662–8671.
[24] G. Greyling, A. Lederer, H. Pasch, Thermal Field-Flow Fractionation for the Investigation of the Thermoresponsive Nature of Star and Linear Polystyrene, Macromol. Chem. Phys. 219 (2018) 1800417.
[25] M.E. Schimpf, L.M. Wheeler, P.F. Romeo, Copolymer Retention in Thermal Field-Flow Fractionation, in: Chromatogr. Polym.,, American Chemical Society, 1993, pp. 63–76.
[26] C.A. Ponyik, D.T. Wu, S.K.R. Williams, Separation and composition distribution determination of triblock copolymers by thermal field-flow fractionation, Anal. Bioanal. Chem. 405 (2013) 9033–9040.
[27] M.E. Schimpf, J.C. Giddings, Characterization of thermal diffusion of copolymers in solution by thermal field-flow fractionation, J. Polym. Sci. Part B Polym. Phys. 28 (1990) 2673–2680.
[28] E.P.C. Mes, R. Tijssen, W.T. Kok, Rapid detection of compositional drift of polydisperse copolymers using thermal field-flow fractionation and multi-angle light scattering, Chromatographia 50 (1999) 45–51.
[29] J.R. Runyon, S.K.R. Williams, Composition and molecular weight analysis of styrene-acrylic copolymers using thermal field-flow fractionation, J. Chromatogr. A. 1218 (2011) 6774–6779.
[30] Greyling, G., Pasch, H., Thermal Field-Flow Fractionation (ThFFF), in: G. Greyling, H. Pasch (Eds.), Springer International Publishing, Cham, Switzerland, 2019, pp. 13–29.
[31] U.L. Muza, G. Greyling, H. Pasch, Stereocomplexation of Polymers in Micelle Nanoreactors As Studied by Multiple Detection Thermal Field-Flow Fractionation, Anal. Chem. 90 (2018) 13987–13995.
[32] U.L. Muza, H. Pasch, Thermal field-flow fractionation with quintuple detection for the comprehensive analysis of complex polymers, Anal. Chem. 91 (2019) 6926–6933.
[33] N.W. Radebe, T. Beskers, G. Greyling, H. Pasch, Online coupling of thermal field-flow fractionation and Fourier transform infrared spectroscopy as a powerful tool for polymer characterization, J. Chromatogr. A. 1587 (2019) 180–188.
[34] G. Greyling, H. Pasch, Characterisation of block copolymer self-assemblies by thermal field-flow fractionation, Polym. Int. 66 (2017) 745–751.

[35] G. Greyling, H. Pasch, Multidetector Thermal Field-Flow Fractionation: A Unique Tool for Monitoring the Structure and Dynamics of Block Copolymer Micelles, Macromolecules 49 (2016) 1882–1889.
[36] C. Soret, Sur l'état d'équilibre que prend, au point de vue de sa concentration, une dissolution saline primitivement homogène, dont deux parties sont portées à des températures différentes, J. Phys. Theor. Appl. 9 (1880) 331–332.
[37] C. Ludwig, Diffusion zwischen ungleich erwärmten Orten gleich zusammengesetzter Lösungen, Sitzungber, Bayer. Akad. Wiss. Wien Math.-Naturwiss. Kl. 20 (1856) 539.
[38] E.P.C. Mes, W.T. Kok, R. Tijssen, Prediction of Polymer Thermal Diffusion Coefficients from Polymer-Solvent Interaction Parameters: Comparison with Thermal Field Flow Fractionation and Thermal Diffusion Forced Rayleigh Scattering Experiments, Int. J. Polym. Anal. Charact. 8 (2003) 133–153.
[39] J.R. Runyon, S.K.R. Williams, A theory-based approach to thermal field-flow fractionation of polyacrylates, J. Chromatogr. A. 1218 (2011) 7016–7022.
[40] D. Stadelmaier, W. Köhler, Thermal diffusion of dilute polymer solutions: The role of chain flexibility and the effective segment size, Macromolecules 42 (2009) 9147–9152.
[41] A. Einstein, Eine neue Bestimmung der Moleküldimensionen, Ann. Phys. 324 (1906) 289–306.
[42] Korber, H., Lappan, U., Geißler, U., Lunkwitz, K., Hanke, R., Vorrichtung zur physiko-chemischen Modifizierung von Materialproben mittels eines Elektronenstrahls, German Patent, DE19930742, 2001.
[43] H. Dorschner, W. Jenschke, K. Lunkwitz, Radiation field distributions of an industrial electron beam accelerator, Nucl. Instruments Methods Phys. Res. Sect. B Beam Interact. with Mater. Atoms. 161 (2000) 1154–1158.
[44] U. Gohs, R. Böhm, H. Brünig, D. Fischer, L. Häussler, M. Kirsten, M. Malanin, M.T. Müller, C. Cherif, D.S.J. Wolz, H. Jäger, Electron beam treatment of polyacrylonitrile copolymer above the glass transition temperature in air and nitrogen atmosphere, Radiat. Phys. Chem. 156 (2019) 22–30.
[45] B.J. Lee, Y. Zhou, J.S. Lee, B.K. Shin, J.A. Seo, D. Lee, Y.S. Kim, H.K. Choi, Discrimination and prediction of the origin of Chinese and Korean soybeans using Fourier transform infrared spectrometry (FT-IR) with multivariate statistical analysis, PLoS One 13 (2018) e0196315.
[46] W.B. Fischer, P. Pötschke, G. Pompe, K.J. Eichhorn, H.W. Siesler, Rheo-optical Fourier transform infrared spectroscopy of polyurethanes and their blends with polyolefins, Macromol. Chem. Phys. 198 (1997) 2057–2072.
[47] J. Hiltz, J. Szabo, FT-IR study of poly(ether)urethanes, Report No. 2001-073, Defense Research Establishment Atlantic, Canada, 2001.
[48] G.G. Suchkova, L.I. Maklakov, Amide bands in the IR spectra of urethanes, Vib. Spectrosc. 51 (2009) 333–339.
[49] G. Socrates, Infrared and Raman characteristic group frequencies: tables and charts, John Wiley & Sons, 2004.
[50] D.O. Hummel, F. Scholl, Atlas of Polymer and Plastics Analysis, Verlag Chemie International, Munich, 1978, p. 387.
[51] M.M. Coleman, D.J. Skrovanek, J. Hu, P.C. Painter, Hydrogen Bonding in Polymer Blends. 1. FTIR Studies of Urethane-Ether Blends, Macromolecules 21 (1988) 59–65.
[52] B.S. Jursic, Z. Zdravkovski, A simple preparation of amides from acids and amines by heating of their mixture, Synth. Commun. 23 (1993) 2761–2770.
[53] J. Cossy, C. Pale-Grosdemange, A convenient synthesis of amides from carboxylic acids and primary amines, Tetrahedron Lett 30 (1989) 2771–2774.
[54] O. Mrad, J. Saunier, C. Aymes Chodur, V. Rosilio, F. Agnely, P. Aubert, J. Vigneron, A. Etcheberry, N. Yagoubi, A comparison of plasma and electron beam-sterilization of PU catheters, Radiat. Phys. Chem. 79 (2010) 93–103.
[55] K.A. Murray, J.E. Kennedy, B. McEvoy, O. Vrain, D. Ryan, R. Cowman, C.L. Higginbotham, The influence of electron beam irradiation conducted in air on the thermal, chemical, structural and surface properties of medical grade polyurethane, Eur. Polym. J. 49 (2013) 1782–1795.
[56] I.M. Hodge, Physical aging in polymer glasses, Science (80-.). 267 (1995) 1945–1947.
[57] L.C.E. Struik, Physical aging in amorphous polymers and other materials, 2nd ed., Elsevier Scientific Publishing Company, Amsterdam, The Netherlands, 1978, pp. 97–122.
[58] B. Wunderlich, Single Component Materials, in: B. Wunderlich (Ed.), Therm. Anal. Polym. Mater., Springer, Berlin Heidelberg, Germany, 2005, pp. 591–704.
[59] R.J. Seyler, Assignment of the Glass Transition, Astm International, West Conshohocken, PA, USA, 1994.
[60] M.A. Sharaf, J.E. Mark, Effects of Cross-Linking and Strain on the Glass Transition Temperature of a Polymer Network, Rubber Chem. Technol. 53 (1980) 982–987.
[61] J.T. Koberstein, A.F. Galembos, L.M. Leung, Compression-Molded Polyurethane Block Copolymers. 1. Microdomain Morphology and Thermomechanical Properties, Macromolecules 25 (1992) 6195–6204.
[62] J.T. Koberstein, A.F. Galembos, Multiple Melting in Segmented Polyurethane Block Copolymers, Macromolecules 25 (1992) 5618–5624.
[63] J. Balko, B. Fernández-D'Arlas, E. Pöselt, R. Dabbous, A.J. Müller, T. Thurn-Albrecht, Clarifying the Origin of Multiple Melting of Segmented Thermoplastic Polyurethanes by Fast Scanning Calorimetry, Macromolecules 50 (2017) 7672–7680.
[64] J.T. Koberstein, R.S. Stein, Small-Angle X-Ray Scattering Studies of Microdomain Structure in Segmented Polyurethane Elastomers, J. Polym. Sci. Part A-2, Polym. Phys. 21 (1983) 1439–1472.
[65] J.T. Koberstein, R.S. Stein, Small-Angle X-Ray Scattering Measurements of Diffuse Phase-Boundary Thicknesses in Segmented Polyurethane Elastomers, J. Polym. Sci. Part A-2, Polym. Phys. 21 (1983) 2181–2200.
[66] A. Saiani, W.A. Daunch, H. Verbeke, J.W. Leenslag, J.S. Higgins, Origin of multiple melting endotherms in a high hard block content polyurethane. 1. Thermodynamic investigation, Macromolecules 34 (2001) 9059–9068.
[67] A. Mishra, P. Maiti, Morphology of polyurethanes at various length scale: The influence of chain structure, J. Appl. Polym. Sci. 120 (2011) 3546–3555.
[68] I.D. Fridman, E.L. Thomas, Morphology of crystalline polyurethane hard segment domains and spherulites, Polymer 21 (1980) 388–392.
[69] R. Navarro, A. Rubio Hernández-Sampelayo, E. Adem, A. Marcos-Fernández, Effect of electron beam irradiation on the properties of poly(tetramethylene oxide) and a poly(tetramethylene oxide)-based polyurethane, Radiat. Phys. Chem. 174 (2020) 108905.
[70] A. Chapiro, Chemical modifications in irradiated polymers, Nucl. Inst. Methods Phys. Res. B. 32 (1988) 111–114.
[71] R. Kltamaru, L. Mandelkern, Irradiation Cross Linking of Polyethylene. The Temperature Dependence of Cross Linking in the Crystalline and Amorphous States, J. Am. Chem. Soc. 86 (1964) 3529–3534.
[72] C. Guignot, N. Betz, B. Legendre, A. Le Moel, N. Yagoubi, Degradation of segmented poly(etherurethane) Tecoflex® induced by electron beam irradiation: Characterization and evaluation, Nucl. Instruments Methods Phys. Res. Sect. B Beam Interact. with Mater. Atoms. 185 (2001) 100–107.
[73] A. Dannoux, S. Esnouf, J. Begue, B. Amekraz, C. Moulin, Degradation kinetics of poly(ether-urethane) Estane® induced by electron irradiation, Nucl. Instruments Methods Phys. Res. Sect. B Beam Interact. with Mater. Atoms. 236 (2005) 488–494.
[74] C.V. Stephenson, J.C. Lacey, W.S. Wilcox, Ultraviolet irradiation of plastics III. Decomposition products and mechanisms, J. Polym. Sci. 55 (1961) 477–488.
[75] L. Irusta, M.J. Fernandez-Berridi, Photooxidative behaviour of segmented aliphatic polyurethanes, Polym. Degrad. Stab 63 (1999) 113–119.
[76] P. Scholz, V. Wachtendorf, U. Panne, S.M. Weidner, Degradation of MDI-based polyether and polyester-polyurethanes in various environments - Effects on molecular mass and crosslinking, Polym. Test. 77 (2019) 105881.
[77] P. Scholz, V. Wachtendorf, A.M. Elert, J. Falkenhagen, R. Becker, K. Hoffmann, U. Resch-Genger, H. Tschiche, S. Reinsch, S. Weidner, Analytical toolset to characterize polyurethanes after exposure to artificial weathering under systematically varied moisture conditions, Polym. Test. 78 (2019) 105996.
[78] J. Gerber, W. Radke, Separation of linear and star-shaped polystyrenes by two-dimensional chromatography, E-Polymers 5 (2005) 44.
[79] M. Al Samman, W. Radke, A. Khalyavina, A. Lederer, Retention behavior of linear, branched, and hyperbranched polyesters in interaction liquid chromatography, Macromolecules 43 (2010) 3215–3220.
[80] A. Lederer, M.A. Elrehim, F. Schallausky, D. Voigt, B. Voit, Molecular weight and contraction factors of hyperbranched poly(urea-urethane)s, E-Polymers 6 (2006) 1–14.
[81] J.C. Giddings, Field-flow fractionation: an alternative to size exclusion chromatography, in: B.J. Hunt, S.R. Holding (Eds.), Size Exclusion Chromatogr, Springer, Boston, MA, USA, 1989, pp. 191–216.
[82] P.J. Wyatt, Light scattering and the absolute characterization of macromolecules, Anal. Chim. Acta. 272 (1993) 1–40.
[83] P.J. Wyatt, The "Size" of macromolecules and some observations on their mass, J. Liq. Chromatogr. 14 (1991) 2351–2372.
[84] M. Geisler, A. Lederer, Non-Parabolicity correction for fifty-nine solvents and a retention study for strongly distorted flow-profiles in thermal field-flow fractionation, J. Chromatogr. A. 1621 (2020) 461082.
[85] M.E. Hansen, J.C. Giddings, M.R. Schure, R. Beckett, Corrections for Secondary Relaxation in Exponentially Programmed Field-Flow Fractionation, Anal. Chem. 60 (1988) 1434–1442.
[86] D. Čožíková, T. Šílová, V. Moravcová, D. Šmejkalová, S. Pepeliaev, V. Velebný, M. Hermannová, Preparation and extensive characterization of hyaluronan with narrow molecular weight distribution, Carbohydr. Polym. 160 (2017) 134–142.

Supporting Information for

Impact of Electron Beam Irradiation on Thermoplastic Polyurethanes Unraveled by Thermal Field-Flow Fractionation

Martin Geisler [a, b], Tuhin Subhra Pal [c], Kerstin Arnhold [a], Mikhail Malanin [a], Michael Thomas Müller [a], Brigitte Voit [a, b], Jürgen Pionteck [a, *], Albena Lederer [a, b, d, *]

[a] Leibniz-Institut für Polymerforschung Dresden e. V., Hohe Str. 6, 01069 Germany

[b] Faculty of Chemistry and Food Chemistry, Technische Universität Dresden, 01062 Dresden, Germany

[c] Rubber Technology Centre, Indian Institute of Technology, Kharagpur, 721302 West Bengal, India

[d] Department of Chemistry and Polymer Science, Stellenbosch University, Private Bag X1, Matieland 7602, South Africa

* Email of corresponding authors: lederer@ipfdd.de, pionteck@ipfdd.de

Table of content for the Supplementary data:

1. Theory
   1.1. The basic principle of thermal field-flow fractionation S-2
   1.2. The concept of the S_T distribution angle and the $\Delta S_{T,D}$ distribution width S-3
2. Experimental
   2.1. Electron beam irradiation S-3
   2.2. Thermal field-flow fractionation with absolute molar mass detection S-4
3. Additional results and calculations
   3.1. Thermal analysis S-4
   3.2. NMR spectroscopy S-8
   3.3. Determination of the refractive index increment $dn\,dc^{-1}$ S-9
   3.4. SEC analysis S-9
   3.5. ThFFF analysis
      3.5.1. Molar mass and size via MALS-dRI S-11
      3.5.2. Thermophoretic analysis S-13
   3.6. Comparison of the molar mass distributions between calibrated SEC, SEC-MALS and ThFFF-MALS S-16
4. References S-17

1. Theory

1.1. The basic principle of thermal field-flow fractionation (ThFFF)

The separation principle of field-flow fractionation in general relies on an externally applied separation force to an analyte mixture to be separated in an empty ribbon-like channel of large aspect ratio. As illustrated in Figure S1, in the first step the analyte mixture is allowed to relax in response to the field force after injection at the beginning of the channel forming an exponentially decaying concentration profile. Following in the second step a laminar flow is pumped through the channel in perpendicular direction to the field force. Due to differences in the response to the field force, analytes may reach their equilibrium between accumulation and back diffusion driven by Brownian motion in different mean layer thicknesses of faster or slower flow velocities and thus a separation in the overlay of flow and field force is realized.[1] If the relaxation equilibrium is reached fast enough, stop-flow prior to elution is not required.

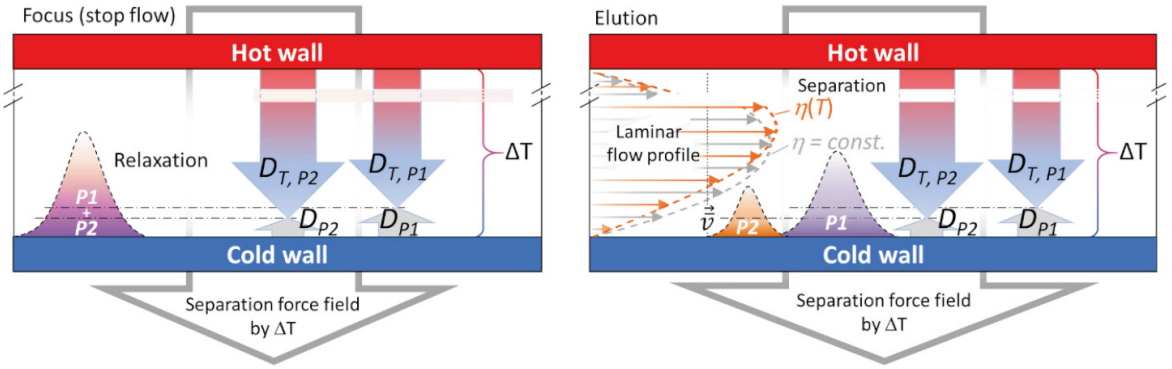

Figure S1 Basic principle of ThFFF shown for a hypothetical analyte mixture of P1 and P2 with their translational diffusion coefficients D and their thermal diffusion coefficients D_T representing the response to the applied field force ΔT. The cold wall is accounted here to be the accumulation wall.

In ThFFF the separation force field is realized by a strong temperature difference ΔT between a heated and an actively cooled channel wall. Thereby the separation relies on thermophoresis causing a down-forcing moment described by the thermal diffusion coefficients D_T, which is in equilibrium with the up-forcing moment caused by translational diffusion D. The ratio D_T to D is defined as the Soret coefficient S_T. Unlike all other FFF sub techniques, due to the temperature gradient the non-constant viscosity of the carrier liquid leads to a distortion of the laminar flow profile (normally described as parabolic flow profile), which has to be respected for an accurate description of the retention, as given in Eq. (1).

$$R = \frac{t_0}{t_R} = 6\lambda\left[\nu + (1 - 6\lambda\nu)\left(coth\left(\frac{1}{2\lambda}\right) - 2\lambda\right)\right] \quad (1)$$

The retention ratio R as fraction of void time t_0 over retention time t_R is dependent on the dimensionless FFF parameter λ and a non-parabolicity parameter ν for the correction of the flow profile distortion. ν can be calculated by a polynomial approach in dependency to ΔT and the cold wall temperature with the help of polynomial coefficients tabulated in the literature for many different solvents.[2,3] The parameter λ is defined by physicochemical parameters depending on the FFF separation mechanism and the field force. In ThFFF λ is therefore defined as given in Eq. (2)

$$\lambda = \frac{1}{S_T \Delta T} = \frac{D_T}{D\ \Delta T} \quad (2)$$

1.2. The concept of the S_T distribution angle and the $\Delta S_{T,D}$ distribution width

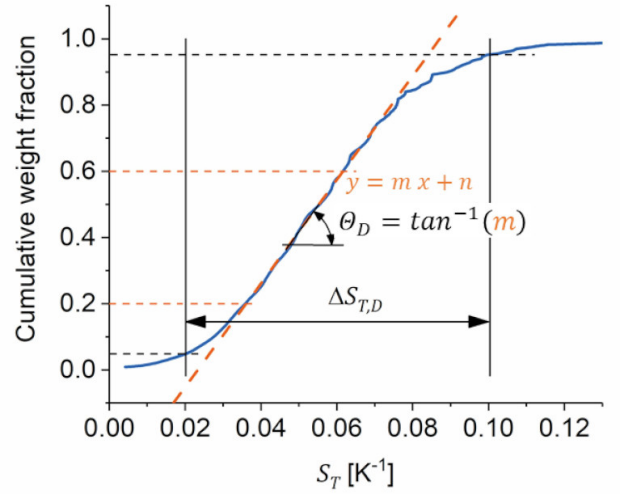

Figure S2 Concept of the S_T distribution angle, determined by linear fit of the steep region. For all series in this study, the distribution angle was fitted between 0.2 and 0.6 of the cumulative weight fractions (see Fig. S17). This concept was adapted from the molar mass distribution angle as reported earlier.[4] Meanwhile, the width of the distribution $\Delta S_{T,D}$ was measured in the confidence interval of 0.05 to 0.95 of the cumulative weight fraction.

2. Experimental

2.1. Electron beam Irradiation (EBI)

Figure S3 Electron accelerator ELV-2 used for irradiation of the polyurethane samples.

2.2. Thermal field-flow fractionation with absolute molar mass detection

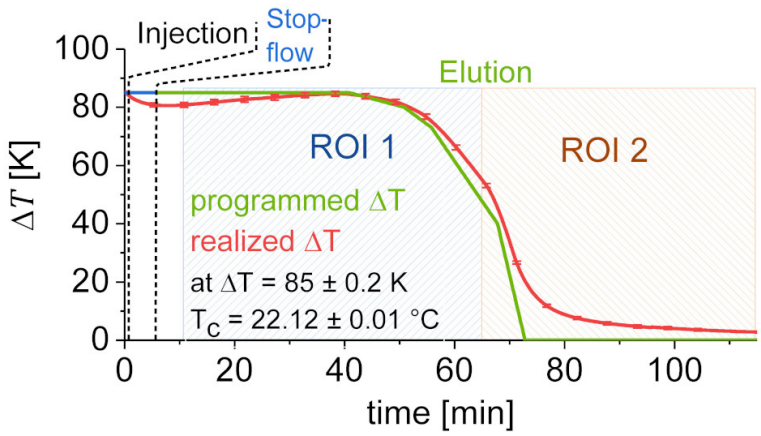

Figure S4 Optimized separation method used for separations of all TPU series in this study with the assigned regions of interest ROI 1 ad ROI 2 referring to the fractograms given in Fig. 5 in the main article and in in Fig. S14.

3. Additional results and calculations

3.1. Thermal analysis

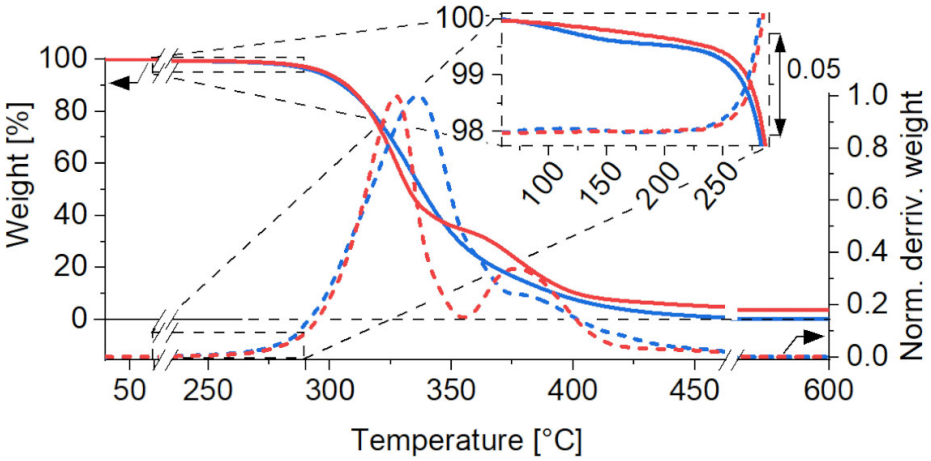

Figure S5 Thermogravimetric analysis of Aliph-TPU and Ar-TPU, both irradiated with a dose of 300 kGy at room temperature.

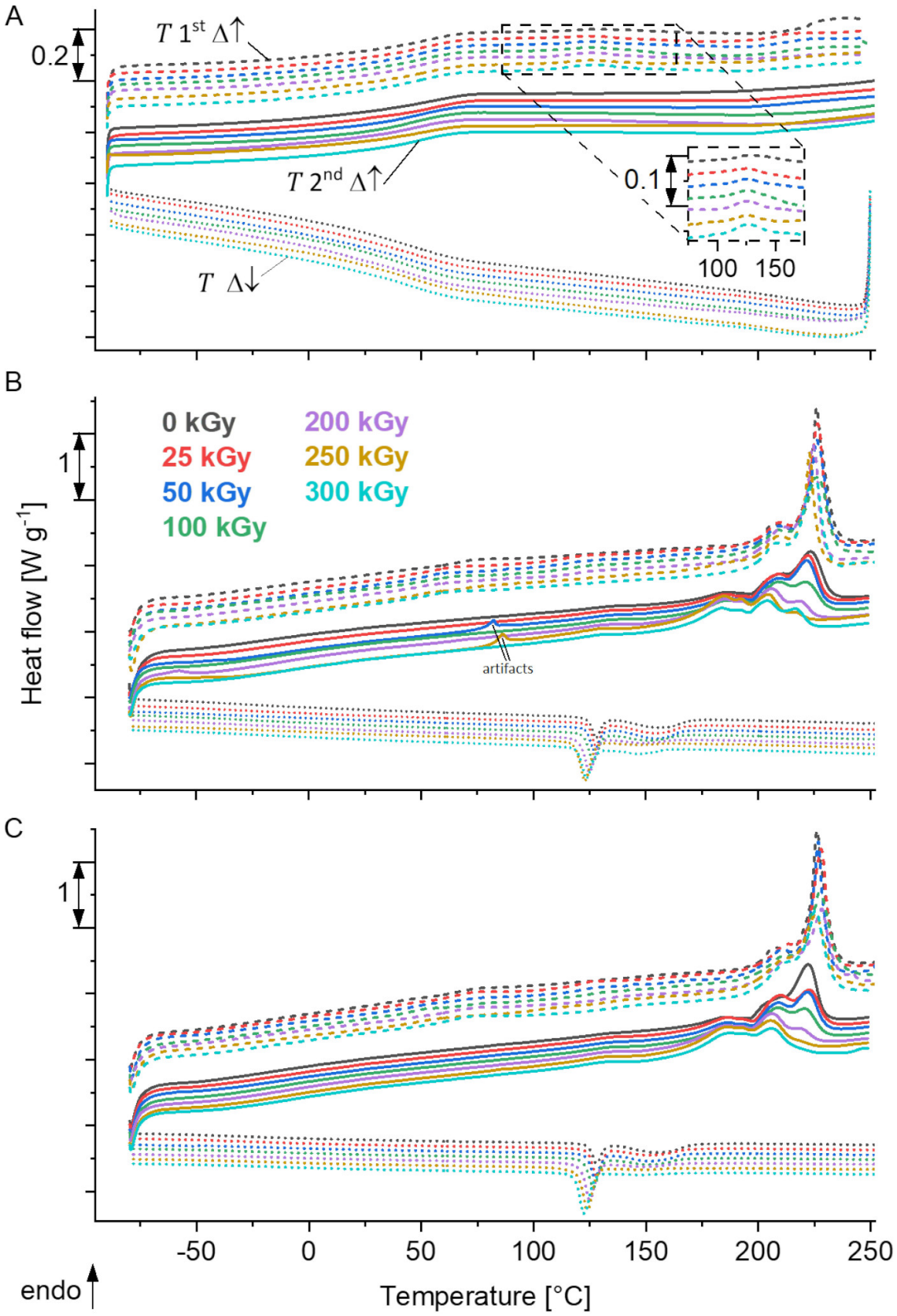

Figure S6 Thermograms of the DSC analysis of Aliph-TPU (**A**) and Ar-TPU irradiated at room temperature (**B**) and at 100 °C (**C**). The dashed line shows the first heating scan, the dotted line shows the cooling scan and the solid line shows the second heating scan.

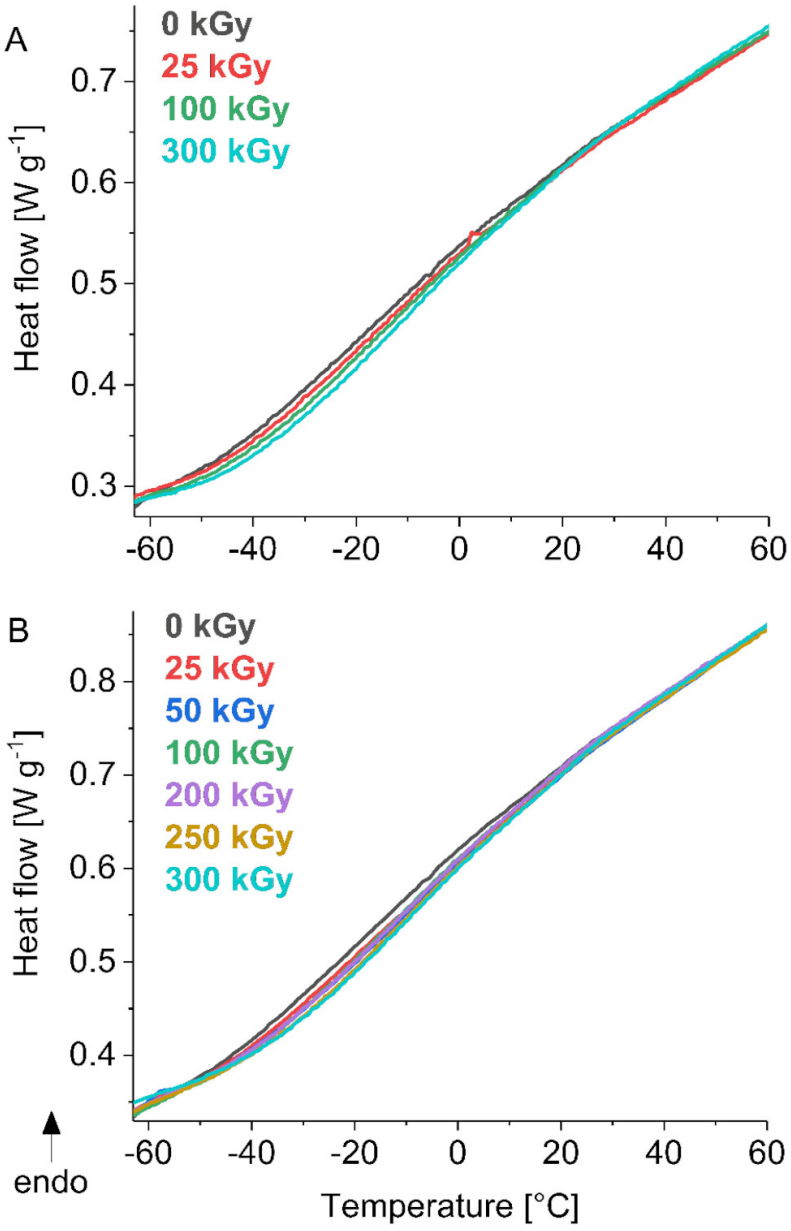

Figure S7 Region of the soft segment glass transition in the DSC thermograms (second heating) of the aromatic TPU irradiated at room temperature (**A**) and at 100 °C (**B**)

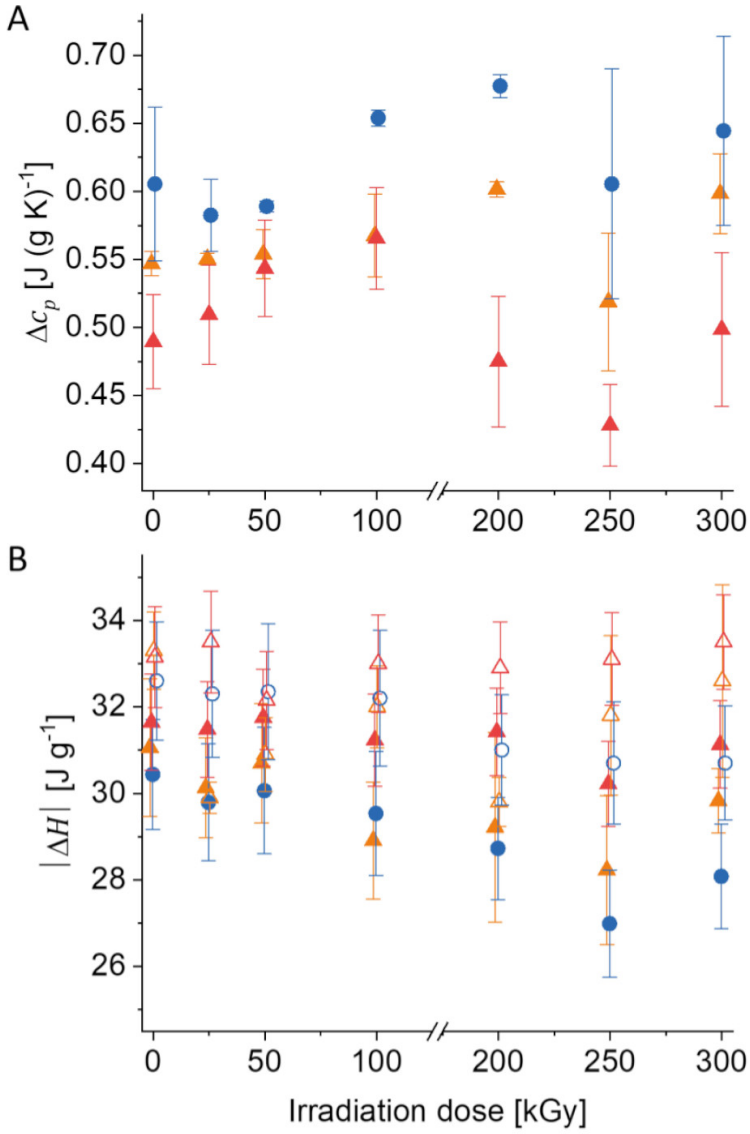

Figure S8 A Heat capacity drops of Aliph-TPU corresponding to the glass transition temperatures given in Fig. 2 in the main article. **B** Total enthalpies of fusion and of crystallization for Ar-TPU. Values from the first heating are displayed in orange, values from the cooling scan are given in blue and values from the second heating scan are shown in red. Filled symbols in B represent the series irradiated at room temperature and open symbols refer to the series irradiated at 100 °C.

3.2. NMR-spectroscopy

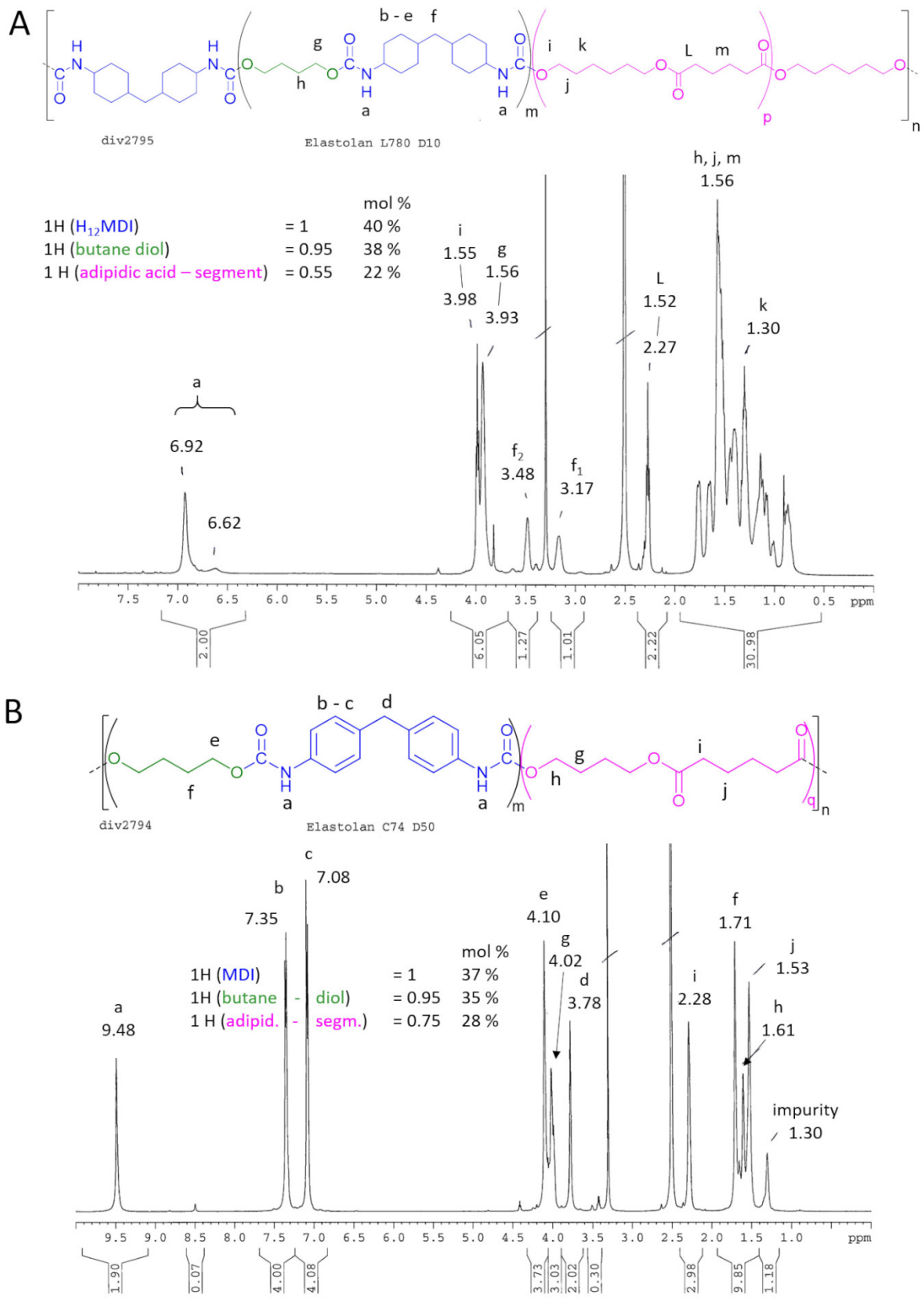

Figure S9 ^{1}H-NMR spectra of the aliphatic thermoplastic poly(ester urethane) (A) and of the aromatic poly-(ester urethane) (B) used in this study, containing hard segments composed of either 4,4′-dicyclo-hexylmethane diisocyanate (H_{12}MDI) (A, blue) or diphenylmethane diisocyanate (MDI) (B, blue) coupled to 1,4-butanediol (green). The soft segments (magenta) consist of poly(1,6-hexane adipate) (A) or poly(1,4-butane adipate) (B).

3.3. Determination of the refractive index increment *dn dc*$^{-1}$

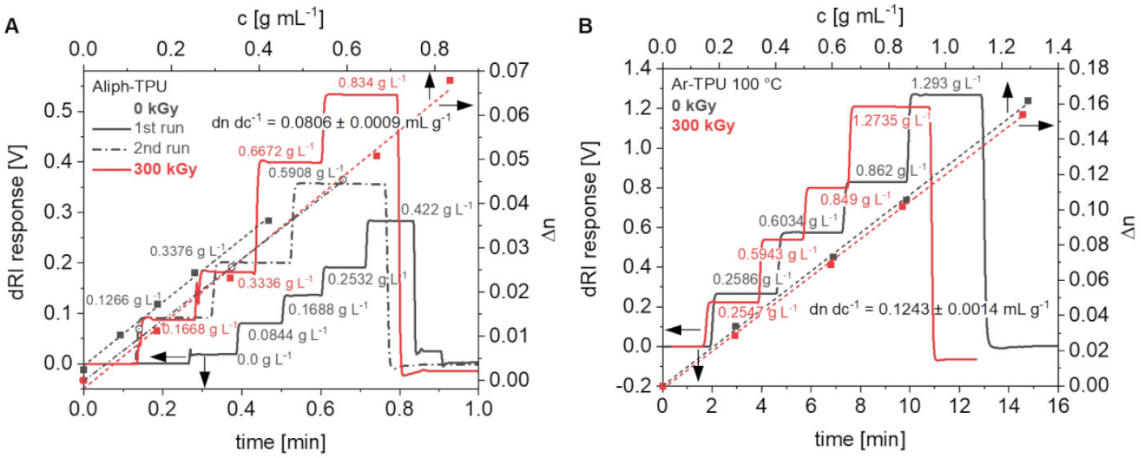

Figure S10 Determination of the *dn dc*$^{-1}$ in batch for Aliph-TPU (**A**) and Ar-TPU (**B**), dissolved in pure *N,N*-dimethylacetamide. No differences between non- and highly irradiated samples were found.

The *dn dc*$^{-1}$ found by batch measurements as reported in Fig. S10 were used for the molar mass and size characterizations in ThFFF only. For the SEC analysis, the influence of the added LiCl has to be taken into account. Hence, *dn dc*$^{-1}$ for Aliph-TPU is to increase from 0.0806 to 0.1330 mL g^{-1} and for Ar-TPU from 0.1243 to 0.1760 mL g^{-1} with a dRI detector constant of 0.12 RIU V^{-1}. With this *dn dc*$^{-1}$ for both TPU a mass recovery of 90 to 98 % is found in the SEC analysis confirming the validity of this correction as proposed in the literature.[5]

3.4. SEC analysis

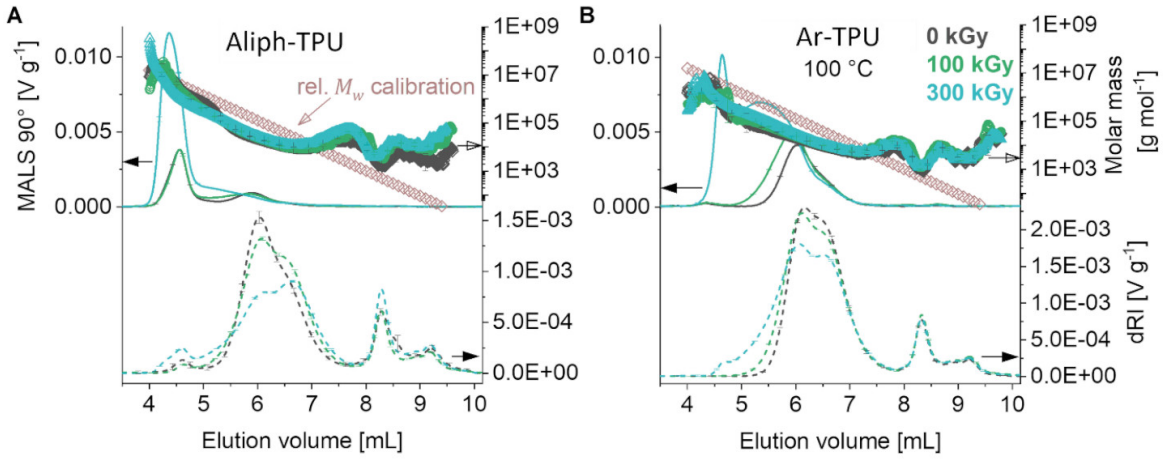

Figure S11 SEC-MALS-dRI chromatograms of Aliph-TPU (**A**) and Ar-TPU (**B**) irradiated at 100 °C performed in *N,N*-dimethylacetamide (+ 3 g L^{-1} LiCl). For comparison, the molar mass trace of a relative calibration with narrowly dispersed polystyrene standards is shown.

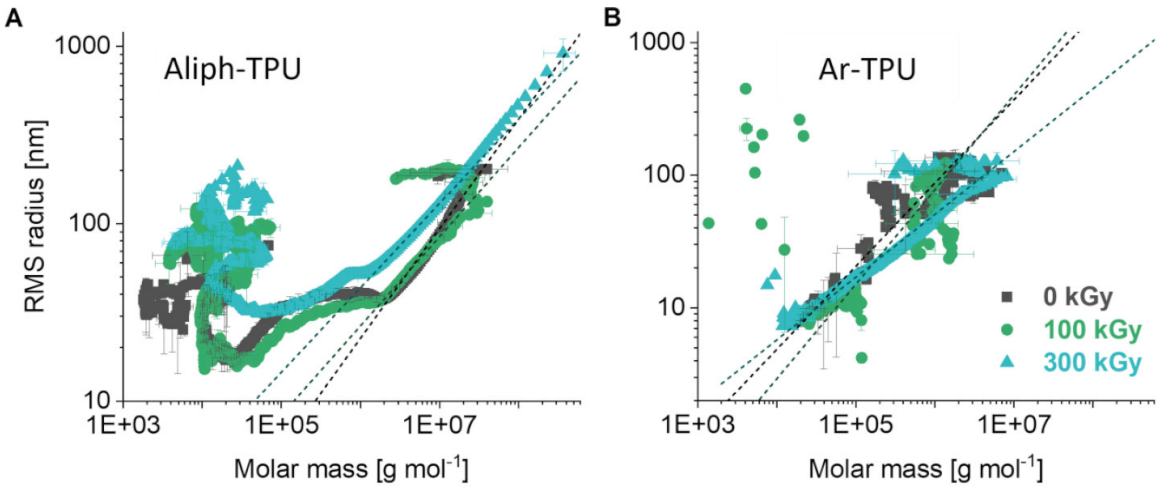

Figure S12 RMS radius – molar mass conformation plots derived from the SEC-MALS-dRI analysis for Aliph-TPU (**A**) and Ar-TPU 100 °C (**B**). The full data are shown here to elucidate abnormal elution behaviour particularly seen for Aliph-TPU (**A**). Only the linear scaling data in the higher molar mass rages have been fitted to determine scaling parameters ν_R.

Table S1 Summary of the SEC-MALS-dRI-analysis.

	Aliph-TPU			Ar-TPU 100 °C		
Irradiation dose	M_n [kg mol^{-1}]	$Đ$	ν_R [kg mol^{-1}]	M_n [kg mol^{-1}]	$Đ$	ν_R [kg mol^{-1}]
0 kGy	16.7 ± 1.9	8 ± 4	0.62 ± 0.02	33.4 ± 0.2	37.1 ± 0.2	0.63 ± 0.02
100 kGy	15.6 ± 1.7	5.5 ± 1.3	0.5 ± 0.02	30.0 ± 0.2	33.3 ± 0.2	0.64 ± 0.05
300 kGy	23.1 ± 2.6	28 ± 11	0.48 ± 0.01	36.3 ± 0.5	40.3 ± 0.5	0.47 ± 0.01

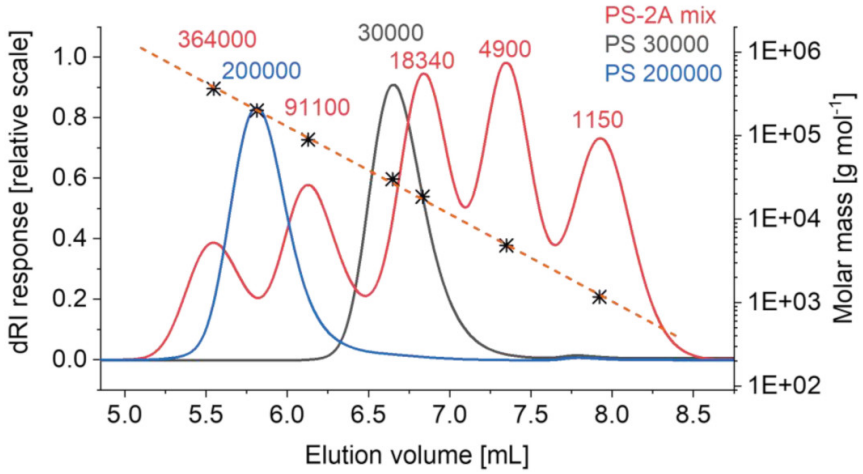

Figure S13 Molar mass calibration performed with narrow polystyrene standard mix PS-2A by Agilent technologies Inc., PS 80317 and PS 50912 by Pressure Chemical Co. The molar mass trace of calibration is illustrated in Figure S11 and the calibration is further used in Figure S19 for comparison. The measurements were done with the set up and the conditions described in sect. 2.4 in the main article.

3.5. ThFFF analysis

3.5.1. Molar mass and size measured by MALS-dRI detection

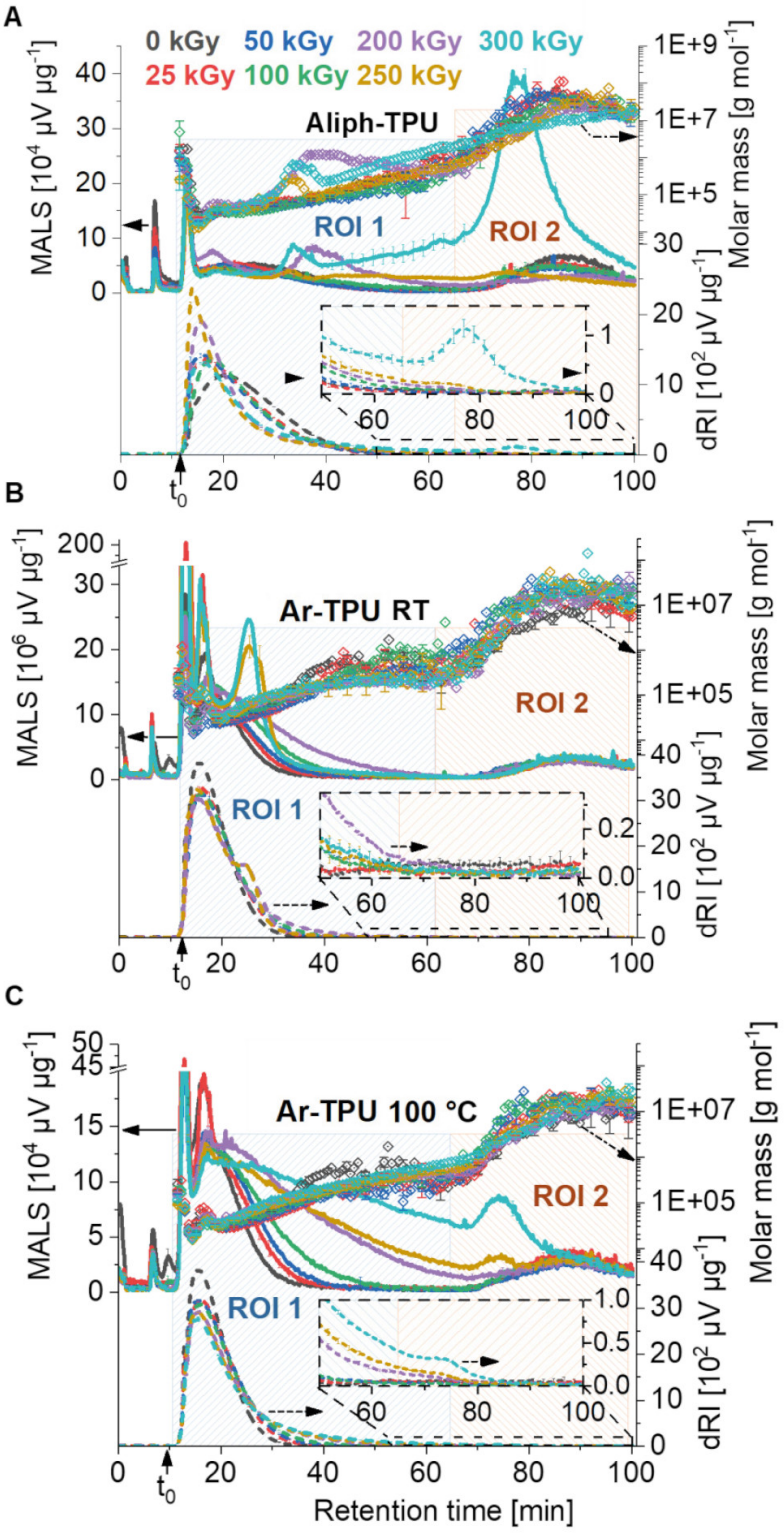

Figure S14 ThFFF fractograms of Aliph-TPU (**A**) and Ar-TPU irradiated at room temperature (**B**) and at 100 °C (**C**). The separation was performed with the optimized separation method shown in Fig. S4.

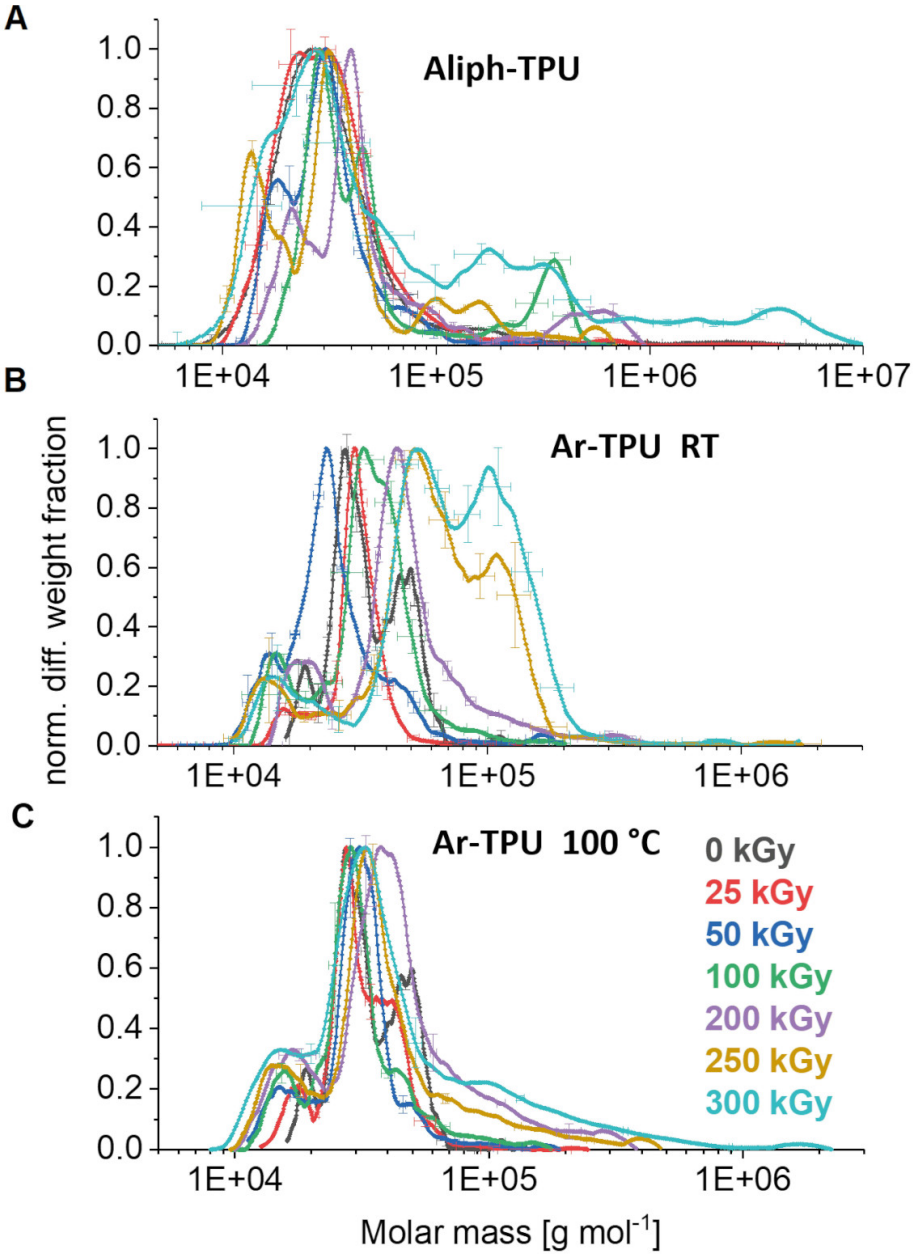

Figure S15 Normalized molar mass differential distributions from the ThFFF analysis of Aliph-TPU (**A**), Ar-TPU irradiated at room temperature (**B**) and at 100 °C (**C**), calculated for the entire fractogram.

Table S2 Summary of the ThFFF-analysis.

	Aliph-TPU		Ar-TPU RT		Ar-TPU 100 °C	
Irradiation dose	M_n [kg mol^{-1}]	$Đ$	M_n [kg mol^{-1}]	$Đ$	M_n [kg mol^{-1}]	$Đ$
0 kGy	45.8 ± 1.1	3.78 ± 0.16	37.1 ± 0.2	1.66 ± 0.01	37.1 ± 0.2	1.66 ± 0.01
25 kGy	42.2 ± 2.9	3.57 ± 0.11	43.1 ± 0.4	2.45 ± 0.01	37.3 ± 2.2	2.03 ± 0.29
50 kGy	36.6 ± 1.5	3.7 ± 0.5	25.4 ± 0.9	2.49 ± 0.04	32.7 ± 0.4	1.71 ± 0.01
100 kGy	37.9 ± 6.5	4.02 ± 0.05	36.5 ± 0.6	2.04 ± 0.01	33.3 ± 0.2	1.87 ± 0.03
200 kGy	47.9 ± 0.6	4.26 ± 0.03	39.5 ± 0.4	2.03 ± 0.01	42.6 ± 2.4	2.0 ± 0.1
250 kGy	29.5 ± 0.6	4.0 ± 0.1	53 ± 5	2.1 ± 0.1	37.6 ± 1.6	2.3 ± 0.1
300 kGy	48.0 ± 0.1	13.7 ± 0.4	55.3 ± 0.9	1.96 ± 0.04	40.3 ± 0.5	2.92 ± 0.01

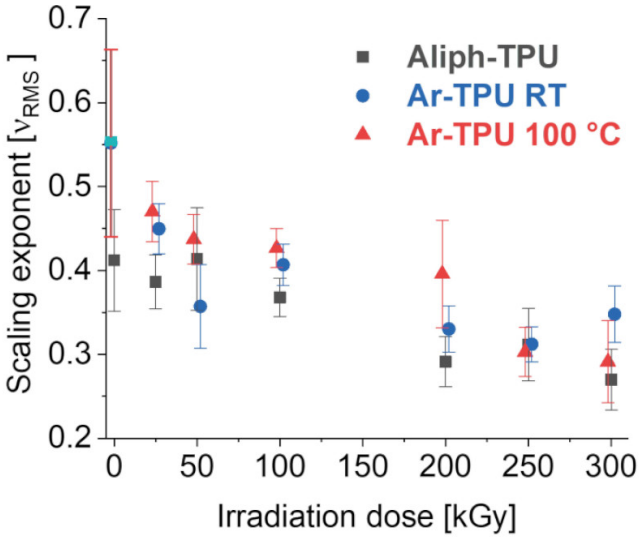

Figure S16 Scaling exponents of Aliph-TPU and Ar-TPU irradiated at room temperature (RT) and at 100 °C. The scaling exponents were determined with data from the interval 40 to 100 min in the ThFFF fractograms, given in Figure S14.

3.5.2. Thermophoretic analysis

The ThFFF separation has been carried out under programmed nonconstant field conditions as illustrated in Fig. S4. Therefore, additionally to the retention description given in Eq. (1) secondary relaxation phenomena needs to be taken into account in case the changes in the field force are fast. In that case, the relaxation equilibrium lags increasingly behind the drop of the field force resulting in later retention times than expected for an instantaneous reaction on the field force. Thus, the description of the retention time needs to be corrected by the introduction of a departure term Δ as stated in Eq. (3)

$$R = R_{instant} \cdot (1 + \Delta) \tag{3}$$

For sedimentation FFF, where secondary relaxation plays a major role in field programming conditions, Δ can be readily approximated.[6] However, for ThFFF of drained well-solvated polymers no investigation of this phenomenon has been carried out yet. In fact, polymers were so far assumed to follow changes in the field force instantaneously. In order to approximate the influence of secondary relaxation in the programmed method used in this study, a reference experiment with known polymer standards was performed. In that, a broad polystyrene and a broad PMMA sample were first analyzed by ThFFF under constant field conditions of ΔT = 80 K (T_c = 23.1 °C) and a calibration of S_T against the molar mass was fitted in a double logarithmic plot (see Fig. S17 A). Based on this calibration, the effective ΔT was then retraced by the means of Eqs. (1) and (2) in field programmed separations of these reference samples using a shortened version and the original version of the optimized separation method (given in Fig. S4). For that, S_T was recalculated based on the detected molar masses in dependency to the retention time. To avoid further elaborative calibrations, a simple S_T to molar mass calibration approach was used, where S_T is assumed to not vary with the cold wall temperature. For PMMA, this assumption holds true for a change of about 5 °C as reported previously.[7]

The so retraced effective ΔT revealed a significant delay to the instantaneous change of the programmed ΔT in particular for high decay rates of the field. Based on this finding an approximation for the departure term was empirically found in dependency to the field decay, as defined in Eq. (4)

$$\Delta = \frac{-0.005}{R_{init.}} \cdot ln\left(\left|\frac{d\Delta T}{dR}\right|\right) \quad (4)$$

with $R_{init.}$ as the retention ratio at the initial time of the field decay. The calculated retention times with correction of the secondary relaxation delay are found in good agreement to the retraced effective ΔT (in nominal retention time), as shown in Fig. S17 B. The S_T distributions illustrated in Fig. 4 in the main article were calculated with the help of the secondary relaxation correction approximation

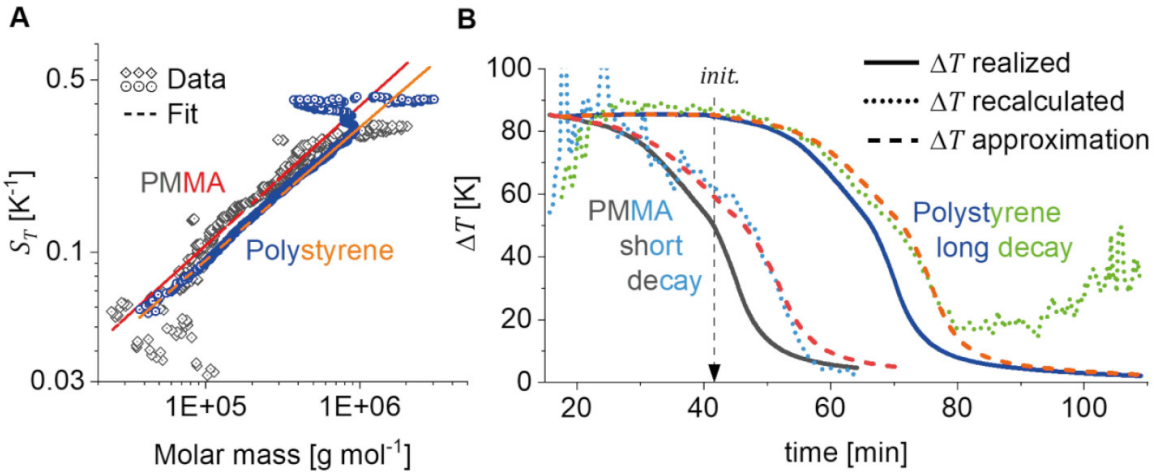

Figure S17 S_T – molar mass calibration of broad polystyrene and PMMA reference samples (**A**) as basis for the approximation of the secondary relaxation influence by retracing the effective ΔT from the measured molar mass retention (**B**); init. refers to the initial time of the field decay.

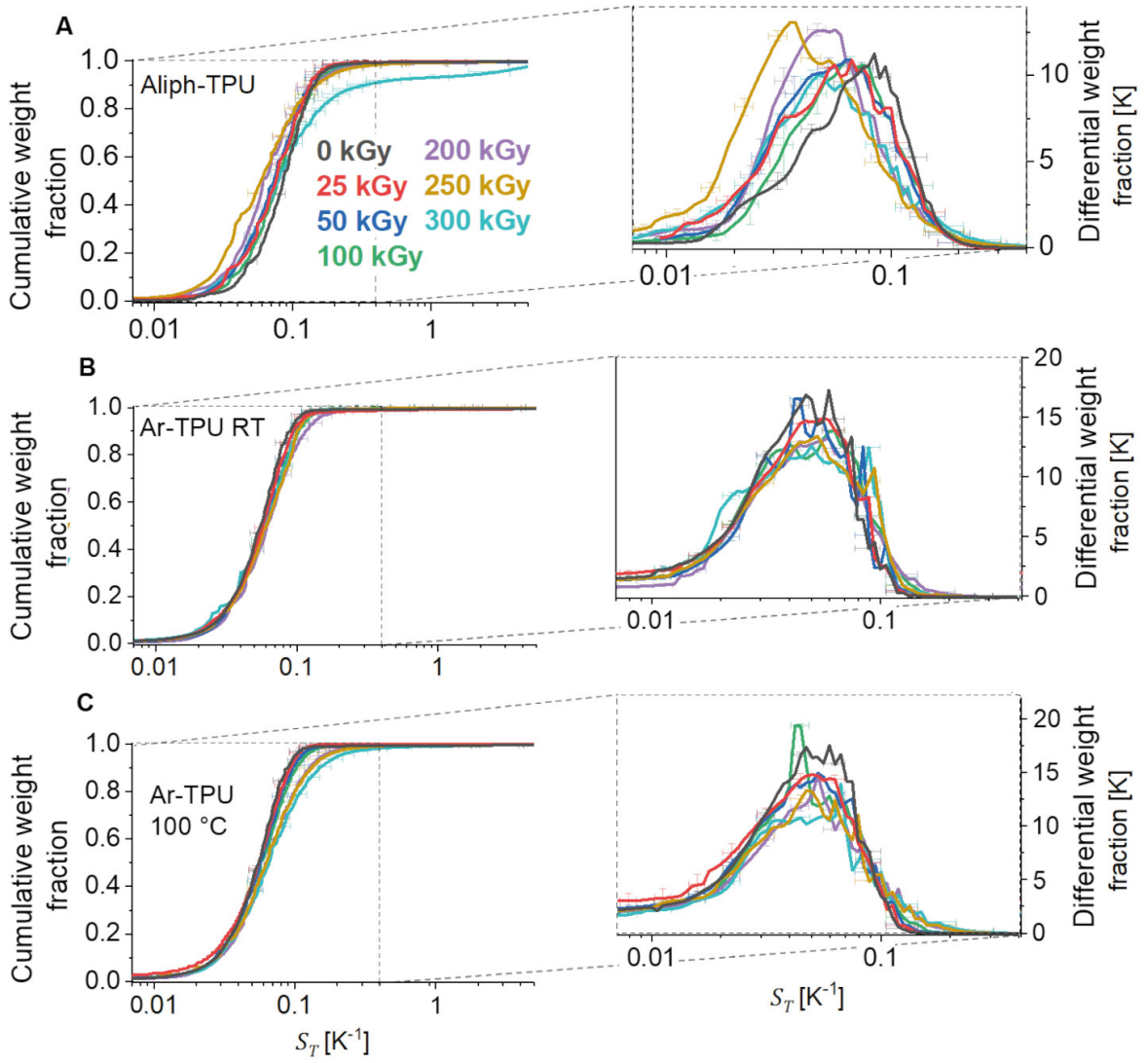

Figure S18 Cumulative S_T distributions with their derived differential S_T distributions of Aliph-TPU (**A**), Ar-TPU irradiated at room temperature (**B**) and at 100 °C (**C**) as presented in Fig. 4 in the main article.

3.6. Comparison of the molar mass distributions between calibrated SEC, SEC-MALS and ThFFF-MALS

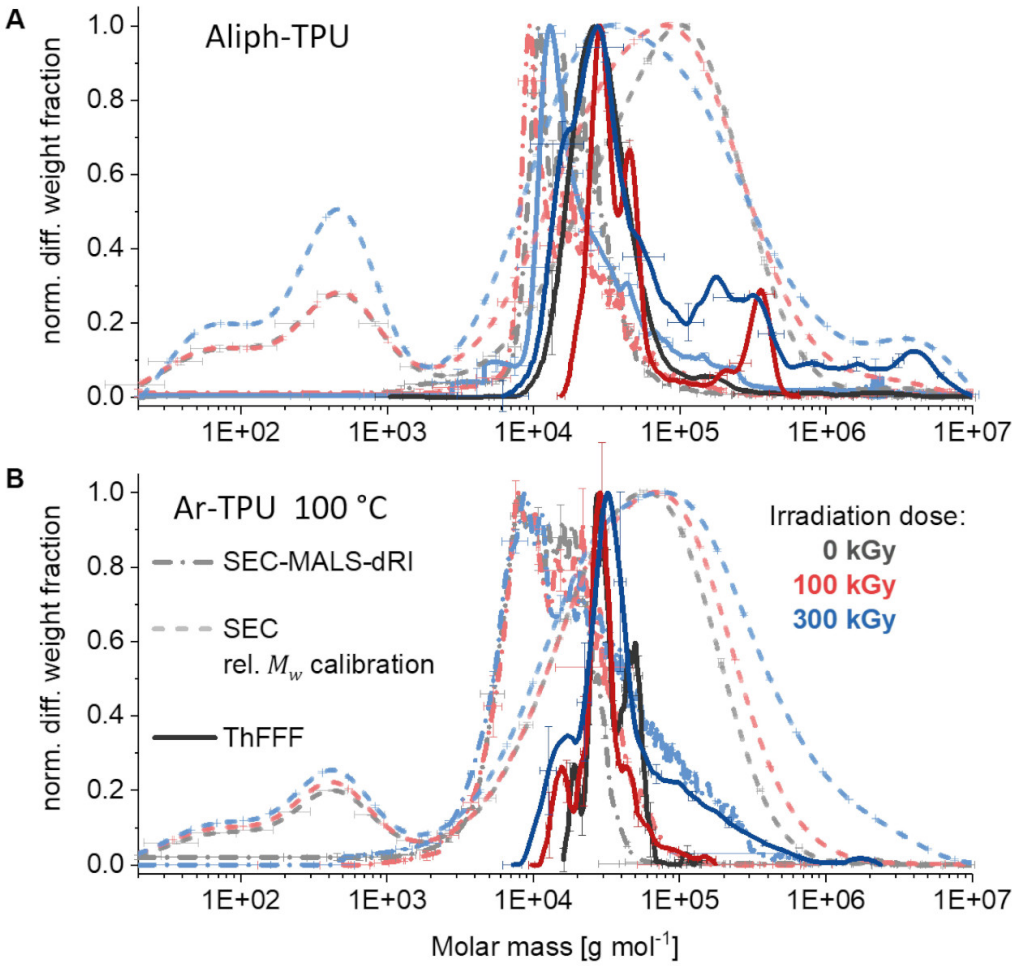

Figure S19 Normalized molar mass differential distributions of the different molar mass analysis approaches in comparison to each other of Aliph-TPU (**A**) and Ar-TPU irradiated at 100 °C (**B**).

4. References

[1] Schure, M. R.; Schimpf, M. E.; Schettler, P. D. Retention—Normal Mode. In *Field-Flow Fractionation Handbook*; Schimpf, M. E., Caldwell, K. D., Giddings, J. C., Eds.; John Wiley & Sons, Inc.: New York, USA, 2000; pp 31–48.

[2] Belgaied, J. E.; Hoyos, M.; Martin, M. Velocity Profiles in Thermal Field-Flow Fractionation. *J. Chromatogr. A* **1994**, *678* (1), 85–96. DOI: 10.1016/0021-9673(94)87077-2.

[3] Geisler, M.; Lederer, A. Non-Parabolicity Correction for Fifty-Nine Solvents and a Retention Study for Strongly Distorted Flow-Profiles in Thermal Field-Flow Fractionation. *J. Chromatogr. A* **2020**, *1621*, 461082. DOI: 10.1016/j.chroma.2020.461082.

[4] Čožíková, D.; Šílová, T.; Moravcová, V.; Šmejkalová, D.; Pepeliaev, S.; Velebný, V.; Hermannová, M. Preparation and Extensive Characterization of Hyaluronan with Narrow Molecular Weight Distribution. *Carbohydr. Polym.* **2017**, *160*, 134–142. DOI: 10.1016/j.carbpol.2016.12.045.

[5] Ono, Y.; Ishida, T.; Soeta, H.; Saito, T.; Isogai, A. Reliable Dn/Dc Values of Cellulose, Chitin, and Cellulose Triacetate Dissolved in LiCl/N,N-Dimethylacetamide for Molecular Mass Analysis. *Biomacromolecules* **2016**, *17* (1), 192–199. doi:10.1021/acs.biomac.5b01302.

[6] Hansen, M. E.; Giddings, J. C.; Schure, M. R.; Beckett, R. Corrections for Secondary Relaxation in Exponentially Programmed Field-Flow Fractionation. *Anal. Chem.* **1988**, *60* (14), 1434–1442. DOI: 10.1021/ac00165a018.

[7] Cao, W.; Williams, P. S.; Myers, M. N.; Giddings, J. C. Thermal Field-Flow Fractionation Universal Calibration: Extension for Consideration of Variation of Cold Wall Temperature. *Anal. Chem.* **1999**, *71* (8), 1597–1609. DOI: 10.1021/ac981094m.

Reprinted with permission from Geisler, M.; Pal, T. S.; Arnhold, K.; Malanin, M.; Müller, M. T.; Voit, B.; Impact of Electron Beam Irradiation on Thermoplastic Polyurethanes Unraveled by Thermal Field-Flow Fractionation. *Polymer Degrad. Stab.* **2021**, 183, 109423. DOI: 10.1016/j.polymdegradstab.2020.109423.

DECLARATION

Eidesstattliche Versicherung

Hiermit versichere ich, dass ich die vorliegende Arbeit ohne unzulässige Hilfe Dritter und ohne Benutzung anderer als der angegebenen Hilfsmittel angefertigt habe; die aus fremden Quellen direkt oder indirekt übernommenen Gedanken sind als solche kenntlich gemacht. Die Arbeit wurde bisher weder im Inland noch im Ausland in gleicher oder ähnlicher Form einer anderen Prüfungsbehörde vorgelegt.

Die vorliegende Arbeit wurde unter der wissenschaftlichen Betreuung von Frau Prof. Brigitte Voit und Frau Prof. Dr. Albena Lederer in der Zeit von Januar 2017 bis Oktober 2020 an der Technischen Universität Dresden und am Leibniz-Institut für Polymerforschung Dresden e.V. angefertigt.

Bisher haben keine weiteren Promotionsverfahren stattgefunden.

Hiermit erkenne ich die Promotionsordnung der Fakultät Mathematik und Naturwissenschaften der Technischen Universität Dresden in der zuletzt geänderten Fassung vom 23.05.2018 an.

Dresden, den 06. November 2020

Martin Geisler